



# NUI MAYNOOTH

Ollscoil na hÉireann Má Nuad

## Investigation of slow oscillations in blood pressure

Oliver P. Kinnane (B.E.)

Ph.D. Thesis

Department of Electronic Engineering

November 2004

Supervisor: Prof. John Ringwood

# Table of Contents

<b>1.</b>	<b>Introduction</b>	<b>1</b>
1.1	Introduction	1
1.2	Objectives of the thesis	3
1.3	Contributions of the thesis	5
1.4	Thesis layout	7
<b>2.</b>	<b>Blood pressure control</b>	<b>9</b>
2.1	Blood pressure and homeostasis	9
2.1.1	The short-term control of blood pressure and the baroreflex	11
2.2	The physiological components	17
2.2.1	Blood pressure sensors	18
2.2.1.1	Models of the baroreceptors	20
2.2.2	The central nervous control of blood pressure	22
2.2.2.1	The central nervous system	25
2.2.2.2	The autonomic nervous system	25
2.2.2.3	Modelling the central arc	30
2.2.2.4	Modelling the neural arc	33
2.2.3	Blood pressure effectors	38
2.2.3.1	The heart	38
2.2.3.2	The vasculature	57
2.2.3.3	Long term effectors of blood pressure	55
2.2.4	Complete control of blood pressure	59
2.3	Cardiovascular variability	60
2.3.1	Cardiovascular rhythms	63
2.3.2	The slow oscillation in blood pressure	67
2.3.3	The origin of the slow oscillation in blood pressure	69

2.3.3.1	The central oscillator theory	70
2.3.3.2	The baroreflex feedback theory	71
2.3.3.3	Roles of the heart and vasculature in the genesis of the slow oscillation in blood pressure	74
2.4	Modelling review	75
2.4.1	Models of the baroreflex control of peripheral resistance	77
2.4.2	Models of the complete baroreflex	80
<b>3.</b>	<b>Analysis of chaos in blood pressure</b>	<b>85</b>
3.1	Introduction	85
3.1.1	Rationale for analysis of blood pressure time series for chaos	87
3.1.2	Chaos and health	88
3.1.2.1	Chaos in cardiovascular systems	89
3.2	Analysis of blood pressure data	90
3.2.1	Description of available data	90
3.2.2	Preprocessing the data	91
3.3	Determining chaos from a one-variable time series	98
3.3.1	Surrogate data analysis	99
3.3.2	Lyapunov exponents	100
3.4	Results	103
3.4.1	Reconstruction of the phase space	103
3.4.2	Noise reduction	105
3.4.3	Nonlinearity of blood pressure signals	106
3.4.4	Chaos in the blood pressure system	107
3.5	Discussion	109

3.6	Conclusions	113
<b>4.</b>	<b>Predicting the slow oscillation in blood pressure using a nonlinear analysis of a model of baroreflex control of peripheral resistance</b>	<b>115</b>
4.1	Introduction	115
4.2	Modelling the baroreflex	118
4.2.1	The nonlinear model	118
4.2.2	Analysis approach	119
4.2.3	The sigmoidal baroreflex curve	120
4.2.3.1	The describing function	125
4.2.3.2	Calculating the describing function for the sigmoid	127
4.2.3.3	An approximation to the describing function for the sigmoid	128
4.2.4	The vascular dynamics	130
4.2.4.1	ARX modelling of the vascular dynamics	130
4.3	The slow oscillation, mean SNA and baroreflex gain	134
4.3.1	Changes in the strength of the slow oscillation during different physiological conditions	134
4.3.2	Mean changes in SNA and the slow oscillation	135
4.3.3	Changes in the characteristics of the baroreflex curves during different physiological conditions	136
4.4	Available data	137
4.5	Prediction of limit cycle oscillation	142
4.6	Results	145
4.7	Discussion	151
4.8	Conclusions	156

<b>5.</b>	<b>Describing function approximations</b>	<b>157</b>
5.1	Introduction	157
5.1.1	The case for a new describing function approximation	158
5.2	A new approximation to the describing function	161
5.2.1	Orthogonal polynomial approximation methods	162
5.3	Comparison of the describing function approximations	169
5.4	Discussion	172
5.5	Conclusions	173
<b>6.</b>	<b>Modelling the complete baroreflex</b>	<b>175</b>
6.1	Introduction	175
6.2	Modelling approach	176
6.3	Modelling the neural arc	177
6.3.1	Dynamical characteristics in the neural arc	179
6.3.2	Nonlinearity in the neural arc	180
6.3.3	A dynamical linear-static nonlinear neural arc model	180
6.3.4	Nonlinearities in the central nervous control of the heart	183
6.3.5	Nonlinearities in the central nervous control of the vasculature	187
6.4	Modelling the baroreflex control of the heart	189
6.4.1	Sympathetic control of the heart	189
6.4.2	Parasympathetic control of the heart	191
6.4.3	Parasympathetic- sympathetic control of heart rate	192
6.4.4	Control of stroke volume	194
6.5	Modelling baroreflex control of the vasculature	194
6.5.1	Response characteristics of the vasculature beds	196
6.6	Delay terms in the model	199
6.7	Model of the complete baroreflex	207
6.8	Model simulation results	209

6.9	Discussion	211
6.10	Conclusions	217
<b>7.</b>	<b>Nonlinear analysis of the complete baroreflex</b>	<b>218</b>
7.1	Introduction	218
7.2	Model Simplification	220
7.3	Preliminary model analysis	224
7.3.1	Frequency domain analysis based on the convolution of the time domain signals	226
7.3.2	Frequency domain analysis based on the Laplace transform	230
7.3.3	Development of the conditions for sustained oscillation	231
7.3.4	Numerical example	238
7.4	Discussion	241
7.5	Conclusions	245
<b>8.</b>	<b>Conclusions</b>	<b>247</b>
8.1	Conclusions	247
8.2	Recommendations for future research	250
	<b>References</b>	<b>253</b>

# Abstract

This thesis addresses blood pressure regulation from a mathematical modelling perspective. Blood pressure is controlled via a number of different negative feedback mechanisms. The baroreflex loop is the most dominant of these mechanisms for short-term control of blood pressure, and soft-limiting nonlinearities inherent in this loop, are thought to give rise to a slow limit cycle oscillation in blood pressure at 0.1 Hz in the human. Measurement of the strength of this slow oscillation has been proposed as the basis for the development of a diagnostic test of cardiovascular dysfunction or disease. Due to this hypothesis, extensive effort has been invested in measuring the strength of this slow oscillation in blood pressure in a range of physiological and pathophysiological conditions. However, the momentum of this research has continued with little consideration given to the fundamental cause of this oscillation. The means of genesis of the slow oscillation in blood pressure is the major focus of this research, and a mathematical modelling approach was undertaken to analyse the nonlinear mechanisms that give rise to this slow oscillation.

The theory that the slow oscillation in blood pressure results due to the feedback nature of the baroreflex loop, and is a limit cycle oscillation established by the nonlinear elements in this feedback loop, is initially investigated by the analysis of blood pressure data recorded during different physiological conditions in which the strength of the slow oscillation in blood pressure was observed to change.

Nonlinear time series analysis methods were used to investigate for the existence of a limit cycle oscillation in blood pressure, and so that insight may be attained into the effects of changes of the nonlinear characteristics on the slow oscillation. Following this, changes in the strength of the slow oscillation were investigated, again during different physiological conditions, via a model of baroreflex control of the vasculature.

Complications to this analysis, due to the difficulty of developing an analytical describing function representation of the nonlinear sigmoid characteristic inherent to the baroreflex, led to the investigation of a range of describing function approximation methods for the sigmoid nonlinearity, which permeates the cardiovascular literature.

A nonlinear model of the complete baroreflex, including the cardiac branch, which has often been ignored, was developed. The ability of the model to replicate the slow oscillation in blood pressure was assessed. A significant role for the heart in the development of the oscillation was identified. An analytical analysis technique was developed to investigate the significance of the different pathways of the baroreflex involved in the genesis of the slow oscillation. This analysis resulted in the development of conditions under which a sustained limit cycle oscillation can occur. In particular the role of mean levels of cardiac output and vascular resistance, previously thought to be relatively unimportant, in establishing and maintaining sustained oscillations, was highlighted.

The ultimate aim of this research was to develop the understanding of the mechanisms involved in the genesis of the slow oscillation, and thereby, to assist in the development of a diagnostic test based on non-invasive measurement of the slow oscillation in blood pressure.

## Acknowledgements

Many people must be thanked, for without their help, either specifically in relation to this research or, in a more general sense in the past 4 years, this thesis may never have been compiled.

First and foremost, I would like to express my sincere gratitude to my supervisor Prof. John Ringwood for his supervision, dedication, patience and persistence. Thanks for getting me to the end John.

I would like to thank Prof. Simon Malpas for all his help. It has been a pleasure to study physiology under his guidance and a wonderful education. Many thanks to all at the Circulatory Control Laboratory at the University of Auckland for their help, welcoming spirit and generosity with their hard earned data.

Thanks to John and Simon for sending me around the world on so many occasions.

Thanks to Orla and John Malocco for their help with the numerous administrative and technical problems and thanks to those of the staff at NUI Maynooth who were so generous with their time and knowledge. Thanks to the postgrads, old and new, for making the four long years in Maynooth so enjoyable. Thanks especially to Tarek for his help and constant good humour, to Bernard for his unbounded generosity with his time and knowledge and to Ken for his untiring help when it was often most needed.

I also gratefully acknowledge the financial support that I have received from NUI Maynooth and The Wellcome Trust.

On a personal level I wish, first and foremost, to thank my family for their kindness and support. I wish to convey my eternal gratitude to my parents and use this opportunity to thank them for their love, support and their unbounded generosity throughout all the years of my life. I feel truly fortunate to have had the educational opportunities in life that I've had, and this is wholly due to their unflinching kindness and generosity.

It would be remiss of me not to also express my gratitude to the many people who's friendships have formed the foundations of what has made the last four years always so good. My gratitude must be extended to a few people in particular, with whom this thesis would perhaps never have been completed. I thank Louise for her wonderful friendship and for putting up with the incessant moaning. Thanks to Cian for being so giving of his time. Thanks Dr. Hennelly for the sanity support in the awful final days, and for always keeping the faith. Thanks to all my friends from the Spioraid Naoimh and UCC years and all from the Portobello, Lombard Street and Grove Park years. A special thank you to Jenny. Finally a very special thanks to Damien for his help, friendship, support and enthusiasm throughout my engineering education. Without him this thesis would probably not have made it on this the eleventh hour.

It would be impossible for me to overstate the debt of gratitude that I owe to my family and friends and to all those who have helped me in so many ways in the course of this Ph.D. The last four years have been a truly wonderful personal and educational journey. Here's hoping the next four are just as good.

For my brother Tony,  
Thank you for showing me that happiness is a method of life.

## Declaration

I hereby certify that this material, which I now submit for assessment on the programme of study leading to the award of Doctor of Philosophy in Electronic Engineering is entirely my own work and has not been taken from the work of others save and to the extent that such work has been cited and acknowledged within the text of my work.

Signed: \_\_\_\_\_

Date: 15<sup>th</sup> November, 2004

# Chapter 1

## Introduction

### 1.1 Introduction

Cardiovascular disease is the leading cause of death in many countries, accounting for 40% of all deaths in Ireland, as an example (Codd 2001). High blood pressure plays a major role in the development of cardiovascular diseases, including stroke and coronary heart disease (Chalmers 1999), yet little is known about the cause and effect of high blood pressure and of the means by which it is developed.

In order to avoid the onset of cardiovascular disease, good regulation of blood pressure is essential. An understanding of the mechanisms of blood pressure control is fundamental to the understanding of the causes of cardiovascular disease, and its prevention. Blood pressure control involves the integrated action of various regulatory mechanisms that operate over time scales of minutes to days, in order to maintain blood pressure at normal operating levels.

Blood pressure is controlled in the long-term through the regulation of the fluid and electrolyte balance (also related to blood volume control). The short-term control of

blood pressure is specifically the duty of the autonomic neural mechanisms, which effect changes in blood pressure on a moment-to-moment basis by causing rapid changes in heart rate and in the resistance of the blood vessels. More recent research also indicated a possible role for neural mechanisms in the long term control of blood pressure (Malpas 2004).

Periodicities in the cardiovascular variables, blood pressure and heart rate, were identified almost 300 years ago (Hales 1733). However, it was the suggestion, that certain frequencies present in these cardiovascular signals were indicative of autonomic nervous function, which stimulated great clinical interest in using measures of cardiovascular variability as a diagnostic tool (Akselrod 1981; Parati 1994; Parati 1995; Parati 1998; Parati 2001). Extensive research has since been undertaken to quantify the changes in these periodicities of blood pressure and heart rate over a range of physiological and pathophysiological conditions (Inoue 1991; Bigger 1992; Teich 2000).

Of particular interest is an oscillation in blood pressure that manifests itself at 0.1 Hz in the human, otherwise known as the *slow oscillation* in blood pressure. Measurement of the strength of this oscillation has been proposed as the basis for the development of a diagnostic test of cardiovascular dysfunction or disease (Malliani 1991). It is hypothesised that measurement of the strength of this oscillation may provide a surrogate, clinical measure of sympathetic nerve activity (SNA) (Pagani 1986). There is a growing body of evidence that suggests that the over-activity of the sympathetic nervous system plays a critical role in the development of hypertension (Goldstein 1981; Grassi 1998; Grassi 1998). Therefore, a noninvasive, surrogate measure of SNA would be of great value to the clinical assessment of subjects at risk of cardiovascular disease, especially considering the ease with which electronic measurement of blood pressure (and other physiological variables) is currently available.

The momentum of this clinical research into the slow oscillation in blood pressure has, however, continued without due reflection and understanding of the fundamental causes of this variability and without reference to the possibility that not all changes in cardiovascular variability are indicative of changes in autonomic function (Malpas 2002). As a result, the mechanisms that give rise to this slow oscillation, and the reasons for its existence, are still strongly disputed. Two main theories (De Boer 1987; Cooley 1998) exist that describe the conflicting hypotheses that the slow oscillation is generated either (a) by a central nervous oscillator or (b) as a result of the closed-loop feedback nature of the baroreflex control mechanism.

The research, described in this thesis, performs a detailed analysis of the slow oscillation in blood pressure and the mechanisms that are responsible for the generation of this oscillation. It is proposed that a mathematical modelling approach to the analysis of the blood pressure controlling mechanism may enable insight into the specific mechanisms responsible for the genesis of this oscillation.

Mathematical models may be useful in determining the relative importance of various factors involved in producing cardiovascular variability, in determining the nature of their effect, and in allowing predictions be made on the behavior of the oscillations under conditions that may be difficult to test experimentally.

Considerable evidence exists to suggest that observed nonlinear relationships between the variables of cardiovascular control are inherently involved in developing a limit cycle oscillation – the slow oscillation in blood pressure. The nonlinear control of blood pressure is therefore a central theme of the thesis and leads to definitive conclusions regarding the origin, and characterisation of, the slow oscillation in blood pressure.

## 1.2 Objectives of this research

The primary goal of this research is the advancement of the present understanding of the mechanisms of blood pressure control that give rise to the slow oscillation in blood pressure. It is proposed that only attainment of this insight will enable conclusions to be drawn regarding the usefulness of this oscillation as a diagnostic measure.

- The initial aim of this work was to examine both theories in relation to the genesis of the slow oscillation, by examining the physiological evidence available in support of both and through the examination of feedback models of the baroreflex. The theory that the oscillation is a feedback oscillation around the baroreflex feedback loop has received most currency in recent years (De Boer 1987; Ringwood 2001). However, recent studies that have supported the baroreflex feedback hypothesis, have proposed alternative descriptions of the feedback mechanism and hence, the means of oscillation genesis differ.
- A second objective looks at resolving the correct structure of the baroreflex mechanism. Some authors have proposed that the oscillation results from a linear process (Burgess 1997). In this case, the requirement for strict relationships between the parameters of the different components of the feedback loop, would imply that the slow oscillation is deliberate and may have a functional purpose and that the central nervous system would go to great lengths to maintain this oscillation. An alternative hypothesis proposes that the oscillation arises as a result of the inherent characteristics of the blood pressure control mechanisms (Ringwood 2001) and hence is not deliberate. Nonlinear characteristics that are well established to exist in blood pressure controlling mechanisms (Iriki 1972; Korner 1972) may give rise to a limit cycle oscillation (Ringwood 2001) and this hypothesis is investigated in this thesis.

- A further objective examines the role of the heart in the genesis of a slow oscillation via the baroreflex. Many studies (Burgess 1997; Ringwood 2001) of the slow oscillation have based their analysis on the baroreflex control of vascular resistance only and have ignored baroreflex control of the heart. The assumption that the heart is not involved in the genesis of the slow oscillation in blood pressure has been pressed by a number of authors (Malpas 2000; Liu 2002). Considering the role of the heart as the principal cardiovascular controller, it is proposed that an analysis of the mechanisms of blood pressure control excluding the heart is incomplete. A major focus of this study is the analysis of the role of the heart in the genesis of the slow oscillation in blood pressure.
- Finally, it is also an objective of this thesis to, where possible, enumerate the conditions for development of a slow oscillation and to develop algebraic measures for oscillation conditions, under both nominal situations and also any substantial changes due to experimental intervention or pathologies. The scope of this objective is obviously limited by the quantity of experimental data accessible to the author either directly, or through experimental results reported in the literature.

### 1.3 Contributions of this thesis

The main contributions of the thesis are as follows:

- A comprehensive review of the physiological literature is undertaken and critiqued in Chapter 2, in order to answer the question as to whether the slow oscillation is a feedback oscillation or not. In addition, this review documents all blood pressure controlling mechanisms, which operate on time scales relevant to the slow oscillation in blood pressure.

- The possible existence of a limit cycle oscillation is analysed using techniques derived from chaotic analysis. This investigation is the focus of Chapter 3 and the results of this analysis were presented at the IFAC Symposium on Modelling and Control of Biomedical Systems (Kinnane 2003).
- The feedback oscillation theory and the limit cycle hypothesis were investigated with regard to relative changes in the central nervous system *and* vasculature, which result from various interventions and pathologies. This is unique, since previous work has not considered the importance in (particularly gain) variations in the vasculature, focusing instead on the controlling mechanism of the CNS. This analysis is presented in Chapter 4 and is under revision following submission to the American Journal of Physiology (Kinnane 2004).
- Inherent to baroreflex control are the sigmoid baroreflex curves, for which describing functions, facilitating stability analysis, are difficult to develop. Describing function approximations for the nonlinear sigmoid characteristic, common to physiological systems, were investigated and extended in this chapter. This work was presented at the 2004 Irish Signals and Systems Conference, in Belfast (Kinnane 2004) (received Best Control Paper award).
- A comprehensive mathematical model that accurately describes the short-term control of blood pressure, including the vascular *and* heart components, is also a major contribution of this thesis. Clearly, an accurately parameterized model can play an important role in scenario testing and examination of the likely variation in, for example, the slow oscillation in blood pressure, under a variety of circumstances, including pathologies. This work has been submitted for presentation at the 2005 IFAC World Congress in Prague (Ringwood 2005).
- The final major contribution of the thesis is the development of an analytical technique, which allows quantification of the amplitude and frequency of limit

cycle oscillations (developed through a combination of heart and vasculature paths) in relation to physiological parameters. This is significant, since traditional describing function techniques allow only limited (lumped series or parallel) combinations of nonlinear characteristics. A description of this analysis is to be submitted for future publication.

## 1.4 Thesis layout

This thesis follows the progression of the research necessary to answer the issues posed in Section 1.2. The logical progression of the thesis is as follows.

**Chapter 2 (Blood pressure control)** provides a detailed description of the mechanisms of blood pressure control in the short-, medium- and long-term. The components of these mechanisms are examined and the relationships between the many cardiovascular and neural variables that might affect the control of blood pressure are documented. The multiple periodicities of the cardiovascular signals, and the methods of quantification of the ‘variability’ of these signals are reviewed. Conclusions drawn from these measures of variability are examined. The different theories that have been hypothesised to describe the means of genesis of these periodicities are discussed and the experimental evidence in support of these various theories is presented. Following this, the mathematical models that have been developed to describe the periodicities of cardiovascular variables are documented and the physiological accuracy of these models, considering what was introduced in the chapter to this point, is assessed.

Following this review, Chapters 3 and 4 contain detailed analysis pertaining to the possible development of feedback oscillations through the peripheral resistance system. In particular, **Chapter 3 (Chaotic analysis of blood pressure signals)** attempts to gain insight into the nonlinear mechanisms responsible for a limit cycle

and to confirm, using measures of chaotic behaviour, that the slow oscillation is, indeed, a limit cycle. **Chapter 4 (Predicting the slow oscillation in blood pressure using nonlinear analysis of a model of baroreflex control of peripheral resistance)**, on the other hand, looks at the relative changes which may occur in both the central nervous system *and* the vasculature in mediating oscillations via a limit cycle and examines the likelihood of increases/decreases in oscillation amplitude in relation to a set of interventions and pathologies. Central to the analysis of Chapter 4 is the requirement for a describing function for the sigmoidal characteristic typical of neural processing mechanisms. **Chapter 5 (Developing the describing function approximation)** documents a number of describing function approximation methods that can be used to overcome the difficulty of calculating describing functions for the sigmoid nonlinearity, common to cardiovascular control.

Chapters 6 and 7 now expand the consideration to include the heart as a mediating influence of slow oscillations. In particular **Chapter 6 (Modelling the complete baroreflex)** develops a comprehensive nonlinear model of the complete baroreflex, including both cardiac and peripheral resistance branches. The development of the model, based on experimentally derived characteristics of the components of the baroreflex, is documented. **Chapter 7 (Nonlinear analysis of the complete model)** then, using the model of Chapter 6 as a basis, develops an analytical technique (broadly similar to a traditional describing function analysis), which may be used to algebraically determine the amplitude and frequency of limit cycle oscillations. The technique of Chapter 7 utilises a slightly simplified model of that developed in Chapter 6, in order to provide tractable solutions, but focussing on those components most likely to play a significant role in feedback oscillations.

Finally, **Chapter 8 (Conclusions)** presents the conclusions developed through the course of this research. The possible significance and impact of the various conclusions is assessed and directions for future work are indicated.

## Chapter 2

### Blood pressure control

#### 2.1 Blood pressure and homeostasis

The regulatory mechanisms of the body can be understood in terms of a single, shared function: that of maintaining constancy of the internal environment. This state of relative constancy of the internal environment is known as homeostasis (Fox 1996). The regulation of blood pressure may be seen as an integral part of homeostasis (Guyton 1991).

Blood pressure is the force exerted by blood against any unit area of blood vessel wall (Sherwood 1997). Both the heart and resistance of the blood vessels have the capacity to facilitate the control of blood pressure, via the 'Ohm's law' relationship:

$$p_b(t) = q_c(t)r_p(t) \quad (2.1)$$

where,

$p_b(t)$  is mean arterial blood pressure, (mmHg)

$q_c(t)$  is cardiac output (ml/min), and

$r_p(t)$  is total peripheral resistance of the vasculature system (mmHg.min/ml) and where,

$$q_c(t) = f_c(t)v_c(t) \quad (2.2)$$

where,

$f_c(t)$  is the cardiac rate (beats/min), more commonly termed heart rate, and

$v_c(t)$  is the cardiac volume, more commonly termed stroke volume

(ml/beat)

The control of blood pressure involves the adjustment of these parameters, through negative feedback mechanisms, to maintain blood pressure close to a set point value (Parati 1995), thereby contributing to the maintenance of homeostasis.

Blood pressure must be constantly high enough to ensure sufficient driving pressure so that the brain and tissues of the body receive adequate blood flow. However, it is important that blood pressure is closely regulated to guard against sustained increases or decreases in blood pressure, both of which are strongly correlated with the onset of cardiovascular disease (Fox 1996).

A healthy blood pressure is defined by the World Health Organisation as around 120/80 mmHg (Chalmers 1999), where the higher value is the blood pressure value at the peak of systole (the contraction of the heart) and the lower value is the blood pressure value during diastole (the filling of the heart).

However, blood pressure control mechanisms may not always function correctly and may be unable to completely compensate for sustained changes in pressure. Blood pressure may be above the normal range in the case of hypertension (140/90 mmHg) (Chalmers 1999) or below the normal range in the case of hypotension (100/60 mmHg) (Chalmers 1999). Sustained hypotension results in, amongst other things, circulatory shock; inadequate blood delivery to the tissues, whereas sustained

hypertension can cause an abundance of cardiovascular disease including heart failure, stroke or renal failure (Fox 1996).

Blood pressure regulation comprises the complex and sophisticated integrated action of various regulatory mechanisms which operate over a wide time scale range of between seconds and days (Guyton 1987). The first line of defence against a sudden pressure change is served by the neural mechanisms (Guyton 1987) which have the capability to facilitate change of the blood pressure effectors, the heart and vasculature (via Equation 2.1), within seconds. Locally acting, and as yet poorly understood, paracrine mechanisms also participate in this short-term regulation (Persson 1992; Just 1994; Stauss 2000) (see Section 2.2.3.2). Although dependent on the class of hormone, a greater latency is generally associated with the humoral mechanisms and the full influence of most hormones is experienced over a period of minutes to hours (Guyton 1987) (see Section 2.2.3.2). The long-term control of blood pressure is specifically the duty of the kidney, which plays the fundamental role of maintaining fluid balance and hence, blood volume and blood pressure (Guyton 1991) (see Section 2.2.3.3). The effectors of blood pressure and the mechanisms by which they are affected are introduced in the subsequent sections, with the emphasis placed on the short-term control of blood pressure.

### 2.1.1 The short-term control of blood pressure and the baroreflex

Blood pressure is regulated in the short-term predominantly by negative feedback neural mechanisms that control blood pressure, as a primary function in the case of the arterial baroreflex mechanism and as what may be considered an ancillary function in the case of the cardiopulmonary and chemoreceptor mechanisms. The affects of the potent paracrine, nitric oxide, released in response to shear stress along the blood vessel walls, are also felt within seconds (Rubanyi 1990). Though these

effects are primarily experienced locally, there is growing evidence of overlap between nitric oxide and the baroreflex mechanism (Malpas 2002).

The structure, significance and components of the arterial baroreflex feedback mechanism are well documented in the physiology literature. The cardiopulmonary receptor and chemoreceptor mechanisms are less well understood, but because they share neural pathways and impact on the same neural centres. A level of cooperation with the baroreflex in the short-term regulation of blood pressure has been proposed for these mechanisms (Persson 1989; Eckberg 1992; Komer 1995) (see Section 2.2.4). All of these cardiovascular reflex mechanisms are negative feedback mechanisms that are triggered by afferent nerve signals, which transport sensory information from blood pressure sensors that originate at different sites in the circulatory system. The arterial baroreflex is generally accepted as the most influential of these mechanisms (Sherwood 1997) and capable of dominating cardiovascular function (Berne 1996).

The arterial baroreflex is a negative feedback mechanism that works to stabilise fluctuations in arterial pressure, by changing heart rate and the resistance of the vasculature, via the central nervous system (Guyton 1987). The baroreflex feedback loop is illustrated in Figure 2.1.

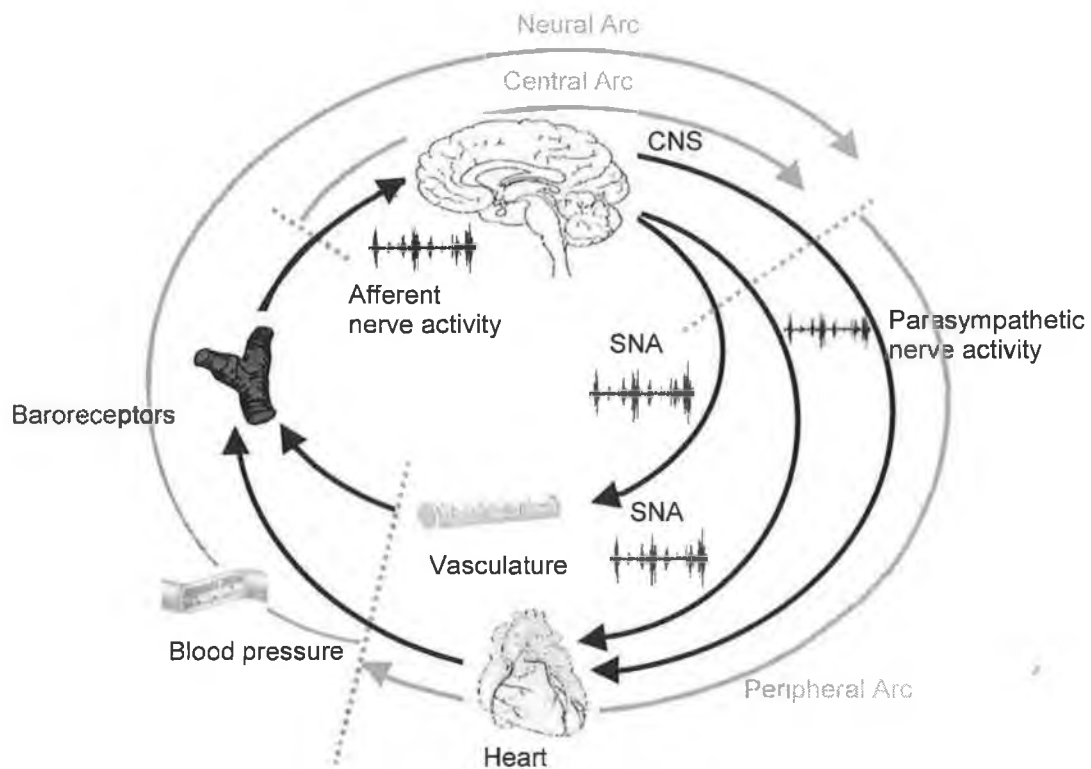


Figure 2.1: The baroreflex feedback loop.

Pressure sensors, known as baroreceptors, constantly monitor mean arterial pressure within the circulatory system (Eckberg 1992). A change in pressure will induce a change in the firing rate of the afferent nerve travelling to the central nervous system (CNS). Here, the afferent signal is processed and efferent nerve signals of varying frequency and amplitude are released (Deutsch 1993). The efferent signals are the signals of the autonomic nervous system, which innervates the heart, via parasympathetic nerve activity and sympathetic nerve activity (SNA), and the blood vessels of the vasculature via SNA alone (Sherwood 1997). In response to changing efferent nerve signals, heart rate, stroke volume and total peripheral resistance are adjusted so as to regulate blood pressure according to Equations 2.1 and 2.2.

It is traditionally thought that the baroreflex is of little or no importance in the long-term regulation of blood pressure (Guyton 1987), although recent experimental studies have challenged this theory (Lohmeier 2001; Thrasher 2002; Barrett 2003; Lohmeier 2003; Sleight 2004; Thrasher 2004). However, the importance of the

baroreflex to the momentary control of blood pressure, so as to keep blood pressure close to the normal level and thus constantly maintain homeostasis, is very evident when considering the situation when the baroreflex loop has been opened. As is shown in Figure 2.2, the fluctuations of blood pressure increase substantially when the baroreflex loop is disabled by opening of the loop at the afferent nerves.

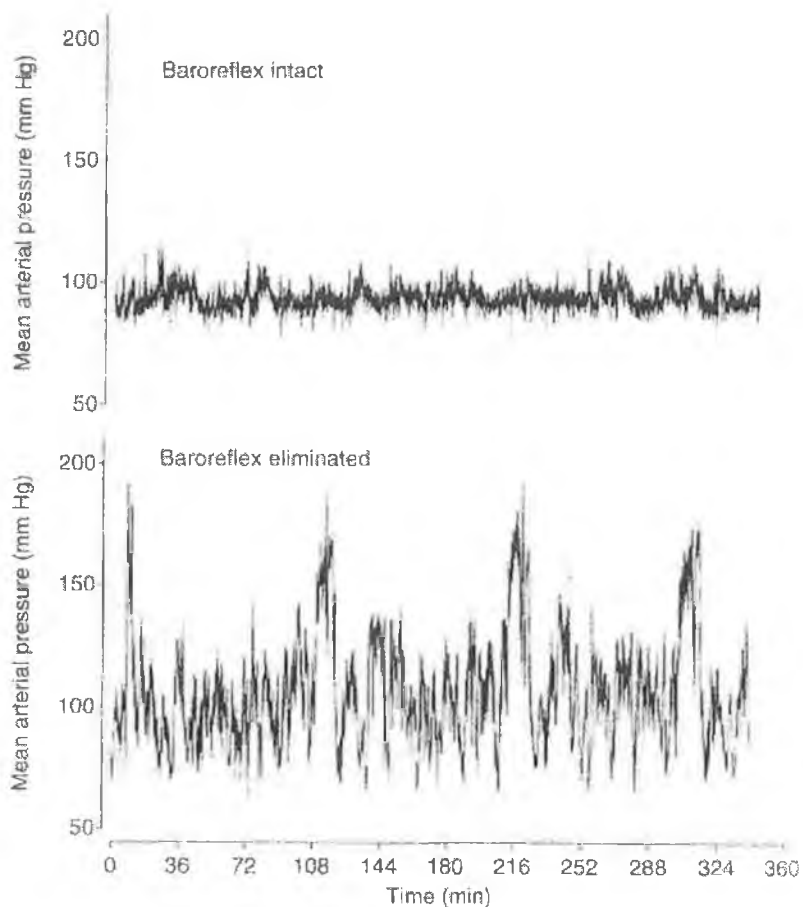


Figure 2.2: A 6-hour recording of mean arterial blood pressure in the rat with an intact baroreflex loop (top) and with the baroreflex loop eliminated (bottom). Adapted from Richardson *et al* (Richardson 1998).

Since the seminal work of Koch (Koch 1931), the standard approach for quantification of baroreflex responses has been the development of the so-called “baroreflex curves”. The responses of heart period (Eckberg 1980), heart rate (Malpas 1997) and SNA (Iriki 1977) describe a nonlinear sigmoidal shaped characteristic when plotted against invoked changes in blood pressure, as shown in Figure 2.3 for the blood pressure–SNA and blood pressure–heart rate baroreflex

curves. Baroreflex curves commonly appear in the physiology literature, calculated during different experimental situations.

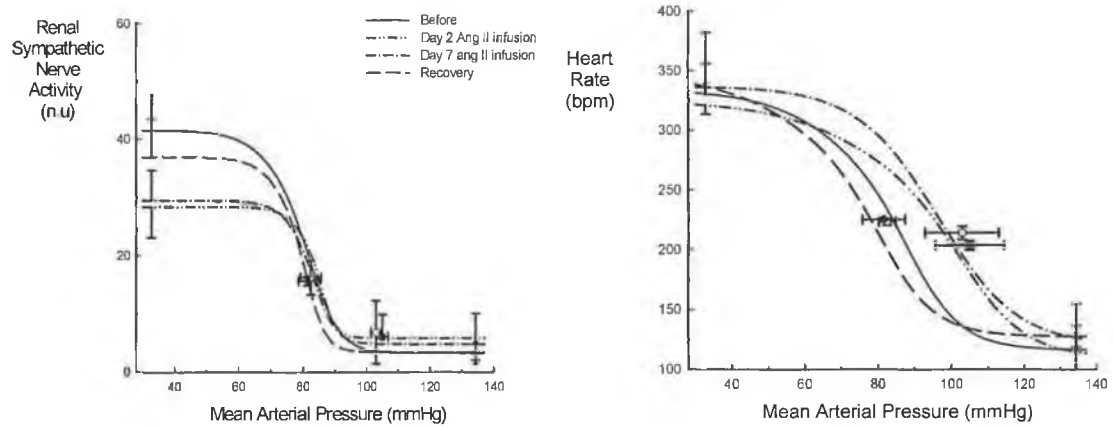


Figure 2.3: The baroreflex curves relating renal sympathetic nerve activity (normalized units (n.u.)) and heart rate (beats/min (bpm)) to mean arterial blood pressure of the rabbit. SNA was normalised to the maximum SNA value evoked by smoke inhalation, 100 n.u.

Taken from Barrett *et al* (Barrett 2003).

The static input-output relationship between blood pressure perturbations in the vicinity of the baroreceptors (input to the baroreflex) and arterial blood pressure (output of the baroreflex) also approximates a sigmoidal curve (Sagawa 1965; Allison 1969; Angell-James 1970; Kent 1972; Yamazaki 1989). The nonlinear sigmoidal relationship is a commonly observed characteristic in many areas of physiology (Coleridge 1981; Sun 1998; Gu 2001) and is otherwise referred to as the logistic (Kent 1972) or Hill curve (Abbiw-Jackson 1998).

The discovery of these sigmoidal characteristics, along with other nonlinear characteristics, implies that the inherent nonlinear nature of cardiovascular control systems is well established by research physiologists (Iriki 1977; Eckberg 1980; Head 1987; Seals 1993; Ursino 1998; Rudas 1999). Systems that comprise nonlinear elements are capable of a wide range of nonlinear phenomena, such as sustained limit cycle oscillation (Slotine 1990). Hence, these static nonlinear baroreflex curves have stimulated much interest and have been strongly linked to the nonlinear

behaviour of blood pressure signals, particularly the 0.1 Hz oscillation in blood pressure (Ringwood 2001), which is the focus of this thesis.

Knowledge of both the static and dynamic characteristics of the baroreflex is essential for the understanding of the means of blood pressure regulation via the baroreflex. Hence, the dynamical nature of the baroreflex is also characterised using frequency response plots of the open-loop baroreflex (Bertram 1998; Liu 2002) (*i.e.* the frequency response of blood pressure to the stimulation of the sectioned afferent nerves). The dynamic characteristics of the (almost) full baroreflex loop (central arc + peripheral arc) have been characterised by means of the frequency response analysis of blood pressure to electrical stimulation of the afferent nerves emanating from a baroreceptor location (Bertram 1998; Liu 2002). Figure 2.4 illustrates the dynamic low-pass characteristics of the baroreflex loop of the rabbit.

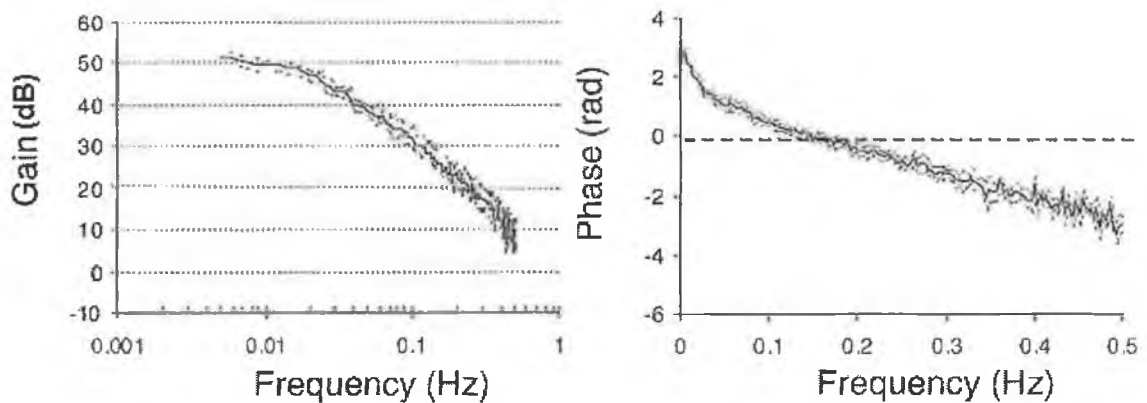


Figure 2.4: Transfer characteristics of the baroreflex, calculated as the response of blood pressure to afferent nerve stimulation. Adapted from Liu *et al* (Liu 2002).

The complete baroreflex may be assumed to combine the properties of the so-called neural arc (from blood pressure to autonomic nervous activity) and peripheral arc (from autonomic nervous activity to blood pressure) (Ikeda 1996), which are commonly characterised by their transfer functions (Ikeda 1996; Kawada 1997; Kawada 2000; Kawada 2001). Other arcs or sections of the baroreflex loop, which

may be subsections of these two major half arcs, have also been characterised by their transfer function characteristics (e.g. the central arc from afferent nerve activity to efferent nerve activity (Kezdi 1968)). These different arcs of the baroreflex loop are illustrated in Figure 2.1.

Both the dynamic and static characterisations of the baroreflex are documented and analysed in detail in the subsequent sections of this chapter and in Chapter 6. Knowledge of these characteristics is essential to the understanding of how the baroreflex regulates blood pressure in the short-term and to the understanding of the 0.1 Hz oscillation in blood pressure.

The reason for, and genesis of, this 0.1 Hz oscillation in the blood pressure of the human, is a highly contentious issue (Malpas 2002). However, all theories share a common agreement that the neural pathways of the baroreflex are influential in the development of the oscillation (De Boer 1987; Cooley 1998; Malpas 2002). The baroreflex feedback theory (Section 2.3.3.2), which hypothesises that the oscillation occurs as a result of the feedback nature of the baroreflex mechanism, has received most currency of late (Malpas 2002). The slow oscillation, evident at 0.1 Hz in the human, varies with frequency for animals of different size (Ringwood 2001). Significantly, with regard to this research, this oscillation is apparent at 0.3 Hz in the rabbit (Janssen 1997). This slow oscillation in blood pressure has a variety of names and has been termed, amongst others, the Mayer wave (Mayer 1876), third order wave (Penaz 1978), low-frequency oscillation (Ringwood 2004) and the mid-frequency oscillation (Janssen 1997) by different research groups. For consistency, this oscillation is referred to as the slow oscillation throughout this thesis.

The physiological components involved in the regulation of blood pressure, and hence those contained in the mechanisms responsible for the genesis of the slow oscillation, are detailed in the subsequent sections of this chapter.

## 2.2 The physiological components in blood pressure regulation

### pressure regulation

The description of the components involved in blood pressure regulation commences with a description of the sensors where a change in blood pressure, which invokes a control action, is sensed.

### 2.2.1 Blood pressure sensors

Blood pressure is monitored by different groups of sensors, specifically the baroreceptors, the chemoreceptors and the cardiopulmonary receptors. The baroreceptors form the sensors of the baroreflex feedback mechanism and constantly monitor blood pressure, with the responsibility of instigating regulatory manoeuvres in the case of blood pressure alterations.

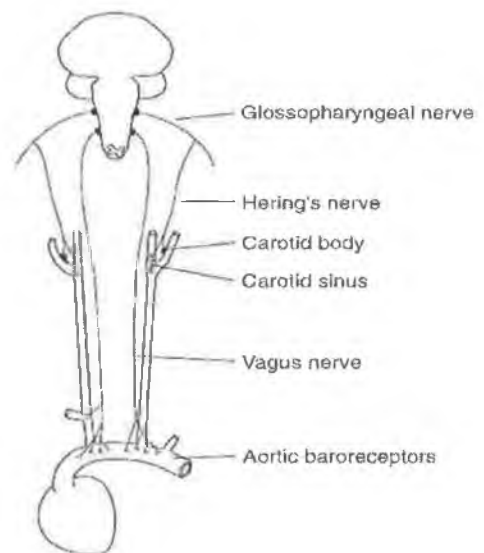


Figure 2.5: (left) The anatomy of baroreceptor areas, published by Antonio Scarpa in 1794 (Scarpa 1974) and taken from Eckberg and Sleight (Eckberg 1992). (right) The location and structure of the baroreceptors taken from Guyton (Guyton 1987).

The baroreceptors are mechanical stretch receptors, with spray like nerve endings, that are located in the walls of major arteries (Eckberg 1992). Baroreceptors are located at the aortic arch (aortic arch baroreceptor), through which blood is transported to the tissue of the body, and along the carotid sinus (carotid sinus baroreceptor), through which blood is transported to the brain. The locations of the baroreceptors are shown in Figure 2.5.

Baroreceptors are sensitive to changes in both mean arterial pressure and pulse pressure, and continuously generate action potentials in response to the ongoing pressure within the arteries (Sherwood 1997). Afferent nerves, shown in Figure 2.5, carry this sensory information to the CNS. These signals travel from the aortic arch baroreceptors through the vagus aortic depressor nerve (ADN) and from the carotid sinus baroreceptors through the carotid sinus nerve (Sherwood 1997) to the *nucleus tractus solitarius* (NTS) of the CNS. However, the neurotransmitter released by the afferent nerves at the NTS is not known with certainty (Eckberg 1992) (see Section 2.2.2.1 for a discussion of the nerves and nerve junctions).

Other receptors form the sensors of other reflex pathways that are also capable of affecting blood pressure. The most significant of these are the chemoreceptors and the cardiopulmonary receptors.

The cardiopulmonary receptors exist in the cardiac chambers and pulmonary vasculature and form the sensors of the cardiopulmonary reflex loop (Johnson 1998). The function of this reflex, and hence the cardiopulmonary receptors, is poorly understood with their best-understood function appearing to be the sensing of total blood volume (Richardson 1998). The cardiopulmonary afferent fibers converge on the same neural sites in the CNS as the baroreceptors (Persson 1989). Hence, it has been proposed that the sensory nerve information emanating from the cardiopulmonary receptors interacts with the central nerve centres which process

information emanating from the baroreceptors and, thereby, the baroreflex regulation of blood pressure (Persson 1989).

The chemoreceptors are sensory receptors that monitor the chemical composition of blood. The principle function of the chemoreceptors is to incite a change in the rate of breathing through the chemoreceptor reflex (Guyton 1987). Chemoreceptors are located in close vicinity to the baroreceptors of the carotid sinus and aortic arch. Physiological conditions, which result in an altered chemical composition of the blood, such as hypoxia (lowered O<sub>2</sub> availability), acidosis (an increase in H<sup>+</sup>) or hypercapnia (excess CO<sub>2</sub>), stimulate the chemoreceptors (Tortora 2003). It is proposed that the chemoreceptors and baroreceptors interact in response to stimulation and that chemoreceptor input has a suppressive effect on the baroreflex blood pressure mechanism (Marshall 1981).

#### 2.2.1.1 Models of the baroreceptors

Both the static and dynamic characteristics of the baroreceptors have been characterised and presented in the literature.

The dynamic transduction properties of the baroreceptors can be characterised by the frequency response characteristics of afferent nerve activity to blood pressure perturbations. To attain accurate characteristics of this relationship, experiments should be performed in the open-loop situation to avoid the effects of the closed-loop feedback regulatory mechanism. However, many studies of the baroreflex via the baroreceptors have been performed under closed-loop conditions because the isolation of the baroreceptors was considered difficult (Thoren 1977; Brooks 1995).

Other authors evaluated baroreceptor properties under open-loop conditions by isolating and recording the activity of the carotid sinus nerve (Franz 1971). However, the difficulty of this experimental procedure and the concomitant effects of the chemoreceptors may have resulted in erroneous results (Sato 1998). Sato *et al*

(Sato 1998) endeavoured to precisely characterise the transduction properties of the baroreceptors of the rat by calculating the transfer function from blood pressure to ADN (aortic depressor nerve) activity.

The baroreceptor gain and phase plots for the rabbit, evaluated by Sato *et al* (Sato 1998), are shown in Figure 2.6.

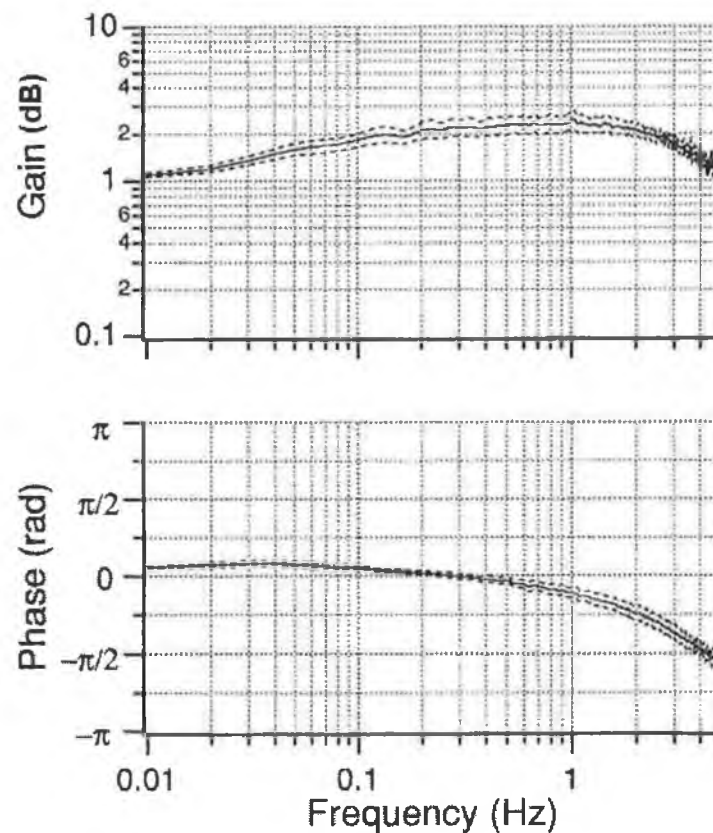


Figure 2.6: The gain, normalized to the value at the lowest frequency, and phase plots averaged between blood pressure perturbations and afferent nerve activity. Taken from Sato *et al* (Sato 1998).

These results indicate that the baroreceptors show high-pass or derivative characteristics up to the cut-off frequency of between 3 and 4 Hz and display low-pass characteristics at higher frequencies (Sato 1998).

The characteristics of the baroreceptors, characterised by the response of the afferent nerves to step changes in blood pressure have been well-documented in the literature

(Bronk 1932; Landgren 1952; Landgren 1952; Warner 1958; Coleridge 1981; Iglar 1981). The steady-state response of afferent nerve activity to step changes in blood pressure inscribes a nonlinear sigmoid characteristic (Landgren 1952; Sato 1998) of similar shape to the baroreflex curves (see Sections 2.2.2.2 & 2.2.3.1). The sigmoidal relationship between blood pressure and the firing rate of the afferent nerve is shown in Figure 2.7. The sigmoidal characteristic described is different for rising and falling pressures, exhibiting hysteresis. This characteristic was observed for the response of afferent nerves emanating from the carotid sinus (Angell-James 1970) and from the aortic arch (Coleridge 1981). During periods of hypotension and hypertension the response curve was reported to shift, or reset, to the left or right respectively (Krieger 1970; Brown 1980; Iglar 1981). Figure 2.7 illustrates the characteristics of hysteresis (Figure 2.7 (top)) and resetting (Figure 2.7 (bottom)).

The sensory neural activity recorded along the afferent nerve displays a trait termed “adaptation” by Taher *et al* (Taher 1988) which describes the tendency of the baroreceptor firing rate to decay with time after a sudden step change in pressure (Landgren 1952). The level of afferent nerve activity is also sensitive to both the mean level of blood pressure and the rate of change of blood pressure, a characteristic included in some models (Warner 1958; Seidel 1998).

Comprehensive models of the baroreceptors, developed using differential equations to describe a number of the characteristics described here, were developed by Taher *et al* (Taher 1988) and Ottesen (Ottesen 1997).

## 2.2.2 The central nervous control of blood pressure

The nervous system may be organised into the central nervous system (CNS), consisting of the brain and spinal cord, and the peripheral nervous system (PNS), consisting of nerve fibers that carry information between the CNS and other parts of

the body. The nervous system is a highly complex and integrated 'wired' system (Sherwood 1997).

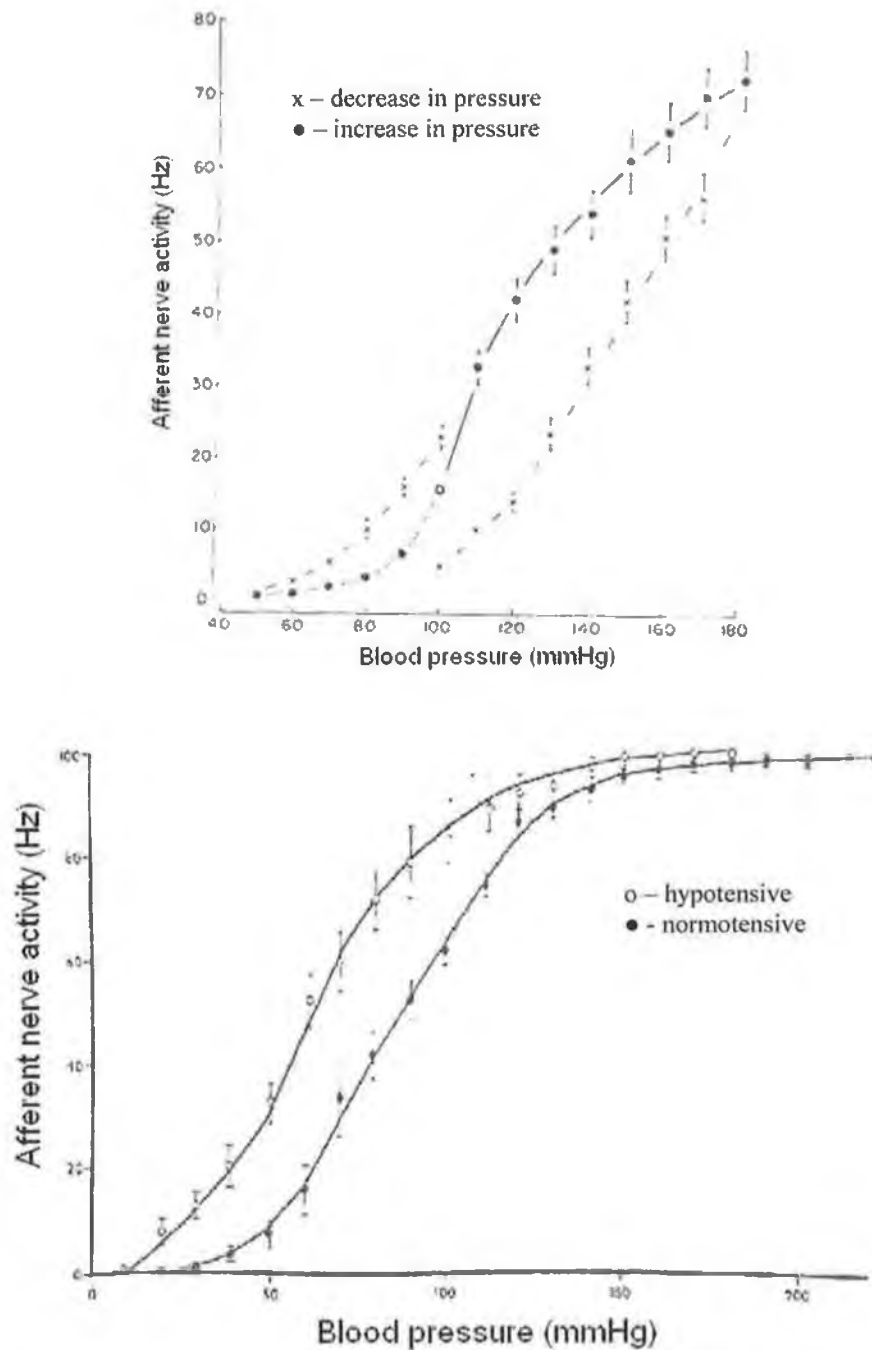


Figure 2.7: The sigmoidal relationship between perturbations of blood pressure at the carotid sinus and the firing rate of the afferent nerves. Adapted from Coleridge (Coleridge 1981) (top) and Igler (Iglar 1981) (bottom).

Only that part of the nervous system involved in the control of blood pressure is introduced in this section. Other nervous systems (such as the somatic motor system) are excluded for brevity and because they do not play a significant role in the regulation of blood pressure. The afferent division of the peripheral nervous system and its role as transporter of sensory information from the blood pressure sensor sites to the central nervous system was described in Section 2.2.1. Figure 2.8 shows the divisions and pathways of the nervous system specifically involved in the regulation of blood pressure.

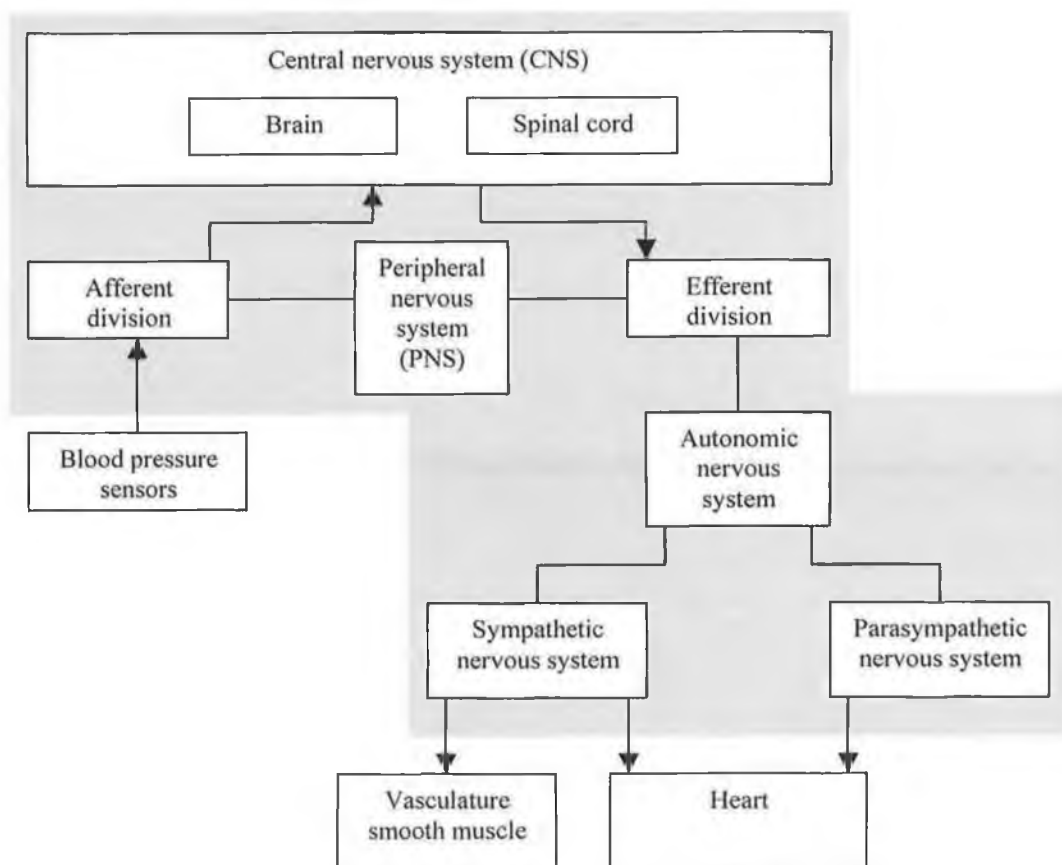


Figure 2.8: Central nervous control of blood pressure.

Adapted from Sherwood *et al* (Sherwood 1997).

### 2.2.1.2 The central nervous system

The central nervous system (CNS), as its name suggests, is central to all neural mechanisms and is the central decision-making unit where information received via the afferent nerves, is processed and transmitted to the required destinations via the efferent nerves. The CNS is responsible for the maintenance of a significant amount of functions engaged in homeostasis and is integral to the constant regulation of blood pressure.

Many different regions of the CNS are involved in the short-term baroreflex regulation of blood pressure. The afferent nerves from the receptor sites (see Section 2.2.1) project to the *nucleus tractus solitarius* (NTS), where much of the processing of information is carried out and from where information is sent through a complex circuitry network to other areas of the brainstem. The parasympathetic and sympathetic outflows are sourced from the *nucleus ambiguus* and *rostral ventrolateral medulla* (RVLM) respectively (Richardson 1998).

Due to the complexity and poor understanding of the internal systems of the CNS, it is often viewed as a black box (Seidel 1997). Hence, models of the CNS are usually developed using input and output data. These models either characterise the relationship between the afferent and efferent nerve activities, termed the central arc, or between a stimulus that activates the afferent nerves (constant blood pressure perturbations) and the efferent nerves (these models are documented in Sections 2.2.2.3 & 2.2.2.4).

### 2.2.1.3 The autonomic nervous system

The peripheral nervous system is divided into nerve fibers that carry information to the CNS, the afferent nerves, and nerve fibers, which carry information away from the CNS, the efferent nerves. Instructions from the CNS are transmitted via the

efferent division to the effector organs – those organs that carry out the desired effect (Sherwood 1997). The autonomic nervous system is that part of the efferent division of the peripheral nervous system that innervates the heart and the smooth muscle of the vasculature, which may facilitate changes in blood pressure (Equation 2.1). The autonomic nervous system may be further subdivided into the parasympathetic nervous system and the sympathetic nervous system, which are responsible for the activation/deactivation of a range of subsystems. Usually both these systems are constantly active, and hence, constantly influence blood pressure. This ongoing activity is called sympathetic or parasympathetic tone or tonic activity (Sherwood 1997). The activity of these systems is increased or decreased from this mean level as is required.

Both the parasympathetic and sympathetic nervous systems are composed of two successive groups of fibers, which synapse with each other at the ganglionic junction (Sherwood 1997). These fibers are the preganglionic fibers, which originate in the CNS, and postganglionic fibers, which innervate the effector organs and may be either myelinated (coated in myelin) or unmyelinated. The myelinated fibers allow for a faster propagation rate along the nerve (Sherwood 1997). A chemical substance known as a neurotransmitter is released at the junctions of the fibers and at the nerve endings attached to the effector organs. The two most common neurotransmitters are acetylcholine and norepinephrine and the fibers that release them are known as cholinergic and adrenergic fibers respectively. Different receptor types are responsive to the neurotransmitters at the synaptic junctions of the postganglionic fibers and effectors (Sherwood 1997). Both the parasympathetic and sympathetic nerves have (different) time-delays associated with them, due to the conduction delay along the nerve fibers (Bertram 1998) and due to the delay at the synaptic junctions (Seidel 1997). The time taken for a nerve signal to transit along the nerve depends on the length of the nerve in question and hence these time-delays vary considerably between species of different size (Ringwood 2001).

### *Sympathetic nerve activity*

The sympathetic nervous system, is a widely distributed nervous system, which innervates a wide range of organs (Berne 1996). SNA provides one of the fundamental aspects in the control of blood pressure (Malpas 1998). The sympathetic nerves function as one of the efferent pathways of the baroreflex loop, innervating both the smooth muscle of the blood vessels, the sino-atrial (SA) node and the muscles of the heart. The sympathetic nervous system also affects blood pressure through its ancillary effects on the endocrine system (Sherwood 1997) (see Section 2.2.3.2).

The sympathetic nerves generally consist of short cholinergic preganglionic fibers and long adrenergic postganglionic fibers. Preganglionic sympathetic fibers may be either myelinated or unmyelinated and as a result may have widely varying conduction velocities (Polosa 1967; Coote 1988), calculated as between 3 and 5 m/s for renal (McAllen 1990) and muscle outflows in animals (Janig 1985) and humans (Wallin 1988). Postganglionic fibers are unmyelinated and therefore, have a slower conduction velocity than the preganglionic fibers, calculated as 1 m/s in humans (Fagius 1980) and rats (Yamazakik 1990). The principle neurotransmitter for sympathetic preganglionic and postganglionic neurons are acetylcholine (Feldberg 1934) and norepinephrine (otherwise known as noradrenaline) (Dale 1934) respectively.

The combination of the short preganglionic, myelinated fibers and long postganglionic unmyelinated fibers results in a relatively long time delay along the sympathetic nerves. These delays were calculated during experimental studies that are discussed in the subsequent sections of this chapter but are given most attention in Chapter 6 (Section 6.6.1).

The first recordings of SNA by Bronk *et al* (Bronk 1936) illustrated the ‘bursty’ nature of the SNA signals. That is, that discharges occur in a synchronised fashion,

with many of the nerves in the bundle being active at approximately the same time. The intermittent bursts of SNA vary in amplitude and frequency (Ninomiya 1990; Malpas 1992). The bursty SNA signal does not occur with a single periodicity but instead contains numerous rhythms at various different frequencies (Cohen 1970; Malpas 1998), detailed in the subsequent section.

It is well established that SNA is an inherently periodic signal, with rhythms at a number of different frequencies (Cohen 1970; Malpas 1998). These rhythms have stimulated much interest, in part, due to the strong relationship between SNA and blood pressure and the possibility that certain oscillations in blood pressure, particularly the slow oscillation with frequency between 0.1 and 0.4 Hz, may be used as surrogate, diagnostic measures of cardiovascular function (Malliani 1991) and of neural activity (Akselrod 1988). These ideas are further developed in Section 2.3 of this chapter. Here, the rhythms present in SNA are (*briefly*) introduced.

There are four major frequency bands of activity: high frequency (~10 Hz), cardiac, respiration and slow oscillation.

The origin of the high frequency 10 Hz oscillation remains unknown (Guild 2002). However, it has been observed in barodenervated animals and, hence, has been proposed to result from a central oscillator, different to that responsible for generating the cardiac rhythm in SNA (Malpas 1998).

The early study of Bronk *et al* (Bronk 1936) illustrated the tendency of sympathetic bursts to occur at a certain phase of the cardiac cycle. This rhythm in SNA (2-6 Hz in the cat) is not a subharmonic of the 10 Hz rhythm (Malpas 1995) but instead it has been proposed that it is inherently generated by the central nervous system and entrained by the baroreceptor input to discharge at a certain phase in the cardiac cycle (Gebber 1980). The oscillation is not abolished by barodenervation, and still retains a large proportion of power in the 2-6 Hz band (Ninomiya 1990), but does lose its entrainment to the cardiac cycle (Barman 1980; Zhong 1992).

Another oscillation occurs in SNA (observed in the rabbit at  $\sim 0.9$  Hz (Janssen 1997)), which is in phase with the respiratory cycle (Cohen 1970; Koizumi 1971). Again, the baroreceptors are not essential for the production of this respiratory related rhythm in SNA, although they do maintain the SNA oscillation in phase with ventilation (Miyawaki 1995).

An oscillation manifests in SNA and in the cardiovascular variables; heart rate, blood pressure and blood flow, at between 0.1 and 0.4 Hz, depending on the species in question. This oscillation is of primary interest to this thesis and has been introduced in earlier sections (Section 1.1 & Section 2.2.1) and a more in depth discussion of the slow oscillation of the cardiovascular variables, their means of genesis, their significance and a summary of the experimental studies that have investigated them is detailed in Section 2.3 of this chapter.

The origin of this slow oscillation in SNA is an area of particular contention and understanding of this topic could prove key to understanding the greater significance that has been associated with this oscillation. The slow oscillation in SNA is either the product of a central oscillator (Section 2.3.3.1) or caused by the baroreflex feedback loop (Section 2.3.3.2). The slow oscillation of the cardiovascular variables is of particular interest to researchers as it has been proposed that they may provide a possible non-invasive diagnostic measure of SNA (again see Section 2.3).

#### *Parasympathetic nerve activity*

The parasympathetic nervous system innervates the heart at the SA node but unlike the sympathetic nervous systems has no effect on the vasculature and only very sparsely innervates the cardiac muscles of the heart (Guyton 1996). The parasympathetic nerve to the heart is commonly known as the vagus nerve (Sherwood 1997).

In contrast to the sympathetic nerves, the parasympathetic nerves generally consist of short cholinergic preganglionic fibers and long cholinergic postganglionic fibers. Acetylcholine is the principle neurotransmitter of both the parasympathetic preganglionic and postganglionic neurons.

The time delay along the parasympathetic nerve is much shorter than that along the sympathetic nerve as is reviewed in subsequent sections.

#### 2.2.1.4 Modelling the central arc

Attempts to characterise the central nervous system, and thus assess its contribution to the regulation of SNA and blood pressure, have involved the development of models based on input/output data of the CNS. The central arc of the baroreflex (see Figure 2.1) is specifically that part of the loop between afferent nerve activity and efferent nerve activity, which have been described in earlier sections. Models of the central arc are not very common in the literature. The modelling of the neural arc (see Figure 2.1), from blood pressure perturbations to SNA (hence, including the baroreceptors), has received more currency (Section 2.2.2.4). Petiot *et al* (Petiot 2001) report a nonlinear sigmoidal relationship between ADN stimulation and renal SNA but this relationship is not commonly reported.

Similarly, there is a paucity of studies that have analysed the dynamic relationship between afferent nerve activity and efferent nerve activity (e.g. ADN activity and SNA); only two studies in the anaesthetised rabbit (Imaizumi 1994; Kubo 1996) and one in the rat (Petiot 2001).

The experimental techniques used, in the quest for central arc characterisation, have differed significantly. Imaizumi *et al* (Imaizumi 1994) randomly perturbed blood pressure by balloon inflation and recorded aortic depressor nerve activity and renal SNA. In another study, this same group (Kubo 1996) stimulated the aortic nerve

with frequencies up to 0.8 Hz. Petiot *et al* (Petiot 2001) used a similar technique in a study on the rat but stimulated the nerve to the much higher frequency of 20 Hz.

These experimental studies have reported conflicting results with regard to the transfer function of the central arc. Both studies in the rabbit reported all-pass filter characteristics (i.e. constant gain across all frequencies). However, Petiot *et al* (Petiot 2001) suggest a major limitation to these studies; that the frequency range investigated did not include frequencies at which baroreceptors are normally exposed to blood pressure fluctuations, especially the frequency of the heart rate (~3-4 Hz in the rabbit). These authors propose a more complex description of the central arc, combining high-pass and low-pass characteristics in different frequency ranges (Petiot 2001).

These different filter characteristics can be observed in the frequency response models of the central arc of the rabbit (Kubo 1996) and the central arc of the rat (Petiot 2001), shown in Figure 2.9.

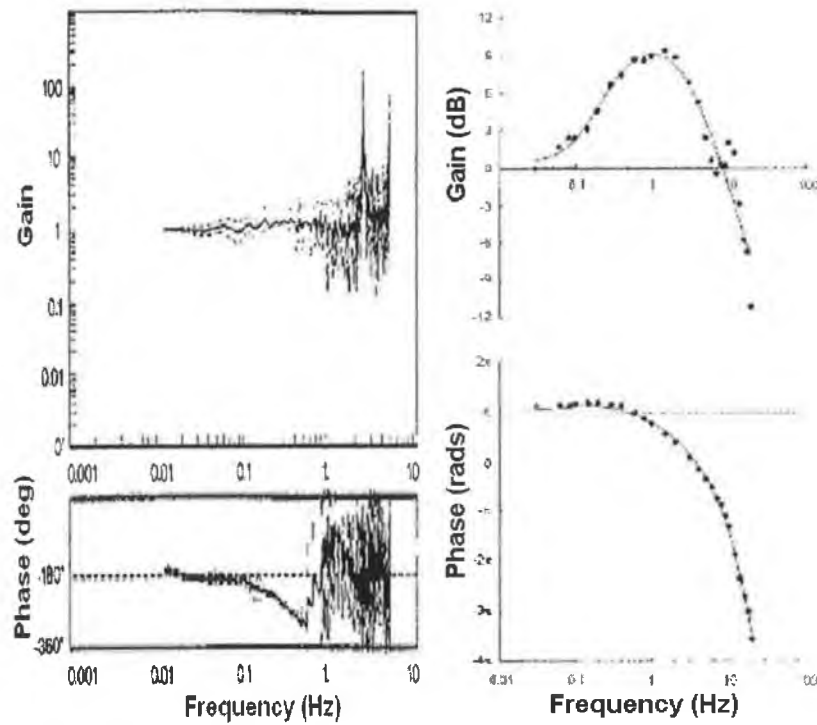


Figure 2.9: Magnitude (top) and phase (bottom) plots of the central arc of the baroreflex, for the rabbit (left) (Kubo 1996) and the rat (right) (Petiot 2001). The gains are again normalized for the rabbit.

A flat frequency response characteristic implying an all-pass transfer function is evident from the magnitude plot of the central arc of the rabbit. A fixed time delay of  $\sim 440$  ms between ADN stimulation and SNA is calculated from the phase plot.

Conversely, the rat model proposed by Petiot *et al* (Petiot 2001) combines a derivative gain with corner frequency  $\sim 0.15$  Hz, a second-order low-pass filter with natural frequency of  $\sim 1$  Hz and a fixed time delay of  $\sim 100$  ms.

Models of the neural arc, which amalgamate the baroreceptors and the central arc, are described in the subsequent section.

### 2.2.1.5 Modelling the neural arc

The research group of Kawada *et al* (Ikeda 1996; Kawada 1997; Kawada 1999; Kawada 2001; Kawada 2002; Kashihara 2003; Kawada 2003; Sato 2003) advanced the term 'neural arc' to describe that part of the baroreflex between blood pressure and SNA. The neural arc may, therefore, be accepted to include the baroreceptor transduction properties, afferent signal conduction, central processing and efferent signal transduction (Kawada 2003). Hence, the neural arc includes all aspects of the central arc in addition to the baroreceptor transduction properties.

Models of the relationship between blood pressure and SNA are frequent in the physiological literature (Kezdi 1968; Iriki 1977; Ikeda 1996; Malpas 1996). Documentation of the static nonlinear (characterised by the baroreflex curve (Iriki 1977; Malpas 1996; Barrett 2003)), and dynamic linear, (characterised by the frequency response plots (Kezdi 1968; Ikeda 1996; Kawada 2001)) relationships between blood pressure perturbations and SNA are common.

#### *Baroreflex curves between blood pressure and SNA*

The baroreflex curve, which illustrates the steady-state relationship between blood pressure and SNA, was introduced in Section 2.2.2.2. Baroreflex curves are derived by slow rises and falls in mean blood pressure induced by drugs that act to increase and decrease blood pressure. A decrease in blood pressure is often invoked by the administration of sodium nitroprusside. Phenylephrine is often used to increase blood pressure (Altimiras 2000).

Blood pressure is recorded at each invoked alteration and the resulting SNA value is also recorded. Using a nonlinear least-squares technique (Marquardt 1963) a nonlinear function is fitted to the data (see Section 6.4.3 for more detail of this technique). Figure 2.10 shows data for an individual rabbit, to which the nonlinear function of Equation 2.3 is fitted. This data was obtained from the physiologists of

the Circulatory Control Laboratory at the University of Auckland, who collaborate on this work.

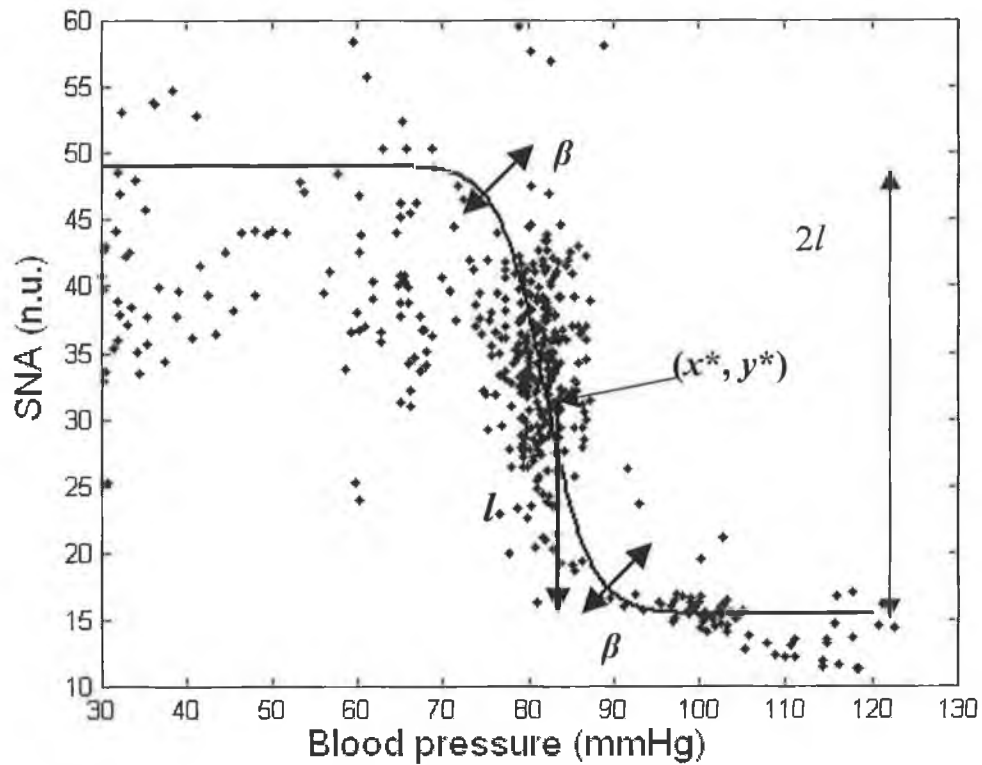


Figure 2.10: SNA for an individual rabbit recorded during invoked changes in blood pressure.

Documented in Equation 2.3 is one functional representation of the sigmoid characteristic. Other representations exist in the literature and these are documented in Chapter 4 (Section 4.3.2).

$$s(x) = \frac{l}{1 + e^{-\beta(x-x^*)}} - \frac{l}{1 + e^{\beta(x-x^*)}} + y^* \quad (2.3)$$

where,

$l$  is half of the full range of the curve

$\beta$  is the curvature at the top and bottom of the sigmoid, and

$(x^*, y^*)$  is the midpoint of the curve

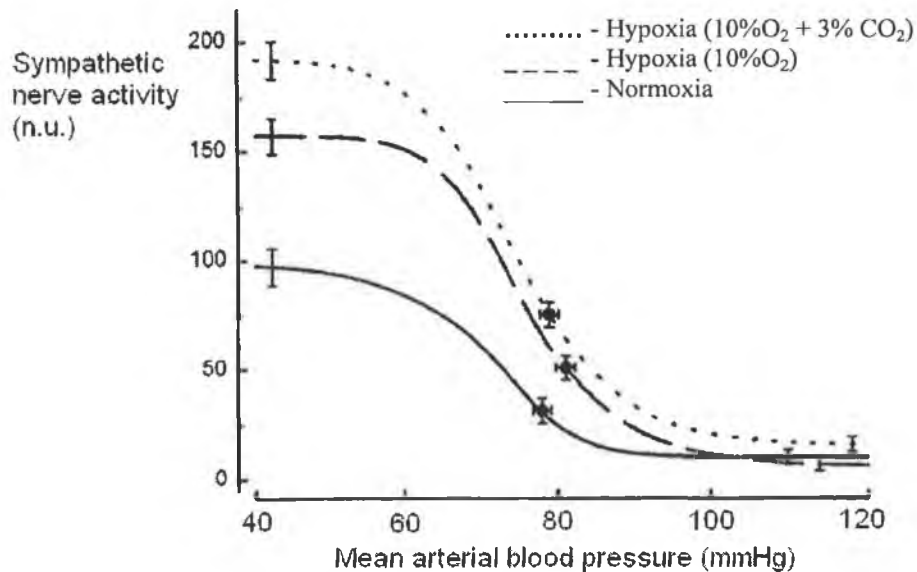


Figure 2.11: The baroreflex curves between blood pressure and renal SNA. In this case the maximum SNA value during normoxia was taken to equal 100 normalised units (n.u.).  
Taken from Malpas *et al* (Malpas 1996).

The baroreflex curves between blood pressure and SNA are often derived for different physiological conditions (Iriki 1977; Burke 1988; Leonard 2000; Head 2001; Barrett 2003; Ramchandra 2003). Changes in the parameters of the baroreflex curves,  $(l, \beta, x^*, y^*)$ , result when the physiological conditions are changed, and this is the subject of an investigation documented in Chapter 4. Examples of baroreflex curves, taken from the physiological literature, are shown in Figure 2.3. Figure 2.11 illustrates more baroreflex curves derived during different conditions of hypoxia, when the animal receives air of a lower than normal oxygen level.

SNA is not uniform to all organs of the body. The baroreflex differentially modulates sympathetic drive to the different organs (Ninomiya 1971; Nishimaru 1971; Ninomiya 1976). SNA to the lungs, spleen and kidney have been shown to be highly sensitive to baroreflex activity (Ninomiya 1971; Shirai 1995). In contrast the skin is only weakly sensitive to baroreflex activity (Ninomiya 1976). This differential sensitivity may have crucial implications for the analysis of the

baroreflex controlling mechanism and it is proposed that it is SNA to a few key organs that may dominate in the production of the slow oscillation in blood pressure (Malpas 2002).

#### *Dynamic models of the neural arc*

Dynamic models of the neural arc are also common in the physiology literature. Kawada *et al* have undertaken a number of studies (Ikeda 1996; Kawada 1997; Kawada 1999; Kawada 2001; Kawada 2002; Kashihara 2003; Kawada 2003; Sato 2003), under open- (Ikeda 1996) and closed-loop (Kawada 1997) conditions, to characterise the frequency response of the neural arc. Derivative or high-pass characteristics were reported for the transfer function of the rabbit (Ikeda 1996) and rat (Sato 2003).

The dynamic characteristics of the neural arc of the rabbit, from blood pressure perturbations to cardiac SNA and renal SNA are illustrated in Figure 2.12. Kawada *et al* (Kawada 2001) report different dynamic neural regulation of cardiac and renal sympathetic activities. They report that the normalised gain of the high-pass transfer characteristic is significantly greater in the neural control of cardiac SNA than in the neural control of renal SNA. These results imply differential central processing in the CNS. However, the authors do not confirm any physiological significance of this differential control in relation to blood pressure (Kawada 2001). The authors report the response of the renal sympathetic nerves to be ~50 ms slower than the response of the cardiac sympathetic nerves to a perturbation of blood pressure. The time-delay of the neural arc between blood pressure and cardiac sympathetic activity was previously reported as 0.55 s (Ikeda 1996).

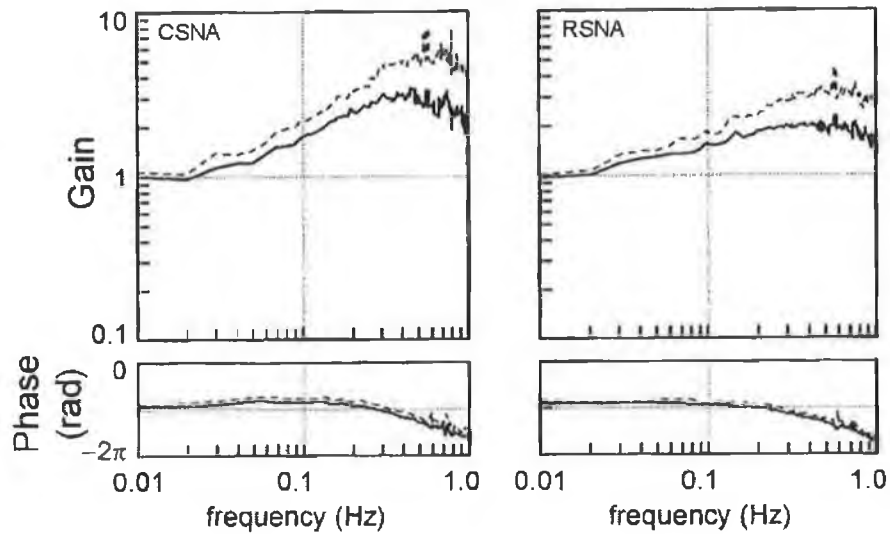


Figure 2.12: The magnitude (top) and phase (bottom) responses of the neural arc between blood pressure and renal (left) and cardiac (right) SNA. The gains are normalized to the value at the lowest frequency. Taken from Kawada *et al* (Kawada 2001).

The primary function of the baroreflex is to quickly and sufficiently react to a change in blood pressure (Sato 1999), hence the high-pass or derivative nature of the neural arc is proposed as key to enabling quick stabilisation of blood pressure (Ikeda 1996). These derivative characteristics of the neural arc have been proposed to compensate for the sluggish response of the peripheral arc (see Section 2.2.3), and hence play a significant role in accelerating the response of the complete baroreflex loop (Ikeda 1996; Sato 2003).

It is evident from this and the previous review sections that both nonlinear static and linear dynamical characteristics are present in the central nervous system. These characteristics play a significant role in the control of blood pressure (Ikeda 1996) and are also key to the slow oscillation in blood pressure (Ringwood 2001). Recently, Kawada *et al* (Kawada 2003) published an investigation of a linear-nonlinear model structure to describe the neural arc. This study is reviewed in greater detail in a later section (Section 6.3.3).

## 2.2.2 Blood pressure effectors

### 2.2.2.1 The heart

The contractile activity of the muscular walls of the heart propels blood throughout the body, delivering nutrients to and removing wastes from the organs of the body (Katz 1992). Considering the function of the heart as the blood pumping mechanism its inherent role as a major effector of blood pressure is obvious. The heart and specifically the amount of blood output by the heart, the cardiac output,  $q_c(t)$ , has the capacity to facilitate the control of blood pressure, via Equation 2.1. The two determinants of cardiac output, heart rate,  $f_c(t)$ , and stroke volume,  $v_c(t)$  (Equation 2.2), are both under neural control.

#### *Heart rate*

The heart contracts, or beats rhythmically, as a result of action potentials that it generates itself. This occurs in the absence of stimulation from the nervous system and is known as autorhythmicity. The cells of the heart display pacemaker activity, which enables the cyclic beating of the heart and the cells with the fastest potential initiation are localised in the SA node (Sherwood 1997). Hence, the SA node is often called the pacemaker of the heart as it sets the rate at which the heart beats in the absence of any neural or hormonal influences. The SA node is innervated by both the sympathetic and parasympathetic branches of the autonomic nervous system, which have the ability to increase and decrease the heart rate respectively (Katz 1992). The individual and joint effects of these nervous systems on heart rate are reviewed in the subsequent sections.

### *The effect of SNA on heart rate*

The sympathetic nervous system has the responsibility of controlling heart action during emergency or exercise conditions when a greater cardiac output is required to supply blood to the tissues in need of a greater blood flow (Sherwood 1997). As well as being able to affect stroke volume the sympathetic nervous system has the capability of increasing heart rate. Sympathetic stimulation of the SA node results in an increased release of norepinephrine which causes the SA node to discharge quicker and hence an increase in heart rate results (Richardson 1998).

In an attempt to understand the response of heart rate to sympathetic nerve activity, research physiologists have sectioned and electrically stimulated the sympathetic nerve and characterised the heart rate response to this electrical stimulation for a range of stimulation frequencies (Kawada 1996).

The response of heart rate to sympathetic nerve stimulation is characterised by a low-pass filter system and pure time delay (Warner 1962; Warner 1969; Berger 1989; Saul 1991; Kawada 1996). First (Berger 1989) and second (Kawada 1996; Nakahara 1999) order descriptions of these low-pass characteristics have been fitted, by different authors, to the frequency response plots attained from the dog (Berger 1989) and rabbit (Kawada 1996; Nakahara 1999).

The frequency response of heart rate to band-limited Gaussian white noise stimulation of the sympathetic nerves of the rabbit is shown in Figure 2.13.

The gain of the transfer characteristic is relatively constant up to 0.02 Hz and decreases above this frequency. The response characteristics observed in the rabbit (Kawada 1996; Nakahara 1999) are comparable to those observed in the dog (Berger 1989), although the filter characteristics are of different order (Kawada 1996). In contrast, Mokrane and Nadeau (Mokrane 1998) identified two distinct components in the heart rate response to SNA. With low-intensities of sympathetic activation, the

heart rate response was faster than at higher intensities of nerve stimulation. However, this difference in the filter behaviour may result from different stimulation protocols (Mokrane 1998).

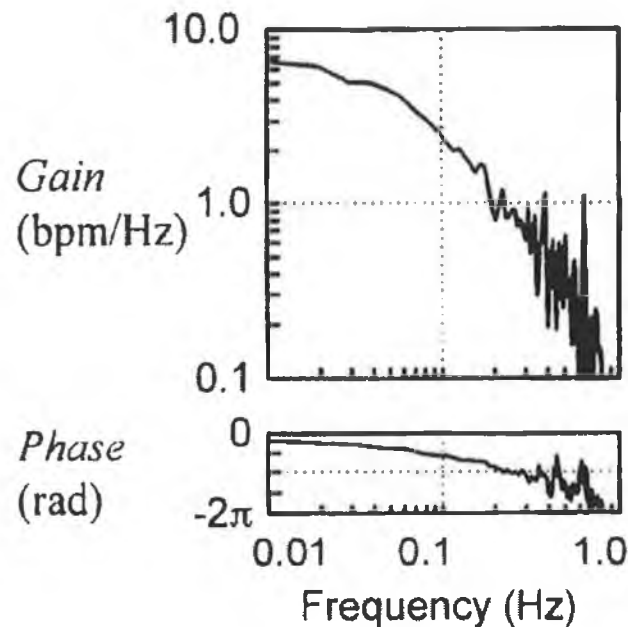


Figure 2.13: The magnitude (top) and phase response (bottom) of the transfer characteristic between electrical stimulation of the sympathetic nerves and the heart rate response. Taken from Kawada *et al* (Kawada 1996).

Following a step change in SNA, the heart rate response of the rabbit is characterised by a time delay of  $\sim 0.5$  s followed by a slow increase with a time constant of  $\sim 10$  s (Kawada 1996). Also, for similar steady-state conditions, the heart rate response of the dog is characterised by a time delay of between 1 and 3 seconds plus a time constant of 10 to 20 s (Berger 1989). The delay differences may be attributed to the difference in size between the animals.

The frequency response of the heart rate is significantly different, and specifically slower, than the frequency response of the vasculature to sympathetic nerve stimulation, as is discussed in more detail in the Section 2.2.3.2.

### *The effect of PSNA on heart rate*

The parasympathetic nervous system has an inhibitory effect on heart rate, slowing it from the intrinsic level set by autorhythmicity (Sherwood 1997). The parasympathetic branch of the baroreflex continuously controls heart action, by maintaining a constant parasympathetic tone, when the body is relaxed and not demanding an enhanced cardiac output (Sherwood 1997; Richardson 1998). Withdrawal of this normal parasympathetic tone allows heart rate to increase toward the intrinsic heart rate (Richardson 1998).

The heart rate response to parasympathetic nerve stimulation is also characterised by a low-pass filter system (Warner 1962; Warner 1969; Berger 1989; Kawada 1996). Using similar method of nerve stimulation as used when stimulating the sympathetic nerves Kawada *et al* (Kawada 1996) calculated the response of heart rate to the electrical stimulation of the parasympathetic nerve in the rabbit. The resulting frequency response characteristics are shown in Figure 2.14.

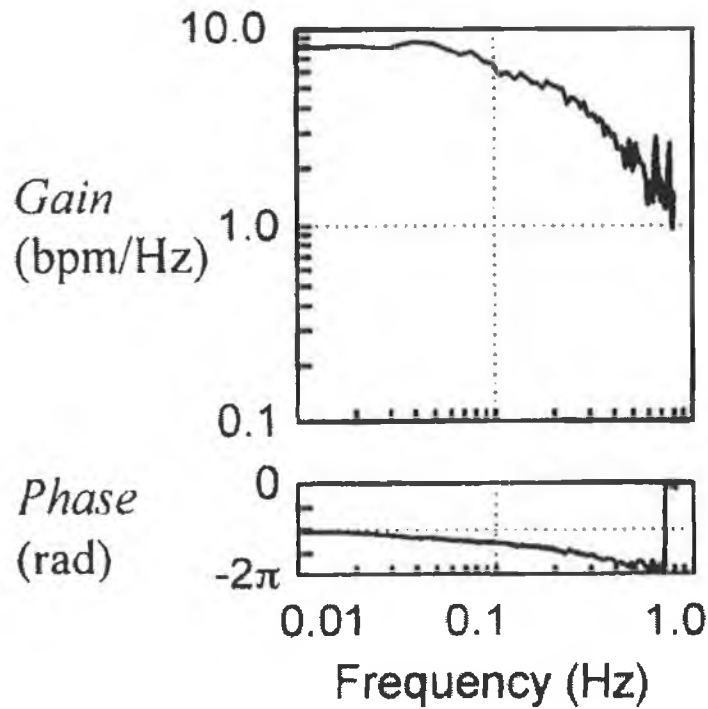


Figure 2.14: The magnitude (top) and phase response (bottom) of the transfer characteristic between electrical stimulation of the parasympathetic nerves and the heart rate response (Kawada 1996). Taken from Kawada *et al* (Kawada 1996).

The gain of the magnitude response is relatively constant up to  $\sim 0.08$  Hz and decreases above this frequency. The structure of the transfer function and corner frequency reported by Kawada *et al* (Kawada 1996) are supported by the findings of Berger *et al* (Berger 1989). However, in contrast to these, Mokrane *et al* (Mokrane 1995) identified two frequency response characteristics of the SA node to parasympathetic activity: one associated with low levels of parasympathetic tone and having a cut-off frequency of 0.065 Hz and another capable of responding to stimulation frequencies up to 0.8 Hz. This phenomenon was also observed by Berger *et al* (Berger 1989).

#### *The interaction of SNA and PSNA*

Parasympathetic and sympathetic nervous activities have antagonistic effects on heart rate (Sherwood 1997). At any given moment the heart rate will be determined mainly by the balance between the inhibitory parasympathetic and excitatory

sympathetic systems, which interact in a complex fashion at the SA node to change heart rate as required.

Various investigators (Glick 1964; James 1966; Levy 1969; Berger 1989) have analysed this interaction by the alternative stimulation of the sympathetic and parasympathetic nerves and have documented the resulting effects on heart rate. These studies have focussed on producing the static characteristic of the heart rate response to simultaneous sympathetic and parasympathetic nerve stimulation (Levy 1969; Levy 1969).

The seminal work of one group of researchers in particular (Levy 1969; Levy 1969; Levy 1984) proved that the cardiac response to neural activity in one autonomic division depends on the level of activity in the other autonomic branch. Levy *et al* (Levy 1969; Levy 1969; Levy 1984), through the electrical stimulation of the parasympathetic and cardiac sympathetic nerves of the dog, investigated the interaction of these nerve signals and their concomitant effect on heart rate. The resulting experimental recordings were presented as a three-dimensional nonlinear curve. Kawada *et al* (Kawada 1999) developed a similar characteristic curve for the rabbit's heart rate response following several combinations of parasympathetic and sympathetic stimulation. The characteristic they reported is illustrated in Figure 2.15. This data was generously provided to this author by Kawada and colleagues from the Department of Cardiovascular Dynamics at the The National Cardiovascular Centre Research Institute in Osaka, Japan.

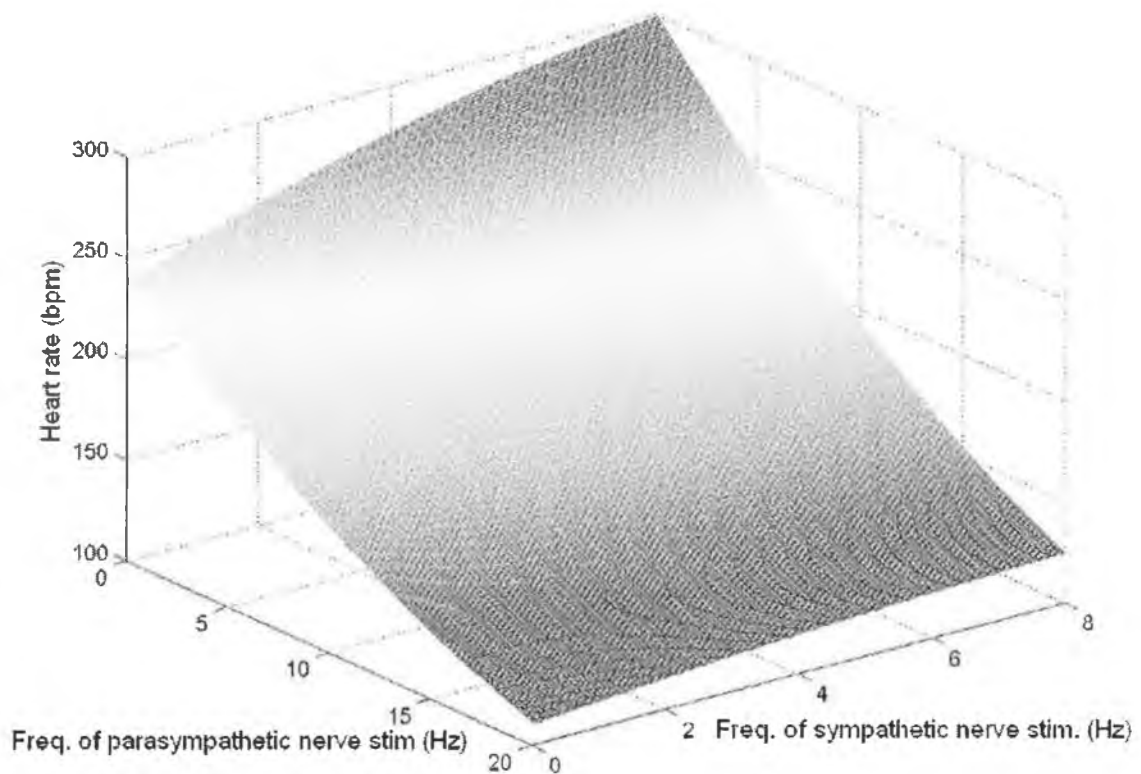


Figure 2.15: The proposed static relationship between heart rate and the electrical stimulation of sympathetic and parasympathetic nerves of the rabbit (Kawada 1999).

There is also good evidence to suggest that the parasympathetic and sympathetic influences also interact in a dynamical fashion (Kawada 1996; Kawada 1997). In particular, sympathetic stimulation combined with tonic parasympathetic nerve stimulation increased the gain of the transfer function and by virtue of this interaction appears to extend its dynamic range of operation (Kawada 1996; Kawada 1997).

#### *Blood pressure to heart rate baroreflex curves*

Similar to the baroreflex curves between blood pressure and SNA, baroreflex curves from blood pressure to heart rate, sometimes called the cardiac baroreflex curve (Korner 1995), are also common in the literature (Head 1987; Malpas 1996; Malpas

1997; Barrett 2003). These curves are developed using similar methods as are used when developing the baroreflex curves from blood pressure to SNA (Section 2.2.2.6) and the response of heart rate to invoked changes in blood pressure describes a similar sigmoid characteristic as that which exists between blood pressure and SNA (Head 1987; Malpas 1996; Malpas 1997; Barrett 2003).

Examples of this sigmoidal relationship are shown in Figure 2.16 for six different rabbits in the control condition (Malpas 1997).

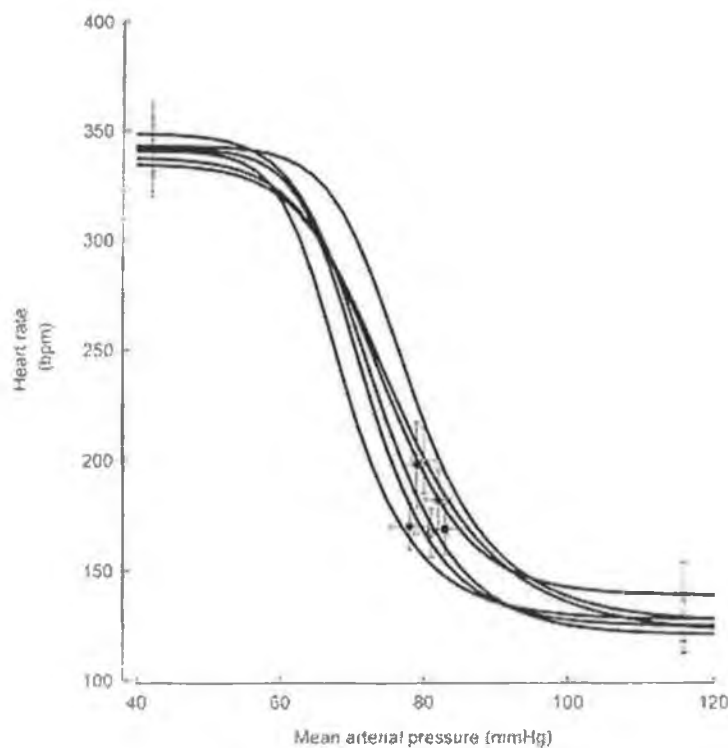


Figure 2.16: The baroreflex characteristic that exists between blood pressure and heart rate (Malpas 1997).

Korner (Korner 1995), who studied the relationship between blood pressure and heart rate (Korner 1974; Korner 1974; Korner 1975; Korner 1994; Korner 1995), asserted that the cardiac branch of the baroreflex is a compound reflex consisting of the cardiopulmonary receptor reflex and the arterial baroreflex. Korner proposes that 70% of the heart rate range described by the baroreflex curve between blood pressure and heart rate is due to the baroreflex and 30% to the cardiopulmonary

receptor reflex. However, there is a paucity of experimental evidence to support this proposed division of effect.

The division of effect of the sympathetic and parasympathetic branches of the autonomic nervous system on the blood pressure to heart rate baroreflex curve has been investigated and is documented in the subsequent section.

*Contributions of cardiac sympathetic and parasympathetic activity to the baroreflex curve between blood pressure and heart rate*

A number of physiologists have attempted to establish the individual impact of the cardiac sympathetic and parasympathetic branches of the autonomic nervous system on the blood pressure to heart rate baroreflex curve (Korner 1972; Head 1987; Weinstock 1988; Kingwell 1991). These investigations involved the sequential blocking of the parasympathetic and sympathetic nervous pathways so as to assess the parasympathetic and sympathetic components of the blood pressure to heart rate baroreflex. Although different experimental protocols exist by which the parasympathetic and sympathetic components of the blood pressure to heart rate baroreflex may be identified (Weinstock 1988; Kingwell 1991) the method most common to these studies involves the administration of drugs, which selectively block the pathways of the autonomic nervous system (Head 1987). Atenolol is administered to block the effects of cardiac SNA on heart rate. Hence, the effect on heart rate, plotted against blood pressure to form the baroreflex curve, is purely parasympathetic. Likewise, methyl atropine is administered to block parasympathetic nerve activity.

Figure 2.17 shows the baroreflex curve from blood pressure to heart rate in the rat, and the resulting baroreflex curves in the presence of atenolol and methylatropine (Head 1987).

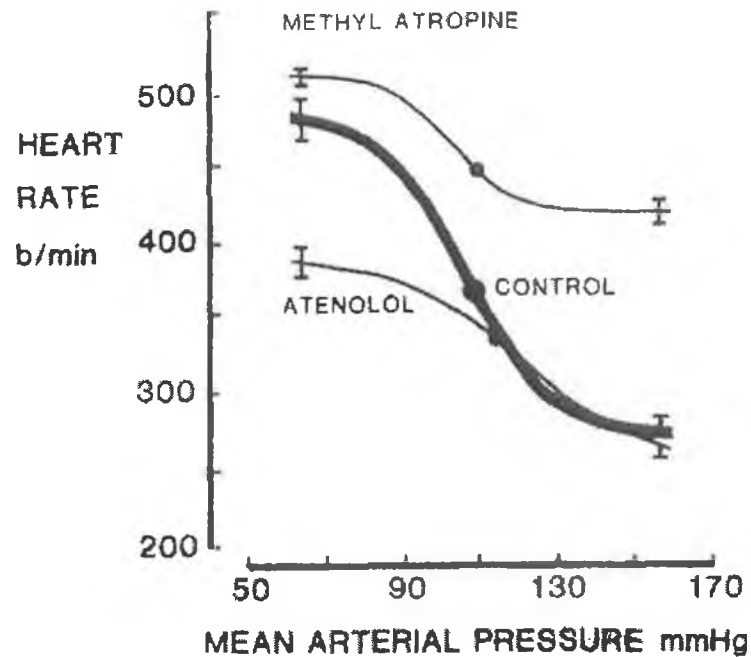


Figure 2.17: The baroreflex curves between mean blood pressure and heart rate, in the control case (thick line) and in the presence of methylatropine and atenolol. Taken from Head and McCarty (Head 1987).

These curves and other similar curves are analysed in more detail in Section 6.3.2.

### *Stroke volume*

Along with the heart rate,  $f_c(t)$ , the pumping ability of the heart and, hence the cardiac output,  $q_c(t)$ , is a function of the amount of blood pumped from the heart each time it beats, termed the stroke volume,  $v_c(t)$  (see Equation 2.2). The stroke volume is regulated by the autonomic nerves but also significantly by mechanisms that are intrinsic to the cardiovascular system (Fox 1996). The intrinsic control of stroke volume is dependent on the degree to which the cardiac muscle of the ventricles is stretched and, as a result, contracts more forcefully at the next contraction. This intrinsic relationship between end-diastolic volume and stroke volume is described by the Frank-Starling law of the heart (Katz 1992).

The effect of the baroreflex on the contractility of the heart is much less well known than the effect of the baroreflex on the heart rate. The contractility of the cardiac muscle increases when blood pressure decreases but, due to the heart rate also increasing, the filling time for the heart chambers decreases (Suga 1974; Wesseling 1982). Hence, stroke volume has been generally observed to remain relatively constant in the physiological operating range (Allison 1969; Suga 1976).

#### *The effect of SNA on stroke volume*

The autonomic nervous system supplies the neural control of stroke volume. SNA originating in the CNS terminates at the sympathetic endings in the cardiac muscle of the heart chambers. Sympathetic stimulation enhances the heart's contractility resulting in a more complete ejection of blood from the heart. The exact dynamical response of the cardiac muscle to sympathetic stimulation is not documented in the literature.

The parasympathetic system has little effect on ventricular contraction due to the scarcity of parasympathetic innervation of the ventricles (Sherwood 1997).

#### 2.2.2.2 The vasculature

The blood pumped by the heart circulates inside a closed circulatory network of blood vessels, known as the vasculature or vascular system (Marieb 2003). The blood vessels of the circulatory system have constantly a level of resistance, to the flow of blood through them, known as vascular tone. The blood vessels are however, compliant and hence, this resistance may vary. The resistance of these peripheral blood vessels is often termed the peripheral, or vascular, resistance (see Equation 2.1).

### *Total peripheral resistance*

The resistance of the entire circulatory system to blood flow is referred to as total peripheral resistance (Guyton 1987) (or the systemic vascular resistance). The arterioles and smaller blood vessels offer the majority of this resistance as their walls are thickly layered with smooth muscle (Tortora 2003). This smooth muscle is richly innervated with sympathetic fibers and hence, the contractility of the muscle is controlled by the sympathetic nervous system. The parasympathetic system has no effect on the vascular resistance.

Arteriolar radius is also influenced by other intrinsic and extrinsic factors. Certain locally acting paracrines, and in particular nitric oxide, have in recent years been shown to have a powerful influence over the resistance of the vessels. Hormones such as vasopressin and angiotensin II, which play a significant role in the long-term control of blood pressure (see Section 2.2.3.3), are also potent effectors of the vessel resistance (Sherwood 1997) and further enhance the neural control supplied by SNA.

The effect on the vasculature of SNA and some of the numerous paracrines and hormones is introduced in subsequent sections.

### *Total peripheral resistance and SNA*

Stimulation of the smooth muscle walls of the arterioles, via the sympathetic nerves, results in the constriction of the vessels of the vasculature, termed vasoconstriction. Similar to the case of sympathetic stimulation of the SA node, sympathetic stimulation of the smooth muscle results in the release of norepinephrine (Sherwood 1997).

Under resting conditions, the sympathetic nervous system maintains a constant level of vasoconstriction, by maintaining a continuous sympathetic tone, which in turn preserves a constant vascular tone (Sherwood 1997). It is proposed that a number of

the faster rhythms in SNA add to the tonic constriction of certain vasculature beds (Janssen 1997; Guild 2002). An increase in vasoconstriction is accomplished by an increase in sympathetic activity above this tonic activity. Due to the lack of parasympathetic control, dilation of the vessels (vasodilation) is not the specific function of a particular neural pathway, but rather results when sympathetic tone to the smooth muscle is decreased.

The dynamics of the vasculature to stimulation of the sympathetic nerves have been characterised by different authors, for a number of different vasculature beds (Rosenbaum 1968; Holstein Rathlou 1994; Cupples 1996; Stauss 1996; Stauss 1997; Just 1998; Stauss 1998; Malpas 1999; Bertram 2000; Guild 2001).

#### *Response of the renal vasculature to SNA*

The dynamics of the vasculature have been most precisely characterised for the renal vasculature (Holstein Rathlou 1994; Cupples 1996; Burgess 1997; Just 1998; Malpas 1999; Guild 2001). The kidney is a key organ in the regulation of blood pressure and although its response to SNA does not offer a global definition of the vasculature response to SNA, its response is of considerable importance to the dynamic control of blood pressure (Malpas 2002).

The kidney receives a rich supply of sympathetic nerves that enter the organ with the blood vessels and extend along the arteries to terminate on smooth muscle cells of the arterioles within the kidney (Barajas 1992; Luff 1992).

The frequency response of the renal vasculature has been characterised by electrical stimulation of the renal sympathetic nerves by either sinusoidal stimulation (Malpas 2001) or, more recently, a pseudo-random binary sequence (PRBS) signal (Guild 2001). The renal vasculature has the ability to respond to oscillations up to  $\sim 0.6$  Hz in the rabbit (Malpas 1999) and rat (Grisk 2002). Malpas *et al* (Malpas 1999) originally used a first-order low-pass filter to characterise the response of the renal

vasculature (Malpas 1999). A more composite frequency response was identified in a later series of experiments and a more complex transfer function was used to describe these characteristics (Guild 2001) (See Section 6.5). The frequency response of the renal blood flow to electrical stimulation with a PRBS signal is shown in Figure 2.18 for three individual rabbits, as presented by Guild *et al* (Guild 2001).

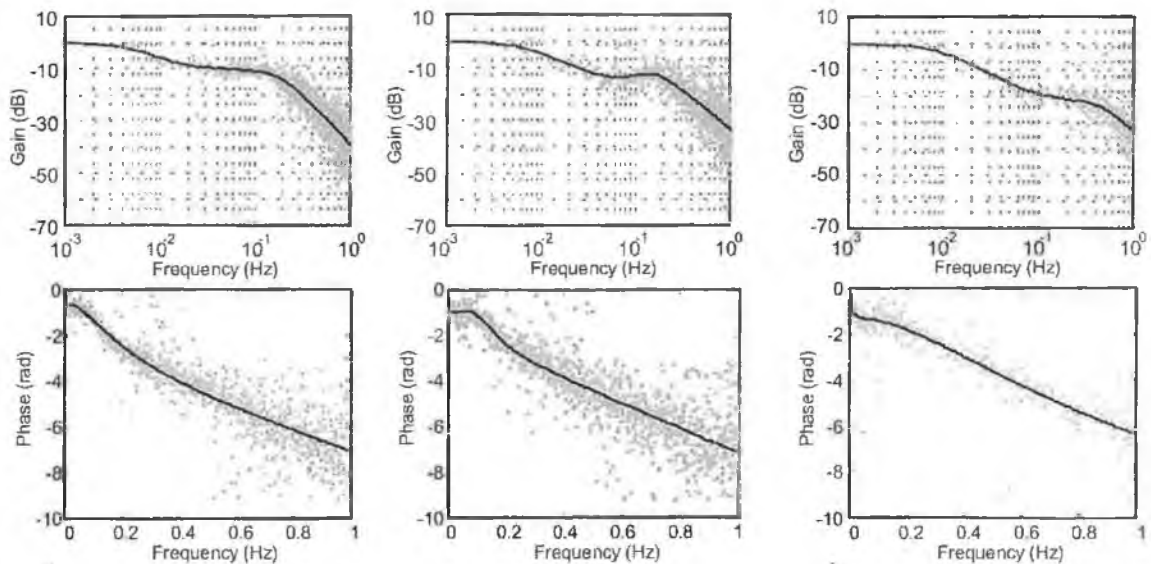


Figure 2.18: Magnitude (top) and phase (bottom) plots of the frequency response of renal blood flow to PRBS stimulation (Guild 2001).

These dynamical models of the vasculature, as for the heart, have a pure time-delay associated with them. The average time-delay, observed by Guild *et al* (Guild 2001), between stimulation of the renal sympathetic nerves and the initiation of the renal vasculature response of the rabbit was measured at 0.672 s, similar to the delay reported by Burgess *et al* (Burgess 1997) in the rat (0.4-0.6 s).

Regarding the response of the renal vasculature to changes in mean SNA, the renal vasculature of rabbits (Malpas 1996) and rats (Grady 1992) has been shown to be sensitive to even moderate changes in mean renal SNA. Changes in mean renal blood flow have been shown to occur in coordination with changes in mean SNA, during a range of stimuli including, hypoxia, air jet stress and noise (Malpas 1998).

Changes in cardiovascular and specifically parameters of the vasculature, associated with changes in SNA, are reviewed in Chapter 4 and calculation and analysis of these changing parameters form a basis for the study presented in that chapter.

#### *Response of other vasculature beds to SNA*

The response of other vasculature beds including the mesenteric, iliac and skin vasculature have also been investigated. However, the dynamic characteristics of these beds are not nearly as well defined as they are for the kidney.

The transfer function from sympathetic stimulation to hind limb (iliac) vascular conductance of the rat was characterised as a second-order low-pass filter combined with a fixed time delay of ~0.4 s (Bertram 2000). These authors further investigated whether norepinehrine neutralisation is the frequency-limiting step of the vascular response, as has been suggested for the sympathetic neuroeffector junction in the SA node of the rabbit (Nakahara 1999). However, they concluded that this mechanism does not play a major role in the dynamic response of the vasculature to sympathetic modulation (Bertram 2000).

The dynamical response of the skin was investigated in humans using a novel technique which enabled the electrical stimulation of efferent skin fibers and the simultaneous recording of skin blood flow (Stauss 1998). The skin blood flow had the capability to respond to stimulation at 0.1 Hz but not at 0.5 Hz. The sluggish nature of this response in humans was surprisingly similar to the response of the skin vasculature in rats (Stauss 1999). The frequency response of skin blood flow of the rat to sympathetic activity activity is reported to display a corner frequency of 0.085 Hz and decrease at 17.1 dB per decade, which approximates a first order low-pass filter characteristic (Stauss 1999).

The response of the mesenteric vasculature of the rat to SNA was also investigated by Stauss and colleagues (Stauss 1996) and was shown to have a faster frequency

response that that of the skin (Stauss 1999). These authors did not document the full frequency response and hence do not document a transfer function fit to the frequency response. However, they report that the mesenteric vasculature of the rat was easily able to follow SNA up to a frequency of ~0.5 Hz but had negligible response beyond 1.0 Hz (Stauss 1996). In their later study, in which they stimulated centres of the CNS, these authors showed that the CNS component does not introduce a frequency-limiting step of the response (Stauss 1997).

A comparison of the response of heart rate and the vasculature to sympathetic nerve stimulation reveals a significant difference between the responses of both blood pressure effectors, despite evidence that the pattern of sympathetic outflow to the heart and kidney is similar (Ninomiya 1971). The sluggishness of the heart rate response in comparison the vasculature response to sympathetic nerve stimulation seems to be due to the frequency-limiting step resulting from the removal rate of norepinephrine at the neuroeffector junction (Nakahara 1999; Bertram 2000).

#### *Other effectors of total peripheral resistance*

Besides the baroreflex mechanism, which affects peripheral resistance through the sympathetic innervation of the smooth muscle of the blood vessels, other locally acting paracrines and extensive hormonal regulatory mechanisms are also intrinsic to the greater control of blood pressure.

Nitric oxide is an example of a locally released paracrine, of the endothelial-derived-relaxation category, which causes vasodilation. The effects of nitric oxide on blood vessel activity have only been discovered in the last quarter century (Furchgott 1980) but this significant vasodilator has stimulated a lot of interest due to its ability to rapidly alter blood pressure.

Nitric oxide is released in response to a shear stress, which stimulates the endothelium cells that line the lumen of the blood vessels. On the release of nitric

oxide the neighbouring smooth muscle cells relax causing vasodilation and hence a decrease in vascular resistance (Nafz 1986). This mediator of vasodilation has a short half-life and has been reported to cause the relaxation of smooth muscle cells within seconds (Rubanyi 1990).

Along with its vasodilatory effects, which directly effect vascular tone, nitric oxide also inhibits the release of norepinephrine at the sympathetic neuroeffector junction (Cohen 1990) and it has also been proposed (Cohen 1999), and investigated (Iida 1999), that neurally released nitric oxide may modulate sympathetic vasoconstriction at pre- and postganglionic stages as well as postjunctional levels. Nitric oxide synthesis has also been observed to attenuate the actions of the parasympathetic system on heart rate (Conlon 1998). Hence, it is a wide-acting and significant effector of blood pressure, yet its synthesis, release mechanism and full effects are still poorly understood and still the focus of much research.

Other paracrines also have the capability to affect blood pressure. Histamine is one such example but this only displays its vasodilatory abilities under certain specific conditions when a tissue has been damaged or invaded. Endothelin is a vasoconstrictive paracrine that works antagonistically with the vasodilatory paracrines to maintain normal blood vessel radius and hence, blood pressure (Sherwood 1997).

Blood pressure is controlled over longer-time scales, than those associated with the baroreflex and nitric oxide, by hormonal mechanisms. The endocrine glands discharge hormones in response to chemical stimuli, nerve stimulation and to stimulation by other hormones (Fox 1996). These hormones are then distributed by the blood circulatory system to all parts of the body, although their actions may be restricted to specific target organs, as only certain organs can respond to particular hormones (Fox 1996).

In the earlier subsection on SNA it was pointed out that along with the direct effects of sympathetic stimulation on the blood vessels and heart, sympathetic activity also has ancillary effects on endocrine glands (adrenal glands) in the vicinity of the kidney; causing the release of epinephrine and norepinephrine into the blood (Guyton 1987). Approximately 80% of the hormone output of the adrenal glands is norepinephrine (the neurotransmitter of the postganglionic sympathetic neurons) and the remaining 20% is epinephrine (Sherwood 1997). The combined release of these hormones cause essentially the same effects on blood pressure control as the sympathetic system *i.e.* an increase in heart rate and peripheral resistance. These hormones circulate in the blood for between one and three minutes before they are eliminated, thus maintaining the effects of the sympathetic system for a prolonged excitation period (Guyton 1987).

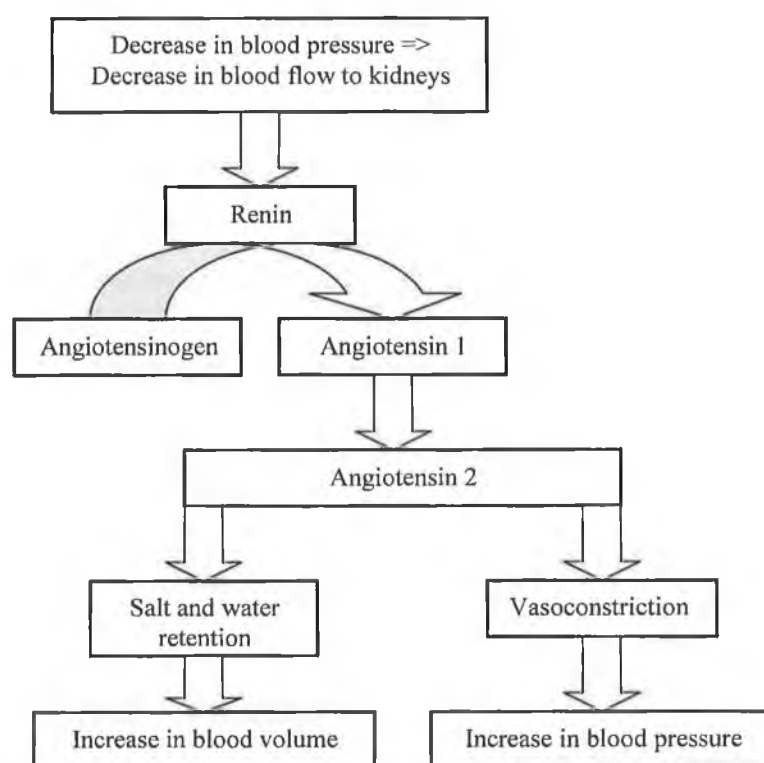


Figure 2.19: The vasoconstrictive and long-term blood pressure control mechanisms involving angiotensin II. Adapted from Richardson *et al* (Richardson 1998).

When arterial blood pressure falls to low levels large quantities of the hormone angiotensin II can be found travelling in the blood circulatory system. Angiotensin is a potent vasoconstrictor which requires approximately 20 minutes to become fully active (Guyton 1987). Hence, it is much slower than the baroreflex control mechanisms and than other paracrines and hormonal mechanisms but it has a longer duration of action. Angiotensin II is a significant effector of long-term blood pressure (see Section 2.2.3.3) and the vasoconstrictive and long-term regulating mechanisms involving angiotensin II are illustrated in Figure 2.19.

Another hormone, vasopressin, is also released when blood pressure falls to very low values. Similar to angiotensin II, this hormone is a potent vasoconstrictor and also plays a role in the long-term control of blood pressure.

The role played by these hormones in the long-term control of blood pressure is discussed in Section 2.2.3.3.

#### *Distribution of cardiac output to the different vasculature beds*

As discussed in the earlier sections describing the heart, the heart pumps blood to the different vascular beds, as required. The distribution of cardiac output to the different vascular beds is well documented in the physiology textbook literature. This distribution is significantly varied during such activity as exercise, when blood is diverted to certain vasculature beds. Cardiac output is also increased in this situation. The apportionment of this distribution, during resting and moderate exercise conditions, is illustrated in Figure 2.20.

Cardiac output also undergoes a major redistribution under certain physiological conditions such as hypoxia when SNA is profoundly increased to the kidney and the gut but decreased to the heart and skin (Iriki 1972; Iriki 1979).

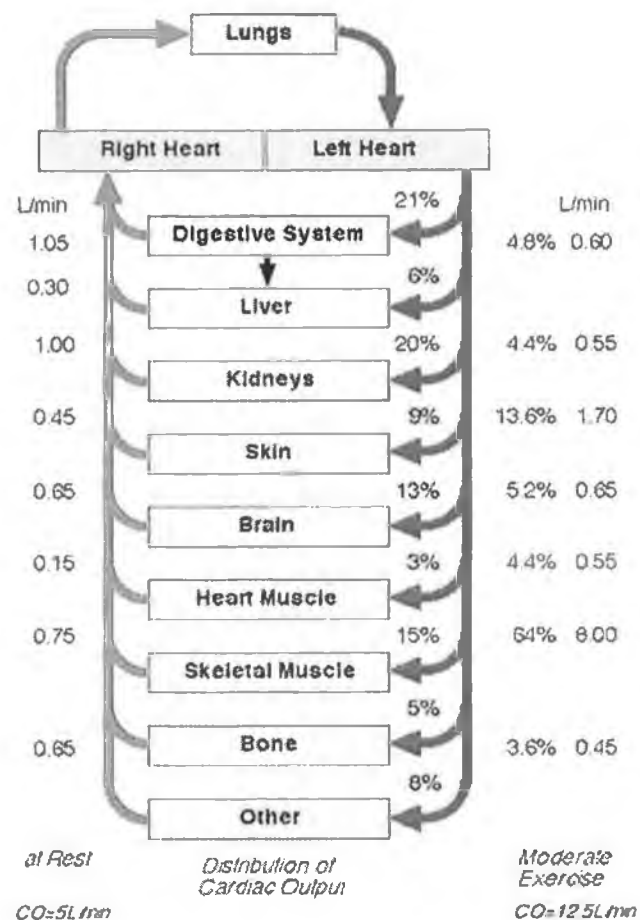


Figure 2.20: The distribution of cardiac output to the different parts of the body, at rest and during moderate exercise. Figure from Bergen.org (Bergen 2004).

### 2.2.2.3 Long term effectors of blood pressure

Until recently, it was generally accepted that the baroreflex regulatory mechanism has no influence over the long-term control of blood pressure (Guyton 1987; Guyton 1991). Recent research has led to a re-think of this view (Lohmeier 2001; Thrasher 2002; Barrett 2003; Lohmeier 2003; Sleight 2004; Thrasher 2004). However, there is no doubt that the most important mechanism for long-term control of blood pressure is the renal-body fluid mechanism (Guyton 1987). The regulatory process of the renal body fluid mechanism is illustrated in Figure 2.21 and described below.

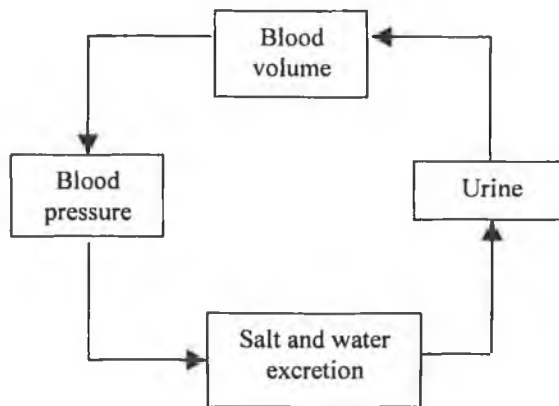


Figure 2.21: The renal-body fluid system. Adpated from Guyton (Guyton 1991).

An increase in blood pressure results in an increase in salt and water output from the kidney, which in turn causes a decrease in both extracellular fluid volume and blood volume. A decrease in blood volume implies a decrease in venous return to the heart. Hence, less blood is available during the pumping action of the heart which results in a decrease in cardiac output and, hence, blood pressure (via Equation 2.1). The converse of this process occurs when a decrease in blood pressure results.

The renal-fluid system, and its long-term regulatory process, is affected by the renin-angiotensin mechanism. Angiotensin causes retention of salt and water and promotes the secretion of the steroid hormone aldosterone that also affects the salt and water balance in the kidneys. Similarly, vasopressin can also cause the retention of water.

In general, the mechanisms involved in the long-term control of blood pressure are beyond the scope of this research because the time scales with which these mechanisms are associated are much longer than those associated with the mechanisms involved in the development of the slow oscillation in blood pressure. This postulation is supported by the analysis of the model, of blood pressure regulatory mechanisms involved in the genesis of the slow oscillation in blood pressure, which is documented in Chapter 7.

### 2.2.3 Complete control of blood pressure

As may be understood from the preceding documentation of the mechanisms and effectors of blood pressure, the regulation of blood pressure involves the integrated action of a number of different mechanisms that operate over different time scales to effect a regulation of blood pressure. The mechanisms involved in blood pressure regulation are not stand-alone mechanisms but interact in a complex fashion to constantly maintain a stable blood pressure.

The mechanisms of blood pressure control may be grouped into short-term, medium-term and long-term regulatory mechanisms. Those that act in the short-term are principally the baroreflex, and the chemo- and cardiopulmonary reflexes (Marshall 1994). These reflexes are further affected by the local release of paracrines. The short-term regulatory mechanisms are of specific interest to this work as they are proposed to be involved in the development of oscillations of cardiovascular variables, and specifically the slow oscillation in blood pressure.

Inherent to these feedback mechanisms are the time delays due to the conduction time along the nerves. The significance of time delays in feedback systems is documented in the control systems literature (Dutton 1997). Significantly, these time delays are proposed by some authors to be essential to the generation of the slow oscillation in blood pressure (See Section 2.3.3.2) due to the phase effects they introduce.

The components of the short- to medium-term blood pressure control mechanisms, introduced in previous sections, are illustrated in Figure 2.22.

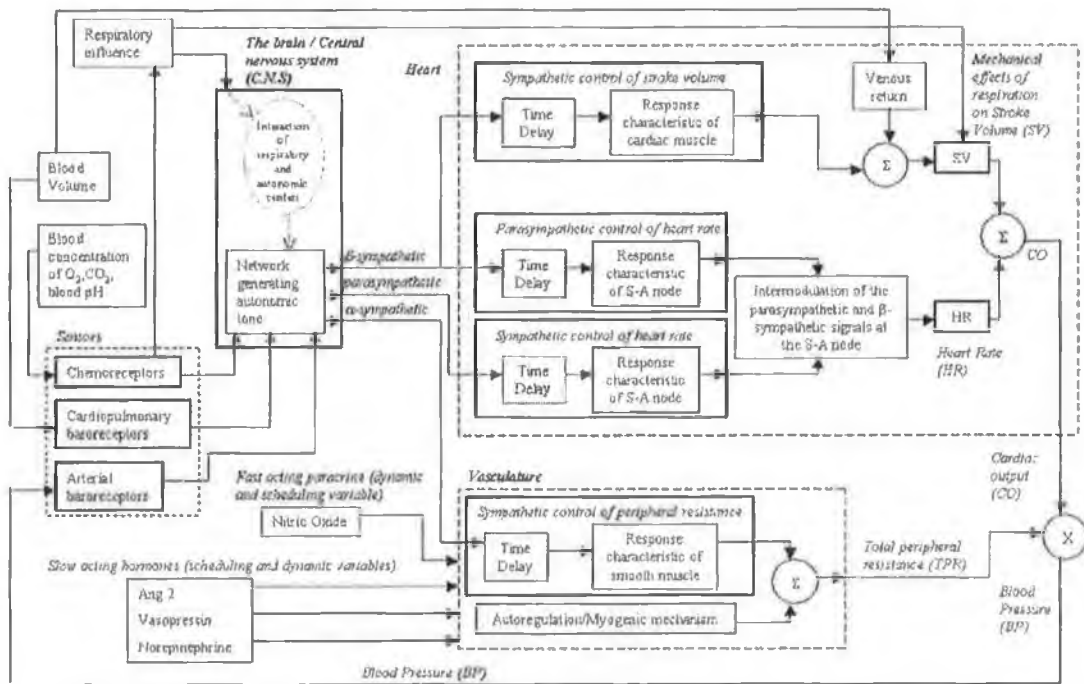


Figure 2.22: Schematic diagram of the mechanisms involved in the short- and medium-term control of blood pressure

The oscillations of cardiovascular variables associated with these mechanisms and the reason why they have received so much attention are studied in the following section (Section 2.3).

## 2.3 Cardiovascular variability

The complex interaction of hemodynamic, paracrine, humoral and electrophysical variables, integrated by sophisticated controlling mechanisms, results in cardiovascular signals containing multiple periodicities. These periodicities in cardiovascular variables were observed many years before any attempt to probe their greater significance was made. As far back as 1733, Hales (Hales 1733) remarked upon the oscillatory behaviour of blood in a glass pipe connected to the crural artery

of a mare. The variability in blood pressure that he observed occurred at a slower rate than that of the beating heart. During subsequent years these oscillations were confirmed by Ludwig (Ludwig 1847) with the development of the manometer. Then in 1876, Mayer (Mayer 1876) discovered the existence of an oscillation in the blood pressure of the dog, at a rate slower than that related to respiration. The slow oscillation in blood pressure, which manifests itself at 0.1 Hz in the human and which is the focus of this thesis and of much other research work, is often referred to as the “Mayer wave”, in recognition of his work. However, closer examination of Mayer’s seminal work (Mayer 1876) reveals the discovery of an oscillation, in the blood pressure of the rabbit, of amplitude between 15 and 40 mmHg, which is greater than the amplitude of the slow oscillation in blood pressure observed by other authors (Malpas 2000), and of a frequency of  $\sim 0.05$  Hz which is far slower than the slow oscillation in the blood pressure of the rabbit (0.3 Hz) often termed the “Mayer wave” (Janssen 1997).

Examples of this inconsistency of terminology are widespread in the loosely defined field of cardiovascular variability, because measures of variability have altered as the many facets and intricacies of cardiovascular signals were revealed during the many years of research. Hence, the “variability” of the cardiovascular variables, blood pressure, and heart rate, has been defined using significantly different quantifiers (Akselrod 1985; Yip 1995; Zaza 2001). Linear and nonlinear dynamics have been observed within the variability of the cardiovascular system. Studies that document these dynamics, and the means of their quantification, have been well-reviewed in the physiological literature (Electrophysiology 1996; Goldberger 1996; Wagner 1996; Mancina 1997; Lombardi 2000; Zaza 2001; Lanfranchi 2002; Malpas 2002; Stauss 2003), yet still much uncertainty surrounding the field of cardiovascular variability remains.

The focus of attention in recent times has been rooted in the pursuit to characterise this so called “variability” within specific frequency bands, which are presumed to encode clinically pertinent information regarding the competence of neural control

(Malliani 1991). Two frequency bands in particular have stimulated most interest; the slow oscillation, which is the focus of this thesis, and a faster oscillation associated with respiration (see Section 2.3.1). It was originally proposed that the power of these two individual frequency bands may quantify the control of blood pressure by the sympathetic and parasympathetic systems respectively (Akselrod 1981), and that the ratio of the powers in these frequency bands may enable the development of an index of “sympathovagal” balance (Pagani 1986; Malliani 1994; Montano 1994). The clinical usefulness of such indexes is undoubted and, hence, this research has been embraced with great enthusiasm (Brown 1993). However, the direct relating of the power in these frequency bands to specific autonomic signals may be unwise, considering the integrated action of neural, paracrine and hormonal variables in the control of cardiovascular function. The calculation of an index of sympathovagal function has also been the subject of strong criticism (Eckberg 1997).

A second method of quantification of cardiovascular variability is also common, particularly in earlier studies. Rather than defining this variability at any particular frequency, these authors used global indices of variability such as the standard deviation of heart rate or blood pressure (Cowley 1973; Littler 1978; Mancia 1983; Mancia 1986; McAreavey 1989; Nolan 1992) as the quantifier of variability. A strong correlation between increased heart rate variability and increased risk of mortality from myocardial infarction has been established (Larovere 1997; Larovere 1998). These studies have also shown consistent relationships between reduced heart rate variability and a number of pathophysiological conditions including atrial fibrillation, coronary artery disease (Casolo 1995) and heart failure (Coumel 1994).

In addition to this periodic oscillatory behaviour of cardiovascular signals, which forms the basis of the methods of cardiovascular variability introduced to date, a less specific variability occurs with nonperiodic behaviour, often quantified using techniques taken from the nonlinear time series analysis; techniques of chaos theory and fractal analysis. These methods are subject to greater consideration in the

ensuing chapter, which focuses on the chaotic characterisation of blood pressure signals. Similar to the other quantifiers of variability, the physiological basis for this nonperiodic behaviour is still unresolved but variations in the quantifiers have displayed a definite consistency when applied to heart rate and blood pressure data recorded in subjects with a wide range of pathophysiological symptoms (Wagner 1995; Yip 1995; Mrowka 1996; Sugihara 1996).

The development of reliable and clinically relevant indices of any of these cardiovascular variabilities would be of great value. A diagnostic index of autonomic activity may be of particular value considering that elevated SNA is strongly correlated to a range of pathophysiological diseases (McCance 1993; Eisenhofer 1996; Julius 1996). This index would enable instantaneous analysis of the dynamical interrelations of autonomic signals using a non-invasive method (Malliani 1991).

Although the physiological basis of “cardiovascular variability” and the authenticity of the present quantifiers introduced in the previous paragraphs are still widely debatable, there is no doubt that analysis of cardiovascular variability has proven useful in understanding cardiovascular regulation (Malpas 2002) and that diagnostic indices are worth striving for. However, the momentum of the research into cardiovascular variability has continued without reflection and understanding of the fundamental causes of this variability (Malpas 2002). The rhythms that exist in cardiovascular signals are introduced in the subsequent sections and it is the aim, in the subsequent chapters of this thesis, to add to a more fundamental understanding of the causes of certain aspects of the variability of blood pressure.

### 2.3.1 Cardiovascular rhythms

Cardiovascular signals are rich in rhythms of different frequency and amplitude (Parati 1995). These rhythms manifest themselves at the same frequency in heart

rate and blood pressure. Due to the easy availability of ECG recordings, heart rate oscillations are more extensively studied than blood pressure oscillations (Karemaker 1999). However, these oscillations may be understood as analogous to each other as an oscillation in one variable will produce an oscillation in the other (Karemaker 1999).

### *The cardiac rhythm*

The actions of the cardiac cycle, the filling of the ventricles and their emptying into the arteries, sets up the oscillation of the largest amplitude that is observed in the blood pressure signal. The average resting heart beats at a rate of ~70 beats/min in humans, hence creating an oscillation in blood pressure at close to 1 Hz (Fox 1996).

### *The respiratory rhythm*

The rhythm slower than the heart rate, that was first observed by the early researchers of cardiovascular variability, is the oscillation in heart rate and blood pressure that is associated with respiration (Hales 1733; Ludwig 1847) (other authors also). Along with the slow oscillation of heart rate and blood pressure, this respiratory related oscillation has stimulated much interest amongst researchers as it has been proposed that it may form the basis of a diagnostic measure of parasympathetic control (Malliani 1999), and form part of a sympathovagal balance index (Pagani 1986).

Respiration forces an oscillation in blood pressure at the breathing rate by cyclically varying intrathoracic pressure. Venous return to the heart is perturbed by the mechanical actions of breathing, which in turn changes cardiac output and hence blood pressure (via Equation 2.1). The blood pressure perturbations developed by this process are sensed by the baroreceptors, which activate the baroreflex mechanism, which causes a change in autonomic activity to the heart and, hence, adjusts heart rate.

The frequency response of heart rate to stimulation of the parasympathetic nerves displays the characteristics of a low-pass filter with a relatively high cut off frequency (Berger 1989; Saul 1991; Kawada 1996) (see Section 2.2.3.1). In contrast, the frequency response of heart rate to stimulation of the sympathetic nerves has a much lower cut off frequency, which demonstrates the limited ability of the SA node to respond to sympathetic influences at frequencies as high as the respiration rate. Hence, it is thought that the oscillation, in the cardiovascular variables, associated with respiration, is mediated by the parasympathetic nervous system. In support of this, experimental studies showed that the inhibition of the parasympathetic activity resulted in an abolition of the respiratory related oscillation in heart rate (Katona 1975; Eckberg 1983; Fouad 1984; Saul 1991; Triedman 1995).

If the low frequency oscillation is a function of the baroreflex, then the oscillation in heart rate at the respiratory rate may only be present as a result of the same oscillation in blood pressure. However, a number of researchers have presented strong evidence to support central coupling of a central respiratory oscillator and the parasympathetic neural centres (Pilowsky 1995; Hayano 1996). Changes in heart rate at the frequency of respiration have been observed in the absence of respiratory movements (Davies 1967; Valentinuzzi 1974). Also, abolition of the respiratory related oscillation with parasympathetic blockade results in a reduction in the oscillation in blood pressure of ~50% (Taylor 1998) and the sino-aortic denervation of the cat, which significantly impairs parasympathetic activity, markedly reduces the power in the frequency band of the respiratory oscillation of heart rate with only a minor reduction in the power of the same frequency band in blood pressure (Di Rienzo 1991).

Malpas (Malpas 2002) challenges the hypothesis that the respiratory related oscillation in heart rate may be used as an index of parasympathetic activity on a number of points.

1. If the changes in parasympathetic activity are induced by baroreceptor sensing of respiratory disturbances of blood pressure, any measurement of the amplitude/power of the oscillation at this frequency must be indicative of all branches of the baroreflex and not just the parasympathetic branch alone.
2. Other nonneural factors, such as reduced respiratory capacity (Saul 1991) and body position (Taylor 1996), that alter the amplitude of the respiratory related oscillation in blood pressure, in turn alter the amplitude of the oscillation in heart rate (via the parasympathetic pathways). Hence, with regard to developing a generic diagnostic tool, problems will ensue when attempts are made to compare across different patient groups, as different patients will have different levels of respiratory capacity (Malpas 2002).

#### *The slow oscillation*

The next oscillation that can be observed at the next lowest frequency in the frequency spectrum of the cardiovascular variables is the slow oscillation that manifests itself at 0.1 Hz in the human. Due to its importance to this research, this oscillation is discussed in detail, and in isolation in the subsequent section (Section 2.3.2).

#### *The very low frequency rhythm*

Spontaneous fluctuations of cardiovascular parameters have also been observed at still lower frequencies (~0.03 Hz in rats (Leyssac 1983)). These oscillations have been observed in blood pressure (Barcroft 1932; Nisimaru 1984) and blood flow (Janssen 1995). Although the mechanisms of this oscillation are contentious, they have been related to fluctuations in the vasomotor tone due to the autorhythmic nature of blood vessels (Fuji 1990; Ursino 1992) and influenced by thermoregulatory, autoregulatory or hormonal mechanisms. Holstein-Rathlou and colleagues (Holstein-Rathlou 1993; Holstein Rathlou 1994; Holstein-Rathlou 1994;

Holstein Rathlou 1995; Holstein-Rathlou 1998) have investigated the autoregulatory mechanisms of the kidney and also fluctuations in this frequency range.

### *The circadian rhythm*

The slowest oscillation observed in blood pressure, is that which is governed by the light-dark cycle, known as the circadian rhythm (Berne 1996). For a human following a regular daily pattern, the peak in blood pressure occurs at mid-morning, followed by a progressive fall during the day, and the lowest value of the cycle is reached at ~3 a.m. (Millar 1978).

## 2.3.2 The slow oscillation in blood pressure

A slow oscillation exists in blood pressure at 0.1 Hz. This oscillation is referred to in this thesis as the *slow oscillation* in blood pressure, but is often termed the Mayer wave, amongst other things (see Section 2.1). This oscillation exists at different frequencies in different animal species and has been observed at 0.1 Hz in humans (Malliani 1991; Sleight 1995), 0.14 Hz in the dog (Akselrod 1985; Berntson 1997), 0.3 Hz in the rabbit (Janssen 1997; Malpas 2000), and 0.4 Hz in the rat (Brown 1994) and mouse (Janssen 2000). This variance of frequency is accounted for by the difference in species size resulting in longer efferent and afferent delays, due to longer conduction times, in larger species (Ringwood 2001) (see Section 2.2.2.2).

This slow oscillation in blood pressure is of particular interest to researchers. The “strength” of this oscillation, usually quantified by the power in the frequency band of this oscillation, has been proposed to provide a non-invasive surrogate measure of efferent SNA (for a review, see (Persson 1997)). SNA is well established to be elevated in heart failure (Eisenhofer 1996; Esler 1997) and coronary artery disease (McCance 1993) and may be associated with hypertension (Julius 1996; Julius 1996; Grassi 1998). Hence, a diagnostic measure of sympathetic tone, based on the easily

measured slow oscillation of the cardiovascular variables, could be of immense value.

The slow oscillation in the blood pressure is well established to exist at  $\sim 0.3$  Hz in the rabbit. However, this oscillation is not always obvious. A number of authors have been unable to consistently identify a peak in the frequency spectrum of blood pressure for all rabbits studied (Janssen 1997; Leonard 2000; Ringwood 2001). When a peak is evident at the frequency of the slow oscillation ( $\sim 0.3$  Hz), it often manifests as a broad peak, as shown in Figure 2.23.

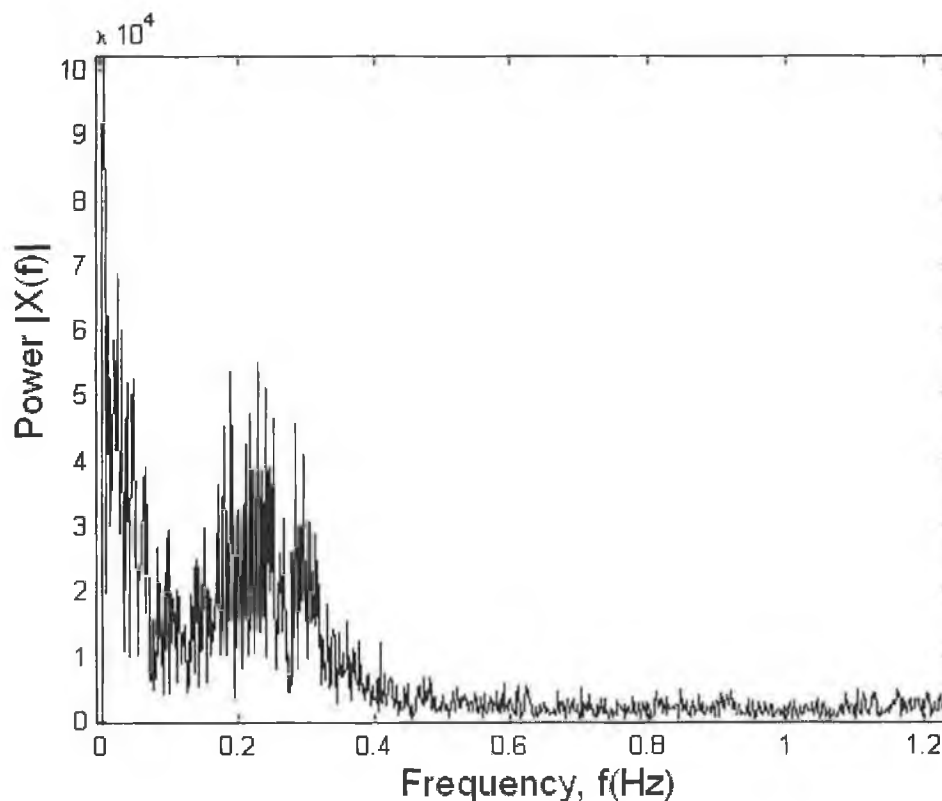


Figure 2.23: The frequency spectrum of the raw 500 Hz sampled blood pressure signal from an individual rabbit plotted against frequency.

The slow oscillation is sometimes more obvious in humans and rodents than in rabbits. A distinct peak, at the frequency of the slow oscillation, is evident in the spectrum of the blood pressure photoelectric plethysmograph (PPG) of the human.

This data was obtained from the Biomedical-Optics Research Group at NUI Maynooth.

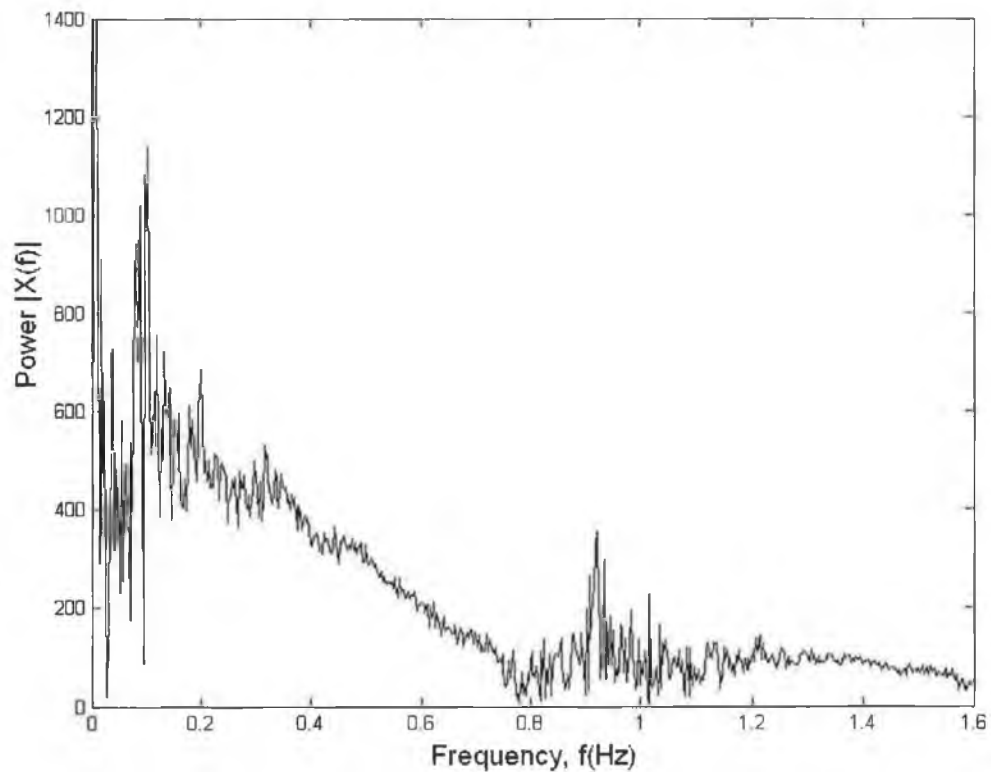


Figure 2.24: The frequency spectrum of the raw 100 Hz sampled PPG signal from an individual human plotted against frequency.

The slow oscillation in blood pressure is probably the most contentious aspect with respect to cardiovascular variability (Malpas 2000). As was already introduced, the information that can be inferred from measurements of this slow oscillation is a definite aspect of contention. Similarly, different theories exist as to the mechanisms involved in the genesis of the oscillation. Two theories dominate, the so-called central oscillator and baroreflex feedback theories, which are described in the subsequent section.

### 2.3.3 The origin of the slow oscillation in blood pressure

With regard to the origin of the slow oscillation, both camps of theorists have mounted convincing arguments and have presented experimental evidence to support their theories. It is accepted by both sides that there is a role for the autonomic nervous system in the genesis of the slow oscillation. The action of the sympathetic nervous system on the vasculature has been particularly promoted by both sides, and experimental studies, which report an abolition of the oscillation during ganglionic blockade, support a significant role for this branch of the baroreflex (Cerutti 1994). The opposing schools of thought undergo a significant divergence with regard to the role of the baroreceptors and whether they are involved, as part of the feedback loop, in the genesis of the slow oscillation.

#### 2.3.3.1 The central oscillator theory

Considering the inherently periodic nature of SNA and particularly the presence of a slow oscillation in SNA between 0.1 and 0.4 Hz, depending on the species in question, some researchers have proposed a central oscillator to account for the slow oscillation in blood pressure (Preiss 1974; Malliani 1991; Vandeborne 1997; Cooley 1998; Montano 1998). It is proposed that the neurons in the CNS that generate the faster rhythms in SNA also have the capability to generate the slow oscillation in SNA and it is further postulated that this slow oscillation in SNA is directly transmitted to blood pressure. Hence, resulting in a slow oscillation in blood pressure at the same frequency as the slow oscillation in SNA.

Researchers who advance this theory of the central oscillator, to account for the slow oscillation in blood pressure, have presented an abundance of experimental evidence to support their theory. This evidence is comprehensively appraised in the recent review paper by Malpas (Malpas 2002). Examples of this evidence and the salient points of the review are reproduced here.

Preiss and Polosa (Preiss 1974) observed slow oscillations of preganglionic SNA in the absence of related changes in blood pressure and in both baroreceptor and chemoreceptor denervated cats. The oscillation reported by these authors is somewhat induced using repeated haemorrhage or carotid artery occlusion. This experimental practice is somewhat dubious for the purposes of analysing the mechanisms of the slow oscillation as haemorrhage has been shown to result in oscillations in blood pressure that do not rely on SNA but reflexly affect SNA through the baroreflex feedback mechanism (Malpas 2000). Although this does not explain the existence of an oscillation in SNA in the barodenervated case, the oscillation observed is at a much slower frequency than that associated with the slow oscillation in the blood pressure of an animal of similar size to the cat (Ringwood 2001) (e.g. the rabbit (Janssen 1997)).

A similar criticism holds for more recent studies that also purport to reveal evidence supporting the central oscillator theory. Grasso et al (Grasso 1995) reported blood flow to exhibit a self-sustained oscillation when the carotid sinus pressure was held constant. However, the frequency of the oscillation these authors report is 0.05 Hz (Grasso 1995). Similarly, another group of central oscillator theorists report activity, in central neurons associated with sympathetic activity, at 0.12 Hz, which is again a slightly slower frequency than the frequency of the slow oscillation (Ringwood 2001).

While the existence of these oscillations is not challenged, it is more likely that these oscillations are an inherent feature of the vasculature (Malpas 2002). The physiological evidence relating the slow oscillation in blood pressure is dubious and hence, the central oscillator theory, which is championed by a relatively small number of research groups (Preiss 1974; Malliani 1991; Vandeborne 1997; Cooley 1998; Montano 1998), does not receive much currency.

### 2.3.3.2 The baroreflex feedback theory

The more dominant theory is the so-called baroreflex feedback theory, which is endorsed by a wider range of physiology groups (Guyton 1951; Hyndman 1974; De Boer 1987; Burgess 1997; Ringwood 2001; Malpas 2002; Stauss 2002) and supported by various models of the baroreflex (De Boer 1987; Burgess 1997; Ringwood 2001; Seydnejad 2001). In this hypothesis, a disturbance, which causes a change in blood pressure, activates the baroreflex feedback mechanism, *i.e.* is sensed by the baroreceptors, from where, sensory information, reporting the change in blood pressure, is transmitted to the CNS. Subsequently, the CNS adjusts the parasympathetic and sympathetic signals, which in turn change heart rate and vascular resistance. Inherent to this process are the time delays due to the conduction times of the nerves and the processing time of the CNS, and the slow dynamical time constants of the vascular and cardiac muscle response to SNA, and SA node response to sympathetic and parasympathetic stimulation (see Sections 2.2.3.1 & 2.2.3.2). These time delays and time constants introduce phase effects, which increases the chances of oscillatory behaviour as the total phase shift of the complete negative feedback loop nears  $360^\circ$  (Dutton 1997) (see Chapter 7).

The nonlinear nature of the baroreflex feedback loop is also well established (see Sections 2.2.1.1 & 2.2.2.5) and nonlinear systems are easily capable of sustained oscillation (Atherton 1982). A nonlinear system is capable of maintaining a stable oscillation for a wide variety of situations, a situation that is not possible for a linear model based on a stringent set of parameters (see Section 2.3 for a discussion of nonlinear models).

The baroreflex feedback theory is strongly supported by a number of physiological experimental investigations which showed that removal of different sections of the baroreflex loop significantly reduced the amplitude or power in the spectral band of the slow oscillation (Malpas 2002).

Studies in which the baroreceptors were deafferented confirm the considerable contribution of the baroreflex in the genesis of the slow oscillation. These studies showed a consistent reduction in the spectral power at the frequency of the slow oscillation in blood pressure and heart rate (Di Rienzo 1991; Cerutti 1994; Cerutti 1995; Jacob 1995). However, this practice may not fully abolish the slow oscillation as a residual variability, in the frequency band of the slow oscillation, is still observed after baroreceptor deafferentation. The considerable contribution of the sympathetic nervous system was also demonstrated by removal of the sympathetic nervous system, which also decreased the spectral power at the slow oscillation in the rat (Cerutti 1991).

These studies, in which certain elements of the baroreflex are removed, may not be sufficient in establishing the significance of the baroreflex alone as such actions may cause interventions and are likely to cause compensation in other control mechanisms (Malpas 2002). As an alternative means of investigation of the role of the baroreflex in the genesis of the slow oscillation, other authors found that fluctuations could also be produced at the frequency of the slow oscillation by stimulation of the baroreceptors of rats (Bertram 1998) and of the carotid blood pressure of humans (Bernardi 1994).

The slow oscillation that manifests itself in heart rate appears to be driven via the baroreflex, since the heart rate oscillation disappears in the absence of the slow oscillation in blood pressure (Cevese 2001) and has been related to cardiac sympathetic modulation resulting from the baroreflex response to the slow oscillation in blood pressure (Sleight 1995). However, other authors have shown that the slow oscillation in heart rate is eliminated by parasympathetic blockade (Taylor 1998).

Nitric oxide, due to its short half-life (~6 s), may have a crucial role to play in the short-term regulation of blood pressure. This may interact with the baroreflex feedback loop and may dampen the slow oscillation in blood pressure (Malpas

2002). It is proposed that blood pressure oscillations may result in alterations in the shear stress along the blood vessel walls and hence stimulate the endothelial cells responsible for the release of nitric oxide. Blockade of nitric oxide in both rats and dogs has resulted in a significant increase in blood pressure variability in the same frequency range in which the effects of SNA are evident (Nafz 1986; Nafz 1997; Stauss 1999). Although doubts remain as to whether nitric oxide displays its dampening effects at the exact frequency of the slow oscillation, it is possible that its effects on the vasculature plays a role in the development of the slow oscillation.

There is a generous amount of physiological evidence to support a hypothesis, which proposes the feedback loop, including the baroreceptors, as integral to the genesis of the slow oscillation. This hypothesis is further supported by a number of models of the baroreflex loop that have reported a corresponding oscillation at the frequency of the slow oscillation and these models are reviewed in Section 2.4 of this chapter. However, many of the recent investigative studies, both experimental (Malpas 2000) and modelling (Burgess 1997; Ringwood 2001), have focused specifically on the sympathetic pathway to the vasculature and dismissed the role of other pathways in the genesis of the slow oscillation. These studies and this hypothesis are reviewed in the subsequent section.

### 2.3.3.3 Roles of the vasculature and the heart in the genesis of the slow oscillation in blood pressure

The experimental physiological studies commented on in the above sections, along with others, have led to conclusions been drawn regarding the role of the different neural pathways, and the different effectors (heart or vasculature) of the baroreflex, involved in the genesis of the slow oscillation in blood pressure.

The presumption in recent times has been that the slow oscillation represents sympathetic effects on the blood pressure effectors (Pagani 1986). The specific focus has been on the effect of the sympathetic system on the vasculature, particularly the

renal vasculature (Grady 1992; Janssen 1997; Leonard 2000; Malpas 2000). Hence, any role for the heart, in the genesis of the slow oscillation, has generally been down-played with the accepted view being that the slow oscillation exclusively involves the role of the sympathetic nervous system on the vasculature (Liu 2002).

The majority of evidence in support of this hypothesis has stemmed from experimental studies that have removed the effects of the parasympathetic and sympathetic pathways to the heart (Liu 2002) or from studies that have reported a decrease in the spectral power at the frequency of the slow oscillation when the sympathetic nervous system (Cerutti 1991) is removed or the baroreceptors are denervated (Di Rienzo 1991; Cerutti 1994; Cerutti 1995; Jacob 1995). Although many of these 'removal' studies do support a significant role for the sympathetic control of the vasculature in the generation of the slow oscillation, these studies alone should not be accepted to preclude a role for the heart in the genesis of the slow oscillation in blood pressure as all pathways and even other mechanisms may be involved in this process. The possibility for enhanced compensatory activity of other mechanisms, once one mechanism has been removed, is also ignored (Malpas 2002).

A possible role for the heart in the generation of the slow oscillation in blood pressure is discussed in more detail in Chapter 6. Models of the short-term blood pressure control mechanisms, that both include and exclude the heart, are introduced in the subsequent section.

## 2.4 Modelling review

Concerning the mathematical investigation of the variability of cardiovascular signals using spectral analysis techniques, standard indices of variability and chaos and fractal theory were briefly described in the previous section (Section 2.3). These

analysis techniques have proven to be powerful tools in the investigation of causal relationships between rhythms present in cardiovascular signals. However, these methods provide no information regarding the mechanisms underlying these oscillations present in cardiovascular signals and the genesis and changes observed in these oscillations. As has been discussed, understanding of these issues will prove key to the possible future use of these oscillations, and in particular the slow oscillation, as a diagnostic test.

Mathematical modelling enables a greater level of understanding of the fundamental processes involved in the regulation of blood pressure and specifically in developing the observed oscillatory characteristics.

Mathematical modelling studies have followed two main approaches. One approach is inherently founded on experimental data recordings of cardiovascular and neural variables. System identification (Chon 1997; Mullen 1997), linear time series analysis (Di Virgilio 1997; Nakata 1998) and artificial neural networks (Allen 1999) are used to study the relationships between these cardiovascular and neural variables. These methods have advanced the understanding of the relationships between different cardiovascular and neural variables. For example, Nakata *et al* (Nakata 1998) analysed the relationship between heart rate, systolic pressure and SNA at the frequency of the slow oscillation and suggested that sympathetic oscillations predict ~70% of the power of the slow oscillation in blood pressure, a result supported by experimental investigations (See Section 2.3.3.2). However, these modelling techniques are limited to a small number of parameters and hence, only the relationship between certain variables can be analysed.

The second approach involves the development of physical linear and nonlinear models of the regulatory mechanisms of the cardiovascular system. These models are based on physical principles that have been experimentally derived and described by linear or nonlinear equations. These models are of importance for analysing the role and relative significance of various factors involved in the

different aspects of baroreflex control including the development of oscillations. Mathematical models also enable predictions to be made regarding cardiovascular control and the behaviour of the oscillations under conditions that are difficult to test experimentally (Malpas 2002). Many physical models of the cardiovascular mechanisms involved in the development of the slow oscillation have been developed to date (Hyndman 1971; Kitney 1979; De Boer 1987; Cavalcanti 1996; Burgess 1997; Cavalcanti 2000; Seydnejad 2001; Ursino 2003). These models have enabled useful insight into the mechanisms involved in the genesis of the slow oscillation. However, many of these models are either physiologically unrealistic and inaccurate or based on a simplified description of cardiovascular control.

The development of a comprehensive physiologically realistic, physical model of the short-term blood pressure control mechanisms, which is capable of accurately describing the mechanisms involved in the development of the slow oscillation in blood pressure, is the primary aim of this research

#### 2.4.1 Models of baroreflex control of peripheral resistance

Due to the substantial school of thought which dismisses the role of the heart in the genesis of the slow oscillation in blood pressure, an abundance of models, which describe baroreflex control of the peripheral resistance excluding the baroreflex control of the heart, are presented in the literature (Hyndman 1971; Kitney 1979; Burgess 1997; Ringwood 2001; Chapuis 2004).

The first models of baroreflex control of peripheral resistance were developed during the 1970s (Hyndman 1971; Kitney 1979). These seminal studies explained the 0.1 Hz oscillations in blood pressure as a limit cycle oscillation present, in part, as a result of the nonlinearity in the feedback loop. Figure 2.26 illustrates the model, which was developed to simulate the limit cycle oscillation in blood pressure.

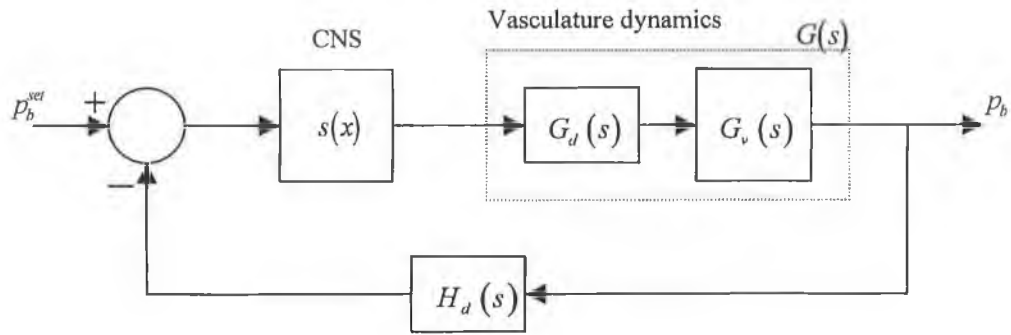


Figure 2.25: The nonlinear feedback model that represents baroreflex control of peripheral resistance.

where,

$$s(x) = \begin{cases} K, & 0 \leq t \leq T/2 \\ -K, & T/2 \leq t \leq T \end{cases} \quad (2.4)$$

where,

$K$  is the saturation limit of the hard saturating nonlinearity.

$$G_v(s) = \frac{(1+12s)}{(1+92s)(1+2s)} \quad (2.5)$$

and,

$$G_d(s) = e^{-\tau_e s} \quad (2.6)$$

where,

$\tau_e$  is the efferent delay in the forward path of the baroreflex.

Equation 2.5 describes the unity gain representation of the frequency response of the vasculature bed as calculated by Scher and Young (Scher 1963). No delay or dynamics are included in the feedback path by Kitney (Kitney 1979) and, hence,  $H_d(s) = 1$ .

The nonlinearity included in the forward path of the model  $s(x)$  is a hard nonlinear characteristic used to approximate the sigmoidal baroreflex curve present in the

central nervous system (Section 2.2.2.4), which were experimentally identified around the same period (Korner 1972; Korner 1973; Iriki 1977). Although, this hard nonlinearity is physiologically unrealistic, these early models proved a sound foundation for explaining the genesis of the slow oscillation in blood pressure via a limit cycle.

More recently, Burgess *et al* (Burgess 1997) proposed a linear feedback model to account for the slow oscillation in blood pressure. They included a linear proportional-derivative (PD) controller to represent the central nervous control. This structure ignores the nonlinear relationship that is well established to exist in the CNS and also requires a very strict relationship between the vasculature and controller parameters in order to maintain sustained oscillation.

Subsequent to this, Ringwood and Malpas (Ringwood 2001) reintroduced the idea of a limit cycle oscillation, this time replacing the hard nonlinearity included in the earlier nonlinear models (Hyndman 1971; Kitney 1979) with the more physiologically realistic sigmoid-shaped amplitude-limiting nonlinearity. This nonlinear characteristic is well established to exist in the baroreflex (Sections 2.2.3.1 & 2.2.3.2) and is described by Equation 2.3 of Section 2.2.3.2.

Also included in the model are delay terms to account for conduction delays along the nerves ( $G_d(s), H_d(s)$ ) and a linear transfer function to represent the dynamics of the vasculature ( $G_v(s)$ ). As illustrated in Figure 2.25,  $G(s)$  is the amalgamation of  $G_v(s)$  and  $G_d(s)$ . Hence, the model takes the same structure as that illustrated in Figure 2.25, where in this case,

$$G_v(s) = \frac{K}{1 + s\tau_v} \quad (2.7)$$

where,

$K$  is the gain of the transfer function, and

$\tau_v$  is the vasculature lag.

$G_d(s)$  is as given in Equation (2.6), where in this case the delay is specified for the rabbit at 0.6 s (Ringwood 2001). Also the feedback path is specified as:

$$H_d(s) = e^{-\tau_a s} \quad (2.8)$$

where,  $\tau_a$  is the afferent delay (0.2 s) (Ringwood 2001).

This nonlinear model, unlike the previously published linear model of Burgess *et al* (Burgess 1997), allows for the slow oscillation in blood pressure under a mild set of assumptions and unlike the previously published nonlinear models, is a physiologically realistic representation of the baroreflex control of peripheral resistance, that is proposed to generate the oscillation (Malpas 2002). This model serves as the basis for the study documented in Chapter 4, in which the model is parameterised and analysed for different physiological conditions.

## 2.4.2 Models of the complete baroreflex

Mathematical models for the heart and other effectors of short-term control of blood pressure are also presented in the literature. Possibly, the most cited model in the literature is the model that was proposed by de Boer *et al* (De Boer 1987). This model is developed using a set of difference equations, which describe baroreflex control of the interbeat interval and peripheral resistance, mechanical effects of respiration on blood pressure, the contractile properties of the myocardium and the input impedance of the systemic arterial tree. Simulation of this model produces an oscillation in heart rate at the frequency of the slow oscillation, which the authors ascribe to a resonance in the baroreflex due to the time delay in the sympathetic path. However, this model represents quite a simplified description of the

cardiovascular regulatory mechanisms and has only been examined in its linearised form. Other researchers have re-parameterised (Whittam 2000) and modified de Boer's model to enable investigation of the nonlinear dynamics of the model (Eyal 2000).

In contrast to the model of de Boer *et al* (De Boer 1987) most other physical models of the baroreflex consist of differential equations (Grodins 1963; Guyton 1972; Wesseling 1982; Cavalcanti 1996; Ottesen 1997). The model of Cavalcanti and Belardinelli (Cavalcanti 1996), which simply describes the baroreflex control of heart rate and stroke volume, also replicates the slow oscillation in heart rate. The emphasis of this study is on the analysis of the influence of the time delays in this simplified description of the baroreflex. These authors show how an increase in the time delay may drive the system to complex behaviour and in particular, to oscillate chaotically, as is also demonstrated by the model of Seidel and Herzel (Seidel 1998). However, neither Cavalcanti and Belardinelli (Cavalcanti 1996) nor Seidel and Herzel (Seidel 1998) associate any physiological reality with this changing delay (Cavalcanti 1996; Seidel 1998) and it is generally accepted that the delays of the baroreflex system due to conduction delay along the nerves are constant.

The cardiac output of the model of Cavalcanti and Belardinelli (Cavalcanti 1996) utilises a Windkessel description of the circulatory system, which is common in a number of developed models (Kano 1984; De Boer 1987; Madwed 1989; Cavalcanti 1996; Abbiw-Jackson 1998; Seidel 1998; Ottesen 2000). A wide variety of Windkessel representations of the arterial tree exist (Westerhof 1971; Burrattini 1982; Campbell 1984). The basic electrical analogue models of the Windkessel model generally include resistors to represent the resistance of the vascular beds and capacitors to represent the compliance of blood vessels. Abbiw-Jackson and Langford (Abbiw-Jackson 1998) altered the Windkessel model by incorporating two pumps, one for each side of the heart, and incorporated the baroreflex via a nonlinear transfer characteristic from blood pressure to heart rate (Abbiw-Jackson 1998). This model simulated a slow oscillation in blood pressure, which the authors proposed

was due principally to baroreflex gain and not primarily influenced by the delays of the baroreflex.

Cavalcanti followed his earlier study (Cavalcanti 1996) with a second, somewhat more complex, model which included different parasympathetic and sympathetic pathways of the heart. The static characteristics included in the baroreflex pathways of the heart were obtained from the study of Head and McCarty (Head 1987), who document sigmoidal relationships between blood pressure and heart rate, separately influenced by each branch of the autonomic nervous system (see Section 2.3.3.1).

Seidel undertook a comprehensive investigation of the mechanisms of short-term blood pressure control (Seidel 1995; Seidel 1997; Seidel 1997; Seidel 1998). This model includes complex nonlinear descriptions of the heart, vasculature, baroreceptors and branches of the autonomic nerve activity, and models the mechanical and central effects of respiration and the control of stroke volume. Much emphasis is given to the modelling of the phase dependency of the SA node on the moment of parasympathetic stimulation during the cardiac cycle (Seidel 1997), which has been experimentally derived (Yang 1984).

In recent years, comprehensive models have also been published by Seydnejad and Kitney (Seydnejad 2001) and Ursino and Magosso (Ursino 2003). The model of Seydnejad and Kitney (Seydnejad 2001) consists of many aspects of the baroreflex including parasympathetic and sympathetic control of heart rate, sympathetic control of the vasculature, a respiration oscillation and a centrogenic oscillator. However, instead of maintaining a purely physical representation of the baroreflex mechanism, the dependence of blood pressure on heart rate, respiration and peripheral resistance is identified empirically through a Volterra expansion (Seydnejad 2001). The authors also include a piecewise nonlinearity in the forward path as “a nonlinearity seems to be essential to satisfactorily explain the observed fluctuations in variability signals”. Although the authors report oscillations at the frequency of respiration and of slow oscillation in blood pressure this result is hardly surprising considering the inclusion

of two signal generators, one at each of these frequencies and the poorly justified inclusion of a nonlinear element which enables oscillations between its limits of threshold and saturation.

Possibly the most comprehensive physical model of the short-term control mechanisms involved in the development of cardiovascular variability, is that which was presented by Ursino and Magosso (Ursino 2003). These authors report simulant oscillations in heart rate at the frequency of the slow oscillation and the frequency of respiration of the human. Their model incorporates descriptions of systemic and pulmonary circulation, sympathetic control of peripheral resistance, heart period, unstressed volume and heart contractility, parasympathetic control of heart period, the mechanical effect of respiration on venous return and a very low-frequency vasomotor term. Although this model is especially inclusive of the mechanisms of short-term cardiovascular control, a number of criticisms of the model remain, specifically related to the contentious parameter choices made by the authors. Due to the inability to do invasive experiments in humans, there is a paucity of parameters available for a model derived for humans. Hence, the model incorporates parameters derived from humans and dogs and although the authors claim otherwise, reference to the physiological literature, from where the model parameters were obtained, is sparse. The locations and parameters of the gain and nonlinear elements are also contentious (see Section 6.3) and the justification of the choice of the physical structure of the model is tentative. This model and the parameter choices are again analysed in Chapter 6 and are compared to the choices made for the model of the complete baroreflex, documented in that chapter

Olufsen developed models (Olufsen 1999; Olufsen 2000) based on sets of hydrodynamic equations. These models are used to predict fluid and pressure waveforms in the arterial tree rather than directly examine the oscillations of cardiovascular variables. Nevertheless, these models offer useful insight into the workings of the cardiovascular system and in support of their model these authors validate their simulated results by comparing them with MRI flow data.

The models reviewed in this section are all distinctly different and attribute the slow oscillation to quite different aspects of the short-term blood pressure control mechanisms. Although many of these models enable insightful investigation and analysis of the possible mechanisms leading to cardiovascular oscillations, many tend to be either physiologically unrealistic or based on a simplified description of cardiovascular control. Considering these facts, a new model of the short-term controlling mechanisms involved in the genesis of the slow oscillation in blood pressure is presented in this thesis. The case for a new model is further justified in Chapter 6 where the model and its development are documented.

## Chapter 3

# Analysis of chaos in blood pressure signals

### 3.1 Introduction

A nonperiodic “variability” exists in cardiovascular signals (see Section 2.3). This nonperiodic variability has attracted much research interest in recent years and quantification of this variability has been enthusiastically embraced. However, similar to the other measures of variability introduced (see Section 2.3) this research has continued with little understanding of what causes this variability.

The techniques for analysis of this nonperiodic variability are derived from “chaos theory”. Chaos is the term used to describe the apparently complex behavior of what are accepted to be simple, well-behaved systems (Hilborn 2001). Chaos can only occur in deterministic nonlinear, dynamical systems, but when initially observed appears erratic and random (Williams 1997).

Researchers have claimed to have found chaos in all types of diverse and incomparable fields, including everything from lasers (Flepp 1991) and electronic circuits (Chen 1988) to oil market prices (Panas 2000) and even in the cries of the newly born (Mende 1990). To this extent, chaotic behavior seems to be regularly occurring and universal.

The search for chaos in medical and biological systems is a research area that has attracted much attention from specialists of nonlinear dynamics and chaotic behavior, in the last twenty years (Babloyantz 1988; Goldberger 1996; Lombardi 2000). Nonlinear dynamical behaviour has been observed in a number of physiological variables, including arterial blood pressure (Wagner 1995; Wagner 1996; Lovell 1997), heart rate (Hagerman 1996; Casaleggio 1997; Pavlov 2000), blood flow (Holstein-Rathlou 1993; Yip 1995) and sympathetic nerve discharge (Zhang 1994; Zhang 1998).

When analysing and quantifying the chaotic nature of a system, time-series data of variables of the system are the key basics. It is proposed that the sampled values of one continuous variable are sufficient to describe the dynamics of the underlying system (Hilborn 2001). Hence, the quantification of the chaotic behavior of a system is generally achieved by researchers, through the analysis of sampled time-series recordings of variables of the system, often using a quantifier known as the largest Lyapunov exponent.

Due to the complex fluctuations in time of physiological systems (see Section 2.3), time-series recordings of physiological variables are popular with researchers wishing to analyse systems for chaos. Heart rate time-series data has been the subject of much investigation and the possible presence of chaos has been studied in heart rate signals taken from subjects with symptoms ranging from depression (Yeragani 2002) and panic disorder (Rao 2001) to those suffering from diabetes (Claesen 1994) and cardiac vascular disease (Pavlov 2000). The study of chaos in cardiovascular signals is reviewed in Section 3.1.2 and the association of different states of health to the varying levels of chaos is examined.

However, rather than add to this growing research, the primary intension of the investigation documented in this chapter was to probe for information regarding the nonlinear nature of the short-term blood pressure control mechanisms.

### 3.1.1 Rationale for analysis of blood pressure time series for chaos

The broader focus of this research project is rooted in the modelling of the mechanisms that control blood pressure in the short-term. As was reviewed in Chapter 2, the mechanisms that control blood pressure are inherently nonlinear (Malpas 1996; Rudas 1999). Of specific interest to this research is the slow (limit cycle) oscillation in blood pressure that is proposed to result from the nonlinear elements present in the blood pressure controlling mechanism. Other nonlinear phenomena have also been reported (Michaels 1987; Rudas 1999). Analysis of these phenomena, the nonlinearities and mechanisms that are responsible for both the genesis of this slow, limit cycle, oscillation and other nonlinear phenomena is key to the future development of a diagnostic test based on cardiovascular variability.

One well-documented nonlinearity that exists in the blood pressure regulatory mechanisms is the nonlinear relationship that occurs between blood pressure and sympathetic nerve activity, described by the baroreflex curves (see Section 2.2.2.4). The characteristics of this nonlinearity have been observed to change during different physiological conditions (Malpas 1996; Barrett 2003). Examples of these changing characteristics have been illustrated in Figure 2.3 and 2.11 already and form a large part of the focus of the study documented in Chapter 4 of this thesis. Ringwood and Malpas (Ringwood 2001) demonstrated, in their modeling study, that this nonlinearity is key to the development of a limit cycle oscillation in blood pressure. Changes in the parameters that describe the baroreflex curve have been related to changes in the strength of the slow oscillation in blood pressure, with the oscillation reported to disappear during certain physiological conditions (see Section 4.3). Such changes in the baroreflex curve have been observed during the inhibition and enhancement of certain hormones and paracrines including, for example, angiotensin II (Barrett 2003) and nitric oxide (Ramchandra 2003).

Considering that chaos can only develop in nonlinear systems, the chaotic analysis of blood pressure signals during physiological conditions where the integral nonlinearities are seen to change is an obvious extension of this research. The methods of nonlinear time series analysis, used in this study to analyse blood pressure signals, enable identification of a number of characteristics of the blood pressure system including the system dimension, levels of complexity, nonlinearity and chaos. This analysis, in theory at least, enables insight into those nonlinear elements in the blood pressure controlling mechanisms that are responsible for nonlinear behavior, and in particular, chaos in blood pressure.

### 3.1.2 Chaos and health

A few different measures of cardiovascular variability have been proposed as the basis for possible future diagnostic tests. It has recently become common to assess the state of health by analysis of the nonperiodic, chaotic nature of cardiovascular signals (Yeragani 1993; Goldberger 1996).

It was originally proposed that chaotic behaviour resulted only during pathophysiological situations such as hypertension (Yip 1991). In contrast to this early observation, more recent studies have consistently reported that healthy systems are those characterised by high levels of chaos, and that reduced health may be associated with reduced levels of chaos (Wagner 1995; Guzzetti 1996; Hagerman 1996; Patzak 1996; Sugihara 1996).

It is not the main objective of this research to relate the level of chaos observed in the physiological situations under analysis to a state of health. As previously stated, the focus of this investigation is primarily on the identification of aspects of cardiovascular control involved in the mechanisms responsible for the development of the slow oscillation.

### 3.1.2.1 Chaos in cardiovascular signals

Due to the easy availability of ECG recordings, heart rate signals are more regularly analysed than blood pressure, blood flow and SNA signals. Hence, studies that report the presence of chaos in blood pressure are not as common as their equivalent in heart rate.

Chaos has been reported in heart rate variability in patients with a range of pathophysiological conditions including hypertension (Signorini 1994), heart failure (Signorini 1994), epilepsy (Faustmann 1994), diabetes (Claesen 1994), panic disorder (Rao 2001), depression (Yeragani 2002), multiple sclerosis (Ganz 1994) and heart transplant patients (Signorini 1994), amongst others. The level of chaos is decreased from the control level in the majority of these conditions. Other authors have assessed the level of chaos following intervention, including vagal (Ganz 1993; Hagerman 1996; Zweiner 1996) and sympathetic (Ganz 1993) blockade. Many of these authors report a decrease in the largest Lyapunov exponent following these interventions, although Ganz et al (Ganz 1993) report no significant change in the level of chaos during these blockades.

Chaos has been reported in the blood pressure of the dog (Wagner 1995; Lovell 1997) and the rat (Mrowka 1995). Wagner et al (Wagner 1995) reported a significant decrease in the level of chaos in the barodenervated dog.

The level of chaos in blood flow has been assessed and was reported to be decreased in hypertensive rats (Yip 1991; Yip 1995). SNA signals have also been assessed during similar conditions (Zhang 1994; Zhang 1998).

## 3.2 Analysis of Blood Pressure Data

### 3.2.1 Description of available data

Blood pressure signals were recorded in conscious New Zealand white rabbits. The University of Auckland, Animal Ethics Committee, approved all experiments. All signals were continuously recorded and sampled at 500 Hz using an analog-to-digital data acquisition card (National Instruments). Calibrated signals were continuously displayed on screen and saved using a program written in the LabVIEW graphical programming language (National Instruments).

Data was recorded during seven different physiological conditions:

#### *Physiological recordings*

1. *Control rabbits* (Leonard 2000; Ramchandra 2003); Blood pressure was measured via an implantable telemetry device inserted in a central ear artery of 10 resting and conscious rabbits.
2. *Blood volume expansion* (Leonard 2000); In 5 rabbits a polygeline-electrolyte solution was used to increase plasma volume. This solution was administered at 1.5 ml/min/kg for 15 minutes.
3. *Control after blood volume expansion* (Leonard 2000); Blood pressure was recorded for a further 7 minutes after completion of volume expansion.
4. *Barodenervated rabbits* (Le Fevre 2003); The afferent nerves sensing blood pressure were cut in a group of 6 rabbits. Recordings were taken from rabbits at least 10 days after surgery and with the animals living in their home cages and on a 12 hr light/dark cycle.

5. *Barodenervated rabbits with infused angiotensin II* (Le Fevre 2003); Following barodenervation, the animals were infused with angiotensin II (50 mg/kg/min).
6. *Angiotensin II infused rabbits with intact baroreflex* (Barrett 2003). These baroreflex animals were infused with angiotensin II (50 mg/kg/min).
7. *Nitric oxide blocked rabbits with intact baroreflex* (Ramchandra 2003). In a group of 4 rabbits, nitric oxide blocker L-NAME was induced by oral administration and the daily intake was  $50 \pm 4$  mg/kg/day.

### *Statistical analysis*

ANalysis Of VAriance statistical techniques (ANOVA) were used to assess the effects of the various interventions on the chaotic nature of blood pressure. P values below 0.05 were considered significant.

All values, including mean blood pressure, correlation dimension and largest Lyapunov exponents, are presented as mean  $\pm$  standard deviation (S.D.).

### 3.2.2 Data preprocessing

The existence of noise is inherent in experimentally recorded physiological signals. When dealing with experimentally recorded time series data, the existence of both measurement and dynamical noise may be assumed (Kantz 1997).

Measurement noise refers to the corruption of observations by errors which are independent of the dynamics (Kantz 1997). The dynamics satisfy,

$$x_{i+1} = F(x_i) \tag{3.1}$$

However, what are measured are scalars of the form:

$$S_i = S(x_i) + \eta_i \quad (3.2)$$

where,

$S(x)$  is a smooth function which maps points on the attractor to real numbers and,

$\eta_i$  are random numbers or measurement noise.

Measurement noise exists in experimental time series recordings due to the non-ideal characteristics of the A-D converter, specifically the introduction of a quantisation error, and to the existence of regular electrical noise associated with the electronic measurement equipment. In contrast, the dynamical noise refers to the actual noise on the system 'states':

$$x_{i+1} = F(x_i + \eta_i) \quad (3.3)$$

Dynamical noise may be the result of a number of factors including movement artifacts and varying emotions of the live subject during recordings. Dynamical noise is generally unidentifiable from the time series as it may be indistinguishable from the normal dynamics of the system, and attempts to remove it may be perilous. In order to remove this dynamical noise from the signals, models must be chosen for the dynamics and these models must be fitted to the data in the regions of interest of the attractor (Kostelich 1993).

The presence of a large noise component in the data limits the possibility of reliably extracting quantitative information for time series data (Kostelich 1990). Noise may completely obscure the underlying fractal structure unless the data are preprocessed to reduce it (Grassberger 1991). Considering that noise usually manifests itself at higher frequencies, a common technique amongst researchers, when attempting to minimise the level of noise in an experimentally recorded signal, is to use linear low-pass filtering techniques. However, a defining feature of chaotic signals is that they will generally have a broad spectrum, with

frequency components at all frequencies across the spectrum (Signorini 2001) and therefore share spectral properties generally attributed to random noise (Kantz 1997). Hence, any attempt to reduce noise by using a linear filter will have a detrimental effect on the signal resulting in correlations and nonlinear signal distortion (Kostelich 1993; Yip 1995).

Alternatively, a number of nonlinear noise reduction algorithms exist, which avoid the distortion of the signal due to linear filtering (Kostelich 1988; Kostelich 1990; Schreiber 1991; Cawley 1992; Sauer 1992). The objective of this noise reduction process was to reduce the effects of measurement noise due to quantisation without affecting the dynamics of the system. Hence, the algorithm chosen for this study is that proposed by Schreiber (Schreiber 1993). This method replaces each data point,  $x_i$ , by the average value of this coordinate over points in a suitably chosen neighbourhood as is described by Equation (3.12). However, the data is first set up for analysis, by reconstruction of the phase space. The methods of this are documented in the subsequent section and the noise reduction method is introduced subsequent to this.

#### *Reconstruction of the phase space*

The first step in any analysis of chaotic data is to reconstruct the attractor in phase-space (Kostelich 1993). The most popular method of reconstruction of the phase space is the time-delay embedding method (Packard 1980; Takens 1981). This technique is developed around the idea that, even for a multidimensional system, the time series record of a single variable is often sufficient to determine many of the properties of the full dynamics of the system (Hilborn 2001). For a properly generated phase space, the behaviour of trajectories in this phase space will have the same geometric and dynamical properties that characterise the actual trajectories in the full multidimensional state space for the system (Hilborn 2001). The time-delay embedding method is well documented in the nonlinear time series analysis literature and may be outlined as follows.

For an N-point time series,  $x(i) = \{x_1, x_2, \dots, x_N\}$ , each time-delay vector in phase space is formed as:

$$X_i = [x(i), x(i+\tau), \dots, x(i+(m-1)\tau)] \quad (3.4)$$

where,

$$i = 1, 2, \dots, N - (m-1)\tau,$$

$\tau$  is the time delay, and

$m$  is the minimum embedding dimension.

These vectors,  $X_i$ , form the rows of the matrix  $\mathbf{X}$ , which describes the reconstructed phase-space:

$$\mathbf{X} = [X_1, X_2, \dots, X_M]^T \quad (3.5)$$

where,  $M = N - (m-1)\tau$ .

Hence, the problem of reconstructing the phase space reduces to the calculation of the time delay,  $\tau$ , and the embedding dimension,  $m$ . It is important that appropriate values of  $m$  and  $\tau$  are chosen so that the optimal embedding space is developed (Radojicic 2001).

The *time delay*,  $\tau$ , is chosen to result in vectors of points that are not correlated to previously generated points (Chen 1999). Hence, each component of the vector  $\tau$  is providing new information about the signal source at a given time (Abarbanel 1998). If  $\tau$  is chosen too small, each component of the vector  $X_i$  will not add significant new information about the dynamics (Abarbanel 1998). Just as too small a choice for  $\tau$  is inappropriate, so also is too large a choice of  $\tau$ , as the components of  $X_i$  become independent of each other and cannot properly describe the dynamics of the system (Abarbanel 1998).

A number of different methods of time-delay calculation are available (Fraser 1986; Albano 1988; Liebert 1991; Buzug 1992). In general, these methods are based on the use of a correlation function to calculate the dependence of the sample points on each other. The time at which this correlation function reaches its first minimum is generally chosen as the time lag,  $\tau$ .

The two most common methods for calculation of the time delay are the autocorrelation method and the mutual information method. Both these methods were used in this study but more concentration is given to the mutual information method as this method offers a measure of general dependence (Fraser 1986), whereas the autocorrelation function returns a measure of linear dependence (Rosenstein 1994).

The *embedding dimension*,  $m$ , may also be calculated using a number of different algorithms (Grassberger 1983; Broomhead 1986; King 1987; Mees 1987; Theiler 1987; Kennel 1992). Many of these require a large number of data points to work correctly and, hence, are computationally very intensive. The method proposed by Cao (Cao 1997) is robust to these difficulties (Radhakrishna 2000).

The method proposed by Cao (Cao 1997), for calculating the minimum embedding dimension, uses the time delay vectors to build the function:

$$a(i, m) = \frac{\|X_i(m+1) - X_{m(i)}(m+1)\|}{\|X_i(m) - X_{m(i)}(m)\|} \quad (3.6)$$

where,

$X_i(m+1)$  is the  $i^{\text{th}}$  reconstructed vector in dimension  $m+1$ .

$X_{m(i)}(m)$  is the nearest neighbour of  $X_i(m)$  in the  $m^{\text{th}}$  dimension phase

space, and,  $\|\bullet\|$  is the Euclidean norm.

Starting from a low value of  $m$  and increasing toward the optimal value, the number of false neighbours or neighbours of a point that are projected into a space that is of too small a dimension should decrease to zero, or equivalently  $a(i, m)$  should reach a constant value. A quantity,  $E(m)$ , which is the mean value of all the  $a(i, m)$  is computed as:

$$E(m) = \frac{1}{N-m} \sum_{i=1}^{N-m} a(i, m) \quad (3.7)$$

and in order to investigate the variation from  $m$  to  $m+1$ ,  $E1$  is defined as:

$$E1(m) = \frac{E(m+1)}{E(m)} \quad (3.8)$$

If the time series has a finite dimensional attractor,  $E1(m)$  should stop changing when  $m$  is increased above the correct value of the embedding dimension. For the case of real data, it may be difficult to distinguish whether  $E1(m)$  has attained a constant value or is slowly increasing. In this case, it is recommended to compute the function:

$$E2(m) = \frac{E^*(m+1)}{E^*(m)} \quad (3.9)$$

where,

$$E^*(m) = \frac{1}{N-m} \sum_{i=1}^{N-m} |x_{i+m} - x_{m(i)+mr}| \quad (3.10)$$

where,

$mn(i)$  is as in Equation (3.6), and

$x$  is now an independent random variable.

For random data,  $E2(m)$  is always very close to 1, whereas for deterministic signals there exists some  $m$ , such that  $E2(m) \neq 1$ .

The choice of embedding dimension,  $m$ , may also be calculated using the method of calculation of the correlation dimension proposed by Grassberger and Procaccia (Grassberger 1983). This method is also used in this study as a check for the embedding dimension calculated using the method proposed by Cao (Cao 1997). The correlation dimension is the slope of the plot of the correlation sum verses the radius of the neighbourhood chosen,  $\varepsilon$ . The correlation sum is:

$$C(\varepsilon) = \lim_{N \rightarrow \infty} \frac{1}{N^2} \sum_{i=1}^N \sum_{j=1}^N G\left(\varepsilon - |X_i - X_{n(j)}|\right) \quad (3.11)$$

where  $G$  is the Heaviside function:

$$G(y) = \begin{cases} 0 & \text{if } y \leq 0 \\ 1 & \text{if } y > 0 \end{cases}$$

The double summation in (3.11) counts the pairs  $(X_i, X_{n(j)})$  where the separation between  $X_i$  and its neighbouring point,  $X_{n(j)}$ , is smaller than  $\varepsilon$ . The slope of successive plots of the log of the correlation sum verses the log of the radius of neighbourhoods for increasing embedding dimension will stop changing as the optimum value of the embedding dimension is reached.

The correlation dimension is, in itself, a very popular quantifier of chaos, as it yields an approximate estimation of the fractal dimension. Although the term fractal dimension is sometimes used rather indiscriminately, it is often seen as a measure of the number of degrees of freedom which comprise the dynamics of a system (Holstein-Rathlou 1994).

### *Nonlinear noise reduction*

Following the reconstruction of the phase space, the nonlinear noise reduction may now be implemented. For each data point,  $x_i$ , the set,  $U_i^\varepsilon$ , of all neighbours,

$x_j$ , in the neighbourhood of radius  $\varepsilon$  is found. The original recorded data point,  $x_i$ , is simply replaced by its mean value,  $\bar{x}_i$ , in  $U_i^\varepsilon$ :

$$\bar{x}_i = \frac{1}{|U_i^\varepsilon|} \sum_{U_i^\varepsilon} x_j \quad (3.12)$$

Following this, the root mean squared value of the corrected error is taken as a new value of  $\varepsilon$  and the procedure may be repeatedly iterated, until no neighbours are found and the signal may be assumed as corrected. The initial choice of  $\varepsilon$  and the parameters of the time-delay vectors  $(\tau, m)$  are dealt with in the results section.

An estimate of the level of noise reduction is possible on the basis of the correlation integral (Kantz 1997).

### 3.3 Determining chaos from a one-variable time series

It is possible to identify chaos in a system, using nonlinear time series analysis methods, from the time series of one variable of the system (Hilborn 2001). Chaos can be determined from time series data using methods based on correlation dimension (Grassberger 1983), Kolmogorov entropy (Grassberger 1983), numerical titration techniques (Poon 2001) and Lyapunov exponents (Eckmann 1985; Wolf 1985; Farmer 1987).

The method of phase space reconstruction, which is inherent to the chaotic analysis of time series, was introduced in the previous section for the noise reduction process. All of the nonlinear time series methods introduced in the subsequent sections are based on the use of phase space reconstructed data.

Prior to attempting an investigation for the presence of chaos in the blood pressure time series, nonlinearity is tested for using the method of surrogate data analysis. This method is introduced in Section 3.3.1 and the results of this analysis are presented in Section 3.4.2.

### 3.3.1 Surrogate data analysis

Surrogate data is used to test for nonlinear deterministic structure. Surrogate data is artificially generated data that mimics certain linear features (*e.g.* autocorrelation function, spectral power density) of the specified time series but that is otherwise stochastic. The experimentally recorded time series and this surrogate data are then used to test a specific hypothesis. In this case, a null hypothesis is chosen, which is best described as the default conclusion in the lack of contrary evidence (Theiler 1996). The null hypothesis, in this case, is that the data arose from a linear random process.

In order to test the null hypothesis, a discriminating statistic is chosen. A significant difference between the discriminating statistic calculated for the original experimentally recorded data and for the surrogate data sets indicates the existence of nonlinear structure in the original data. In principle, any nonlinear statistic that assigns a real number to a time series can be chosen as the discriminating statistic (Kantz 1997). The measures chosen for this study are a nonlinear prediction error, calculated using a simple nonlinear prediction algorithm (Kantz 1997) and the largest Lyapunov exponent (Rosenstein 1993). The prediction error was chosen as nonlinear predictability provides a direct test for the presence of determinism in the data set (Sugihara 1990) and the largest Lyapunov exponent, because it is the (chaos) quantifier of primary interest to this study.

The technique used to create the surrogates is that proposed by Theiler *et al* (Theiler 1992). Using this technique, surrogate data is generated by randomising the phases of the Fourier transform of the time series.

The results of the surrogate data tests are documented in Section 3.4.3.

### 3.3.2 Lyapunov exponents

The most striking feature of chaos is the unpredictability of the future despite a deterministic time evolution (Kantz 1997). The slightest change in a variable's starting value or of a system's state at any given time leads ultimately to vast differences in the output. Chaologists refer to such a trait as "the sensitive dependence on initial conditions" (Williams 1997). Such a characteristic is quantified by the analysis of the divergence of trajectories, where a trajectory is the time path of the sequence of successive iterates in phase space.

Therefore, a phase-space trajectory reflects the evolution of a dynamical system and the Lyapunov exponents  $(\lambda_i)$  enumerate the average rate of convergence or divergence of two neighbouring trajectories in phase space.

#### *Lyapunov spectrum*

The number of possible directions for deviation of the two trajectories is equal to the number of degrees of freedom in the phase space (Kaneko 1996), hence the number of Lyapunov exponents equals the number of phase space dimensions (Williams 1997).

The different rates of divergence or convergence of the trajectories within the different dimensions are termed the Lyapunov exponents of the attractor, and when considered as a group are known as the Lyapunov spectrum:

$$\lambda_1 \geq \lambda_2 \geq \dots \geq \lambda_m .$$

The Lyapunov exponents may be positive, negative or zero. Positive and negative exponents respectively signify exponential divergence (unstable) and convergence (stable) of neighbouring trajectories. If the motion settles down onto

a stable limit cycle, two trajectories can only separate at the same rate. In this case, the maximum Lyapunov exponent is zero and the motion is marginally stable.

The method of calculation of the Lyapunov spectrum, used in this study, was first suggested by Eckmann and Ruelle (Eckmann 1985) and applied to data by Sano and Sawada (Sano 1985). However, the available methods of calculation of the Lyapunov spectrum contain a number of fundamental problems and are strongly dependent on the quality of the data (Kantz 1997).

The reconstructed phase space is often of a larger dimensionality than the ‘true’ dimensionality of the chaotic attractor (Takens 1981). Therefore, among the  $m$  Lyapunov exponents, there may be some that are not defined in the true state space and, hence, are referred to as spurious exponents (Kantz 1997). Although a method of distinguishing between spurious and nonspurious Lyapunov exponents has been suggested (Parlitz 1992), the presence of spurious components and the inherent sensitivities of the algorithms of Lyapunov spectrum calculation make it difficult to conclude on the validity of various exponent values.

#### *The largest Lyapunov exponent*

The presence of one positive Lyapunov exponent is enough to denote chaos (Williams 1997). A positive exponent implies the divergence of two trajectories, and therefore, the value of the positive exponent quantifies the sensitivity of the system to initial conditions.

The algorithm begins by searching for the nearest neighbour,  $X_{m(i)}$ , of each reconstructed phase point  $X_i$ , where,  $i = 1, \dots, N - (m - 1)$ . The minimum distance is:

$$d_0(i) = \min \|X_i - X_{m(i)}\| \quad (3.13)$$

The nearest neighbours diverge, approximately at a rate given by the largest Lyapunov Exponent ( $\lambda_1$ ).

$$d_n(i) = d_0(i) e^{\lambda_1(n\Delta t)} \quad (3.14)$$

where,

$d_0$  is the initial separation, and

$d_n$  is the distance between the neighbouring points after iterating to  $n$ .

Taking the logarithm of both sides produces:

$$\ln(d_n(i)) = \ln d_0(i) + \lambda_1(n\Delta t) \quad (3.15)$$

This represents a set of  $i$  approximately straight lines. The largest Lyapunov exponent is calculated as the least-squares fit to the average of these  $i$  lines, which is defined as:

$$\lambda_1 = \frac{1}{n\Delta t} \langle \ln(d_n(i)) - \ln(d_0(i)) \rangle \quad (3.16)$$

where  $\langle \dots \rangle$  donates the average over  $i$  lines.

#### *Other measures of chaos*

Other measures of chaos were also investigated. Along with the correlation dimension, introduced in Section 3.2, a novel method for the detection of chaos, based on what is termed “numerical titration”, has been developed (Poon 2001). This technique involves using additive white noise as a titrant for chaos. The method simply involves adding white noise, of increasing standard deviation, to the data until the nonlinearity in the data goes undetected by a certain chosen nonlinear indicator. The proposed candidates for this nonlinear indicator are a time-reversibility measure (Diks 1995) and the Volterra-Wiener nonlinear identification method.

## 3.4 Results

### 3.4.1 Reconstruction of the phase space

The phase-space is reconstructed using the time delay embedding method, with a time delay of 40 samples and an embedding dimension of 10. The time delay is calculated as the first minimum of the automutual information function and the embedding dimension as the approximate point of saturation of the  $E1$  function of the method of Cao (Cao 1997). Figures 3.1 and 3.2 show examples of plots, derived for blood pressure data of individual rabbits, from which these values were calculated. For comparison purposes, the embedding parameters are maintained at these values across all animals and physiological conditions.

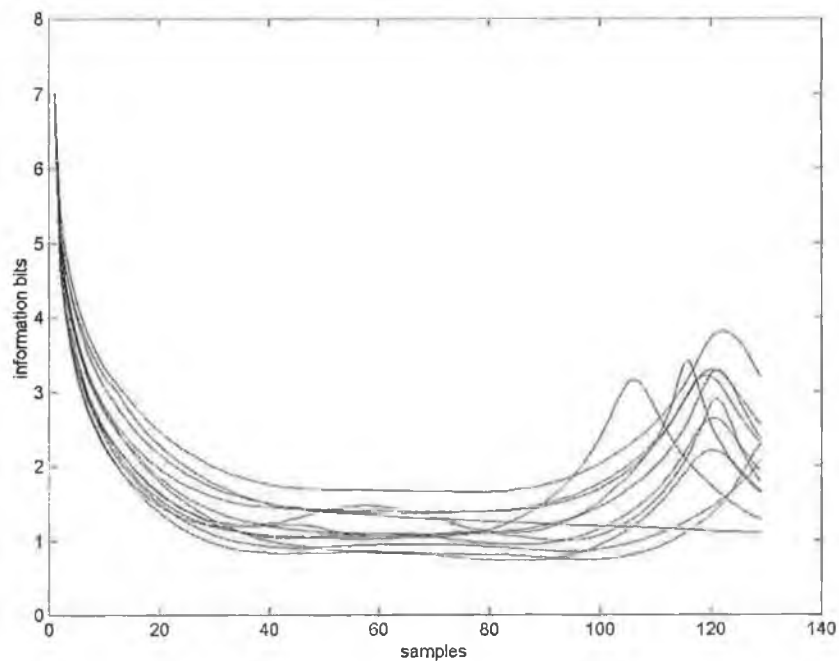


Figure 3.1: Calculation of the time delay using the automutual information function.

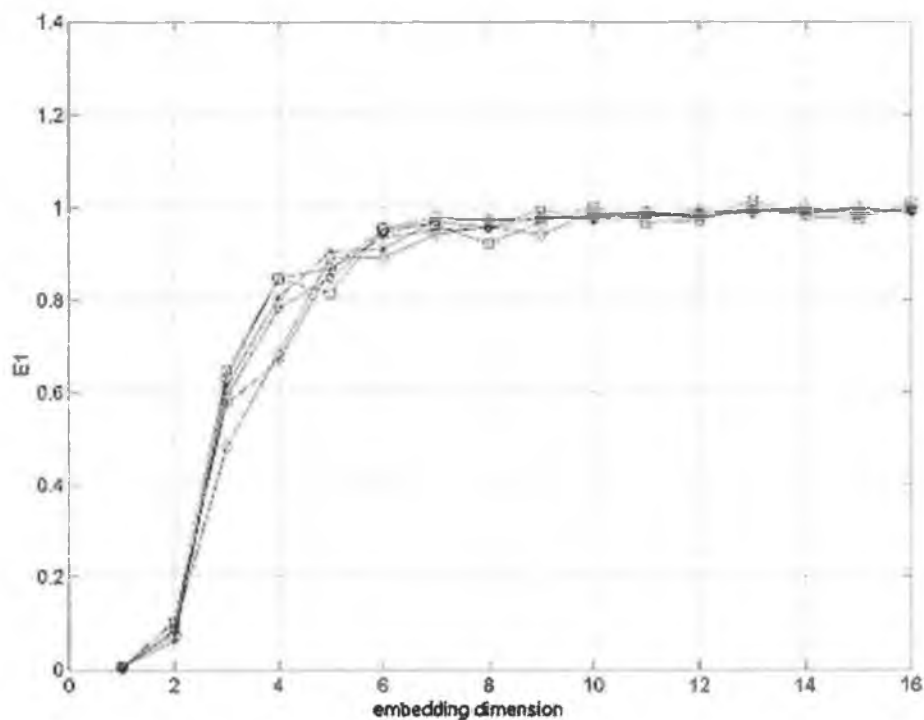


Figure 3.2: Calculation of the minimum embedding dimension.

The plot of the correlation sum versus the radius supports 10 as a good choice of embedding dimension, as the slopes of the consecutive plots become constant at approximately this value of embedding dimension. An example of such a plot is illustrated in Figure 3.3.

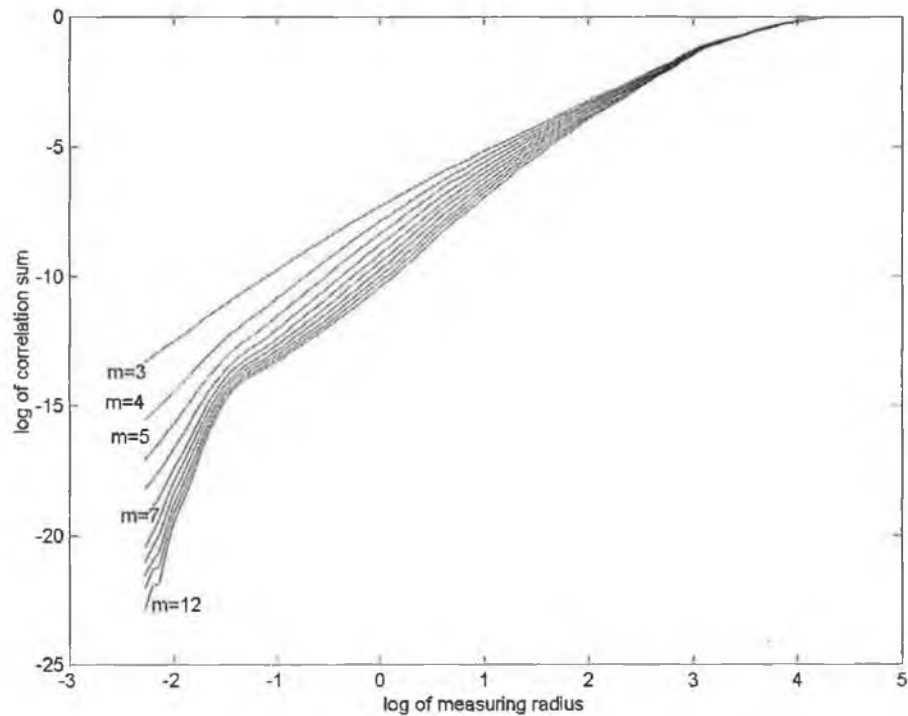


Figure 3.3: Plot of the correlation sum versus measuring radius for blood pressure data of a single animal.

### 3.4.2 Noise reduction

The phase-space is reconstructed for the implementation of the nonlinear noise reduction algorithm. However, rather than reconstruct the phase space using the values of  $\tau$  and  $m$  calculated using the methods introduced in Section 3.2.2, it is recommended that a larger than usual value of  $m$  is chosen, so as to get rid of dubious neighbours (Kantz 1997; Signorini 2001). A unity time delay value is also recommended. Hence, the phase space is reconstructed, for the noise reduction procedure, using unity time delay and an embedding dimension,  $m$ , of 25. These parameter values provided the optimum results for the algorithm chosen.

It is proposed that a good choice of the size of the neighbourhood,  $U_i^\epsilon$ , is given by 2-3 times the noise amplitude (Kantz 1997). The data recordings are to one decimal place, therefore, it may be assumed that the discretisation error is

distributed in the range  $[-0.05, 0.05]$ . The radius was chosen to at least include this range of error, and was decreased exponentially during 3-5 iterations of the procedure. Delay maps of a sample blood pressure time series before and after noise reduction are presented in Figure 3.4.

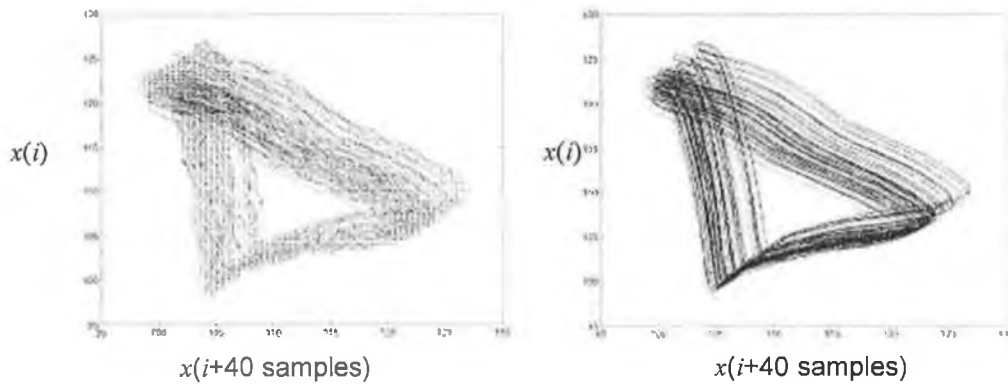


Figure 3.4: Delay maps of 10,000 sample points of a blood pressure time series before (left) and after (right) noise reduction.

### 3.4.3 Nonlinearity of blood pressure signals

Twenty surrogate data sets were created for each time series. Both the largest Lyapunov exponent ( $\lambda_1$ ) and the nonlinear prediction error were used as discriminating statistics. The null hypothesis stated that the time series originates from a linear process. This null hypothesis is rejected, as both the discriminating statistics are significantly different from the original time series to all surrogate data sets ( $P < 0.05$ ).

The prediction error was calculated for 1 to 100 time steps ahead for each time series and the forecasting error in the experimental time series was less than 80% that for the surrogate data sets at each prediction ( $P < 0.05$ ).

The values of the largest Lyapunov exponent calculated for the surrogate data sets, although significantly decreased from the largest Lyapunov exponent ( $P < 0.05$ ) for the original time series, were still positive ( $\lambda_1 = 0.6$ ). This is an

unexpected result, although a positive largest Lyapunov exponent was previously reported for purely stochastic data (Damming 1993).

### 3.4.4 Chaos in the blood pressure system

The spectrum of Lyapunov exponents was calculated for the control subjects. The aim of this investigation was to identify a zero Lyapunov exponent, which was expected due to the periodicities and proposed limit cycles that exist in blood pressure signals. However, following careful calculation, no zero Lyapunov exponent was observed.

The largest Lyapunov exponent for the control subjects was significantly higher than all but one of the other experimental conditions ( $P < 0.01$ ). The exceptional case is for the rabbits in the nitric oxide blocked experimental condition. The average values of the largest Lyapunov exponent, along with the average correlation dimension, calculated for each experimental condition, are documented in Table 3.1. All values are presented as mean  $\pm$  standard deviation (S.D).

<b>Experimental Condition (Number of animals)</b>	<b>Mean BP</b>	<b>Correlation Dimension</b>	<b>Largest Lyapunov exponent (LLE)</b>
Control subjects (10)	75 $\pm$ 9	2.7 $\pm$ 0.3	1.70 $\pm$ 0.10
Baroreceptor denervated subjects (5)	87 $\pm$ 4	2.4 $\pm$ 0.2	1.14 $\pm$ 0.11
Baroreceptor denervated & angiotensin II infused (5)	108 $\pm$ 3	2.6 $\pm$ 0.1	1.23 $\pm$ 0.11
Nitric oxide blocked subjects (5)	84 $\pm$ 3	2.4 $\pm$ 0.5	1.61 $\pm$ 0.05
Blood volume expansion (5)	59 $\pm$ 7	3 $\pm$ 1	1.48 $\pm$ 0.09
Control after blood volume expansion (5)	75 $\pm$ 15	3.9 $\pm$ 0.4	1.24 $\pm$ 0.22
Angiotensin II infused (3)	104 $\pm$ 8	2.7 $\pm$ 0.3	1.33 $\pm$ 0.06

Table 3.1: Averaged values of the largest Lyapunov exponent calculated for the seven different physiological conditions.

The correlation dimension varied greatly across animals, hence, the average values of the correlation dimension calculated for the different experimental conditions are generally not statistically different ( $P > 0.05$ ) from one another, making it impossible to draw clear conclusions.

The largest Lyapunov exponent calculated for the control subjects was significantly higher than the largest Lyapunov exponent calculated for all of the experimental conditions ( $P < 0.01$ ), except for the exceptional case of the rabbits in the nitric oxide blocked experimental condition. Although the largest Lyapunov exponent also decreases for this physiological condition there is not a statistically significant difference between the largest Lyapunov exponent calculated for control and that calculated for the nitric oxide blocked condition.

### 3.5 Discussion

The main aim of this study was to test how the short-term dynamics of blood pressure control are affected when short- to medium-term effectors of blood pressure are either removed or enhanced. This was done in an effort to provide some insight into the mechanisms that are responsible for controlling blood pressure in the short-term and specifically to provide insight into the nonlinear nature of these mechanisms.

Of specific interest to this research is the slow oscillation in blood pressure, which is proposed to be a limit cycle oscillation resulting from the feedback pathways of the baroreflex. Nonlinear elements are well established to exist in the baroreflex feedback loop (Iriki 1977; Coleridge 1981; Iglar 1981; Malpas 1996; Malpas 1997), and these nonlinearities are proposed to be inherently involved in the genesis of this slow oscillation in blood pressure (Ringwood 2001; Ringwood 2004). Changes in these nonlinear characteristics have been associated with the changing strength of the slow oscillation in blood pressure (Leonard 2000), which in turn has been associated with the state of autonomic function in health and disease (Akselrod 1981; Malik 1990; Yeragani 1995).

The results of the surrogate data tests demonstrate that the underlying controlling mechanisms of blood pressure are nonlinear (Theiler 1992). The largest positive Lyapunov exponents of all the animal groups, by definition, indicate that these nonlinear mechanisms exhibit chaotic behaviour (Williams 1997). Preliminary results achieved by this author, using the numerical titration technique, proposed by Poon and Barahona (Poon 2001), also support the findings of the presence of chaos in blood pressure signals.

The spectrum of Lyapunov exponents was calculated for blood pressure signals recorded in the rabbits during the control condition, some of which contained a slow oscillation. The presence of a zero exponent was expected due and a proposed presence of a limit cycle amongst the multiple periodicities in the blood pressure

signals (see Section 2.3). However, none is reported. This result is most likely explained by the fact that the methods of calculating the Lyapunov spectrum are very sensitive to contamination artifacts of real-world data (Kantz 1997). Many authors desist from drawing definite conclusions from the spectrum of exponents calculated for noisy real-world data, due to the presence of noise, finite size of the data files and the occurrence of spurious exponents (Kantz 1997).

Although the presence of a zero Lyapunov exponent was not observed, a positive largest Lyapunov exponent was consistently observed.

#### *Chaos during different physiological conditions*

The values of the largest Lyapunov exponent calculated during each of the eight physiological conditions examined are positive (see Table 3.1). Neither disruption of the baroreflex nor tampering with relevant hormonal (angiotensin II) and paracrine (nitric oxide) concentrations eliminates the evidence of chaos in the mechanisms that regulate blood pressure. However, the values of the largest Lyapunov exponent change considerably from condition to condition, leading to the conclusion that certain effectors of blood pressure play more of a role than others in the establishment of chaos in blood pressure.

Changes in the largest Lyapunov exponent have been related to changes in peripheral vascular mechanisms due to alterations in the sympathetic drive (Rao 2000). Rao *et al* (Rao 2000) reported an increase in the largest Lyapunov exponent, calculated for heart rate variability, from the supine to the standing position. An increase in SNA during such a movement is well documented (Munakata 1999). An increase in sympathetic drive to the vasculature will result in an increase in vascular tone (see Section 2.2.3.2). An increase in power, in the frequency range of the slow oscillation, has also been observed during such a movement (Munakata 1999; Rao 2000) and these authors report a positive correlation between the largest Lyapunov exponent and the power in the region of the slow oscillation (Rao 2000).

The correlation between the increased levels of SNA and an increase in the largest Lyapunov exponent is consistently reported for the conditions analysed in this study.

The value of the largest Lyapunov exponent drops by over 30% from the control subjects to the barodenervated animals, *i.e.* from 1.7 to 1.14 ( $P < 0.01$ ). A similar result was previously documented by Wagner *et al* (Wagner 1995), in the dog. When the animals are barodenervated, the signal becomes less chaotic and more predictable. This may be explained by the fact that after the removal of the baroreflex, the ability to control blood pressure in the short-term is considerably repressed. Wagner, *et al* (Wagner 1996) proposed that other effectors of blood pressure will compensate this loss of control (Brand 1988), hence, perturbing the dynamics of the regulating system in a way that is simpler and less complex.

In keeping with the conclusions of Rao *et al* (Rao 2000), sympathetic control of the vasculature is considerably limited following barodenervation, as the baroreflex feedback mechanism is abolished. Rao *et al* (Rao 2000) report an increase in the largest Lyapunov exponent when SNA to the vasculature is increased, and a significant decrease in the largest Lyapunov exponent is reported in this study when SNA to the vasculature is decreased (*i.e.* following barodenervation).

Infusion of angiotensin II in baroreflex intact animals leads to an increase in the mean level of blood pressure (from  $75 \pm 9$  to  $104 \pm 3$  mmHg) and a decrease in the largest Lyapunov exponent (from 1.7 to 1.33 ( $P < 0.05$ )). Angiotensin II is a potent vasoconstrictive hormone that acts over much longer time scales than the baroreflex (Guyton 1991) (see Section 2.2.3.2).

Interestingly, SNA to the kidney is significantly decreased in the days following angiotensin II infusion (Barrett 2003). Although, in this case, vascular constriction is compensated by angiotensin II infusion, the ability of sympathetic activity to cause significant and quick alterations in vascular resistance, via the baroreflex, is inhibited, due to the increased constrictive state of the blood vessels. Unfortunately, as the mechanisms of blood pressure control responsible for the chaotic nature of the blood pressure signals are unknown, the effect of a decrease in SNA and its association with the largest Lyapunov exponent can only be postulated. Therefore, it is proposed that

the increase in the predictability of the blood pressure signal and the decrease in chaos may be due to the decreased level of SNA.

The largest Lyapunov exponent calculated for the nitric oxide blocked group of animals did not show a significant decrease from the control subjects. This result is surprising, as nitric oxide is known to play a prominent role in the short-term control of blood pressure (Rees 1989), and hence might be expected to affect the largest Lyapunov exponent. Again compensatory effects may come into play, which in this case maintain the level of chaos close to that of the control values. Yuasa, *et al* (Yuasa 2000) documented results that suggest an increase in SNA after nitric oxide inhibition. This increased sympathetic drive may help to maintain the level of chaos in blood pressure after nitric oxide inhibition.

Studies documenting the variation in the largest Lyapunov exponent of heart rate signals abound in the physiology literature. A large percentage of these studies document the decrease in the largest Lyapunov exponent from the healthy to the unhealthy condition such as depression (Yeragani 2002), multiple sclerosis (Ganz 1993) and epilepsy (Faustmann 1994) (see Section 3.1.2). This broad assertion is reflected in the results of this study, in which the largest Lyapunov exponent decreases from the control situation to all other situations, during which the control mechanisms of blood pressure are tampered with. These situations include the unhealthy conditions of a damaged baroreflex control mechanism and elevated blood pressure, amongst others.

In this study we showed that perturbation of the overall blood pressure controlling mechanism, by removal or enhancement of some of the effectors of blood pressure resulted in a decreased level of chaos in the recorded blood pressure signals.

### *Limitations*

The choice of the embedding parameters for the reconstruction of the phase-space was one that had to be made with care, due to the considerable sensitivity of the largest Lyapunov exponent to variations in these values (Abarbanel 1998). This choice is always going to be approximate and subjective, however, care was taken when

calculating these values and, so as to enable accurate comparison, both the time delay and embedding dimension were consistent for all data sets and physiological conditions. It may be argued that the structure of the system may change during barodenervation or hormone and paracrine blockade or enhancement, however, there is not sufficient clarity in the data to suggest that this is the case and the tests for these embedding parameters did not present any obvious results to demonstrate this to be the case. Hence, it is assumed that the structure of the system remains the same but that the parameters of the system change.

With experimentally recorded data, problems and limitations are always to be expected due to errors during the recording, the limited resolution of each data point and the masking of the data by noise. Though use of nonlinear noise reduction minimises the problems created by the measurement noise, the restriction of the resolution of the data points is a limitation posed by the finite number of bits of the A/D converter. There is no ideal solution to this problem, however, the effects of the bias due to truncating quantisation on the calculated values of the largest Lyapunov exponent are diminished by averaging over a large number of data points.

### 3.6 Conclusions

Using nonlinear time series analysis, the mechanisms that control blood pressure are shown to be nonlinear and are capable of displaying chaotic characteristics and, therefore, may be termed chaotic. The different mechanisms and effectors of blood pressure control, including the baroreflex feedback loop, the different hormones and paracrines that effect blood pressure control over different time scales, all play a role in making the blood pressure system chaotic.

However, a lack of understanding of the mechanisms, that give rise to the chaotic nature of the blood pressure system, make it difficult to conclude definitively from the results of changing levels of chaos, as measured by the largest Lyapunov exponent.

Also, because the methods used are very sensitive to disturbances in real data, insight into the slow oscillation based on the spectrum of Lyapunov exponents is limited.

However, although the original aims of this study may not have been met, the results of this study are otherwise very interesting.

In summary, what can be specifically concluded is that, the blood pressure control mechanisms are inherently nonlinear and chaotic. The level of chaos decreases from a high level during control to a lower level during all physiological situations in which the short- to medium-term blood pressure control mechanism are in some way tampered with. Therefore, it is proposed that the results of this study, although failing to add insight to the mechanisms responsible for either the periodic or the nonperiodic variability in blood pressure, may add to the momentum of research into the use of nonperiodic variability as a diagnostic measure.

## Chapter 4

# Predicting the slow oscillation in blood pressure using nonlinear analysis of a model of baroreflex control of the peripheral resistance

### 4.1 Introduction

The idea that the slow oscillation in blood pressure may be used as a basis for a non-invasive, surrogate measure of autonomic function has resulted in the slow oscillation been enthusiastically researched (see Section 2.3). This research has generally used spectral analysis techniques to quantify the power in the frequency band of the slow oscillation in the cardiovascular signals, including heart rate and blood pressure. The strength of the slow oscillation has been reported to vary during different physiological conditions, including a range of pathophysiological conditions (Inoue 1991; Bigger 1992; Bigger 1992; Koh 1994; Teich 2000), during age and gender changes (Murata 1992; Ryan 1994; Taylor 1998; Barnett 1999), and during experimental interventions (Janssen 1997; Leonard 2000; Malpas 2000). These observed changes in the strength of the oscillation have stimulated much interest as quantification of these changes may offer vital information regarding the competence of neural control of

cardiovascular function in disease and other conditions. Variations in the strength of the slow oscillation are documented in Section 4.3.1.

Although the research into the changing strength of the slow oscillation has enabled much insight into cardiovascular function, the fundamental causes and effectors of the slow oscillation in blood pressure are still highly contentious (see Section 2.3.3). Of the theories that explain the origin of the slow oscillation in blood pressure, the baroreflex feedback theory has received most currency (see Section 2.3.3.2), and particularly the baroreflex control, via sympathetic pathways. This has led to a deluge of studies that have investigated the slow oscillation in blood pressure, by solely analysing sympathetic control of the vasculature and thereby ignoring the role of the heart in the development of the slow oscillation (see Section 2.3.3.3). As was introduced in Section 2.4, Ringwood and Malpas (Ringwood 2001) presented a nonlinear model to describe baroreflex control of the peripheral resistance, which produced a limit cycle oscillation at the frequency of the slow oscillation in blood pressure. The study documented in this chapter assumes this description of the baroreflex for the purpose of the forthcoming analysis. It is the aim of this work to explain how observed changes in the slow oscillation in blood pressure might result from changes in physiological conditions, which, in turn, cause variation in the modelled components of the baroreflex.

Changes in the strength of the slow oscillation have previously been proposed to reflect changes in the mean level of SNA and/or baroreflex gain. A number of studies have explored how the strength of the oscillation changes under different stimuli for which the mean level of SNA is observed to increase or decrease (Arai 1989; Houle 1999). However, a causal relationship between changes in mean SNA and changes in the strength of the slow oscillation has not been consistently reported. Results have also proven inconclusive for those who have attempted to explain changes in the strength of the slow oscillation by calculating the gain for specific sections of the baroreflex loop (Bertram 1998; Leonard 2000). These studies, and the associations made by the authors of these studies are reviewed in Section 4.3 of this chapter.

These studies have commonly attempted to relate the strength of the slow oscillation to individual aspects of the blood pressure control system. However, because of the closed-loop nature of the baroreflex, all components in the loop could (in theory) influence the strength of the oscillation. Specifically with reference to that part of the baroreflex under examination in this study, a change of gain either within the neural arc (*i.e.* a change in the gain of the baroreflex curve) or peripheral arc (*i.e.* vasculature) could influence the size of the oscillation (arc illustrated in Figure 2.1). Unfortunately, due to the nature of the SNA recordings, where the value of SNA is dependent on the number of fibers recruited (and hence, all SNA recordings are normalised), realistic *absolute* parameterisation of the model is not possible. Therefore, emphasis is put on the relative changes in the gains of the different elements of the feedback loop in an attempt to explain *changes* in the strength of the slow oscillation in blood pressure.

The main aim of this study is to quantify the impact of the different sections of the feedback loop proposed to be involved in the generation of the slow oscillation. The effect of a change in the curvature or the range of the baroreflex curve, and/or a change in the characteristics of the vasculature on the amplitude of the oscillation is examined. It is also pertinent to examine how a change in the mean level of SNA and/or blood pressure will cause a change in the amplitude of the oscillation due to a shift in the operating point away from the middle region of high slope of the baroreflex curve towards the saturation regions at the top and bottom of the curve, as has been previously observed (Barrett 2003). Specifically, it is proposed that it is the relative relationship between the changing characteristics of the baroreflex curve and the vasculature gain that is of importance when analysing the role of the peripheral resistance branch of the baroreflex loop, in the genesis and maintenance of the slow oscillation in blood pressure.

The baroreflex model, used for analysis of this hypothesis, is presented in Section 4.2.1 and the analysis approach is introduced in Section 4.2.2.

## 4.2 Modelling the baroreflex

The nonlinear feedback model proposed by Ringwood and Malpas (Ringwood 2001) was reviewed in Section 2.4.1. The model structure is illustrated in Figure 4.1. This model represents a reduced model of the baroreflex mechanism, as it includes only the sympathetic control of the vasculature and ignores the baroreflex control of the heart. Also, the model, as presented here, represents a uniform description of the sympathetic effects on the resistance of the vasculature and, as such, cannot represent different changes in resistance through different organs.

### 4.2.1 The nonlinear model

The reduced baroreflex model, shown in Figure 4.1, contains an amplitude-limiting nonlinear function describing the sigmoidal baroreflex curve  $s(x)$ , a first-order transfer function describing the dynamical nature of the vasculature  $G_v(s)$ , and delay terms both in the forward,  $G_d(s)$ , and feedback,  $H_d(s)$ , pathways that account for the conduction delay along the nerves (Figure 4.1).

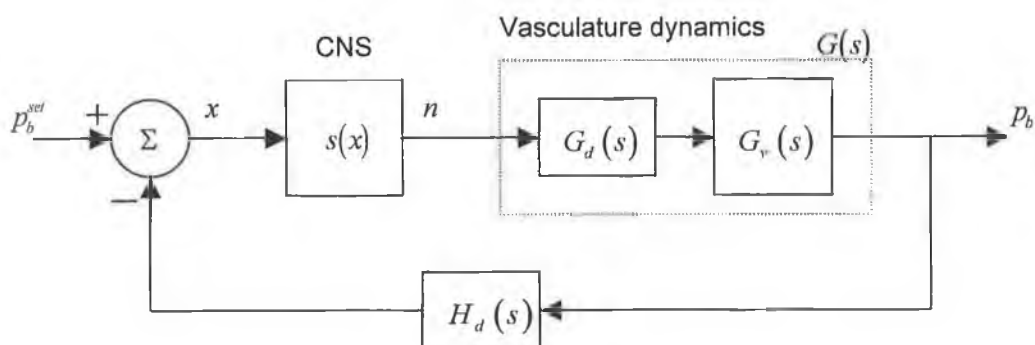


Figure 4.1: Components of the nonlinear feedback model proposed by Ringwood and Malpas (Ringwood 2001).

where,

$p_b$  is blood pressure,

$p_b^{set}$  is the blood pressure set point,

$x(t)$  is the input to the nonlinearity ( $x(t) = p_b^{set} - p_b(t)$ ), and

$n(t)$  represents the SNA signal.

$s(x)$ ,  $G_d(s)$ ,  $G_v(s)$  and  $H_d(s)$  are described by Equations (2.3), (2.6), (2.7) and (2.8) respectively and are further investigated in Section 4.2.2 and 4.2.3. The values of efferent and afferent delay are those chosen by Ringwood and Malpas (Ringwood 2001) ( $\tau_e = 0.7s$ ,  $\tau_a = 0.2s$ ) and are supported by the physiological literature (Burgess 1997; Guild 2001).

## 4.2.2 Analysis approach

The model illustrated in Figure 4.1 is used in this study to analyse the relative gain changes of the different sections of the baroreflex feedback loop. The slow oscillation in blood pressure is proposed to be a limit cycle oscillation, arising due to the presence of the nonlinear, sigmoid baroreflex curve, in the neural arc of the model. The frequency and amplitude of the oscillation can be calculated using Nyquist diagrams, when the ‘gain’ of the nonlinear element is represented by a linear, amplitude dependent ‘gain’ approximation, known as the describing function.

Hence, for the purposes of analysis of the limit cycle developed by the model of Figure 4.1, calculation of the describing function for the sigmoid nonlinearity and the gain of the linear dynamical part of the model at the frequency of oscillation is necessary.

However, the normalised nature of SNA introduces an impediment to the aims of this analysis, because absolute parameterisation of the model is not possible.

Therefore, only relative changes of the gain of the describing function and the linear dynamical parts can be analysed. Due to the fact that only relative movements of the gains can be assessed, the gain of the vasculature may be calculated at its steady state value, as long as relative movements of the steady state gain and the gain at the frequency of the oscillation are consistent. Knowledge of the vasculature gain, and the describing function 'gain', enable conclusions regarding the likelihood of the oscillation increasing or decreasing be drawn.

Descriptions and respective methods of gain calculation of the nonlinear baroreflex curves and the linear vascular dynamics are described in the subsequent sections.

### 4.2.3 The sigmoidal baroreflex curve

The nonlinear function,  $s(x)$ , in the forward path of the reduced model of the baroreflex presented in Figure 4.1 (page 118), describes the steady-state baroreflex curve that results when SNA is plotted for step changes in blood pressure (see Equation 2.3). Examples of the nonlinear baroreflex curves, between blood pressure and SNA, are shown in Figure 2.3 and Figure 2.11 for different physiological conditions and also in Figure 2.10, when the sigmoid function of Equation (2.3) is fitted (Marquardt 1963) to the curve. This function (Equation (2.3)) is used to represent the sigmoid by some authors (Ringwood 2001; Kinnane 2004). However, a modification of this representation is common in many physiological studies (Kent 1972; Dorward 1985; Head 1987; Weinstock 1988; Kingwell 1991), that have derived baroreflex curves. This description is given in Equation (4.1), and is usually written in terms of parameters that specify the upper and lower saturation values. Here, the equation is expressed in terms of the range,  $l$ , curvature,  $\beta$ , horizontal,  $x^*$ , and vertical,  $y^*$ , offset parameters depicted in Figure 2.10.

$$s_1(x) = (y^* + l) - \left( \frac{y^* + 2l}{1 + e^{\beta(x-x^*)}} \right) \quad (4.1)$$

The sigmoid may also be described using a hyperbolic tangent function (Seidel 1998; Eyal 2000). This representation of the sigmoid is described in Equation (4.2) for the parameters  $l, \beta, x^*$  and  $y^*$ .

$$s_2(x) = l \left( \tanh \left( \beta (x - x^*) \right) \right) + y^* \quad (4.2)$$

This hyperbolic tangent representation may also be described in exponential form as:

$$s_3(x) = l \left( \frac{e^{\beta(x-x^*)} - e^{-\beta(x-x^*)}}{e^{\beta(x-x^*)} + e^{-\beta(x-x^*)}} \right) + y^* \quad (4.3)$$

The fact that the hyperbolic tangent function, described by Equation (4.2), may be described in terms of exponential functions, is illustrated here, as this creates difficulties for developing an analytical describing function for this nonlinearity, as discussed in Section 4.2.3.2. The hyperbolic tangent function of Equation (4.2) is plotted in Figure 4.2, for a range of curvature ( $\beta$ ) values and for the same range ( $l$ ) and centre point ( $x^*, y^*$ ) as function Equation (2.3).

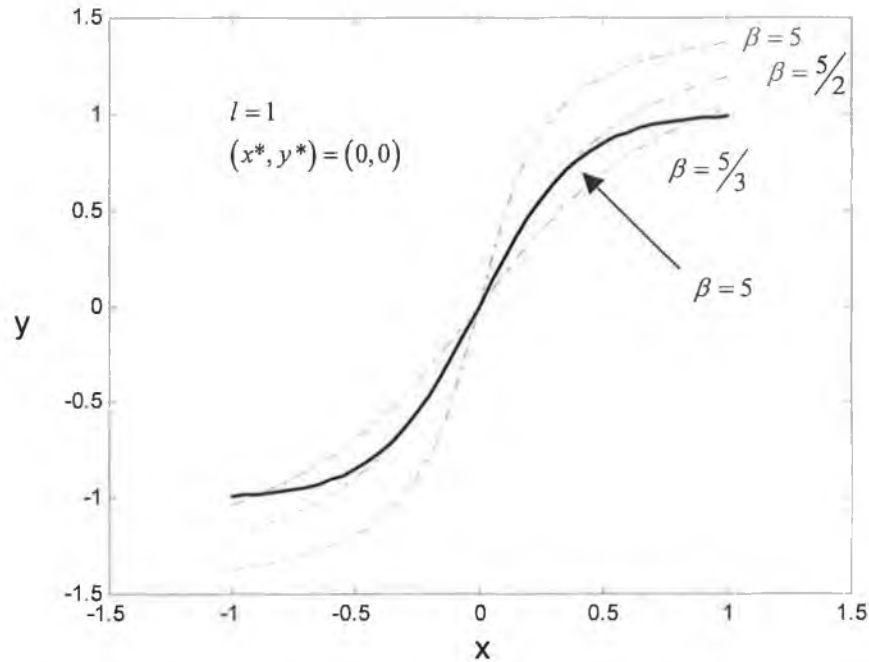


Figure 4.2: The hyperbolic tan description of the sigmoid given in Equation (4.2) (dashed lines) and the sigmoid function of Equation (2.3) (heavy line), plotted for different values of  $\beta$ .

The sigmoid description of Equation (2.3) enables a more accurate description of the baroreflex curves documented in the physiology literature than Equation (4.2) does, since the baroreflex curves documented in the literature are shown to saturate quickly at low and high blood pressures (see Figure 2.3 & 2.11), a characteristic difficult to capture by Equation (4.2).

The representations of the sigmoid given in Equations (2.3), (4.1), (4.2) and (4.3) assume a symmetry of the baroreflex curve. However, experimentally derived baroreflex curves are often asymmetrical (Malpas 1996; Barrett 2003). The original description of this asymmetry involved fitting two hyperbolas to the data of the baroreflex curve, thus enabling differential descriptions of the upper and lower curvature (Korner 1972).

In more recent years, Ricketts and Head (Ricketts 1999) investigated the suitability of a five-parameter function, that was formally fitted to the data of the baroreflex curves (Malpas 1996). This function includes a fifth parameter, so that the curvature at the top and bottom of the curves can be differently defined, so

that the asymmetrical nature of the baroreflex curve may be captured. This five-parameter function is:

$$s_4(x) = (y^* + l) + \frac{2l}{1 + f_x e^{\beta_{top}(x^* - x)} + (1 - f_x) e^{\beta_{bottom}(x^* - x)}} \quad (4.4)$$

where,

$$f_x = \frac{1}{1 + e^{-\bar{c}_f(x^* - x)}} \text{ and } \bar{c}_f = \frac{2\beta_{top}\beta_{bottom}}{|\beta_{top} + \beta_{bottom}|}$$

where,

$\beta_{top}$  describes the curvature of the sigmoid at the top of the curve, and

$\beta_{bottom}$  the curvature at the bottom of the curve.

However, this five-parameter curve only offers small improvements of fit over the four-parameter description of functions (2.3) and (4.1) (Ricketts 1999). This description of the sigmoid may be more suited to the blood pressure – heart rate baroreflex curve where dual neural pathways contribute to the shape of the curve at different ranges of the curve (see Figure 2.17).

An alternative five-parameter function, which does not explain asymmetry as a function of curvature, rather as an amplification of the response nonlinearly dependent on blood pressure, and an even more complex seven-parameter curve, which would require very high quality data and a large amount of data points are also reviewed by Ricketts and Head (Ricketts 1999).

A different representation, not based on exponential functions, was used by Abbiw-Jackson and Langford (Abbiw-Jackson 1998) to describe the sigmoidal baroreflex curve (the Hill function), of the form:

$$s_5(x) = \frac{x^n}{a^n + x^n} \quad (4.5)$$

and may be adjusted to include the range,  $l$ , and vertical,  $y^*$ , and horizontal,  $x^*$ , offsets:

$$s_6(x) = l \left( \frac{(x - x^*)^n}{(a - x^*)^n + (x - x^*)^n} \right) + y^* \quad (4.6)$$

where,

$n$  controls the slope of the function

$a$  is a constant midpoint term

The Hill function of Equation (4.6) is plotted in Figure 4.3 for increasing values of  $n$ . The sigmoid function of Equation (2.3) is also illustrated on this plot for comparison purposes. The Hill function is obviously asymmetrical for low values of  $n$  and only begins to resemble a symmetrical sigmoidal function for the higher values of  $n$  that are plotted. The Hill function therefore describes a discrete set of curves. Clearly, this description of the sigmoid does not allow for as much freedom of fit to the baroreflex curve data as the representation of Equation (2.3) does.

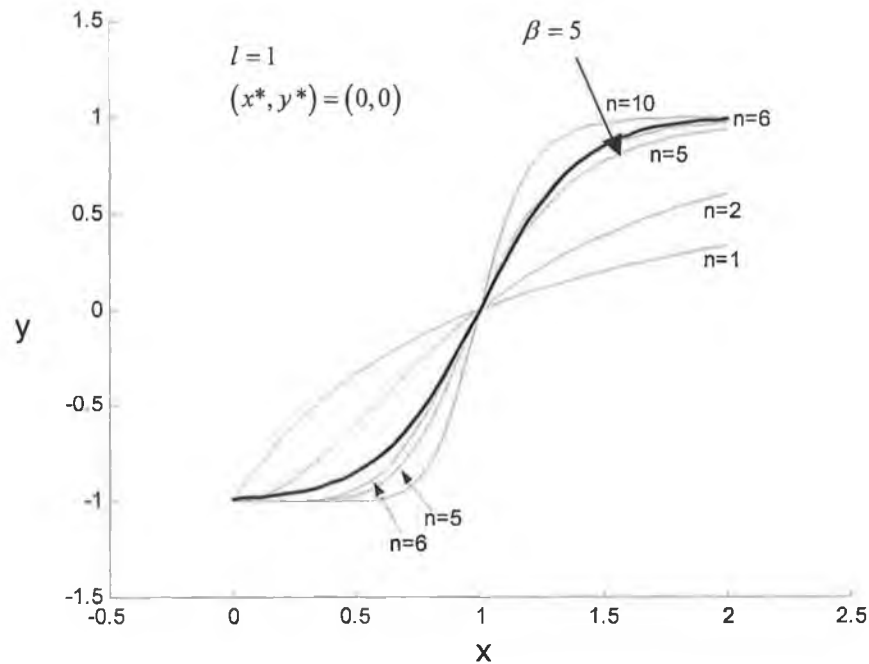


Figure 4.3: The Hill function description of the sigmoid given in Equation (4.6) (light lines) and the sigmoid function of Equation (2.3) (heavy line), plotted for different values of  $n$ .

The function description of the sigmoid described by Equation (2.3) is chosen for use in this study as it allows for accurate description of the sigmoid for any given

parameters and because it is simpler to deal with than the unnecessarily complex five-parameter function of Equation (4.4).

#### 4.2.3.1 The describing function

Frequency domain analysis is a powerful tool in the analysis of linear control systems. Frequency domain analysis cannot, however, be directly applied to nonlinear systems because frequency response functions cannot be defined for nonlinear systems. The describing function method enables the extension of linear frequency response analysis to the nonlinear case, by enabling an approximate gain and phase description of the nonlinearity. The method of describing function calculation is described in this section, followed by documentation of the development of the describing function for the sigmoid, in the subsequent sections.

The *sinusoidal input describing function* is the fundamental approximation that enables this analysis. Considering the system as illustrated in Figure 4.1, a nonlinear component,  $s(x)$ , is included in the forward path and the other blocks of the loop are described using the linear models,  $G_v(s)$ ,  $G_d(s)$  and  $H_d(s)$  (described by Equations (2.6), (2.7) and (2.8) respectively). It is assumed that if the system can exhibit a limit cycle, then the signal at  $x$  during limit cycle operation will approximate a sinusoid, given by Equation (4.7).

$$x(t) = M \sin(\omega t) \quad (4.7)$$

whose period,  $T$ , is defined as  $T = 2\pi/\omega$ .

The output of the nonlinearity is a periodic function that may be described using a Fourier series.

$$n(t) = \frac{A_0}{2} + \sum_{k=1}^{\infty} A_k \cos(k\omega t) + \sum_{k=1}^{\infty} B_k \sin(k\omega t) \quad (4.8)$$

where,

$$A_k = \frac{2}{T} \int_0^T n(t) \cos(k\omega t) dt \quad (4.9)$$

and,

$$B_k = \frac{2}{T} \int_0^T n(t) \sin(k\omega t) dt \quad (4.10)$$

The Fourier series expansion of  $n(t)$  may be also represented as,

$$n(t) = \frac{N_0}{2} + N_1 \sin(\omega t + \theta_1) + N_2 \sin(2\omega t + \theta_2) + \dots \quad (4.11)$$

where,  $N_1$  is the amplitude of the fundamental,  $N_2$  is the amplitude of the second harmonic and so on.  $\theta_1, \theta_2$ , and so on are the phase shifts at the various frequencies.  $N_0$  is the amplitude of the bias component, which is zero if attention is restricted to nonlinear elements whose characteristics exhibit odd symmetry about the origin.

Using only the fundamental component,  $n(t)$  is written as,

$$n(t) \approx N_1 \sin(\omega t + \theta_1) \quad (4.12)$$

or in terms of its Fourier components as,

$$n(t) \approx A_1 \cos(\omega t) + B_1 \sin(\omega t) \quad (4.13)$$

The describing function is defined as the ratio of the fundamental component of the output of the nonlinear element to the sinusoidal input to the nonlinear element, as given in phasor representation by Equation 4.14.

$$N(M, \omega) = \frac{N_1 \angle \theta_1}{M \angle 0} \quad (4.14)$$

where,

$$N_1 = \sqrt{(B_1^2 + A_1^2)} \quad (4.15)$$

and,

$$\theta_1 = \tan^{-1} \left( \frac{A_1}{B_1} \right) \quad (4.16)$$

Justification for assuming a sinusoid at  $x$  and for disregarding the higher harmonics of  $n(t)$  is based on anticipated conditions that will occur when the system is in steady state or limit cycle operation. The composition of the linear dynamical function  $G$  and  $H_d$  will display lowpass characteristics and, hence, all higher-order harmonics than the fundamental are assumed to be filtered out.

#### 4.2.3.2 Calculating the describing function for the sigmoid

Inherent to the method of describing function calculation documented in the previous section is the calculation of the integrals of Equations (4.9) and (4.10). When the input to the nonlinearity,  $s(x)$  (described by Equation (2.3)), is  $M \sin(\omega t)$  the output is  $s(M \sin(\omega t))$ . This can be expanded in a Fourier series expansion. For the sigmoid description of Equation (2.3) and assuming a sinusoidal input signal, the integrals of Equations (4.9) and (4.10) become:

$$A_1 = \frac{2}{T} \int_0^T \left[ \frac{l \cos(x)}{1 + e^{-\beta(M \sin(x) - x^*)}} - \frac{l \cos(x)}{1 + e^{\beta(M \sin(x) - x^*)}} + y^* \right] dx \quad (4.17)$$

$$B_1 = \frac{2}{T} \int_0^T \left[ \frac{l \sin(x)}{1 + e^{-\beta(M \sin(x) - x^*)}} - \frac{l \sin(x)}{1 + e^{\beta(M \sin(x) - x^*)}} + y^* \right] dx \quad (4.18)$$

The symmetrical sigmoid of Equation (2.3) introduces no phase to the signal. In the case where the output signal from the nonlinearity is in phase with the input signal,  $A_1 = 0$  in Equation (4.17) as there will only be sine terms (Dutton 1997).

Hence, the integral of Equation (4.18) remains to be calculated. However, no closed-form expression exists for this integral of (Holohan 2000).

Numerical integration methods (*e.g.* the trapezoidal method) may be used to compute the integral given in Equation (4.18), however, an analytical description of the describing function offers advantages over the numerical integration method of calculation. The describing function of the nonlinearity is inevitably dependent on the parameters of the original function. An analytical expression reveals the effect of varying these parameters, and hence, provides useful insight which numerical integration does not. In the context of this research, an analytical expression for the describing function is required to allow insight into how changes in the parameters of the nonlinearities of the system will effect changes in the strength of the slow (limit cycle) oscillation in blood pressure.

Holohan (Holohan 2000) introduced a method of describing function approximation developed for the example of the sigmoid. This method of approximation enables the calculation of an analytical representation of the describing function, which is accurate for very low amplitude values of the oscillation and enables accurate prediction of the limit cycle oscillation.

#### 4.2.3.3 An approximation to the describing function for the sigmoid

The method of approximation developed by Holohan (Holohan 2000) is based on the Taylor series expansion of the sigmoid function.

The proposed method involves expanding  $s(x)$  in a Taylor series expansion about  $x = x_0$  for a finite number of terms. Truncation of the Taylor series results in a finite polynomial approximation to  $s(x)$ , called  $\hat{s}_{TS}(x)$ , where,

$$\hat{s}_{TS}(x) = \sum_{k=1}^n \frac{s^{(k)}(x_0)}{k!} (x - x_0)^k \quad (4.19)$$

where,

$n$  is the number of terms of the Taylor series expansion, and,

$x_0$  is the point around which the sigmoid is centered.

The approximation was centered on a number of points  $x_0$ , away from the midpoint of the sigmoid, so as to approximate the sigmoid at different sections of its full range. This enabled analysis of how a shift in the operating point affects the role of the sigmoid nonlinearity in the development of a limit cycle oscillation.

In order to develop a describing function approximation for the sigmoid, the Taylor series expansion is developed for the sinusoidal input of Equation (4.7), by replacing  $x$  in Equation (4.19) by  $M \sin(\omega t)$ . When the input to the nonlinearity  $s(x)$  is  $M \sin(\omega t)$ , the output is  $s(M \sin(\omega t))$ . What results, for a finite number of terms of the Taylor series expansion, is an approximation to the Fourier series expansion of  $s(M \sin(\omega t))$ ,  $\hat{s}(M \sin(\omega t))$ .

Use of the trigonometric identities,

$$\begin{aligned}\sin^2(\omega t) &= \frac{1}{2} - \frac{1}{2} \cos(2\omega t) \\ \sin^3(\omega t) &= \frac{3}{4} \sin(\omega t) - \frac{3}{4} \sin(3\omega t) \\ \sin^4(\omega t) &= \frac{3}{8} - \frac{1}{2} \cos(2\omega t) + \frac{1}{8} \cos(4\omega t) \\ \sin^5(\omega t) &= \frac{5}{8} \sin(\omega t) - \frac{5}{16} \sin(3\omega t) + \frac{1}{16} \sin(5\omega t)\end{aligned}\tag{4.20}$$

allows the expansion to be written in terms of  $\sin(\omega t)$  and its higher harmonics  $\sin(k\omega t)$  and  $\cos(k\omega t)$ . Hence, what results is a trigonometric series representation of the output signal of the nonlinearity,  $n(t)$ , that resembles the Fourier trigonometric series (Holohan 2000).

As documented previously, describing function theory assumes that all harmonics are filtered out by the low-pass dynamics of the system. Similar to

what is described in Equation (4.14) the describing function developed using the Taylor series expansion,  $N_{TS}(M)$ , is then the coefficient of the fundamental divided by the amplitude of the input signal,  $M$ .

#### 4.2.4 The vascular dynamics

The frequency response dynamics of the different vascular beds are documented in Chapter 2. The dynamics of the different vasculature beds are most commonly characterised as the blood flow response to sympathetic stimulation (Stauss 1998; Stauss 1999; Bertram 2000; Guild 2001). The frequency response characteristics of renal, mesenteric and skin blood flow are also described in Chapter 2. The dynamical element in the model depicted in Figure 4.1 represents the dynamical response of blood pressure to SNA, rather than the response of blood flow to SNA. The section of the baroreflex between SNA and blood pressure has been termed the ‘peripheral arc’ of the baroreflex (Ikeda 1996; Kawada 1997). This relationship was described by Burgess *et al* (Burgess 1997) using a first-order differential equation. Petiot *et al* (Petiot 2001) recorded renal SNA and arterial blood pressure, and first and second order transfer functions have been fitted to this data (Chapuis 2004). Other authors have characterised the peripheral arc, between blood pressure and cardiac SNA, using a second-order low-pass filter (Ikeda 1996; Kawada 1997).

These frequency response characteristics are usually derived during normal control conditions and are generally not derived during periods of different physiological conditions and stresses. Of interest in this study is the change in the baroreflex loop gain at the frequency of the slow oscillation (*i.e.* in the region 0.3 Hz), during different physiological situations. Hence, system identification techniques are used to calculate the gain of the vasculature based on blood pressure and SNA data recorded during physiological conditions in which the strength of the slow oscillation has been observed to change (see Section 4.3.1). These system identification techniques are documented in the following section.

#### 4.2.4.1 ARX modelling of the vascular dynamics

The gain of the vasculature is calculated using system identification techniques. The vasculature is modelled using blood pressure and SNA data. The simplest multivariate model structure, based on the output data  $y(k)$  and on an exogenous variable time series  $u(k)$ , is the AutoRegressive with eXogenous variable (ARX) model (Ljung 1999) described by the following difference equation, in the delay operator  $q$ , as:

$$A(q)y(k) = B(q)u(k - n_k) + \varepsilon(k) \quad (4.21)$$

where,

$$A(q) = 1 + a_1q^{-1} + \dots + a_{n_a}q^{-n_a},$$

$$B(q) = b_0 + b_1q^{-1} + \dots + b_{n_b}q^{-n_b},$$

$\varepsilon(k)$  is a residual, which is to be minimized by the identification process

$n_k$  is the number of steps delay between  $u(\ )$  and  $y(\ )$ .

The transfer function is then:

$$F(q) = q^{-n_k} \frac{B(q)}{A(q)} \quad (4.22)$$

which may be represented in the z-domain as:

$$\frac{Y(z)}{U(z)} = F(z) = \frac{b_0 + b_1z^{-1} + \dots + b_{n_b}z^{-n_b}}{1 + a_1z^{-1} + \dots + a_{n_a}z^{-n_a}} z^{-n_k} \quad (4.23)$$

Before the system identification method may be implemented, the time series plots of  $u(k)$  and  $y(k)$  must be examined, to identify the characteristics of the data and to check for the presence of outliers, which may introduce erroneous results.

The identification of a model structure involves the selection of model order terms,  $n_a$  and  $n_b$ , and time-delay term  $n_k$ . Two different approaches are available for the calculation of these parameters, which define the model structure. One approach was developed by Box and Jenkins (Box 1976) based on auto- and cross- correlation function methods to calculate the parameters of the model and estimate its accuracy. The second approach involves the estimation of model quality for a number of different model structures ( $n_a, n_b$  and  $n_k$ ) and suitable quality criteria include Akaike's Information Theoretic Criterion (AIC) (Akaike 1973) or Rissanen's Minimum Description Length (MDL) criterion (Rissanen 1978).

However, in keeping with the low-order representations of the peripheral arc presented in the literature, a first-order model structure is chosen. It is also desirable that the model identified is parsimonious *i.e.* that it is developed with the smallest number of parameters required for an adequate representation of the time series. Also, only trends of gain changes are of interest in this study, hence high order choices for  $n_a$  and  $n_b$  which would enable more accurate fits to the data, are unnecessary and would unduly complicate this work. Hence,  $n_a$  is set equal to 1, and  $n_b$  to 0. Therefore, only the time delay  $n_k$  remains to be calculated.

The second approach to model structure estimation described above, involving a criterion function, is used to establish the delay,  $n_k$ . The data set is separated into two parts, one part to estimate  $n_k$  and the second part used to compute the criterion function. A loss function, which is a raw measure of model quality, may be defined as:

$$V = \frac{1}{N} \sum_{k=1}^N (\varepsilon(k))^2 \quad (4.24)$$

where,

$$\varepsilon(k) = y(k) - \hat{y}(k)$$

$\hat{y}(k)$  is the approximated signal

$N$  is the number of samples used in the calculation of the loss function.

The model structure, which results in the minimum value of the loss function, is selected, as it is the most accurate model structure. The loss function is also incorporated in other criterion functions, which also penalise model complexity. The AIC criterion (Akaike 1973) and the MDL criterion are described by Equations (4.25) and (4.26) respectively and are used in this study to estimate the time delay  $n_k$  for the ARX models.

$$AIC = \log(V) + \left(\frac{2d}{N}\right) \quad (4.25)$$

$$MDL = V \left(1 + \log(N) \frac{d}{N}\right) \quad (4.26)$$

where,

$V$  is the loss function,

$N$  is the number of samples used in the calculation of the loss function  
and,

$d$  is the number of parameters estimated in the model.

As described in Section 4.4, sampled data is available for the different physiological conditions analysed in this study. Hence,  $n_k$  is different for the different data sets but each accords well with the time delays documented in the literature (Burgess 1997; Guild 2001).

Following the choice of a suitable model structure, the parameters of the model *i.e.* the coefficients of the polynomial operators,  $(a_1, \dots, a_{n_a})$  and  $(b_1, \dots, b_{n_b})$ , must be estimated. The method of ordinary least squares is used to estimate these parameters.

The first-order ARX model, defining the relationship between blood pressure  $p_b(z)$  and sympathetic activity  $n(z)$ , has the form:

$$F(z) = \frac{p_b(z)}{n(z)} = \frac{b_0}{1 + a_1 z^{-1}} z^{-n_k} \quad (4.27)$$

The frequency response between the input and output data was calculated. Trends between the gain in the region of 0.3 Hz (the frequency of the slow oscillation) and the steady-state gain (gain at 0 frequency) varied consistently from the control situation to after intervention. Hence, for simplicity, steady-state gain values were calculated (by setting  $z=1$ ) and were used for comparison purposes.

### 4.3 The slow oscillation, mean SNA and baroreflex gain

Changes in the strength of the slow oscillation in blood pressure have been associated with changes in baroreflex gain (De Boer 1987; Bernardi 1994) and the mean level of SNA (Malpas 1998; Leonard 2000). The physiological conditions during which the strength of the slow oscillation in blood pressure, the baroreflex gain and the mean level of SNA are altered are discussed in the subsequent sections.

#### 4.3.1 Changes in the strength of the low-frequency oscillation during different physiological conditions

Changes in the strength of the slow oscillation in blood pressure were briefly introduced in Chapter 2. The 'strength' of the slow oscillation is usually characterised by the power in the frequency band of the slow oscillation or by the

amplitude of the slow oscillation. The power at the frequency of the slow oscillation has been used to classify congestive heart failure patients (Teich 2000) and to predict death after heart attack (Bigger 1992; Bigger 1992). The slow oscillation has been both, observed in (Koh 1994), and reported to disappear (Inoue 1991) in spinal cord injury patients.

A range of intervention studies have been undertaken specifically to alter the strength of the slow oscillation and changes in the strength of the slow oscillation, both in blood pressure and heart rate, have been observed during a range of these conditions. Increases in the strength of the slow oscillation in blood pressure are reported during air jet stress (Malpas 1998), haemorrhage (Malpas 2000) and hypoxia (Janssen 1997) in rabbits. In contrast the slow oscillation disappeared following blood volume expansion in rabbits (Leonard 2000) and remained unchanged during hypertension in rats (Stauss 1995). The strength of the slow oscillation increases with standing (Munakata 1999), during head up tilt (Taylor 1996) and during lower body negative pressure (Hamner 2001). A decrease in the strength of the slow oscillation in blood pressure was observed during exercise in the human (Arai 1989) and in the dog with healed myocardial infarctions (Houle 1999).

Gender related differences in the strength of the slow oscillation in blood pressure have also been reported. The slow oscillation in blood pressure and in SNA is reported to be lower in women than in men (Ryan 1994; Taylor 1998; Barnett 1999), although no change in the slow oscillation in heart rate is observed at this frequency (Murata 1992). The strength of the slow oscillation in blood pressure declines with age (Taylor 1998).

#### 4.3.2 Mean changes in SNA and the slow oscillation

Changes in the strength of the slow oscillation in blood pressure have often been associated with changes in the mean level of SNA. A number of authors have

explored how the strength of the slow oscillation changes under different stimuli, which increase or decrease the mean level of SNA.

Increases in the strength of the slow oscillation have been observed during certain stimuli that increase the mean level of SNA such as air jet stress, hypoxia and haemorrhage (Janssen 1997; Malpas 2000). However, more studies have reported a decrease in the strength of the slow oscillation when the mean level of SNA increases. The mean level of SNA is dramatically increased during exercise, however, the strength of the slow oscillation is decreased (Arai 1989; Houle 1999). In addition to these studies, other authors have reported experimental results which have weakened the hypothesis that the strength of the slow oscillation in blood pressure is indicative of the mean level of SNA (Saul 1990; Sleight 1995; Stauss 1995; Taylor 1998).

The point on the baroreflex curve, where the mean level of blood pressure and mean level of SNA intersect, may be termed the operating point, as variations in blood pressure and SNA will occur around this point. The effect of shifts in the operating point, due in part to shifts in SNA, are analysed in more detail in later sections of this chapter.

### 4.3.3 Changes in the characteristics of the baroreflex curves during different physiological conditions

The strength of the slow oscillation in blood pressure has also been proposed to be indicative of 'baroreflex gain' (De Boer 1987; Bernardi 1994). The baroreflex is often characterised by the baroreflex curve, and attempts have been (unsuccessfully) made to relate changes in the strength of the slow oscillation to changes in the gain of the baroreflex curve (Leonard 2000).

As was reviewed in Chapter 2, baroreflex curves, derived during a range of different physiological conditions, are available in the literature and a number of these have been documented in this thesis to date. However, baroreflex curves

are not documented for the majority of situations when the strength of the slow oscillation is altered, as invasive recordings of SNA are not always possible. These curves are generally only derived in animal subjects and, to date, only for a small range of physiological conditions.

Changes in the baroreflex curves observed during angiotensin II infusion and hypoxia were illustrated in Figures 2.3 and 2.11 respectively. Baroreflex curves have also been documented during blood volume expansion (Leonard 2000) and during nitric oxide blockade (Ramchandra 2003). Baroreflex curves are generally not documented during haemorrhage as it is not a steady-state condition and only one previous study (Burke 1988) has documented baroreflex curves for this condition, and this for a small number of rabbits ( $n=3$ ).

The parameters of the baroreflex curves, used for analysis in this study, are documented in Table 4.2 in the subsequent section.

## 4.4 Available data

The analysis of the model of baroreflex control of peripheral resistance is restricted to those conditions for which knowledge of the strength of the slow oscillation in blood pressure, knowledge of the changing baroreflex curve characteristics and availability of data for to calculate the changing gain of the vasculature component exist. Considering this, only the conditions of hypoxia, blood volume expansion and haemorrhage meet these criteria. Hence, the model is analysed for these three conditions.

Blood pressure and sympathetic nerve signals were recorded in New Zealand white rabbits by the physiologists of the Circulatory Control Laboratory at the Department of Physiology, University of Auckland, New Zealand. The University of Auckland, Animal Ethics Committee, previously approved all experiments

The model as presented in Figure 4.1 represents a uniform description of the sympathetic effects on the resistance of the vasculature and, as such, cannot represent different changes in resistance through different organs (Ninomiya 1971; Ninomiya 1976). It is proposed that SNA to a few key organs, including the kidney, may dominate in the development of the slow oscillation (Malpas 2002), and it has been shown that changes in the strength of the oscillation are heavily reliant on the sympathetic pathways to the kidney (Malpas 2000). Hence, considering this proposed significance of the renal vasculature, over other vasculature beds, it is apt that the sympathetic activity is recorded at the renal nerve, and hence, that it is the renal vascular dynamics that are modelled. The raw SNA signal was amplified 10,000 – 100,000 times, filtered between 50 – 5,000 Hz, full wave rectified, and integrated with a time constant of 20 ms. This integrated SNA signal is digitised at 500 Hz and this signal is used for analysis. SNA is presented in Table 4.2 and 4.3 in normalised units (n.u.). The maximum value of SNA during control is given the value of 100 n.u. Blood pressure was measured from a catheter inserted in a central ear artery. The blood pressure signal is also digitised at 500 Hz. A statistical analysis of the data is undertaken for each of the conditions analysed.

### *Statistical analysis*

The values of mean blood pressure, mean heart rate and mean SNA are documented in Table 4.1. Data is presented as mean  $\pm$  standard error. The significance of the difference between groups was assessed from the variance ratio:

$$F = (\text{between groups mean square error}) / (\text{within groups mean square error}).$$

This significance ratio was calculated between 10% O<sub>2</sub> hypoxia and normoxia (F1), between 10% O<sub>2</sub> + 3% CO<sub>2</sub> hypoxia and normoxia (F2), between blood volume expansion and control (F3), and between haemorrhage and control (F4).

These blood pressure and SNA signals were recorded during the three different physiological conditions, of hypoxia, haemorrhage and blood volume expansion.

Detailed descriptions of the animal preparation and conditions for each stimuli have been provided in previous publications (Malpas 1996; Leonard 2000; Malpas 2000). Summarised details are listed in the subsequent section.

#### *Physiological recordings*

- (1) Hypoxia (Malpas 1996); Data was collected before and during 10% O<sub>2</sub> hypoxia. Prior to hypoxia the box containing the rabbit was ventilated with normal air at a rate of 10 L.min<sup>-1</sup> for a 20-minute period. The perfused gas was then switched to 10% O<sub>2</sub> at the same rate for another 20-min period.
- (2) Blood volume expansion (Leonard 2000); Data was collected before, during and after blood volume expansion. A polygeline-electrolyte solution was then used to increase plasma volume (administered at body temperature at 1.5 ml.min<sup>-1</sup> kg<sup>-1</sup> for 15 minute).
- (3) Haemorrhage (Malpas 2000); after a control period blood was withdrawn using a constant withdrawal pump at a rate of 1.35 ml.kg<sup>-1</sup>.min<sup>-1</sup> for 20 minutes.

The values of mean blood pressure and SNA and the results of the statistical analysis of this data are presented in Table 4.1.

Physiological condition	Mean blood pressure (mmHg)	Heart rate (bpm)	SNA (n.u.)
Normoxia	84 ± 2	286 ± 8	38 ± 3
10% O <sub>2</sub> Hypoxia	82 ± 3	258 ± 11	55 ± 6
F1		*	*
Normoxia	84 ± 2	286 ± 8	38 ± 3
10% O <sub>2</sub> + 3% CO <sub>2</sub> Hypoxia	81 ± 3	242 ± 9	69 ± 7
F2		*	*
Control before BVE	71 ± 5	258 ± 21	45 ± 5
BVE	73 ± 4	262 ± 15	33 ± 5
F3			*
Control before haemorrhage	80 ± 2	270 ± 14	35 ± 5
Haemorrhage (15 <sup>th</sup> -20 <sup>th</sup> min)	57 ± 5	320 ± 20	68 ± 15
F4	*	*	*

Table 4.1: Mean values of blood pressure and SNA before and during hypoxia, before and after blood volume expansion (BVE) and before and during haemorrhage.

The averaged parameters of the baroreflex curves documented in the literature for the control condition before blood volume expansion (BVE) and hypoxia and during the two different conditions of hypoxia and after blood volume expansion are documented in Table 4.2. These baroreflex curves are used for analysis in this study.

	Control before BVE	After BVE	Normoxia	10% O <sub>2</sub> Hypoxia	10% O <sub>2</sub> + 3%CO <sub>2</sub> Hypoxia
Lower plateau ( $y - l$ )	32 ± 6	35 ± 6	11 ± 6	6 ± 4	16 ± 6
Upper plateau ( $y + l$ )	100 ± 0	116 ± 0	99 ± 0	151 ± 15	190 ± 0
Full range ( $2l$ )	68 ± 6	81 ± 6	88 ± 6	157 ± 6	177 ± 6
BP50	67 ± 7	67 ± 7	85 ± 7	83 ± 7	80 ± 7
Upper curvature ( $\beta_{top}$ )	-0.17 ± 0.03	-0.14 ± 0.03	-0.13 ± 0.03	-0.22 ± 0.03	-0.17 ± 0.04
Lower curvature ( $\beta_{bottom}$ )	-0.15 ± 0.06	-0.09 ± 0.06	-0.22 ± 0.06	-0.12 ± 0.06	-0.14 ± 0.02
Gain	-2.3 ± 0.5	-2.5 ± 0.5	-3.3 ± 1	-5 ± 1	-5.5 ± 0.9

Table 4.2: Baroreflex parameters describing blood pressure to renal SNA curves in rabbits before and after blood volume expansion (BVE) and before and during hypoxia.

### *Data preprocessing*

The digitised 500 Hz blood pressure and SNA data was available for the normoxia and 10% O<sub>2</sub> hypoxia conditions and for before and after blood volume expansion. The 500 Hz data contained a large portion of high frequency information, which was outside the range of interest. Furthermore, processes using this 500 Hz data were computationally very intensive. Therefore, the data was low-passed filtered and resampled to discard the unwanted high frequency information and to reduce the computer workload, respectively.

The data was resampled to 50 Hz to decrease the number of sample points. Then, following an investigation of filter types, orders and ripple parameters, an 8<sup>th</sup>-order Chebychev filter, with ripple parameter  $\varepsilon = 0.07$ , was chosen to low-pass filter the data. These filter parameters were chosen so as to maintain the ripple effect within 0.05 dB and to minimise the numerical problems that may result when high-order filters are used (Little 1992).

The data for the haemorrhage condition was available as a time series of blood pressure values that were previously averaged over the period of each cardiac cycle. The period of the cardiac cycle varies from beat to beat. Hence, the blood pressure values are averaged over unequally spaced time periods. Prior to the use of discrete time system identification tools, this data is interpolated to produce a time series of blood pressure and SNA data points that are equally spaced in time.

### *Cubic Spline Interpolation*

The data is interpolated using cubic spline interpolation methods.

Consider the data set  $x_i = \{x_1, x_2, \dots, x_n\}$ . The cubic spline method of interpolation uses a piecewise function of the form:

$$f(x) = \begin{cases} f_1(x) & \text{if } x_1 \leq x \leq x_2 \\ f_2(x) & \text{if } x_2 \leq x \leq x_3 \\ \vdots & \\ f_{n-1}(x) & \text{if } x_{n-1} \leq x \leq x_n \end{cases} \quad (4.14)$$

where,  $f_i$  is a third degree polynomial defined by:

$$f_i(x) = a_i(x - x_i)^3 + b_i(x - x_i)^2 + c_i(x - x_i) + d_i \quad (4.15)$$

for  $i = 1, 2, \dots, n-1$

The piecewise function  $f(x)$  will interpolate between all of the data points  $x_i$ . Equally spaced data points are calculated from this function fit to the data. Hence, what results are equally spaced data point sets, of blood pressure and SNA values.

The data, described in this section, is used to calculate the describing function and vascular gains, so that predictions may be made regarding the presence or absence of a limit cycle oscillation in blood pressure.

## 4.5 Prediction of limit cycle oscillations

Nonlinearity in a system may enable the system to exhibit a sustained, repetitive oscillation known as a limit cycle. It is proposed that the slow oscillation in blood pressure is a limit cycle that results from the inflective nature of the baroreflex curve contained in the model presented in Figure 4.1 (see Section 2.4.1). Variations in the characteristics of the nonlinearity and the gain of the vasculature can account for growth and decay of the slow oscillation and situations where the oscillation can disappear altogether. An analysis of the nonlinear model is presented in the subsequent section.

A practical approach to the analysis of nonlinear systems is to include the effects of the nonlinearity as accurately as is feasible in a linear systems analysis of the model. The describing function method, introduced in the subsequent sections, is one such method often used to analyse nonlinearities.

Referring to the block diagram of Figure 4.1, and replacing the nonlinear function by its describing function representation,  $N(M, \omega)$  the stability of the nonlinear closed-loop system depicted in Figure 4.1 can be analysed using Nyquist's criterion applied to the associated linear system shown in Figure 4.4 (Zak 2001).

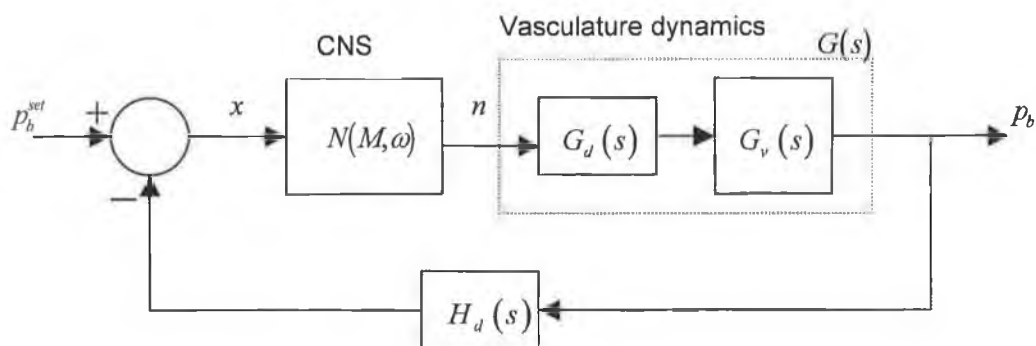


Figure 4.4: The associated linear system of Figure 4.1.

A linear systems approach produces the characteristic equation

$$1 + N(M, \omega)GH_d(j\omega) = 0 \quad (4.27)$$

or,

$$GH_d(j\omega) = -\frac{1}{N(M, \omega)} \quad (4.28)$$

If the nonlinearity is odd (as is the case for the sigmoids of Equations (2.3), (4.1) & (4.2)) the describing function is real and independent of the input frequency,  $\omega$ , in which case  $N(M, \omega)$  is reduced to  $N(M)$  (Slotine 1990).

When considering specific values of input amplitude,  $M$ , the Nyquist stability criterion is easily adapted to the nonlinear system analysis situation by

considering encirclements of the point  $-\frac{1}{N(M)}$  in the  $GH_d(j\omega)$  plane. However, when considering all oscillation amplitudes ( $0 < M < \infty$ ), the representation of  $-\frac{1}{N(M)}$  generates a locus in the  $GH_d(j\omega)$  plane. If the  $GH_d(j\omega)$  contour in the complex plane intersects the  $-\frac{1}{N(M)}$  locus, the intersection satisfies the condition for a sustained limit cycle oscillation. The amplitude and frequency of the limit cycle oscillation can be calculated at the intersection of the  $-\frac{1}{N(M)}$  locus and the  $GH_d(j\omega)$  curve, evident in the Nyquist diagram example in Figure 4.5.

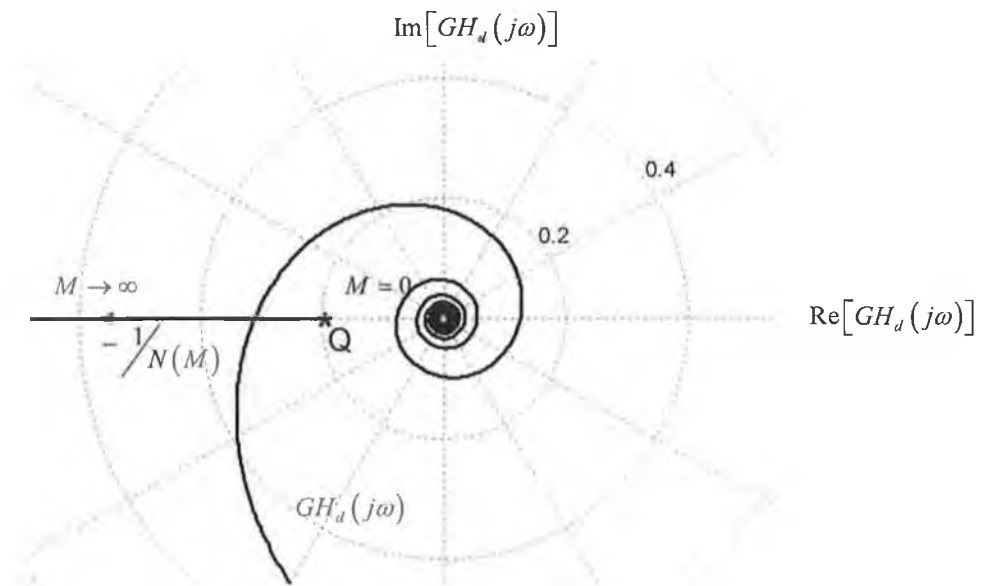


Figure 4.5: The  $-\frac{1}{N(M)}$  contour in the  $GH_d(j\omega)$ -plane of the Nyquist diagram.

The describing function approximation, based on the Taylor series expansion, is used in this study to predict the presence or absence of a limit cycle oscillation during different physiological conditions. As is described in Section 5.1.1, the describing function developed using the Taylor series expansion is only accurate for small values of limit cycle amplitude. However, for the purpose of this study

where prediction of the possible existence of the slow (limit cycle) oscillation this method of approximation suffices.

Therefore, the Q point, or point on the  $-\frac{1}{N(M)}$  locus at which  $M = 0$  (illustrated in Figure 4.5) may be calculated for the baroreflex parameters documented in Table 4.2.

## 4.6 Results

As indicated in the previous section, three stimuli (hypoxia, blood volume expansion and haemorrhage) were analysed to assess the validity of the model and hypothesis presented in this chapter. The results are presented for each of these conditions individually. Due to the fact that the analysis presented in this chapter is inherently based on the analysis of SNA and because SNA is available in normalised, integrated, and rectified values (Malpas 1996), as explained earlier, all results are presented in terms of relative changes, rather than absolute gain changes (see Limitations, Section 4.7).

### *Hypoxia*

Although the slow oscillation in blood pressure has been reported in the rabbit, during the resting, control condition, by a number of authors (Leonard 2000; Malpas 2000), Janssen *et al* (Janssen 1997) present a spectrum of blood pressure during control with no distinct peak in the region of 0.3 Hz. Again, no distinct slow oscillation in blood pressure was reported during 10% O<sub>2</sub> hypoxia (Janssen 1997). The slow oscillation, however, became evident during 10% O<sub>2</sub> + 3% CO<sub>2</sub> hypoxia (Janssen 1997).

A significant increase in the gain of the baroreflex curve ( $51\% \pm 25\%$ ) occurred from control to 10% O<sub>2</sub> hypoxia (Table 4.2). A further increase in the gain of the

baroreflex curve ( $66 \pm 25\%$  increase from control) was observed during 10% O<sub>2</sub> + 3% CO<sub>2</sub> hypoxia.

With regard to the baroreflex model of peripheral resistance, and the resulting describing function analysis, these increases in the gain of the baroreflex curve cause the Q point (initially Q\* in Figure 4.6) to shift to Q' and to Q. These shifts in the Q point will increase the likelihood of a limit cycle oscillation occurring as the likelihood of an intersection between the  $GH_d(j\omega)$ , and the  $-1/N(M)$  curve is increased. An example of such a shift in the Q point (Q\*  $\rightarrow$  Q'  $\rightarrow$  Q) is illustrated in Figure 4.6, for the changes documented in Table 4.3. For illustrative purposes, the  $GH_d(j\omega)$  curve is maintained constant in Figure 4.6.

$l$	$\beta$	Q
20	0.22	-0.45 (Q*)
30	0.22	-0.3 (Q')
44	0.22	-0.2 (Q)
20	0.5	-0.2

Table 4.3: Changing values of the Q point, for changing values of the range,  $l$ , (rows 1-3) and curvature,  $\beta$ , (row 4).

For the values presented in Table 4.3, the  $-1/N(M)$  locus begins at Q\* for the range and curvature values documented in the first line of Table 4.3. Q\* is to the left of the  $GH_d(j\omega)$  curve and hence no limit cycle oscillation results. An oscillation results for the  $l = 30$  and  $l = 40$  conditions of Table 4.3 as the Q' and Q points are on and inside the  $GH_d(j\omega)$  curve respectively.

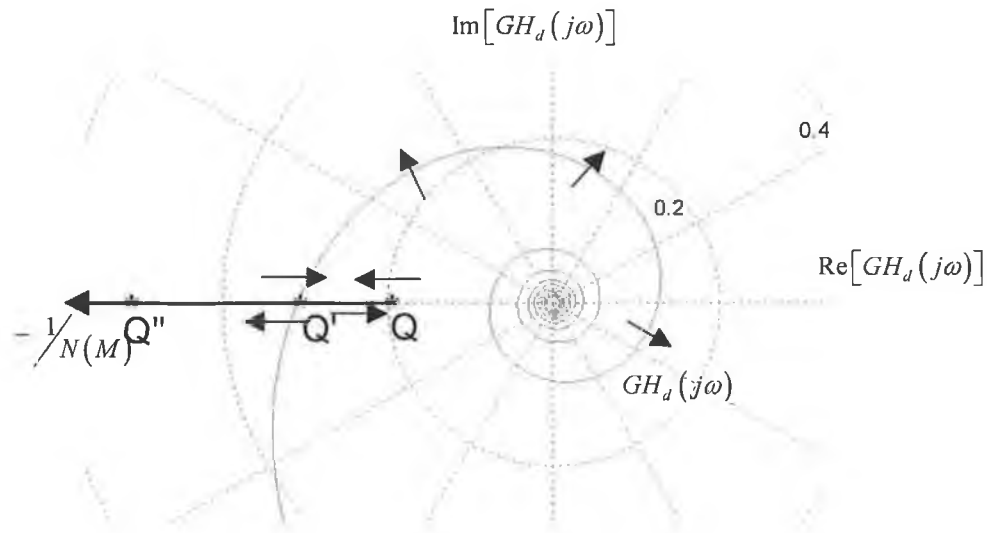


Figure 4.6: Illustration of the effects of a shift in the Q point on the Nyquist plot.

Steady-state vasculature gain decreased in all rabbits ( $n=6$ ) during 10%  $O_2$  hypoxia. An average 40% ( $\pm 30\%$ ) decrease in vasculature gain was calculated during 10%  $O_2$  hypoxia. If this change in gain is consistent at all frequencies, the  $G H_d(j\omega)$  curve to reduce to  $G H_d(j\omega)^*$ . The gains as calculated using the system identification techniques are documented in Table 4.4.

Rabbit	1	2	3	4	5	6
Gain (Control)	1.06	0.31	0.93	0.914	1.5	0.81
Gain (hypoxia)	0.73	0.16	0.4	0.45	1.02	0.6
% gain decrease	31%	48%	57%	51%	32%	26%

Table 4.4: Gains of the vasculature as calculated using ARX model.

This reduction in the  $G H_d(j\omega)$  curve is illustrated in Figure 4.7. For illustrative purposes, the  $-1/N(M)$  locus is maintained constant in Figure 4.7.

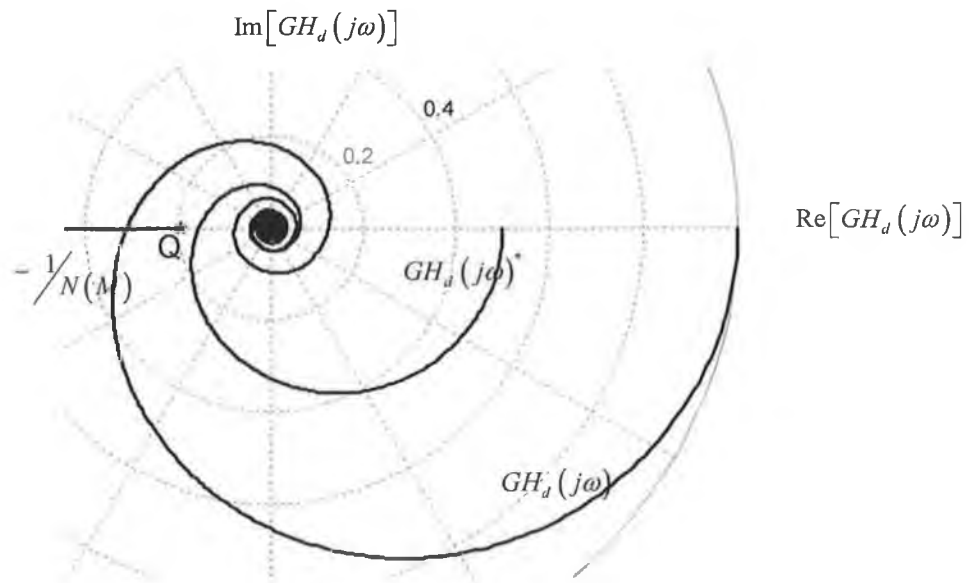


Figure 4.7: Illustration of the effects of a shift in the  $GH_d(j\omega)$  curve to  $GH_d(j\omega)^*$ , on the Nyquist plot.

When such a contraction of the  $GH_d(j\omega)$  curve occurs, no limit cycle oscillation will occur as the  $GH_d(j\omega)^*$  curve will be inside the  $Q^*$  point (for the condition of 10%  $O_2$  hypoxia) and, hence not intersect the  $-\frac{1}{N(M)}$  curve.

During both conditions of hypoxia the mean value of renal SNA increased causing the operating point to shift to a more central region of the baroreflex curve (see Table 4.1). This shift in the operating point is particularly evident during 10%  $O_2 + 3\%$   $CO_2$  hypoxia when the operating point lies in the region of high gain of the baroreflex curve. Movement of the operating point to the central inflection region of high gain significantly increases the likelihood of an oscillation occurring (see Section 2.4.1).

Table 4.5 documents how shifts in the,  $x_0$  coordinate of the, operating point  $(x_0, y_0)$ , away from the midpoint  $(x^*, y^*)$  of the baroreflex curve will shift the Q

point to a more negative value and thereby decrease the likelihood of the system limit cycling.

$x^*$	$x_0$	$Q$
85	95	-0.29
85	90	-0.25
85	85	-0.22

Table 4.5: Changing values of the blood pressure operating point verses the centre point for the baroreflex curve.

The effects of shifts in the operating point on the likelihood of an oscillation occurring are diagrammatically shown in Figure 4.8 for those shifts documented in Table 4.5. However, it needs to be emphasised that a shift in the operating point away from the central inflection region results in a lack of symmetry. Hence, the describing function will no longer be purely real and will instead contain an imaginary component. When illustrated on the Nyquist plot, the imaginary part will cause the  $-1/N(M)$  locus to shift off the real axis and cause a consequent change in the frequency of the oscillation, as the  $-1/N(M)$  curve will then intersect the  $GH_d(j\omega)$  contour at a different point above or below the real axis. For simplicity the  $-1/N(M)$  curve is illustrated on the real axis in Figure 4.8. Also, the  $GH_d(j\omega)$  curve is maintained constant in this example.

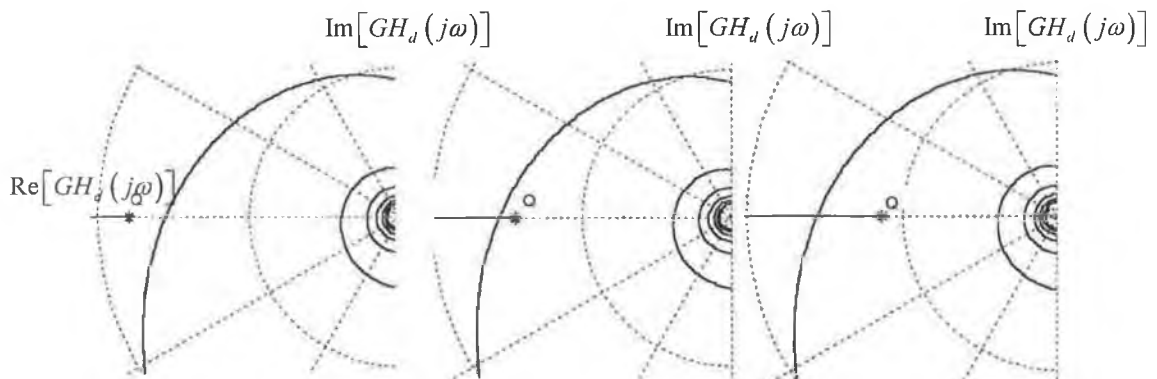


Figure 4.8: Illustration of the effects of a shift in the operating point away from the central inflection region of the baroreflex curve, on the Nyquist plot.

### *Blood volume expansion*

In the control condition, prior to blood volume expansion, a distinct peak was observed in most animals (4 of 5 rabbits) at  $0.3 \pm 0.02$  Hz (Leonard 2000). This peak was decreased significantly in rabbits that underwent blood volume expansion (Leonard 2000). After the rabbits had undergone blood volume expansion a slight increase in the gain of the baroreflex curve was observed ( $8 \pm 2\%$ ). However, most significant was that in the 5-min period following the end of blood volume expansion, renal SNA was  $75 \pm 5\%$  of renal SNA at the control level, whereas mean blood pressure remained constant. This resulted in a downward shift in the operating point to a region of lower gain and away from the central inflection region of the baroreflex curve. This downward shift in the operating point will decrease the likelihood of a limit cycle oscillation occurring as the operating region is now in a region of lower gain away from the operating point, and significantly out of the inflection region of the curve. The result of such a shift in the operating point can be seen on the Nyquist plot of Figure 4.8. The values of vasculature gain calculated for blood volume expansion were inconclusive; a significant decrease in vasculature gain was reported in 3 out of 5 rabbits. No change in vasculature gain is reported in one rabbit and the vasculature gain increases for the fifth rabbit.

### *Haemorrhage*

Baroreflex curves are not reported during haemorrhage, as it is not a steady-state condition (see Section 4.3.2.). The steady-state vasculature gain remains constant from control to the early stages of haemorrhage. However, a dramatic decrease in the vasculature gain from the early stages of haemorrhage to the later stages of haemorrhage is observed (>80% decrease). This decreases the likelihood of the limit cycle oscillation occurring. It is reported that the power in the 0.25–0.45 Hz range decreased during the later stages of haemorrhage (~23% decrease) (Malpas 1998; Malpas 2000).

## 4.7 Discussion

The main aim of this study was to use a model of baroreflex control of the peripheral resistance to analyse changes in the strength of the slow oscillation in blood pressure and to quantify the impact of the different sections of the feedback loop that may be responsible for these alterations in the slow oscillation.

It is to the detriment of this study that, of all the situations in which changes in the strength of the slow oscillation have been observed (see Section 4.3.1), SNA was recorded during only a few of these conditions. Hence, baroreflex curves and vascular dynamics are not documented during these physiological conditions, when alterations of the slow oscillation are observed. As such the analysis presented here in this chapter cannot be applied to these situations.

Also, because the open-loop vasculature dynamics are not documented in the literature for conditions other than the normal control condition, the gain characteristics of the vasculature were calculated only for those physiological conditions for which SNA and blood pressure data was available.

Considering these limitations the model was analysed only for three physiological conditions, hypoxia, haemorrhage and blood volume expansion. Baroreflex curve characteristics were documented in the physiology literature for the control situation and during hypoxia and blood volume expansion (see Table 4.2). System identification techniques were used to calculate the steady state gain of the vasculature, both in the control situation and post intervention. Hence, knowing the changes in the gain of the baroreflex curves and of the vasculature, it was possible to predict the likelihood of changes in the strength of the oscillation occurring. Unfortunately, due to the nature of the SNA signals, where the amplitude of the signal recorded is dependent on the number of fibers recruited and the contact between the nerve and the electrode, absolute values of

SNA cannot be consistently recorded. Therefore, the investigation is restricted to the analysis of trends of gain changes. However, knowing the relative changes in gains between the control and intervention cases, the likelihood of a change in the presence or strength of the oscillation can be predicted.

The importance of this relative relationship between the gain of the static nonlinear baroreflex curve and the steady-state gain of the vasculature is supported when the results of the studies by Malpas *et al* (Malpas 1996) and Janssen *et al* (Janssen 1997) are compared. Malpas *et al* (Malpas 1996) reported dramatic increases in the gain of the baroreflex curve during 10% O<sub>2</sub> hypoxia. However, Janssen *et al* (Janssen 1997) do not report an increase in the strength of the slow oscillation during this hypoxic condition, as might be expected considering the large increase in baroreflex gain. This disparity can be explained by the 50% decrease in vasculature gain, as calculated in this study. Hence, the increase in baroreflex gain is offset by a decrease in the vasculature gain thus, explaining the lack of an oscillation at 0.3 Hz during 10% O<sub>2</sub> hypoxia.

Janssen *et al* (Janssen 1997) do report a distinct peak at 0.3 Hz during the more severe hypoxic condition of 10% O<sub>2</sub> & 3% CO<sub>2</sub>. Unfortunately, data was not available for this hypoxic condition. However, we hypothesize that the increase in the strength of the oscillation at 0.3 Hz is due to the further increase in the gain of the baroreflex curve and to the shift of the operating point into the inflection region of the sigmoid curve. Also, it is predicted that there may be a smaller decrease in the vasculature gain, during this hypoxic condition due to an increase in tonic sympathetic activity, whereas blood pressure remains relatively constant (see Table 4.1). An increase in tonic SNA will cause an increase in vascular tone and hence, the gain may be lower for sympathetic stimulus.

Also it should be noted that variations in the levels of O<sub>2</sub> and CO<sub>2</sub> within the blood will activate the chemoreceptors (Malpas 1996). The chemoreceptors trigger the chemoreflex, which has ancillary effects on blood pressure and can modulate baroreflex function (see Sections 2.2.1 & 2.2.4). Malpas *et al* (Malpas 1996) proposed that the increase in SNA with the addition of CO<sub>2</sub> to the inspired gas may be responsible for producing a greater activation of the chemoreceptors.

Hence, analysis of the baroreflex control loop in isolation, during the hypoxic conditions, may not enable full analysis of the reflex mechanisms involved in the development (and abolition) of the slow oscillation in blood pressure.

Blood volume expansion is reported to cause a disappearance of the slow oscillation in blood pressure (Leonard 2000). After the rabbits have undergone blood volume expansion, renal SNA was reported to be decreased by 25% from the control level, whereas mean arterial pressure remained at the control level. This change caused a vertical downward shift in the operating point, to the region of lower gain, as reported by Leonard *et al* (Leonard 2000). Such a shift in the operating point out of the inflection region coupled with a decrease in gain in the region of operation will result in a decrease in the strength of the slow oscillation. However, following the hypothesis presented in this study, the full picture of the likelihood of an oscillation occurring can only be formed if vasculature gain changes are examined in tandem with changes in the baroreflex gain. Changes in the vasculature gain were not consistent, although, of the 5 rabbits analysed in this study, 3 recorded a dramatic decrease in vasculature gain. No slow oscillation is observed in any of the rabbits following blood volume expansion. Leonard *et al* (Leonard 2000) could not explain this result by analysis of the baroreflex curve alone. Hence, rather than using changes in one component of the loop as a marker of changes in the strength of the oscillation, an analysis of the gains of the relative components offers a more accurate means of prediction of the change in the strength of the oscillation.

Similar to the case for the hypoxic condition where the chemoreflex is activated depending on the level of CO<sub>2</sub> administered, the cardiopulmonary reflex may be activated following blood volume expansion (Leonard 2000). If activated, this reflex will modulate the baroreflex mechanism and, may affect the slow oscillation in blood pressure, and it has been proposed that it may even cause its abolition (Malpas 2002).

Of the intervention studies that have been used in this analysis, changes in the strength of the slow oscillation in blood pressure are probably most evident during haemorrhage (Malpas 2000). However, baroreflex curves are not

developed for the haemorrhage condition (see Section 4.3.3). The steady-state vasculature gain remains constant from control to the early stages of haemorrhage. However, during the later stages of haemorrhage, a dramatic decrease in vasculature gain is observed. Hence, the likelihood of the limit cycle oscillation occurring is decreased. In support of this, studies which have quantified the power in different frequency bands during haemorrhage reported (Malpas 1998; Malpas 2000) a decrease in power in the 0.2 to 0.4 Hz range during the later stages of haemorrhage, following an obvious increase during the first 10 minutes.

Shifts in the operating point are reported in a number of different studies, which documented baroreflex curves during various stimuli. Barrett *et al* (Barrett 2003), in a recent study that measured baroreflex curves for animals undergoing angiotensin II infusion, report a shift in the operating point from the region of high gain in the middle of the curve to a region of low gain at the bottom of the curve. Spectral analysis of the blood pressure signals, before and after angiotensin II infusion, results in no evidence of an oscillation in the later situation, as would be expected from the nonlinear analysis proposed in this study. However, no consistent peak was observed in the spectrum of blood pressure recorded during the control case, prior to angiotensin II infusion.

Most models of the baroreflex control of blood pressure assume operation in the central region of the sigmoid curve (Ursino 2003). However, many physiological studies report the presence of the operating point outside of the central region of the sigmoid (Malpas 1996; Barrett 2003). The results of this study show that knowledge of the operating point position is vital to the prediction of the strength of the slow oscillation in blood pressure, and specifically that shifts in the operating point away from the inflection region will decrease the likelihood of the slow oscillation in blood pressure occurring.

An increase in the available physiological results regarding changes in the strength of the slow oscillation along with an increase in the documented characteristics of the components of the baroreflex loop during different stimuli

would allow further exploitation and development of the analysis presented in this study.

### *Limitations*

The limitations presented by the nature of the SNA recordings are commented on throughout the text of this chapter. However, these difficulties are inherent to physiological experimental studies, where the level of recorded SNA is dependent on the number of nerve fibers recruited, and also to the methods of quantification of nerve activity.

The baroreflex control of the heart rate was not analyzed in this study. Although, as reviewed in Section 2.3.3.3, evidence exists to suggest that the heart is not involved in the generation of the slow oscillation in blood pressure (Liu 2002), it at least plays a role in maintaining gain (Liu 2002). The role of the heart in the genesis of the slow oscillation in blood pressure is analysed in greater detail in Chapters 6 and 7 of this thesis.

The model used for investigation in this study does not enable analysis of the compound influences of the different reflex mechanisms involved in the short-term control of blood pressure such as the chemoreflex and cardiopulmonary reflex. As discussed, these reflex mechanisms may be of particular importance during the physiological conditions under analysis in this study.

The investigation of the three physiological conditions was further limited by the lack of data (particularly for the 10% O<sub>2</sub> + 3% CO<sub>2</sub> hypoxic condition), the limited number of rabbits (for the blood volume expansion condition) and the lack of definitive baroreflex curve characteristics (for the hemorrhage condition). A larger compilation of these would enable more in-depth analysis of the hypothesis presented in this study and even enable the employment of this hypothesis for the analysis to the individual subject.

## 4.8 Conclusions

In summary, it is concluded that the strength of the slow oscillation in blood pressure can be related to changes in the baroreflex curve *and* to changes in the vasculature characteristics. However, it is also accepted that such a simple model and analysis of the baroreflex system may not enable definitive conclusions be drawn regarding aspects of cardiovascular function specifically responsible for the slow oscillation in blood pressure, as other mechanisms and effectors of blood pressure control are not described by this model.

The point that is emphasized, following analysis of this model, is that it is the relative relationship between the gains around the baroreflex loop that is of importance when analysing the conditions necessary for the existence or maintenance of the slow oscillation in blood pressure. However, there is a paucity of documented characteristics available in the literature and a paucity of data available with which the analysis based on this relative relationship may be investigated.

It is proposed that this method of analysis enables a somewhat crude prediction of the strength of the slow oscillation in blood pressure and does offer insight into the components of the baroreflex system that are responsible for the genesis and alteration of the slow oscillation in blood pressure. For these reasons, it is proposed that this analysis furthers the quest for a diagnostic test based on cardiovascular variability.

## Chapter 5

# Developing the describing function approximation

### 5.1 Introduction

A method of describing function approximation (Holohan 2000) was introduced in the previous chapter (Section 4.2.3.1). An approximation is required so that a closed-form analytical expression for the describing function may be developed. As discussed in Chapter 4 (Section 4.2.3.2), this analytical expression allows greater insight into how changes in the parameters of the nonlinearity affect the describing function of the nonlinearity.

However, the method of describing function approximation, introduced in the previous chapter, has a number of shortcomings. In this chapter, a new method of describing function approximation is introduced, which overcomes a number of these deficiencies.

### 5.1.1 The case for a new describing function approximation

The describing function approximation method introduced in the previous chapter was used, with success, to predict the possible occurrence of a limit cycle oscillation. It was specifically used to predict a limit cycle oscillation in blood pressure during different physiological conditions during which the oscillation is present (Janssen 1997) and during which the oscillation disappears (Leonard 2000).

However, although the presence or absence of the oscillation may be predicted using this method of describing function approximation, accurate prediction of the amplitude of the limit cycle oscillation is unachievable, as the approximation is only accurate for very small values of oscillation amplitude. Although, the amplitude of the oscillation is small for the rabbit ( $\sim 10$  mmHg) (Malpas 2000), the amplitude increases during different physiological conditions (see Section 4.3.1), and hence may be greater than the range of approximation of the sigmoid. Also the operating point has been reported to exist in different sections of the baroreflex curve during different physiological conditions (see Section 4.3.2). Knowledge of the position of the operating point would, therefore be necessary, so that the sigmoid may be approximated at different points on the sigmoid. An approximation capable of describing the full range of the sigmoid would overcome this problem.

The Taylor series approximation of the sigmoid ( $\hat{s}_{TS}(x)$ ), for 6 terms of the Taylor series is illustrated in Figure 5.1. As is evident from the plot, the approximation of the sigmoid, developed using the Taylor series, is unable to accurately approximate the sigmoid over its full range.

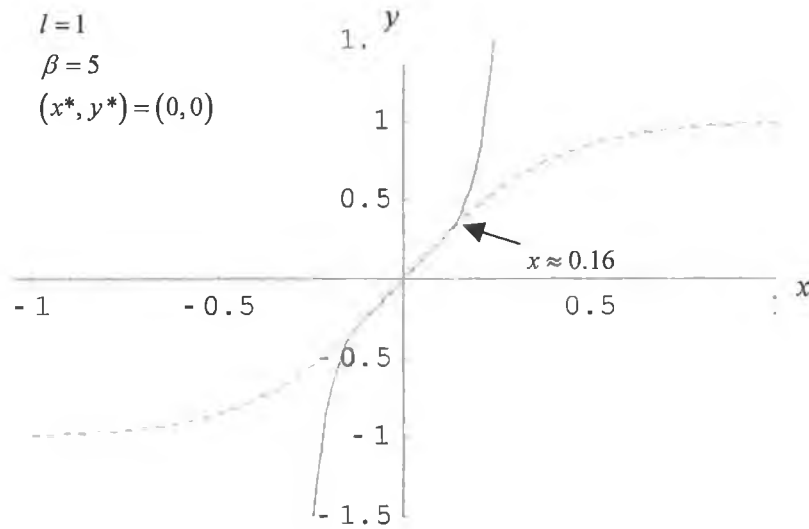


Figure 5.1: The sigmoid (thin line) and the approximation of the sigmoid for 6 terms of the Taylor series expansion (thick line).

The inaccuracy of the sigmoid approximation affects the accuracy of the describing function approximation calculated using the Taylor series expansion. The describing function gain calculated using this approximation method ( $N_{TS}(M)$ ) is compared with the precise describing function approximation to the sigmoid calculated using numerical integration methods ( $N_{NI}(M)$ ) in Figure 5.2.

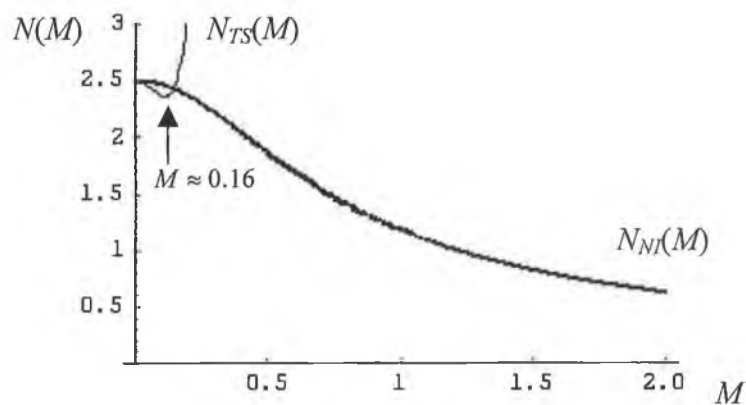


Figure 5.2: The describing function gains calculated using the Taylor series approximation method,  $N_{TS}(M)$ , and using numerical integration,  $N_{NI}(M)$ , calculated for the parameters of

Figure 5.1

The describing function approximation,  $N_{TS}(M)$ , accurately approximates the exact describing function,  $N_M(M)$ , only for very small values of oscillation amplitude ( $M$ ) but quickly loses accuracy as the limit cycle amplitude increases. This inaccuracy is also evident when the describing function is incorporated with the Nyquist stability diagram.

As was described in Section 4.5, when considering all possible limit cycle oscillation amplitudes ( $0 < M < \infty$ ), the representation of  $-1/N(M)$  generates a locus in the  $GH_d(j\omega)$  plane of the Nyquist diagram. If the  $GH_d(j\omega)$  contour in the complex plane intersects the  $-1/N(M)$  locus, the intersection satisfies the condition for a sustained limit cycle oscillation and the intersection point defines values of frequency (from  $GH_d(j\omega)$ ) and amplitude (from  $-1/N(M)$ ) for this limit cycle oscillation (Lewis 1997).

However, using the describing function approximation based on the Taylor series expansion of the sigmoid the  $-1/N_{TS}(M)$  curve produces erroneous results outside the range of accuracy of the sigmoid approximation. Outside this range the  $-1/N_{TS}(M)$  curve doubles back and increases in the opposite direction for increasing values of the limit cycle amplitude,  $M$ , as shown in Figure 5.3.

Hence, this approximation only enables prediction of a limit cycle and accurate calculation of the amplitude and frequency of this limit cycle for a very small range of oscillation amplitudes ( $M \leq 0.16$ ). Considering this, alternative methods of describing function approximation were considered.

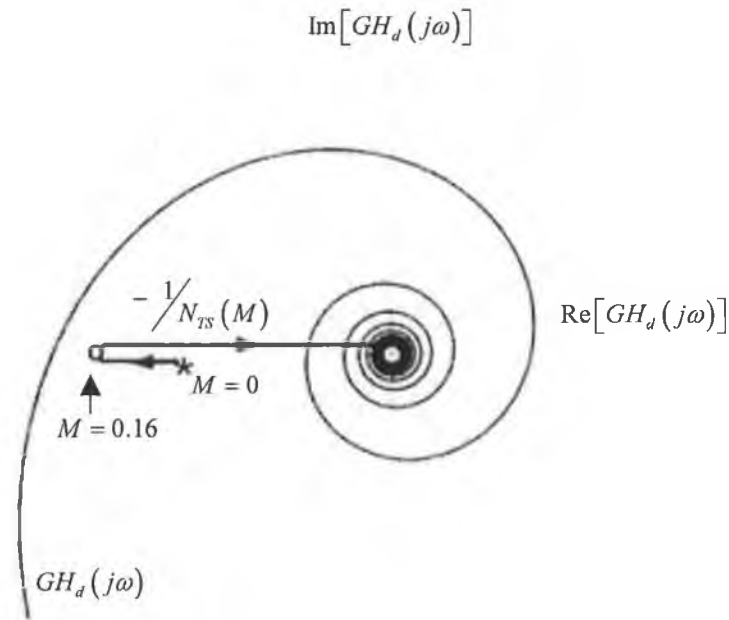


Figure 5.3: Nyquist plot showing the  $GH_d(j\omega)$  curve given by Equation 4.1 and the

$-1/N_{TS}(M)$  locus developed using the Taylor series expansion method.

## 5.2 A new approximation to the describing function

A number of different techniques for the development of the describing function approximation were investigated. The suitability of wavelets for the development of a describing function approximation was examined. However, the approximation procedure results in complicated integrals, for which a closed-form expression cannot be calculated, similar to the case for the Fourier integrals (see Section 4.2.3.2).

The suitability of cubic spline functions, for the development of the describing function approximation of the sigmoid, was examined. Cubic spline functions are

generally used to fit a cubic equation to a data set. However, the aim of this study was to develop an analytical approximation to the sigmoid in terms of the parameters of the sigmoid  $(l, \beta, x^*, y^*)$ , but the cubic spline fit bears no direct relationship to these parameters. Hence, the transparency of the parameters of the sigmoid is not preserved and insight into the effect of variation of these parameters on the describing function is lost.

Considering the limitations of these methods, for the aim of this study, the use of orthogonal polynomials (Szegő 1975; Axler 1997) as a basis set for a polynomial approximation of the sigmoid was investigated.

### 5.2.1 Orthogonal polynomial approximation methods

Various types of orthogonal polynomials exist, including the Legendre, Laguerre and Chebychev polynomials of first and second kind. The development of a polynomial that approximates the sigmoid, and hence enables the development of an analytical describing function, was developed using these polynomial sets. The method of polynomial approximation is first described.

Let the weight function,  $w$ , be a positive function on  $[a, b] \subset \mathbb{R}$ .

Let

$$L^2([a, b], w) = \left\{ f : [a, b] \rightarrow \mathbb{C} : \int_a^b |f(x)|^2 w(x) dx < \infty \right\} \quad (5.1)$$

$L^2([a, b], w)$  is an inner product space (Axler 1997) with inner product

$$\langle f | g \rangle = \int_a^b f(x) \bar{g}(x) w(x) dx \quad (5.2)$$

Let  $\{e_n\}$  be an orthonormal basis for  $L^2([a, b], w)$ , and let  $U_N$  be the finite dimensional subspace of  $L^2([a, b], w)$  spanned by  $\{e_1, \dots, e_n\}$ .

Then, given a function  $f \in L^2([a, b], w)$  the element  $\hat{f} \in U_N$ , such that

$\int_a^b |f(x) - \hat{f}(x)|^2 w(x) dx$  is minimised, is the orthogonal projection

$$P_{U_N} f = \hat{f} = \sum_{n=1}^N \langle f | e_n \rangle e_n \text{ of } f \text{ onto } U_N.$$

The polynomial approximation of the sigmoid is developed for the Legendre, and Chebychev polynomials of the first and second kind. The Laguerre polynomials are defined over the range  $[0, \infty]$ , and therefore are not suited to the example of the symmetrical sigmoid (defined in the range  $[-1, 1]$  in this example).

Let  $U_6$  be the finite dimensional subspace of  $L^2[-1, 1]$  spanned by the first 6 orthonormal polynomials. The first six Legendre polynomials are:

$$\begin{aligned} e_0(x) &= \frac{1}{\sqrt{2}} \\ e_1(x) &= \sqrt{\frac{3}{2}}x \\ e_2(x) &= \sqrt{\frac{5}{2}}\left(\frac{3}{2}x^2 - \frac{1}{2}\right) \\ e_3(x) &= \sqrt{\frac{7}{2}}\left(\frac{5}{2}x^3 - \frac{3}{2}x\right) \\ e_4(x) &= \sqrt{\frac{9}{2}}\left(\frac{3}{8} - \frac{15}{4}x^2 + \frac{35}{8}x^4\right) \\ e_5(x) &= \sqrt{\frac{11}{2}}\left(\frac{15}{8}x - \frac{35}{4}x^3 + \frac{63}{8}x^5\right) \end{aligned} \tag{5.3}$$

The orthonormal Legendre polynomials, that span the subspace  $L^2[-1, 1]$ , are shown in Figure 5.4.

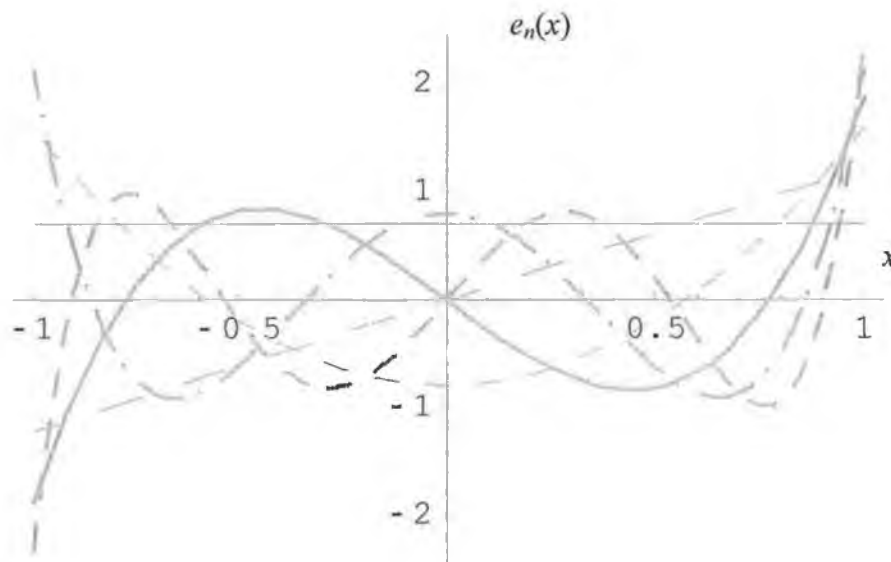


Figure 5.4: The first 6 Legendre polynomials defined over the range  $[-1, 1]$ .

The Chebyshev polynomials of the first kind ( $t_n(x)$ ) are defined over the range  $[-1, 1]$  and are weighted by the function  $w(x) = (1-x^2)^{-1/2}$  (Kreyszig 1999). The first six Chebyshev polynomials, of the first kind, are:

$$\begin{aligned}
 t_0(x) &= 1 \\
 t_1(x) &= x \\
 t_2(x) &= 2x^2 - 1 \\
 t_3(x) &= 4x^3 - 3x \\
 t_4(x) &= 8x^4 - 8x^2 + 1 \\
 t_5(x) &= 16x^5 - 20x^3 + 5x
 \end{aligned}
 \tag{5.4}$$

The Chebyshev polynomials of the second kind ( $u_n(x)$ ) are defined over the range  $[-1, 1]$  and are weighted by the function  $w(x) = \sqrt{1-x^2}$  (Kreyszig 1999). The first six Chebyshev polynomials, of the second kind, are:

$$\begin{aligned}
 u_0(x) &= 1 \\
 u_1(x) &= 2x \\
 u_2(x) &= 4x^2 - 1 \\
 u_3(x) &= 8x^3 - 4x \\
 u_4(x) &= 16x^4 - 12x^2 + 1 \\
 u_5(x) &= 32x^5 - 32x^3 + 6x
 \end{aligned}
 \tag{5.5}$$

The first 6 Chebychev polynomials of the first and second kinds are illustrated in Figure 5.5.

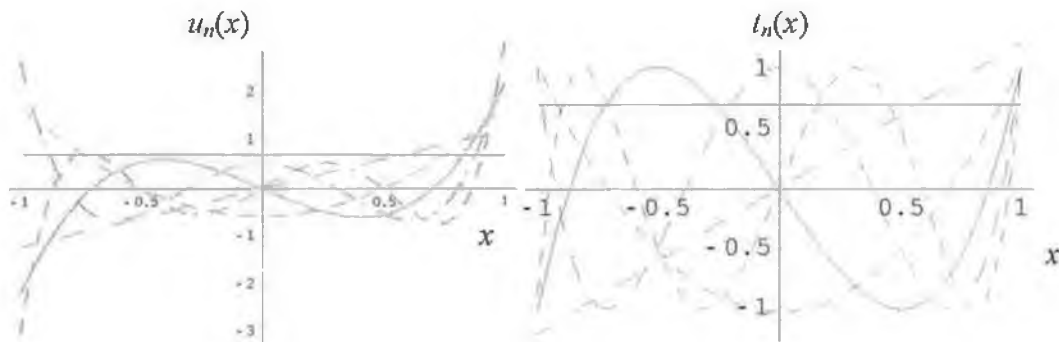


Figure 5.5: The first six Chebychev polynomials (left) of the first kind (right) of the second kind.

The weighting functions for the polynomials are shown in Figure 5.6:

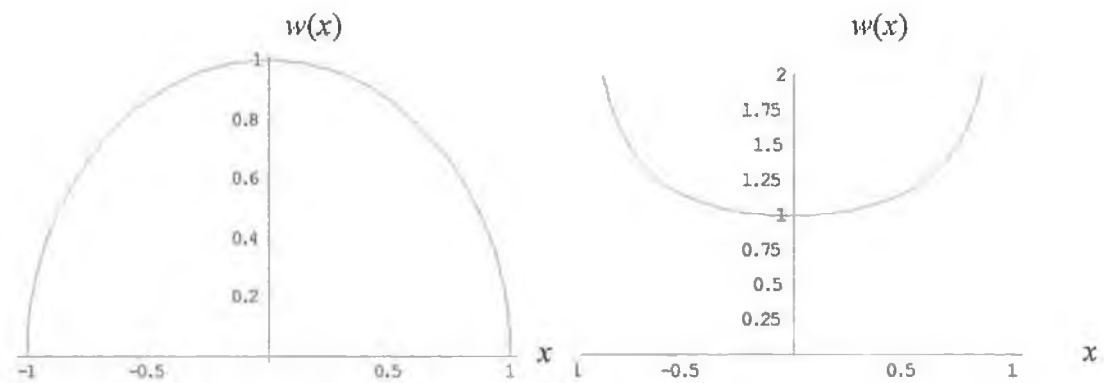


Figure 5.6: The weighting functions of the (left) first kind and (right) second kind of Chebychev polynomials.

The sigmoid,  $s(x) \in L^2[-1,1]$ , described by Equation (2.3), is approximated by

$$P_u s = \sum_{n=1}^6 \langle s | e_n \rangle e_n \in U_6 \quad (5.6)$$

with minimal  $L^2[-1,1]$  error, *i.e.*

$$\int_a^b |s(x) - P_u s(x)|^2 dx = \min \int_a^b |s(x) - \hat{s}_{LP}(x)|^2 dx$$

The sigmoid  $s(x)$  and the approximation of the sigmoid, using the first 6 Legendre polynomials  $\hat{s}_{LP}(x)$ , which have a weighting function,  $w(x) = 1$ , are shown in Figure 5.7.

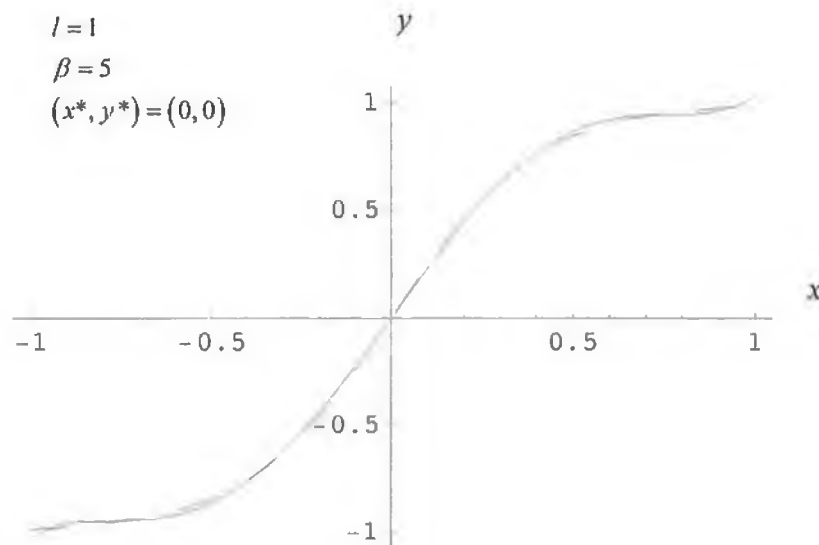


Figure 5.7: The sigmoid (dashed line) and the approximation of the sigmoid for 6 terms of the Legendre polynomial expansion (full line).

The sigmoid and the residual error between the sigmoid and the sigmoid approximation,  $\hat{s}_{LP}(x)$ , are shown in Figure 5.8.

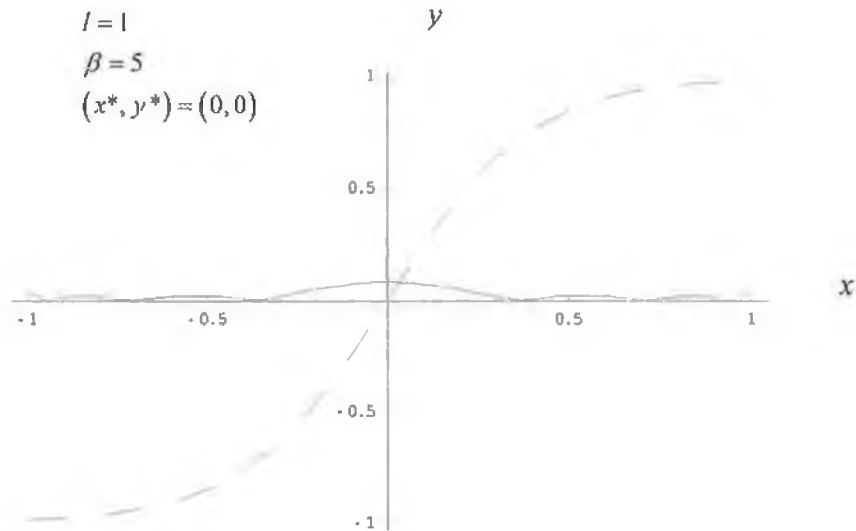


Figure 5.8: The sigmoid (dashed line) and the residual error of the sigmoid and the Legendre polynomial expansion (full line)

The sigmoid  $s(x)$  and the approximation of the sigmoid, using the first 6 Chebychev polynomials of the first  $\hat{s}_{CT}(x)$  and second  $\hat{s}_{CU}(x)$  kind are shown in Figure 5.9.

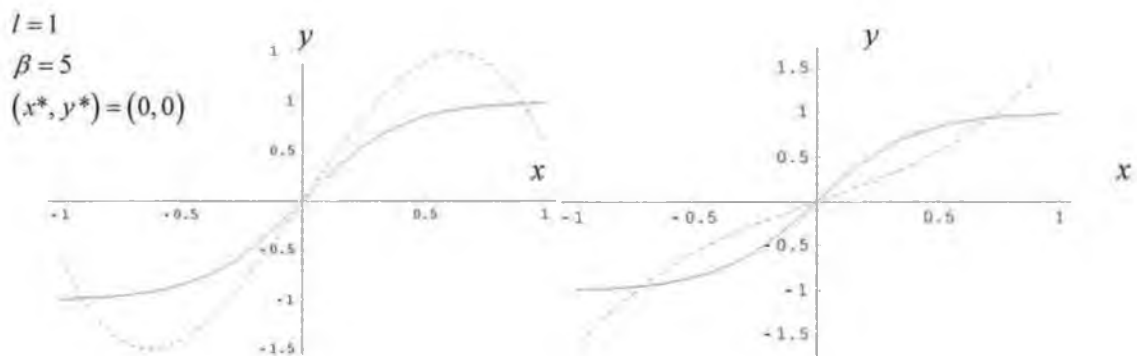


Figure 5.9: The approximations to the sigmoid as approximated by the Chebychev polynomials (left) of the first kind and (right) of the second kind.

The inaccuracies in the shape of the approximations are related to the weighting functions fundamental to the Chebychev polynomial approximations. Around the

origin where the weighting functions have a value of 1, the approximation is at its most accurate. Due to the inaccuracy of the sigmoid approximation using the Chebychev polynomials, the approximation of the sigmoid based on the Legendre polynomials ( $\hat{s}_{LP}(x)$ ) is used to calculate the describing function using the same method as already documented for the Taylor series expansion method (See Section 4.2.3.3).

Using the method of describing function approximation based on the Legendre polynomials, the  $-\frac{1}{N_{LP}}(M)$  locus is generated for a range of oscillation amplitudes equivalent to the full range ( $2l$ ) of the sigmoid approximation. This is shown in Figure 5.10.

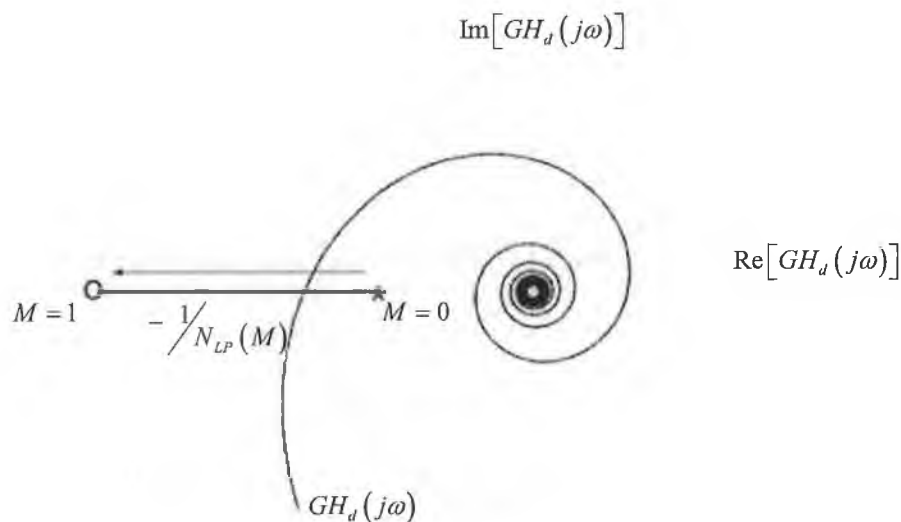


Figure 5.10: Nyquist plot showing the  $GH_d(j\omega)$  curve and the  $-\frac{1}{N_{LP}}(M)$  locus developed utilising the Legendre polynomials.

Using this method of describing function approximation reliable values of amplitude and frequency for a range of input amplitude values, set by the range of approximation of the sigmoid, can be calculated from the intersection of the  $GH_d(j\omega)$  curve and the  $-\frac{1}{N_{LP}}(M)$  curve.

In the above description an approximation is developed for the sigmoid function defined in the range  $[-1,1]$ . The sigmoid may be approximated over different intervals through dilation and normalisation of the orthonormal basis.

### 5.3 Comparison of the describing function approximations

The gains of the describing function approximations developed using the Taylor series expansion,  $N_{TS}(M)$ , and the Legendre polynomials,  $N_{LP}(M)$ , are plotted in Figure 5.11 for the sigmoid parameters given. In this figure these approximations are compared with the true value of the describing function calculated using numerical integration methods  $N_{NI}(M)$ , for a range of limit cycle amplitude values.

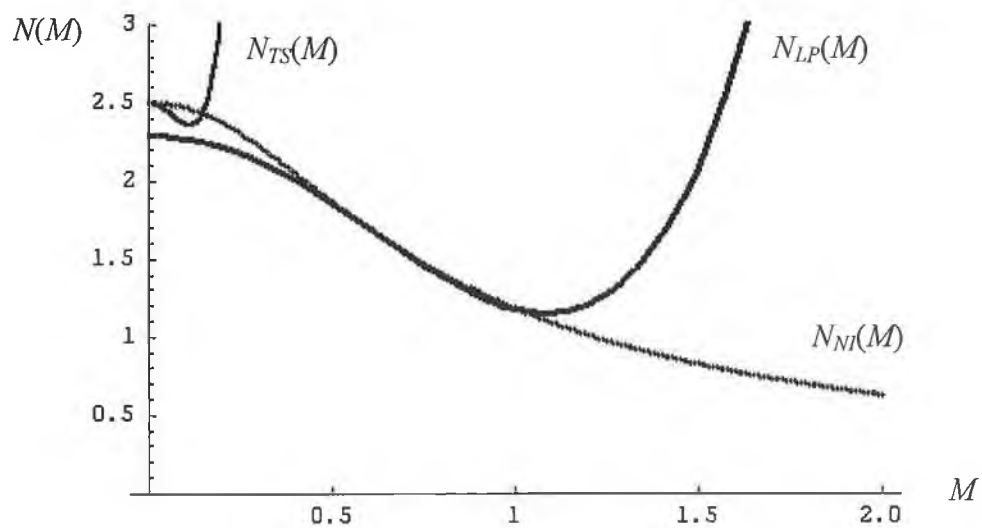


Figure 5.11: The describing function gains calculated using the Taylor series approximation method,  $N_{TS}(M)$ , the Legendre polynomial approximation method,  $N_{LP}(M)$ , and using numerical integration  $N_{NI}(M)$

Values of the describing function based on the Taylor series expansion are more accurate for very low values of oscillation amplitude. However, this approximation quickly loses accuracy as the values of oscillation amplitude increase. The describing function based on the Legendre polynomial approximation of the sigmoid is less accurate for very low values of oscillation amplitude. However, it more closely resembles the precise describing function,  $N_{NI}(M)$ , for a larger range of oscillation amplitude values.

These results are also evident in Figure 5.12, where the difference ( $J$ ) between the describing function approximation methods and the describing function calculated using numerical integration are compared. The difference between the describing function approximation calculated using numerical integration and the describing function approximation calculated using the Taylor series approximation method is:

$$J_{TS} = |N_{NI}(M) - N_{TS}(M)| \quad (5.7)$$

and, the difference between the describing function approximation calculated using numerical integration and the describing function approximation calculated using the Legendre polynomial approximation method is:

$$J_{LP} = |N_{NI}(M) - N_{LP}(M)| \quad (5.8)$$

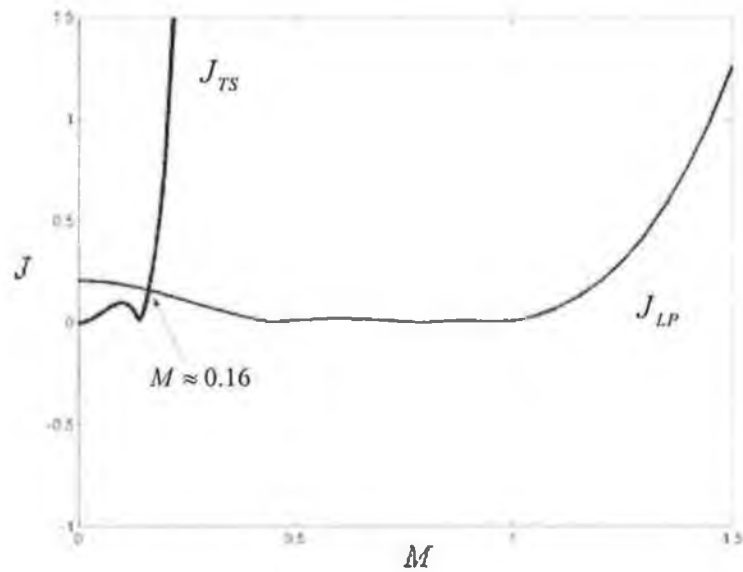


Figure 5.12: The difference,  $J$ , between the describing function calculated using numerical integration and the describing function approximation methods.

Of the 2 describing function approximation methods, the method of approximation based on the Taylor series expansion is more accurate for limit cycle peak-to-peak amplitude values of 16% of the full range of the sigmoid.

The methods of describing function approximation may also be analysed by comparing the predicted amplitude of the limit cycle with that of a simulated example in a limit cycle condition. A model with the structure of that shown in Figure 4.1 was used with results documented in Table 5.1. The gain of the dynamic transfer function,  $|G(j\omega)|$ , of Equation (2.7) was varied so as to alter the amplitude of the limit cycle.

$ G(j\omega) $	<i>M Simulated</i>	<i>Predicted M (TS)</i>	<i>Predicted M (LP)</i>
1.2	0	0	0
1.3	0.08	0.03	0
1.4	0.238	0	0
1.5	0.33	0	0.27
1.6	0.41	0	0.395
1.7	0.48	0	0.47
2	0.65	0	0.658
2.2	0.76	0	0.75
2.5	0.915	0	0.88
3	1.15	0	0

Table 5.1: Simulated results of limit cycle oscillation amplitude,  $M$ , calculated for increasing values of  $|G(j\omega)|$  and predicted values of this amplitude using the 2 approximation methods.

Again it is evident from this simulated example that the Taylor series expansion method allows better prediction of the amplitude of the limit cycle oscillation for small amplitude values and that the Legendre polynomial method of describing function approximation allows for better prediction of the limit cycle oscillation amplitude for a larger range of amplitude values.

## 5.4 Discussion

Two methods of describing function approximation are presented in this thesis. The first describing function approximation introduced in Section 4.2.3.3 is based on the Taylor series expansion of the sigmoid (Holohan 2000). The second describing function approximation introduced in Section 5.2.1 was developed utilising the Legendre orthogonal polynomial approximation of the sigmoid.

The describing function utilising the Taylor series expansion offers a better approximation of the sigmoid around the inflection region for an equivalent number of terms of both expansion methods. The inflection of the curve is key to the genesis of a limit cycle oscillation (Ringwood 2001). The accurate

approximation of the central inflection region enables better detection of the presence or absence of the oscillation for small oscillation amplitude values, ( $M \rightarrow 0$ ).

However, outside the inflection region, the approximation method based on the Legendre orthogonal polynomials, unlike the approximation based on the Taylor series expansion, is capable of approximating the sigmoid nonlinearity. Hence, using this new method of describing function calculation, the describing function may be accurately calculated for a larger range of oscillation amplitude values, enabling the limit cycle amplitude to be accurately approximated for a range of oscillation amplitude values within the full range of the sigmoid. This is of advantage when the amplitude of the slow oscillation in blood pressure increases beyond the range of approximation of the Taylor series approximation to the sigmoid.

The use of an additional weighting function to improve the accuracy of the Legendre polynomial approximation of the sigmoid in the central inflection region of the curve, while still retaining accuracy at the extremities of the curve, was investigated. However, the introduction of an additional weighting function would result in a set of polynomials that would not form an orthonormal basis set for the space defined. Hence, the orthogonal projection theory (Section 5.2.1) could not be used to develop a finite series, which would accurately approximate the sigmoid.

## 5.5 Conclusions

In this chapter approximations to the sigmoid nonlinearity, that is common in physiological systems, are presented. This approximation enables calculation of a closed-form expression for the describing function. Unlike the previous approximation method, utilising the Taylor series, the method of approximation presented in this chapter allows for accurate calculation of the describing function for a large range of oscillation amplitudes. This enables accurate calculation of the amplitude of the limit cycle oscillation.

Of the two methods of approximation used in this study, the method based on the Taylor series expansion is better for the detection of a limit cycle, while the method of approximation based on the Legendre orthogonal polynomials permits accurate calculation of the amplitude of the oscillation.

These results are significant when applied to the field of biomedical engineering and particularly the area of cardiovascular control where the *strength* of the 0.1 Hz oscillation in the blood pressure of the human is proposed as a future diagnostic test (Section 2.3). The development of an accurate closed-form expression for the describing function of the sigmoid allows greater insight into how changes in the parameters of the experimentally observed nonlinearities (Head 1987; Malpas 1996) will affect the amplitude of this limit cycle oscillation in blood pressure.

## Chapter 6

### Modelling the complete baroreflex

#### 6.1 Introduction

A main aim of this thesis is the development of an accurate model of the short-term control of blood pressure. This model should be capable of describing the mechanisms of short-term blood pressure control and, hence, enable investigation of the mechanisms responsible for the genesis of the slow oscillation in blood pressure. The modelling analysis of the slow oscillation in blood pressure, documented so far in this thesis has concentrated on the investigation of baroreflex control of peripheral resistance (see Chapter 4). That model (Ringwood 2001), and other models of baroreflex control of peripheral resistance (Kitney 1979; Burgess 1997), are capable of giving rise to an oscillation at the frequency of the slow oscillation. However, this fact alone does not preclude the heart from also playing a role in the genesis of the slow oscillation. The models of baroreflex control of peripheral resistance provide a sound foundation for explaining the theoretical perception as to how the slow oscillation in blood pressure is produced (*i.e.* as a limit cycle). However, similarly describable neural pathways to those that travel to the vasculature exist to the heart. Due to the presence of nonlinearities in these cardiac pathways (Iriki 1977), limit cycle oscillations may also be generated through these pathways.

The significance of the heart in relation to the genesis of the slow oscillation in blood pressure has been questioned and, in many cases, dismissed by a number of authors (O'Leary 1996; Janssen 2000; Liu 2002). The studies of these authors, and the evidence in support of their conclusions, are reviewed in Section 2.3.3.3. However, the role of the heart as the principal cardiovascular controller, and its inherent ability to generate oscillations, makes a model description of the control of blood pressure, excluding the heart, incomplete.

A model of the complete baroreflex, including the baroreflex pathways to the heart, is presented in this study. Documented in this chapter are the components and parameters used in the model of the baroreflex. Using this model, the role of the heart, and other components, which contribute to the development of the slow oscillation, are analysed.

## 6.2 Modelling approach

This model was developed using experimentally derived characteristics and parameters exclusive to the rabbit so as to investigate the slow oscillation in blood pressure that exists at about 0.3 Hz in the rabbit (Leonard 2000). As was already discussed (Section 2.3.2), this oscillation is analogous to the 0.1 Hz oscillation in the human (Ringwood 2001), which is the frequency of oscillation produced by the majority of models available in the literature (De Boer 1987; Cavalcanti 2000; Seydnejad 2001; Ursino 2003). However, due to the fact that rabbits are more commonly used as the subjects of physiological experiments, there are many more studies available that characterise components of the baroreflex of the rabbit than there are of the human. Hence, accurate representation of short-term blood pressure control of the model is more easily achieved when the model is developed using rabbit data and components derived for the rabbit. The development of the model for the rabbit also benefits the consistency of parameterisation of the model, as the need

to mix or transpose parameters and characteristics obtained from different species is avoided. Also, the rabbit is used as the subject for all experiments performed by the physiologists at the Circulatory Control Laboratory at the University of Auckland, New Zealand, who collaborate on this research. Therefore, data is available to model the various characteristics of the rabbit's baroreflex, where required.

Characteristics have been derived in other animals subjects also, such as the rat (Sato 2003), dog (Berger 1989) or cat (Seller 1991), which are more closely akin, at least in size, to the rabbit than the human is. These characteristics are also available in the literature, and these may be compared to those derived for the rabbit.

### 6.3 Modelling the neural arc

Central nervous control of blood pressure is discussed in Chapter 2, where the experimentally derived static and dynamic characteristics are documented. Due to the complexity of the central nervous system and central processing mechanisms, the CNS is most often viewed as a black box, and is therefore modelled using input and output data of the CNS. The CNS is most precisely characterised by the relationship between afferent nerve activity and SNA (models of the central arc) and these characteristics are documented in 2.2.2.3. However, the more common models are of the neural arc, which lumps the characteristics of the baroreceptors with the central arc (see Section 2.2.2.4). These arcs of the baroreflex are illustrated in Figure 2.1.

As was discussed in Section 2.2.2.4, the neural arc includes the baroreceptor transduction properties, afferent signal conduction, central processing and efferent signal transduction. The characteristics of the baroreceptors are well described, in the literature, by the relationship between blood pressure and afferent nerve activity. Static nonlinear and linear dynamic characteristics have been reported and these are reviewed in Section 2.2.1.1.

Although models of the baroreceptors, central and neural arcs are all available in the literature, they are rarely included in more complete models of the baroreflex system. Some authors have investigated complicated descriptions of the CNS and the baroreceptors (Seidel 1995; Seidel 1997). However, the majority of models of the baroreflex either exclude any kind of description of the CNS (Ursino 2003) or include a very simple description (Ottesen 2000; Seydnejad 2001). Similarly, the characteristics of the baroreceptors are rarely included in these models and the emphasis is instead on the descriptions of the effectors of blood pressure (Seydnejad 2001; Ursino 2003).

The significance of the dynamical characteristics contained within the neural arc was emphasised by Ikeda *et al* (Ikeda 1996), who proposed that the derivative nature of these characteristics may be key to enabling quick stabilisation of blood pressure. A significant role for the nonlinear characteristic of the neural arc in the genesis of the slow oscillation in blood pressure was reported by Ringwood and Malpas (Ringwood 2001) and it was shown, in Chapter 4 of this thesis, that changes in the characteristics of the neural arc component of the baroreflex model can be related to changes in the strength of the slow oscillation. Hence, it is proposed that an accurate description of the neural arc is crucial for a realistic description of the baroreflex.

The different linear and nonlinear characteristics that exist in the neural arc, due to the baroreceptors and the CNS, are detailed in Section 2.2.2.4 and the suitability of these, for inclusion in the model of the baroreflex, is discussed in the following sections.

### 6.3.1 Dynamical characteristics in the neural arc

The dynamic transfer function models of the baroreceptors, central and neural arc were reviewed in Section 2.2.2.1, 2.2.2.3 and 2.2.2.4. Derivative characteristics have been consistently reported by the physiologists who have investigated the characteristics of the neural arc (Kawada 1997; Kawada 2002). The gain of the frequency response plots of the neural arc increases as the frequency increases, up to a given frequency, but decreases for higher frequencies. Importantly with respect to this model, the filter characteristics are high-pass in the frequency range of the slow oscillation (see Figures 2.6, 2.9, 2.12).

Although the derivative characteristics are well established to exist between blood pressure and SNA, there is some argument as to whether the baroreceptors or the CNS are responsible for the high-pass characteristics observed in the neural arc. Transfer functions for both the baroreceptors and the central arc have been reviewed in earlier sections (Sections 2.2.1.1 and 2.2.2.3). However, the published observations of the different authors do not conform.

Sato *et al* (Sato 1998) identified the dynamic transduction properties of the baroreceptors of the rabbit, and reported the gain of the transfer function between blood pressure and afferent nerve activity to increase up to ~2 Hz and decrease at higher frequencies. Kubo *et al* (Kubo 1996) report the transfer function of the central arc to exhibit a flat, all-pass characteristic. Hence, it might be assumed that the high-pass characteristics to the neural arc are attributable solely to the dynamic transduction properties of the baroreceptors, as has been proposed (Sugimachi 1990; Kubo 1996), and that the central component does not affect the dynamic properties of the baroreflex. However, Petiot *et al* (Petiot 2001) challenged the experimental procedure used by Kubo *et al* (Kubo 1996) and, following an experimental investigation of the central arc of the rat, reported high-pass characteristics within the central arc. Kawada *et al* (Kawada 2001) also revealed different frequency

response characteristics of the neural arc, when SNA to different organs was recorded. This result implies differential central processing (Kawada 2001).

Considering these studies, high-pass characteristics cannot be attributed solely to the baroreceptors, and may exist in both the baroreceptors and central arc. The characteristics chosen for inclusion in the model are discussed in Section 6.3.3.

### 6.3.2 Nonlinearity in the neural arc

The presence of nonlinearity in the neural arc is well established. The nonlinear baroreflex curves, between blood pressure and SNA, are well documented in the physiological literature, and were introduced in Section 2.2.2.4. Nonlinear characteristics were reported in both the baroreceptors (see Section 2.2.1.1) and the central arc (see Section 2.2.2.3). The nonlinearity in the neural arc was shown to constitute the primary nonlinear element in baroreflex control of peripheral resistance (Ringwood 2001) (a result supported by Sato *et al* (Sato 1999)) and the inflection of this curve, has been demonstrated as sufficient to induce oscillations.

### 6.3.3 A dynamical linear-static nonlinear neural arc model

Ideally, distinct descriptions of the baroreceptors and the central arc of the baroreflex would be included in the baroreflex model, so that the influence of each individual component on baroreflex function and on the slow oscillation in blood pressure may be assessed. However, the problems introduced by the nature of neural recordings, as documented in Chapter 4, reoccur. Hence, absolute parameterisation of the model components is difficult to achieve.

Correct descriptions of both the baroreceptors and central arc should include (dynamic) linear and (static) nonlinear components. However, the structure of the

models of both the baroreceptors and the central arc are largely unknown, yet are significant to model operation. These models may either be of the class of Wiener models (linear part first followed by nonlinear part), or of the class of Hammerstein models (nonlinear part first followed by linear part). The linear and nonlinear blocks of these two model types do not commute and hence, an incorrect structure choice may result in a misrepresentation of the section of the baroreflex in question.

Documentation of the dynamics and nonlinearities of the central arc is relatively scarce (see Section 2.2.2.3). In contrast the dynamics and nonlinearities of the neural arc are well described and the structure of the neural arc model has been investigated (Kawada 2003; Kawada 2004). These authors have demonstrated, by simulation of both model structures, that a cascade model consisting of the linear dynamical part followed by the nonlinear sigmoid baroreflex curve (Wiener model) is the more likely representation of the neural arc transfer characteristics (Kawada 2003). For these reasons, instead of including different descriptions of the baroreceptors and central arc, a description of the neural arc is included in the model.

Hammerstein-Wiener model identification methods are available in the literature (Zhu 1999; Bai 2002; Dempsey 2004). Unfortunately, data was not available with which to identify the correct model representation of the neural arc using more involved methods than those used by Kawada *et al* (Kawada 2003). However, the nonlinear-linear model structure proposed by these authors offers a good first approximation but, because the linear and nonlinear components of the neural arc model lump the characteristics of the baroreceptors and CNS, no specific anatomical counterparts may be assumed for these components. The model structure of the neural arc is illustrated in Figure 6.1.

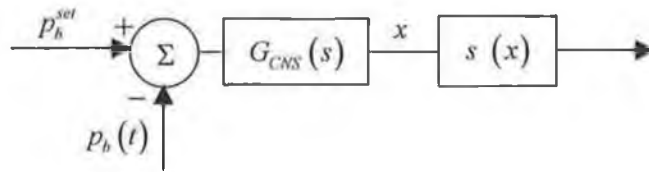


Figure 6.1: The model of the neural arc.

The dynamical transfer function of the neural arc is described by Equation (6.1) (Ikeda 1996).

$$G_{CNS}(s) = e^{-s\tau_{CNS}} \frac{1.326s + 1}{s + 1} \quad (6.1)$$

where,

$s(x)$  is as described by Equation (2.3), and the parameterisation of this function is discussed in the subsequent sections,

$p_b^{set}$  is the blood pressure set point,

$p_b(t)$  is the blood pressure signal,

$\tau_a$  is the processing delay in the CNS, and

$x$  is the input signal to the nonlinearity.

The magnitude characteristic of Equation (6.1) is illustrated in Figure 6.2.

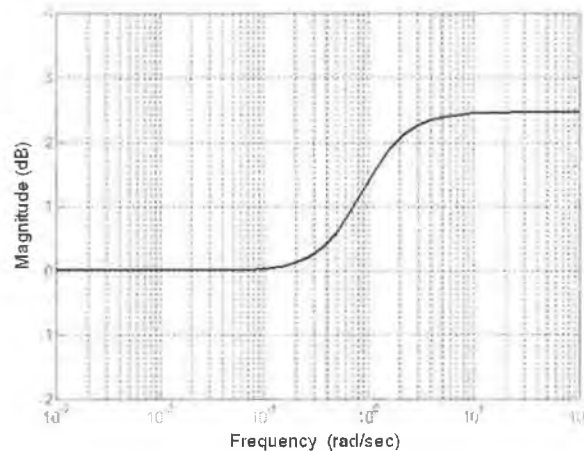


Figure 6.2: Magnitude plot for the transfer function of Equation (6.1).

Although the transfer characteristics of the baroreceptors are lumped with the transfer characteristics of the central arc in the neural arc characteristics a distinct time delay, from the delay in the neural arc, due to the baroreceptor transduction and afferent delays is included in the feedback path. The sigmoid nonlinear element contained in the neural arc is introduced in the subsequent sections.

#### 6.3.4 Nonlinearities in the central nervous control of the heart

The heart is controlled by both the sympathetic and parasympathetic systems. Baroreflex curves have been developed to describe the relationship between blood pressure perturbations and cardiac SNA (Iriki 1977). However, a similar baroreflex curve, between blood pressure perturbations and parasympathetic nerve activity, is not documented due to the difficulty of recording parasympathetic activity from the vagal nerve.

For this reason, and because of the normalised nature of SNA and the restrictions due to model structure already documented, alternative methods of quantification of the nonlinear elements of the CNS were investigated. Although baroreflex curves do

not exist for both branches of the autonomic nervous system, baroreflex curves between blood pressure perturbations and heart rate are well documented (Head 1987; Malpas 1996; Malpas 1997), and these curves have been derived when only individual autonomic pathways can influence heart rate.

Sigmoid nonlinear characteristics are well established to exist in baroreflex control of heart rate. Similar to the case of the sympathetic pathway to the vasculature, the sympathetic pathway to the heart contains a sigmoid nonlinear characteristic in the neural arc (Iriki 1977). Other nonlinear characteristics have also been observed at the SA node. However, these are generally poorly characterised (Eckberg 1980), although hysteresis (Pickering 1972; Rudas 1999) and the nonlinear interaction of the different branches of the autonomic nervous system (Levy 1971; Levy 1984) are examples of nonlinear relationships that have been characterised. Blood pressure to heart rate baroreflex curves are common in the physiological literature (see Section 2.2.3.1), and this characteristic lumps the nonlinearities that exist in the neural arc and at the SA node.

The blood pressure to heart rate baroreflex curves, derived for the rat, in the control case and in the presence of autonomic nerve activity blockers were illustrated in Figure 2.17.

Other authors (Korner 1972; Weinstock 1988; Kingwell 1991) have investigated the role of the different branches of the autonomic nervous system on the blood pressure to heart rate baroreflex curve, in the rabbit. Kingwell *et al* (Kingwell 1991) document the gain of the blood pressure – heart rate baroreflex curve for the rabbit but only during bradycardia and tachycardia, and only when the autonomic neural pathways to the heart are normally active. Weinstock *et al* (Weinstock 1988) use two genetically related strains of rabbits as subjects in their study. One of these groups responded with more pronounced bradycardia than the other. Both these groups of authors investigated different experimental methods of baroreflex curve development, namely the cuff and drug methods (see Table 6.1). Korner *et al*

(Korner 1972) documented changes in the baroreflex curve when the parasympathetic control of the heart is blocked (using atropine) or denervated, but only after other experimental interventions (thalamic, pontine and sham operated rabbits), and never in the purely control condition. The contributions of the parasympathetic and sympathetic nerves to the overall blood pressure – heart rate baroreflex curve are documented in Table 6.1.

Study	Subject	Range		Gain	
		% Vagal	% Sym	% Vagal	% Sym
Head and McCarty, 1987	Rats	62	38	54	46
Weinstock <i>et al.</i> 1988	Rabbits (Group 1)	Cuff: 74 Drug: 68	Cuff: 26 Drug: 32	Cuff: 93 Drug: 80	Cuff: 7 Drug: 20
Weinstock <i>et al.</i> 1988	Rabbits (Group 2)	Cuff: 78 Drug: 77	Cuff: 22 Drug: 23	Cuff: 85 Drug: 76	Cuff: 15 Drug: 24
Kingwell <i>et al.</i> 1991	Rabbits	Cuff: 82 Drug: 73	Cuff: 18 Drug: 27	Cuff: Drug:	Cuff: Drug:
Kingwell <i>et al.</i> 1991	Humans	82	18	86	14

Table 6.1: The contribution of the vagus and the sympathetic to the overall blood pressure – heart rate baroreflex characteristic.

Considering the different grouping of rabbits in the studies of Weinstock *et al* (Weinstock 1988) and Kingwell *et al* (Kingwell 1991), and the complex surgery undergone by the rabbits in the study of Korner *et al* (Korner 1972), the generic contributions of the cardiac sympathetic and parasympathetic pathways is difficult to conclude on, for the rabbit. The results of the study of Head and McCarty (Head 1987), although attained from the rat, are the least convoluted of these studies of the influence of the different autonomic branches on heart rate. Based on the analysis of Korner *et al* (Korner 1972), Head and McCarty propose that the rabbit has a lesser contribution from the sympathetic system, than the rat has, and this contribution accounts for about 40% of the range of the curve and 15% of the gain (Head 1987).

The heart rate ranges of the baroreflex curves calculated by Weinstock *et al* (Weinstock 1988) and Kingwell *et al* (Kingwell 1991) vary considerably. Therefore, the proportions of the heart rate range associated with the different autonomic nervous pathways are related to the range of a recently documented blood pressure – heart rate baroreflex curve (Barrett 2003). Barrett *et al* (Barrett 2003) report a full range of 219 bpm and a gain of 4.87 bpm/mmHg. The range and gain are proportioned as recommended by Head and McCarty (Head 1987) and the values of curvature are calculated from these parameter values according to the equation of gain given in Equation (6.2).

$$'gain' = -\frac{2\beta l}{4.56} \quad (6.2)$$

Descriptions of the sigmoid curve are documented in Section 4.2.3 and the symmetrical sigmoid representation of the curve is described by Equation (2.3). The baroreflex curve parameters are given in Table 6.2.

Parameter	$l$	$\beta$	'gain'
Control	109.5 bpm	0.105 (average)	-4.87 bpm/mmHg
Sympathetic only, $s_{sc} ( )$	43.8 bpm	~0.04	-0.73 bpm/mmHg
Parasympathetic only, $s_{pc} ( )$	65.7 bpm	~0.14	-4.14 bpm/mmHg

Table 6.2: Parameters of the nonlinear sigmoid characteristics in the neural arc.

The baroreflex curves, calculated for the parameters of Table 6.2, are shown in Figure 6.3.

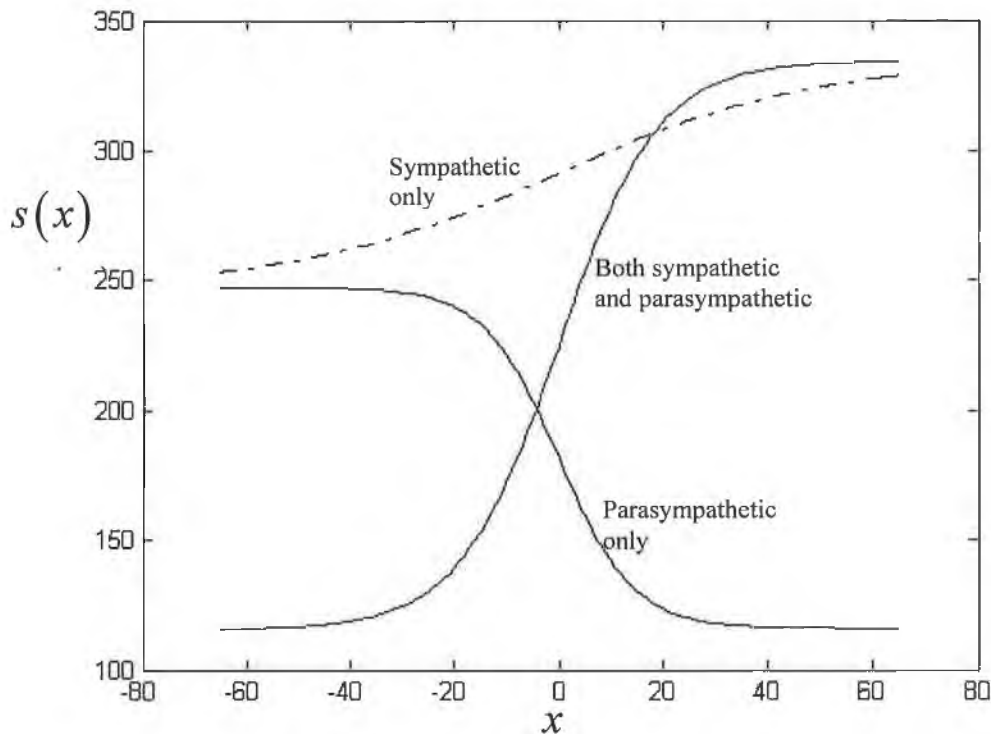


Figure 6.3: The blood pressure to heart rate baroreflex curves illustrated as orientated in the model.

The alternative orientation of the blood pressure – heart rate baroreflex curve compared to that normally documented in the physiology literature (see Figures 2.3, 2.10 and 2.11) is due to the effects of negative feedback of the loop. Due to the fact that the parasympathetic effect has an opposite effect to the sympathetic system (on heart rate), the baroreflex curve, based on parasympathetic control of heart rate, is reversed. The sigmoid curves are centered at zero on the  $x$ -axis. No bias is introduced as the signal input to the sigmoid nonlinearity has a mean of zero.

### 6.3.5 Nonlinearities in central nervous control of the vasculature

As discussed, it has been established that the nonlinear element in the CNS is the significant nonlinearity in baroreflex control of peripheral resistance (Ringwood

2001). The remaining portion of this loop mechanism was shown to be only minimally nonlinear and, significantly, with respect to the slow oscillation in blood pressure, devoid of an inflection (Ringwood 2001). Therefore, the nonlinear element in the sympathetic pathway to the vasculature is confined to the CNS.

The baroreflex curve from blood pressure to cardiac SNA has been shown to be equivalent to the baroreflex curve from blood pressure to renal SNA (Iriki 1977; Kawada 2001). Therefore, the gain due to the nonlinear element in both sympathetic pathways is equivalent, and the inflections of the curves are equivalent. Considering this, the nonlinear sigmoid curve included in the neural arc of the sympathetic pathway to the vasculature is parameterised in an identical way to the sigmoid curve in the neural arc of the sympathetic pathway to the heart (see Table 6.2). A conversion gain term,  $k_{\Delta r}$ , is included in this baroreflex pathway to scale the values of the output signal of the nonlinear curve to peripheral resistance values.

The nonlinear elements in the sympathetic pathways to the different vascular beds are described by  $s_k(\cdot)$ ,  $s_g(\cdot)$ ,  $s_m(\cdot)$  and  $s_s(\cdot)$ , for the nonlinearity in the sympathetic pathways to the kidney, gut, muscle and skin respectively. Considering that the available evidence shows that the blood pressure – SNA baroreflex curves, derived for renal and cardiac SNA, are equivalent (Iriki 1977), the nonlinear elements to the different vasculature elements are also assumed equivalent, and the parameters of the curves,  $s_k(\cdot)$ ,  $s_g(\cdot)$ ,  $s_m(\cdot)$  and  $s_s(\cdot)$  are commonly described by  $s_r(\cdot)$ , with the parameters for this curve are documented in Table 6.3..

Parameter	$l_r$	$\beta_r$	$C_r$	$k_{\Delta r}$
Value	43.8	0.04	102	0.0011

Table 6.3: The parameters of the sigmoid curves in the sympathetic pathways to the vascular beds.

No definite measure of peripheral resistance exists in the literature, and different authors have used different units to quantify peripheral resistance. The unit used in this study, mmHg.min/ml, is given by Equation (2.1), when cardiac output is in terms of ml/min and blood pressure is in terms of mmHg. The offset value of the sigmoid curves,  $C_r$ , is set to 102, so that the range of the possible peripheral resistance values, maintain blood pressure within the physiological range of blood pressure, for the given range of cardiac output values, given by Equation (2.1).

## 6.4 Modelling baroreflex control of the heart

The baroreflex control of the heart is well documented in the literature. Many dynamic and static models are reviewed in Section 2.2.3.1. The emphasis of the model review is on models developed for rabbit data and the characteristics suitable for inclusion in the model are documented in the subsequent sections.

The models of sympathetic and parasympathetic control of heart rate described in the subsequent sections describe the linear dynamics of heart rate control and the nonlinear interaction of these signals, but the significant amplitude limiting nonlinearity is included in the CNS.

### 6.4.1 Sympathetic control of heart rate

Studies that have documented the heart rate response to sympathetic nerve stimulation were reviewed in Section 2.2.3.1. This transfer function is characterised by a low-pass filter. The calculated transfer function between sympathetic stimulation and the heart rate response of the rabbit, calculated by Kawada *et al* (Kawada 1996), is shown in Figure 2.13. This transfer function is described by a

second-order system with time-delay, as given in Equation (6.3) (Kawada 1996). The main aim of the study of Kawada *et al* (Kawada 1996) was to investigate how simultaneous activation of both the parasympathetic and sympathetic nervous systems affect heart rate. Kawada *et al* (Kawada 1996) document the parameters of three different transfer functions, from dynamic sympathetic stimulation to heart rate, for three different frequencies of simultaneous tonic parasympathetic stimulation (0Hz, 5Hz & 10Hz). The parameters calculated for the frequency response of heart rate to sympathetic stimulation are averaged for these three conditions.

$$G_{sc}(s) = e^{-s\tau_{sc}} \frac{1}{1.3s^2 + 3.8s + 1} \quad (6.3)$$

The magnitude response of the transfer function of Equation (6.3) is shown in Figure 6.4.

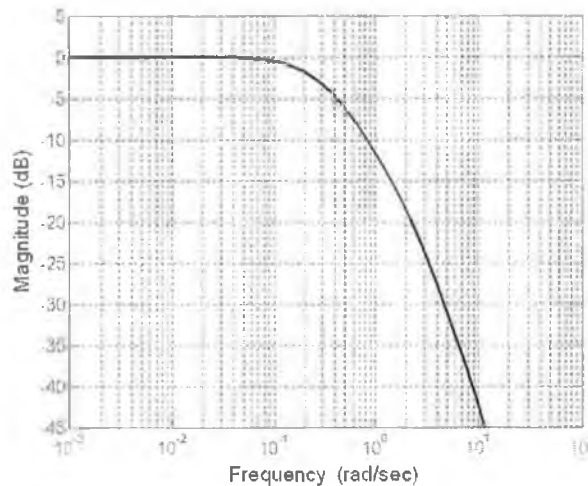


Figure 6.4: Magnitude plot for the transfer function of Equation (6.3).

The nonlinearities in the central nervous control of heart rate are parameterised to heart rate values, for reasons described in Section 6.3.4. Therefore, the gains of the transfer functions are normalised to unity (for convenience) so as to maintain the output within the physiological range of heart rate values.

## 6.4.2 Parasympathetic control of heart rate

The heart rate response to parasympathetic stimulation also displays low-pass characteristics (see Section 2.2.3.1). These low-pass characteristics have been described using a first order differential equation (Berger 1989; Kawada 1996; Kawada 1997). The first order transfer function characteristics of the parasympathetic control of heart rate is expressed mathematically as:

$$G_{pc}(s) = e^{-s\tau_{pc}} \frac{1}{1.22s + 1} \quad (6.4)$$

Similar to the case of the heart rate response to sympathetic nerve stimulation, the parasympathetic nerve stimulation to heart rate transfer function is documented by Kawada et al (Kawada 1996) for three different frequencies of tonic sympathetic stimulation. These parameters are averaged and the transfer function of Equation (6.4) is calculated for these averaged parameters.

The magnitude response of the transfer function is shown in Figure 6.5.

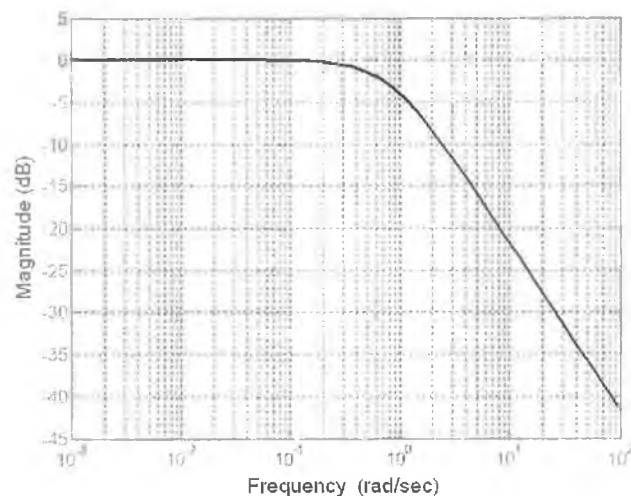


Figure 6.5: Magnitude plot for the transfer function of Equation (6.4).

### 6.4.3 Parasympathetic-sympathetic control of heart rate

The heart rate response to simultaneous parasympathetic and sympathetic activation was discussed in Section 2.2.3.1, where the studies of Levy *et al* (Levy 1969; Levy 1969; Levy 1984) and Kawada *et al* (Kawada 1999) were introduced. The static heart rate response of the rabbit to combined sympathetic ( $u_{sc}$ ) and parasympathetic nerve stimulation ( $u_{pc}$ ), for a range of stimulation frequencies, is displayed in Figure 2.15.

Seidel *et al* (Seidel 1997) fitted a nonlinear function to the data of Levy *et al* (Levy 1969; Levy 1969; Levy 1984). This dual-input nonlinear function is described as:

$$f_c(t) = (\alpha_1 \tanh(\gamma_1 u_{sc}(t))) * (1 - \tanh(\gamma_2 u_{pc}(t))) - (\alpha_2 \tanh(\gamma_3 u_{pc}(t))) + f_c^0 \quad (6.5)$$

where,

$f_c(t)$  represents the heart rate of the rabbit,

$f_c^0$  is the constant heart rate in beats/min regardless of nervous control, and

$\alpha_1, \alpha_2, \gamma_1, \gamma_2, \gamma_3$  are constant terms.

For the purpose of this model, the same nonlinear function was fitted to the data of Kawada *et al* (Kawada 1999), as this model is parameterised using experimentally derived parameters from studies of the rabbit.

The parameters of this equation are calculated using a least squares nonlinear fit to the data of the trained neural network of Kawada *et al* (Kawada 1999). Both the Gauss-Newton and Levenberg-Marquardt (Marquardt 1963) gradient methods were investigated. The parameter values calculated using these least squares methods differed by little. The parameters calculated using the Levenberg-Marquardt (Marquardt 1963) method are documented in Table 6.4.

Parameter	$\alpha_1$	$\alpha_2$	$\gamma_1$	$\gamma_2$	$\gamma_3$	$f_c^0$
Value	181	156.1	0.04	0.035	0.07	245.8

Table 6.4: Parameters of the sympathetic-parasympathetic interaction curve (Equation (6.5)).

The baroreflex curves included in the neural arc of the model are parameterised for heart rate values, for reasons described in Section 6.3.2. The range of heart rate values are taken from the study of Barrett *et al* (Barrett 2003), who calculated a maximum heart rate of 335 bpm, which is outside the range of heart rate values observed by Kawada *et al* (Kawada 1999), following stimulation of the parasympathetic and sympathetic nerves for a range of frequencies. This disparity between values is rectified by calculation of the values of sympathetic stimulation up to 15 Hz, using Equation (6.5).

The input units of the characteristic illustrated in Figure 2.15 are in terms of stimulation frequency. This introduces a discrepancy to the proposed model specification, as the modelled signal is assumed to be amplitude coded. However, the response characteristics of blood flow to stimulation of the renal nerves at varying frequency values was similar to the response characteristic of blood flow to the stimulation of the renal nerves for varying amplitude values (Navakatikyan 2000).

Conversion gain terms are introduced to convert the range of output of the baroreflex curves to the range of stimulation frequencies of the sympathetic and parasympathetic nerves.

Figure 6.6 represents the full model of the forward path of the baroreflex control of heart rate.

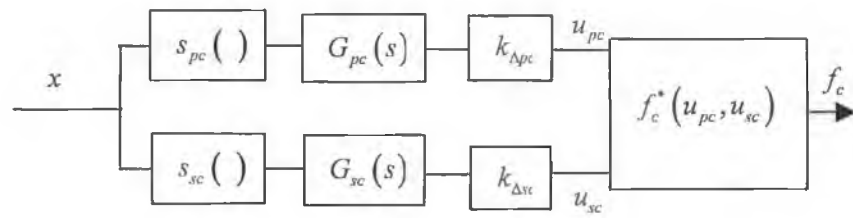


Figure 6.6: Baroreflex control of heart rate.

#### 6.4.4 Control of stroke volume

Baroreflex control of cardiac muscle contractility, and hence stroke volume, is not as well documented as baroreflex control of heart rate (see Section 2.2.3.1). Studies of baroreflex control of the heart have shown the stroke volume to remain nearly constant when the mean blood pressure is within the normal physiological range (Allison 1969; Suga 1976). Data was available with which to test this hypothesis and the stroke volume remained constant ( $\sim 2.5$  ml/min) for the range of blood pressure values available (60 – 120 mmHg). When blood pressure falls below normal physiological levels, stroke volume rapidly decreases (Cavalcanti 1996). Considering that the model is designed to operate in a normal physiological operating region, the stroke volume was assumed to remain constant, at,  $v_c = 2.5$  ml/min.

### 6.5 Modelling baroreflex control of the vasculature

The vasculature comprises a number of different vascular beds. These vascular beds receive significantly different amounts of blood flow during the resting state as described in Section 2.2.3.2. Hence, the resistance of different vascular beds is weighted relative to the amount of blood flow each one receives.

Similarly, the different vascular beds are weighted according to their baroreflex sensitivities (see Section 2.2.3.2). SNA to the lungs, kidney and spleen are highly baroreceptor sensitive (Ninomiya 1971; Shirai 1995), whereas the skin is only weakly regulated by baroreceptor activity (Ninomiya 1976).

The weighting terms that quantify the amount of cardiac output received by, and baroreflex sensitivity of, the different vascular beds at rest are documented in Table 6.5.

Vascular bed	Cardiac output distribution	Baroreflex sensitivity
Kidney (k)	$k_{dk} = 0.2$	$k_{bsk} = 0.9$
Gut (g)	$k_{dg} = 0.27$	$k_{bsg} = 0.25$
Muscle (m)	$k_{dm} = 0.15$	$k_{bsm} = 0.9$
Skin (s)	$k_{ds} = 0.09$	$k_{bss} = 0.1$

Table 6.5: Cardiac output distribution and baroreflex sensitivity weights.

The cardiac output distribution to the different vascular beds changes significantly during different conditions (Fox 1996). Similarly, the baroreflex sensitivity would be expected to change during different physiological conditions, including periods of stress and exercise, as blood is diverted away from certain vascular beds to others. The values documented in Table 6.5 are the parameters for the resting condition.

The contractile state of the smooth muscle of the blood vessels of the vasculature is affected by SNA, as well as by a range of hormones and paracrines. The response characteristics of the blood vessels to the hormones and paracrines are not well defined (see Section 2.2.3.2). However, the response characteristics of the blood vessels to sympathetic stimulation have been investigated and these characteristics are introduced in the subsequent section.

However, a number of vascular beds, such as the brain and bone, are not under baroreflex control, but do receive a significant amount of blood flow. The resistance due to these vascular beds is included as a constant resistance term,  $r_p^*$  (see Table 6.6).

Parameter	$r_p^*$	$k_r$	$k_{\Delta pc}$	$k_{\Delta sc}$
Value	0.121	0.0011	0.14	0.18

Table 6.6: Constant resistance and conversion gain parameters.

### 6.5.1 Response characteristics of the vasculature beds

The response characteristics of the different vascular beds to SNA are described by the frequency response characteristic of blood flow to stimulation of the sympathetic nerves. As was reviewed in Section 2.2.3.2, the dynamical transfer characteristics are only well defined for the vasculature of the kidney. Guild *et al* (Guild 2001) documented the response of renal blood flow to the PRBS stimulation of the renal sympathetic nerves and the corresponding frequency response plots are illustrated in Figure 2.18. These authors fitted a 2-zero/4-pole function to the gain response. The dynamics of the kidney vasculature,  $G_k(s)$ , with the d.c. gains normalised to unity, are described as:

$$G_k(s) = e^{-s\tau_k} \frac{11s^2 + 6.64s + 1}{4.27s^4 + 21s^3 + 36s^2 + 22s + 1} \quad (6.6)$$

The gain plot for this transfer function is illustrated in Figure 6.7.

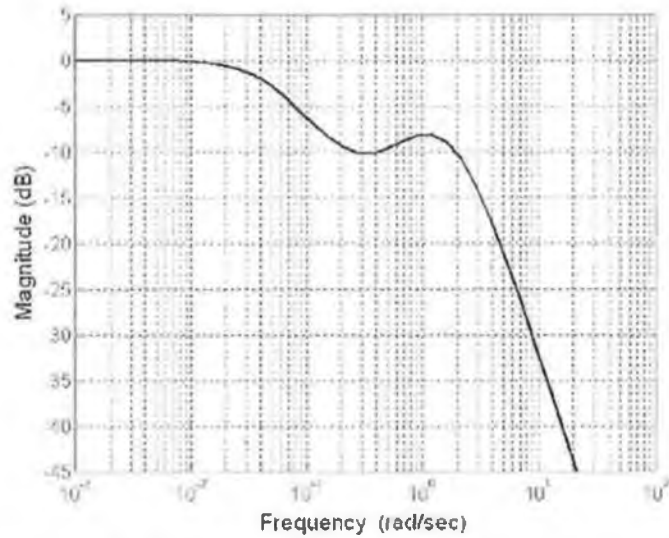


Figure 6.7: Magnitude plot for the transfer function of Equation (6.6).

These characteristics are used in the model of the complete baroreflex to describe the dynamics in the sympathetic pathway to the kidney. Also, due to the paucity of documented dynamic characteristics of other vascular beds, the transfer function of Equation (6.6) is also used to describe the dynamics of the gut,  $G_x(s)$ , and muscle,  $G_m(s)$ .

The frequency response of skin blood flow to sympathetic activity may be approximated by a first order transfer function (Stauss 1999), as:

$$G_s(s) = e^{-sr_s} \frac{1}{1.87s + 1} \quad (6.7)$$

This transfer function is included in the sympathetic pathway to the skin vasculature in the model. The gain plot for the skin transfer function is illustrated in Figure 6.8.

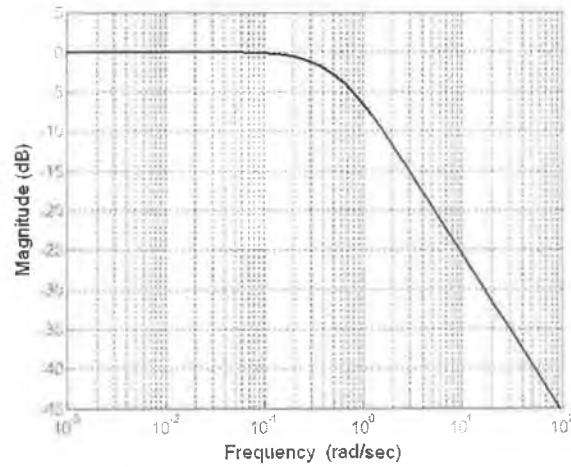


Figure 6.8: Magnitude plot for the transfer function of Equation (6.7).

Other models of the baroreflex generally only include a global description of sympathetic control of the combined vascular beds (Burgess 1997; Ringwood 2001; Seydnejad 2001; Ursino 2003). Figure 6.9, on the other hand, illustrates the baroreflex control of the different vascular beds.

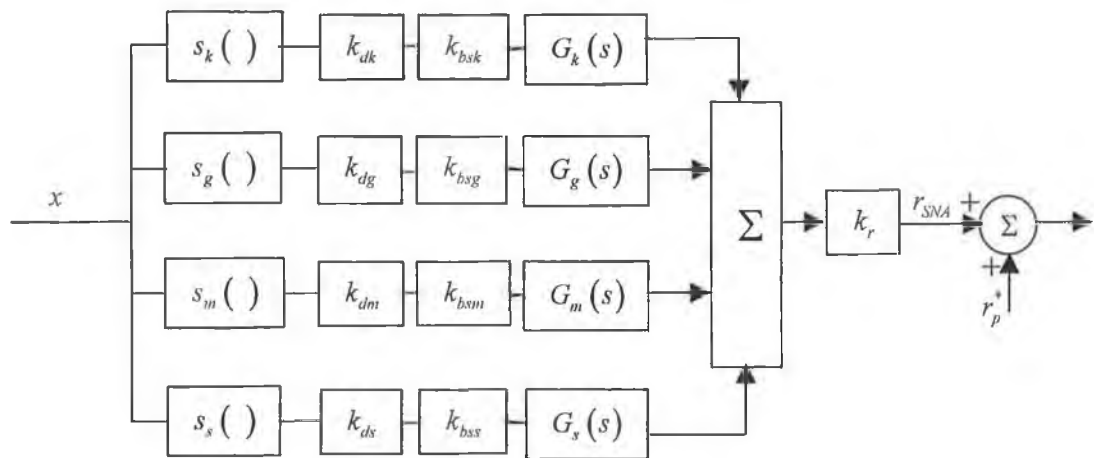


Figure 6.9: Baroreflex control of vasculature.

where,

$$s_{sc}(\cdot) = s_k(\cdot) = s_g(\cdot) = s_m(\cdot) = s_s(\cdot),$$

$k_{ilk}, k_{lfg}, k_{dm}$  and  $k_{ds}$  are as given in Table 6.5,

$k_{bsk}, k_{bsg}, k_{bsm}$  and  $k_{bss}$  are as given in Table 6.5.

## 6.6 Delay terms in the model

The short-term blood pressure control mechanisms, specifically the baroreflex, contain several notable time delays. A time delay exists in the CNS due to the finite (non-zero) time taken for information processing. Transmission delays exist corresponding to the nerve signals to conduct along the afferent and efferent nerves. These delays vary considerably depending on the nervous system in question (*i.e.* sympathetic or parasympathetic) and on the composition of the nerve fibers (*i.e.* whether they are myelinated or unmyelinated) (see Section 2.2.2.2).

These delay terms have been calculated during a range of physiological experiments, and delay terms for the different sections of the baroreflex are documented by a number of authors (Borst 1983; Seller 1991; Burgess 1997; Guild 2001). The types, structure and characteristics of the different nerve fibers are described in Section 2.2.2.2 and the different, experimentally calculated, delay terms are commented on in the various sections of Chapter 2.

It has been proposed by a number of authors that the delays are of major importance to the development of the slow oscillation via the baroreflex (Bertram 1998; Malpas 2000; Guild 2002). In general terms the time delay will have a destabilising effect on a system due to the negative phase contribution which increases linearly with increasing frequency (Dutton 1997). With regard to the model illustrated in Figure 4.1, the delay terms add sufficient phase to create an overall phase lag of  $180^\circ$ , which coupled with the phase shift of  $-180^\circ$ , due to inversion, provides a total of  $360^\circ$  phase shift, corresponding to positive feedback. The time delay is the most

significant element in the determination of the limit cycle oscillation frequency (Bertram 1998; Ringwood 2001). The influence of the delays on baroreflex function have been the focus of a number of studies, and changes in the delay have been shown to lead to changes in nonlinear phenomena and chaotic behaviour (Cavalcanti 2000). Considering these facts, it is important that the delay terms of the model are chosen with care, if the model is to give a true approximation of the underlying mechanism of the slow oscillation. Delay terms can be easily tuned to give rise to an oscillation at the required frequency. However, care needs to be taken in such an exercise, since a number of different parameters could be tuned to produce a specific desired response at a certain operating point, but a concerted model tuning exercise, at a variety of operating points, would be needed to correctly isolate erroneous parameters.

A number of models, that are capable of developing an oscillation at the frequency of the slow oscillation have, however, been created with little care or justification of the delay terms chosen for inclusion in the model. This is not a direct criticism of these modelling studies, however, as there is also a paucity of delay values documented in the literature and delays that are documented, for sections of the baroreflex, are often inconsistent. Much of this inconsistency is due to the inconsistency of definition terms (Eckberg 1976; Borst 1983) and the differing experimental techniques used to determine these delays (Borst 1983) (see Seidel (Seidel 1997) for review). Delay values have become more regularly documented in experimental physiological studies of recent years. Authors have documented delays during the investigation of the dynamical characteristics of the different components of the baroreflex. However, these delays are often calculated in studies where the nerve is sectioned and stimulated at some point along the nerve fiber and hence, the time delay does not represent the delay due to the conduction time along the *full* length of the nerve.

For these reasons, some degree of deduction and extrapolation is inevitable when choosing the delay terms included in the model of the short-term blood pressure control mechanisms.

A number of delay values for many different sections and arcs of the baroreflex have been reported by different authors (Warner 1969; Borst 1983; Rideout 1991). Borst and Karemaker (Borst 1983) published a comprehensive review of the delays calculated in many of these studies. The experimentally calculated delay values, used for calculation of the delay parameters for the model of the baroreflex, and commented on in this text, are documented in Table 6.7.

Delay	Ref	Subject	Section of baroreflex & experimental procedure	Delay value
1	(Ikeda 1996)	Rabbit	Full baroreflex: $p_b$ to $p_b$	1.55 s
2	(Ikeda 1996)	Rabbit	Neural arc: $p_b$ to SNA measurement	0.55 s
3	(Ikeda 1996)	Rabbit	Peripheral arc: SNA measurement to $p_b$	1 s
4	(Liu 2002)	Rabbit	Central + peripheral arcs: afferent nerve stim. to $p_b$	1.01 s
5	(Bertram 1998)	Rat	Central + peripheral arcs: afferent nerve stim. to $p_b$	0.82–0.86 s
6	(Green 1968)	Cat	Central arc	0.2 s
7	(Kezdi 1968)	Dog	Central arc	0.26 s
9	(Kubo 1996)	Rabbit	Central arc	0.43
10	(Terui 1987)	Rabbit	Central arc	0.15 - 3s
11	(Petiot 2001)	Rat	Central arc	0.1 s
12	(Guild 2001)	Rabbit	Renal nerve stimulation to blood flow	0.672 s
13	(Kawada 1996)	Rabbit	Peripheral arc: sympathetic nerve stim. to $p_b$	0.47 s
14	(Kawada 1996)	Rabbit	Peripheral arc: parasympathetic nerve stim. to $p_b$	0.087 s
15	(Berger 1989)	Dog	Peripheral arc: parasympathetic nerve stim. to $p_b$	0.6 s

Table 6.7: Delay values, from the literature calculated for sections of the baroreflex feedback loop.

The delay of the overall baroreflex, for the rabbit, was estimated by Ikeda *et al* (Ikeda 1996). This delay combined the delay in the neural arc with the delay in the peripheral arc. The delay they report is 1.55 s, divided into 0.55 s for the neural arc and 1 s for the peripheral arc (see Figure 2.1). Eckberg (Eckberg 1980) reported a delay of 2.5 s for the human baroreflex using a neck suction procedure to perturb blood pressure at the baroreceptor locations.

Liu *et al* (Liu 2002) investigated the dynamical response of the rabbit's blood pressure to afferent nerve stimulation and calculated the pure time delay along this pathway as 1.01 s (Delay 4, in Table 6.7). The section of the baroreflex loop under analysis in this study may be assumed to be the complete baroreflex loop, excluding the baroreceptor transduction properties or, in other words, the central and peripheral arcs of the baroreflex. Bertram *et al* (Bertram 1998) calculated the delay for the same section of the baroreflex, except for the rat. They report a delay of 0.82 - 0.86 s, which they conclude accords well with summed delays due to the latency of conduction along the nervous pathways and the delay at the neuroeffector junction (Delay 5 in Table 6.7). Delays in individual components are now documented in the following subsections.

#### *Delay in the feedback path*

The delay in the feedback path of the model consists of what may be termed the baroreceptor transduction delay plus a delay due to the conduction along the afferent nerve. The baroreceptor transduction delay is the time taken for the baroreceptors to sense a change in blood pressure, while the afferent delay is the time it takes for the sensory information to be sent from the baroreceptors to the CNS.

Comparison of the delays calculated by Ikeda *et al* (Ikeda 1996) for the complete baroreflex (Delay 1 in Table 6.7) and those calculated by Liu *et al* (Liu 2002) (Delay 4 in Table 6.7) and Bertram *et al* (Bertram 1998) (Delay 5 in Table 6.7) between afferent nerve stimulation and blood pressure, proposes a relatively long afferent

and/or baroreceptor transduction delay. However, some authors have proposed that the transduction delay of the arterial baroreceptors is negligible (Charlton 1982).

Little information exists in the literature regarding correct values of afferent delay. Some authors (Burgess 1997) choose the delay between afferent nerve stimulation and efferent nerve activity as the afferent delay but this delay will include the latency due to central processing and will not include the full delay due to conduction time along the afferent nerves, since the afferent nerve is sectioned. The afferent delay and baroreceptor transduction properties may be roughly approximated as the delay in the neural arc minus the delay in the central arc. This delay is approximately 150 - 200 ms (Delay 2 – Delay 6 in Table 6.7).

#### *Processing delay*

The processing delay is specifically the time that it takes to process the input afferent material in the brain and output the efferent nerve signals. Seller (Seller 1991) proposed that most of the time delay within the central nervous system originates from the very slow conduction velocity (0.15m/s) between the second-order neurons, in the processing sections of the brain.

The CNS is usually characterised by the dynamics of the neural or central arc (see Figure 2.1). The delay in the central arc has been calculated during experiments in a number of different animals (Green 1968; Kubo 1996; Petiot 2001). The delay was estimated to be of the order of 250 – 350 ms in the human (Borst 1983), 260 ms in dogs (Kezdi 1968), 200 ms in cats (Green 1968) and ~100 ms in the rat (Petiot 2001). More recent studies, in the rabbit (Terui 1987; Kubo 1996), reported the latency between aortic nerve stimulation and renal SNA to be between 0.15 – 0.3 s (Terui 1987) or 0.43 s (Kubo 1996), depending on the study. A delay of 0.4 s is deduced for use in the model (deduced from Delays 1, 4 and 9 in Table 6.7).

Considering the structure of the model chosen, the delay due to the feedback path is in series with the delay of the CNS. Hence, emphasis is instead placed on the fact that the sum of these delays should correctly characterise the delay of the neural arc, and hence that the individual values of the delays are not as significant to model integrity.

#### *Delay in the sympathetic innervation of the vasculature*

The delay in the sympathetic pathway is the time it takes for the sympathetic signal, which originates in the CNS, to conduct down the nerve and reach the effector organs. The time delays for the various sympathetic signals to reach the different vasculature beds are not documented for all these different vasculature beds. Delay values, for the conduction time of the sympathetic signal to reach the gut or liver, are generally not documented and because the skin is distributed over the whole body, the choice of a unique time delay may be inappropriate. The kidney is commonly the organ of interest during experimental studies (Burgess 1997; Guild 2001), since it commands such an important position in the neural control of blood pressure. Guild *et al* (Guild 2001) calculated a delay of 672ms between renal nerve stimulation and renal blood flow response, for the rabbit. Burgess *et al* (Burgess 1997) report that a change in blood pressure, in the rat, occurred after 0.4 to 0.6 s, following electrical stimulation of the renal sympathetic nerve. However, these delays may only be the delay time for a small portion of the nerve (and for the onset of vascular response (Bertram 1998)) and, hence, the conduction delay between the CNS and the peripheral vasculature is expected to be greater than this.

The delay value included in the sympathetic pathways to the different vascular beds is chosen as 0.85 s. This delay is deduced from Delays 3,4 and 9, in Table 6.7 documented in Table 6.7. The delay to the skin is also approximated by this single delay value. This should have no significant influence on model operation, since the skin is only weakly weighted, it being a minor recipient of cardiac output and having a weak baroreflex sensitivity (see Table 6.7).

### *Delay in the cardiac sympathetic branch*

The cardiac sympathetic delay is the time it takes for the sympathetic signal, which originates in the CNS, to conduct down the nerve and reach the effector organ, in this case the heart. Kawada *et al* (Kawada 1996) recorded values of the delay between stimulation of the sympathetic nerves (at a point along the nerve) and the heart (Delay 11 Table 6.7). However, the full efferent delay for this pathway is going to be greater than this value due to the extra nerve fiber between the site of stimulation and the CNS.

Kawada *et al* (Kawada 2001) report a of 50ms between stimulation of the response of the renal vasculature and the response of the heart following sympathetic nerve stimulation. Hence, due to this result, the delay of the sympathetic signal to the heart is taken to be 50ms less than the delay time to the vasculature.

### *Delay in the parasympathetic branch*

There is a paucity of investigative studies of the exact delay along the parasympathetic nerve. Rather, a common assumption is that heart rate control by the parasympathetic system is achievable on a beat-to-beat basis (Cavalcanti 2000). This assertion is supported by the few studies that do document the parasympathetic delay. Kawada *et al* (Kawada 1996) recorded a delay between stimulation of the parasympathetic nerves and the heart during tonic stimulation at three different frequencies. This delay averages to 0.087 s. These delay values are less than the minimum heart period of the rabbit. However, because the parasympathetic nerve is stimulated at the neck, this delay may only be the delay time for a small portion of the nerve and, the true delay may be longer than these documented values. In a similar study to that of Kawada *et al* (Kawada 1996), Berger *et al* (Berger 1989) reported a delay of ~0.6s, which is less than the heart period of the dog (Berger 1989).

Different values of the pure time delay of the parasympathetic branch of the baroreflex have been used in modelling studies. Some authors use a delay of within two or three cardiac beats (Ursino 2003), within one cardiac beat (Cavalcanti 2000) or in some cases the delay was viewed as too small to warrant inclusion in the model (Ottesen 1997; Seydnejad 2001).

However, on review of the literature, the viewpoint that holds most currency is that the parasympathetic system responds to blood pressure changes by affecting a change of heart rate within one cardiac cycle. Therefore, for the purpose of this study, the delay of the parasympathetic component is assumed to be approximately the time period of one cardiac cycle at rest  $\sim 0.27$  (Barrett 2003).

The chosen delays for the model are documented in Table 6.8 below.

Delay	Meaning	Value	Units
$\tau_a$	Afferent delay	0.2	seconds (s)
$\tau_{CNS}$	CNS processing delay	0.4	seconds (s)
$\tau_{pc}$	Efferent parasympathetic delay	0.3	seconds (s)
$\tau_{sc}$	Efferent cardiac sympathetic delay	0.8	seconds (s)
$\tau_k$	Efferent sympathetic delay to kidney	0.85	seconds (s)
$\tau_g$	Efferent sympathetic delay to gut	0.85	seconds (s)
$\tau_m$	Efferent sympathetic delay to muscle	0.85	seconds (s)
$\tau_s$	Efferent sympathetic delay to skin	0.85	seconds (s)

Table 6.8: The delays deduced from the delays documented in the literature and chosen for use in the complete model of the baroreflex.

## 6.7 Model of the complete baroreflex

Documented in the previous sections of this chapter are the different components of the baroreflex, to be used in the model of the complete baroreflex. These components are now combined to form the complete model of the baroreflex. The model includes descriptions of sympathetic and parasympathetic control of heart rate and separate distinctions of the sympathetic control of the different vasculature beds. In contrast to other models of the baroreflex, this model combines the effect of cardiac output and peripheral resistance on blood pressure using the simple 'Ohm's law' relationship described by Equation (2.1). The model, as presented in Figure 6.10 does not account for the differential dynamics of neural control of SNA travelling to the different organs. Although this differential dynamical control was observed by Kawada et al (Kawada 2001), no parameterisation of the transfer characteristics is available. Also, the small increase in the derivative gain that was observed will not significantly effect the slow oscillation. The block diagram of the complete model of the baroreflex is illustrated in Figure 6.10.

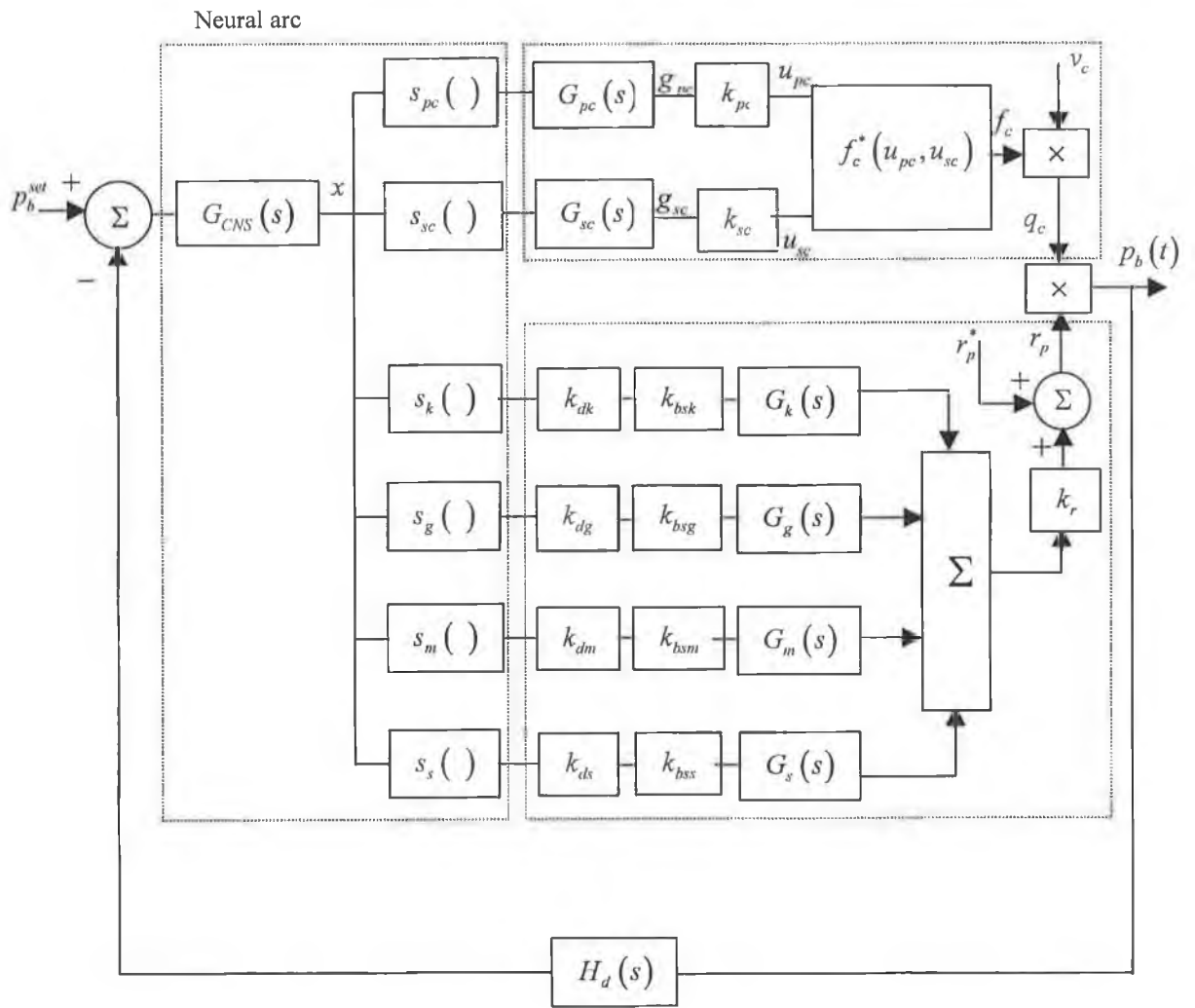


Figure 6.10: The complete model of the baroreflex.

The parameters of the model, illustrated in Figure 6.10, are documented in Tables 6.2, 6.4 and 6.5. All of the parameters are obtained from the rabbit and the choice of these parameters is justified in the previous sections of this chapter.

## 6.8 Model simulation results

When the model, parameterised for the rabbit as documented, is simulated in its closed loop form, a slow oscillation results at the output of the model. The power spectral density of the output signal of the model is shown in Figure 6.11.

The oscillation represents the slow oscillation in blood pressure that occurs at about 0.3 Hz in the rabbits (Malpas 2000), with the actual frequency from the simulation measured as 0.34 Hz.

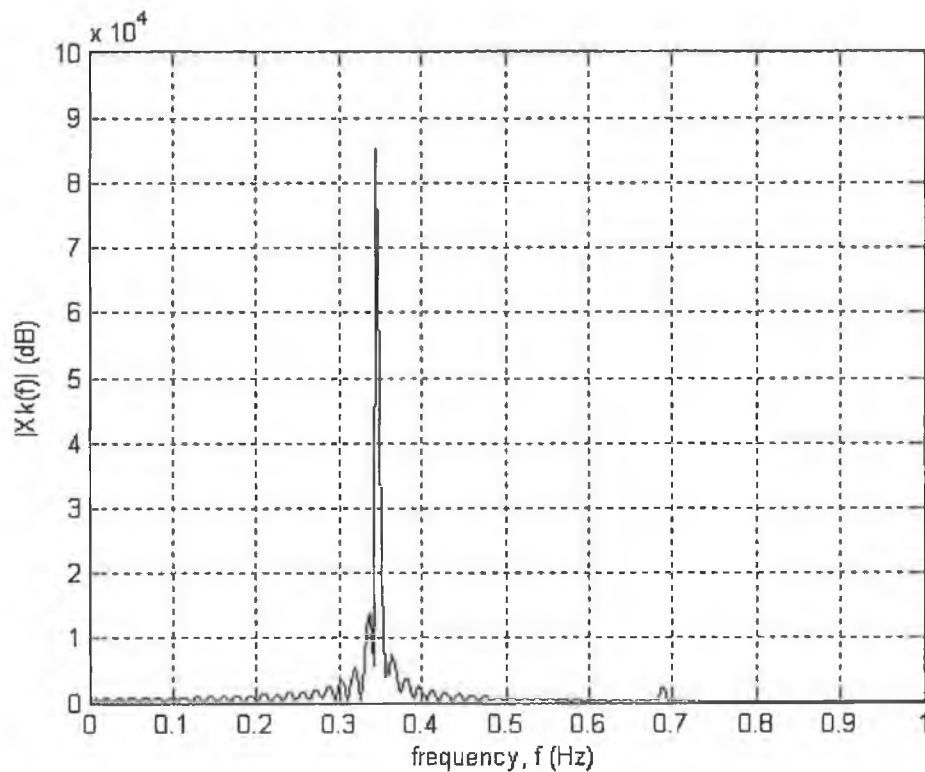


Figure 6.11: Spectrum of simulated blood pressure signal.

To assess the roles of the parasympathetic, cardiac and vascular sympathetic branches of the baroreflex mechanism in the development of the slow oscillation a

simple numerical sensitivity analysis of the gains and delays of the neural branches was undertaken.

The frequency and amplitude of the blood pressure oscillation calculated for the chosen parameter terms (Table 6.9, Value set 1) and for variations in the delay terms, are described in Table 6.9. The delay and curvature of the nonlinearities contained within the sympathetic paths to the multiple vascular beds are described by the universal delay,  $\tau_r$ , and curvature,  $\beta_r$ , respectively.

Parameter set	Oscillation frequency	Oscillation amplitude	$\tau_{pc}$	$\tau_{sc}$	$\tau_r$
1	0.345	9.1760	0.3	0.8	0.85
2	0.318	12.5686	0.4	0.8	0.85
3	0.276	17.4773	0.6	0.8	0.85
4	0.3828	3.4418	0.2	0.8	0.85
5	0	0	0.18	0.8	0.85
6	0.3525	7.5359	0.3	0.15	0.85
7	0.3487	10.4453	0.3	0	0.85
9	0.3638	10.853	0.3	0.15	0
10	0.3563	4.7331	0.3	0.15	1.7
11	0.3487	6.4429	0.3	0.15	10

Table 6.9: Values for oscillation frequency and amplitude following the variation of delays.

To assess the roles of the parasympathetic, cardiac and vascular sympathetic branches of the baroreflex mechanism in the development of the slow oscillation a sensitivity analysis of the gains of the sigmoid curves, in the neural arc of the parasympathetic and sympathetic branches, was undertaken. The gain of the sigmoid curves was varied by changing the curvature,  $\beta$ , of the curves.

With regard to the sensitivity to sigmoidal curve 'gains', the frequency and amplitude of the simulat blood pressure oscillation are described in Table 6.10.

Parameter set	Oscillation frequency	Oscillation amplitude	$\beta_{pc}$	$\beta_{sc}$	$\beta_r$
1	0.345	9.1760	0.14	0.04	0.04
2	0	0	0.1	0.04	0.04
3	0.3486	14.2238	0.2	0.04	0.04
4	0.3525	9.0802	0.14	0	0.04
5	0.3297	10.1148	0.14	0.2	0.04
6	0	0	0.14	0.04	0
7	0	0	0.14	0.04	0.2

Table 6.10: Values for oscillation frequency and amplitude following the variation of the gains of the sigmoid curves.

## 6.9 Discussion

This chapter documents the steps taken in the development of the model of the complete baroreflex, including the neural pathways to the heart. This model is illustrated in Figure 6.10 and the role of this model of the baroreflex in the genesis of the slow oscillation in blood pressure is investigated by simulation.

To date, a number of models of the mechanisms of short-term blood pressure control have been developed (see Section 2.4). However, the model presented here in this chapter overcomes a number of shortcomings of these other models. Previously developed models were introduced in Section 2.4, where aspects of the models were appraised. In general, although each of these models enables significant insight into the mechanisms of blood pressure control and the means of genesis of blood pressure variability, many are based on a simplified description of baroreflex function or are physiologically inaccurate or unrealistic.

The model presented here includes both the cardiac and peripheral resistance branches of the baroreflex, different descriptions of the different vasculature beds and a term to include the vascular resistance due to the vascular beds not under neural control. The model is stringently parameterised for the rabbit using data and characteristics obtained only from the rabbit, from a wide appraisal of the literature and experimental results. The slow oscillation ultimately results as a consequential property, when all the components of the baroreflex are combined, and the model is simulated.

The primary result of this study is that the slow oscillation in blood pressure is a feedback oscillation due to the closed-loop, feedback nature of the baroreflex mechanism. It is also a limit cycle oscillation, due to the nonlinear elements in the neural components of the baroreflex mechanism.

The slow oscillation in blood pressure is dependent on the sympathetic nervous system and removal of the sympathetic pathway to the vasculature results in the abolition of the slow oscillation in blood pressure, a result observed during a number of physiological studies (see Section 2.3.3.2). Although other authors have reported the existence of a level of variability at the frequency of the slow oscillation, following removal of the sympathetic pathways to the vasculature, this is probably due to compensatory effects that come into play following the removal of the sympathetic neural control of peripheral resistance, which is not reproduced by the model in its present form.

Although the simulant slow oscillation is dependent on the sympathetic control of the peripheral resistance, it is also very much dependent on the baroreflex pathways to the heart. Removal of these pathways also results in the abolition of the slow oscillation.

In fact, the heart plays a very significant role in the genesis of the slow oscillation in blood pressure. This is in contrast to the generally accepted view, held by

physiologists, that the heart plays no role in the development of the slow oscillation (see Section 2.3.3.3).

Results of the sensitivity analysis show that the strength of the slow oscillation in blood pressure is very sensitive to changes in the 'gain' and delay terms, particularly the 'gain' and delay of the parasympathetic pathway (see Tables 6.9 and 6.10). Alteration in both the gain and delay in the different pathways results in changes in the amplitude and frequency of the slow oscillation, and in the case of the parasympathetic pathway, which has the largest 'gain' of all pathways due to the steeper slope of the baroreflex characteristic, variations in gain, and delay, result in the abolition of the oscillation (Parameters sets 5 and 2 of Tables 6.9 and 6.10 respectively).

However, changes in the 'gain' and delay of the cardiac sympathetic pathway have little influence on the frequency and amplitude of the slow oscillation. Although the cardiac sympathetic pathway increases heart rate and hence, plays a significant role in maintaining the mean level of cardiac output (and hence, the gain (see Figure 6.12)). However, the results of this study show that the slow oscillation in blood pressure is not dependent on the gain and delay parameters of the cardiac sympathetic pathway.

Physiological studies that dismiss the role of the heart, in the genesis of the slow oscillation, are generally based on the removal of the effects of the heart, via blockade of the neural pathways to the heart (Liu 2002). One such study was recently documented by Liu *et al* (Liu 2002) who documented the dynamical response of blood pressure to renal SNA during afferent nerve stimulation when the parasympathetic and sympathetic neural control of the heart was blocked.

The main conclusion of the study of Liu *et al* (Liu 2002), is easily explained by the model of the complete baroreflex, with an alternative conclusion. In the experiments of Liu *et al* (Liu 2002), mean heart rate was found to drop from 265 bpm to 206 bpm

which gives an effective mean reduction in cardiac output of 3dB, which is almost exactly the mean gain reduction in the renal frequency response (51 → 48.8 dB).

However, this result gives little information regarding the ability of the cardiac loop to sustain oscillations itself. The influence of the mean level of cardiac output is illustrated using the simple example of Figure 6.12. The significance of the mean levels of heart rate and peripheral resistance are accentuated due to the multiplier block at the output.

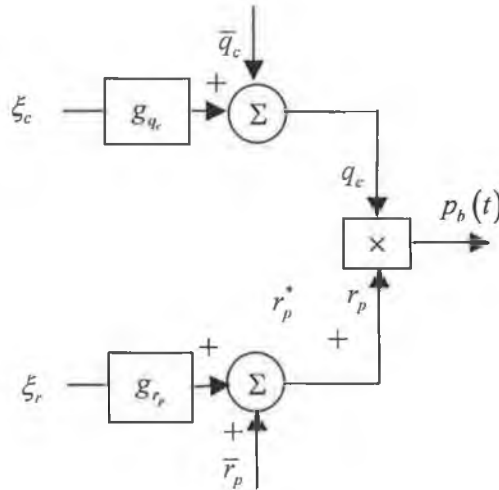


Figure 6.12: The effect of the multiplier.

A simple analysis of this part of the model illustrates the gain effect of the mean levels of cardiac output and peripheral resistance. The blood pressure signal may be described by:

$$p_b(t) = (g_{q_c} \xi_c + \bar{q}_c)(g_{r_p} \xi_r + \bar{r}_p) \quad (6.8)$$

$$= g_{q_c} g_{r_p} \xi_c \xi_r + \bar{q}_c \bar{r}_p + g_{q_c} \xi_c \bar{r}_p + g_{r_p} \bar{q}_c \xi_r \quad (6.9)$$

The mean level of resistance,  $\bar{r}_p$ , multiplies the  $\xi_c$  signal and the mean level  $\bar{q}_c$  multiplies the  $\xi_r$  signal. Hence, the mean level in one path is essentially, the gain of the path. This illustrates how the mean levels are inherently involved in maintaining

gain, and therefore mediating the oscillation. Hence, the conclusion that the heart plays no significant role in the maintenance of the slow oscillation, as its removal results in a decrease in the gain of the frequency response may be misinterpreted, considering the decrease in the mean heart rate level and the described interdependence of gain and mean levels.

A large amount of research has also focused on the association between the mean level of SNA and the slow oscillation in blood pressure. This research focused on the possible causal relationship between the strength of the slow oscillation and the mean levels of blood pressure (see Section 4.3.3). The mean levels of heart rate and peripheral resistance are influenced by the mean levels of SNA and parasympathetic activity. Hence, it is proposed that the mean levels of SNA are indeed of significance in mediating the slow oscillation.

The lack of a role for the heart in the genesis of the slow oscillation of blood pressure has also been proposed by authors of modelling studies of baroreflex function (Burgess 1997). These authors suggested that other pathways of the baroreflex, other than sympathetic pathways to the vasculature, are not necessary for the generation of the slow oscillation in blood pressure. Most interestingly, they propose that given the faster responses of the vagus that, if the changes in heart rate were important in producing the oscillation in blood pressure, then heart rate changes would buffer out the slow oscillation. This proposal is rebuffed by the results of this study. The baroreflex is a closed loop system and the oscillation around the closed loop exists at a unique frequency. The oscillation in the parasympathetic pathway is at the same frequency as the oscillation in blood pressure and hence, the oscillation in blood pressure, is in part, maintained via the parasympathetic pathway.

The influence of the different parameters of the baroreflex in mediating the slow oscillation become even more obvious following an analytical analysis of the limit cycle oscillation, which is the focus of the subsequent chapter.

### *Limitations*

The model developed describes only baroreflex control of blood pressure, via the heart and the vasculature. However, other mechanisms, including the chemoreflex and cardiopulmonary reflex, have been proposed to modulate baroreflex activity and effect blood pressure in the short-term are not described by this model. There is a paucity of information available regarding the working of these mechanisms and because their affect on blood pressure is an ancillary effect these mechanism will show varying influences on blood pressure depending on the conditions under analysis. These mechanisms may modulate the slow oscillation in blood pressure, however, the model of the complete baroreflex shows that the baroreflex feedback loop is capable of creating and sustaining the slow oscillation in blood pressure alone.

Similarly, this model cannot explain longer-term variations in blood pressure as these variations are developed by other blood pressure controllers that act over longer time scales, such as hormonal and renal-fluid balance systems.

Malpas *et al* (Malpas 2003) commented on the difficulty in determining what each level of stimulation of the nerve relates to in terms of changes in endogenous SNA. Hence, as is the case for all such experimental studies, the documented characteristics may not perfectly resemble the true physiological case but are the best means available to analyse this relationship in the open-loop situation.

## 6.10 Conclusions

It is concluded, from the results of the combined heart-resistance model, that the heart plays a significant role in mediating the slow oscillation. This is in contrast to the generally accepted view.

Removal of any of the branches of the baroreflex, in the model, results in the abolition of the slow oscillation. The slow oscillation is dependent on the sympathetic nervous control of vascular resistance but is also, and to a greater extent, dependent on the cardiac loop, particularly the parasympathetic pathway. The influence of the parasympathetic pathway to the heart was demonstrated by the significant variation in the strength and frequency of the oscillation, when the delay, and gain, along these pathways are altered. In contrast the oscillation frequency and amplitude are relatively insensitive to changes in the delay, and gain, of the cardiac sympathetic pathway. Hence, it is proposed that the cardiac sympathetic loop plays a passive role in mediating the slow oscillation, and its role, in sustaining the slow oscillation in blood pressure, is limited to its ability to increase mean heart rate.

In conclusion, it is proposed that the model enables better understanding of the mechanisms of the baroreflex and the influence of the different components and sections of the baroreflex involved in the genesis of the slow oscillation in blood pressure.

## Chapter 7

# Nonlinear analysis of the complete model

## 7.1 Introduction

The model of the complete baroreflex, parameterised for the rabbit, produces an oscillation at  $\sim 0.3$  Hz, the frequency of the slow oscillation in the blood pressure of the rabbit. However, simulation of the model alone does not allow for full insight into the features of the model responsible for the genesis and maintenance of the slow oscillation.

Other modelling studies of the baroreflex, that have been undertaken, have generally only documented simulation results and in some cases a simulated sensitivity analysis of the influence of the different gains of the model (Seydnejad 2001; Ursino 2003). The influence of time delays and the different gain terms in baroreflex models has been investigated and the mathematical route to chaos via alterations of the time delays and gain values has been analysed (Abbiw-Jackson 1998; Seidel 1998; Cavalcanti 2000). However, although the blood pressure system has been shown to exhibit chaotic characteristics (see Chapter 3) the physiological reality of changing time delays or gains are generally not justified (Abbiw-Jackson 1998; Seidel 1998; Cavalcanti 2000).

Due to the fact that the published models of the baroreflex are generally complex, and contain multiple, coupled pathways, analytical analysis of these models is generally avoided. The analytical analysis of baroreflex function is generally confined to the analysis of simplified models of the baroreflex (Ringwood 2001). In this chapter, analytical analysis of the model of the complete baroreflex, described in Chapter 6, is documented.

An analytical analysis of the model is undertaken so that:

1. The frequency and amplitude of the slow oscillation may be calculated analytically from the model description of the baroreflex controlling mechanism.
2. The significance of the different components and parameters involved in the development of the slow oscillation in blood pressure can be identified.

The most popular methods for analytical analysis of systems are based on the theory of linear systems (Brilliant 1958). The techniques of analysis of linear systems are, at this stage, well developed, and these are used for analysis of both linear and nonlinear (in linearised form) systems (Brilliant 1958). However, sometimes, as is the case for the system under analysis in this study, the nonlinearity is essential to the operation of the model, hence, a method of nonlinear analysis of the model is required.

Nonlinear analysis methods have already been introduced in this thesis, in Chapter 3, where, a nonlinear, time series analysis of blood pressure data was documented. The model of baroreflex control of peripheral resistance (Figure 4.1) was analysed in Chapter 4 using describing function analysis techniques. The method of nonlinear model analysis using describing functions is well documented in the control literature (Mees 1975; Woon 1977; Atherton 1982) and this analysis method is described in Section 4.5.1. This traditional describing function approach is pertinent to the analysis of the classic single loop system of Figure 4.1. The expansion of this fundamental analysis to more complex nonlinear systems, including systems with

series and parallel combinations of linear and nonlinear elements, is also documented by a number of authors (Jud 1964; Gran 1965; Bhargava 1970; Davison 1971; Atherton 1982). However, these methods are generally constrained to deal with nonlinear systems of specific configurations.

The model of the complete baroreflex contains multiple interconnected pathways (Figure 6.10). However, the complexity of the baroreflex system is not limited to its multiple path structure, but is further enhanced by complicated nonlinear functions (Equation 6.5), and the multiplier at the system output. Methods of analysis of models containing multipliers are not commonly documented in the control literature.

The analysis approaches of the model of the complete baroreflex, investigated in this work, are based on classic describing function theory. The analysis is developed in the subsequent sections of this chapter.

## 7.2 Model simplification

Models with multiple nonlinear pathways are generally difficult to analyse, as a good deal of the simplicity of the analysis of the simple feedback loop is lost when more than one nonlinear element is contained in the model, unless the nonlinearities are directly in series or parallel (Davison 1971). The model of the complete baroreflex, with its many nonlinear branches is, in general, too cumbersome to examine in terms of limit cycle oscillation. This model, illustrated in Figure 6.15, has common components in some of its multiple branches, and hence, the number of nonlinear pathways may effectively, be reduced. Also, the model contains some complex characteristics that may be simplified. For these reasons, the simplified model of Figure 7.1 is proposed.

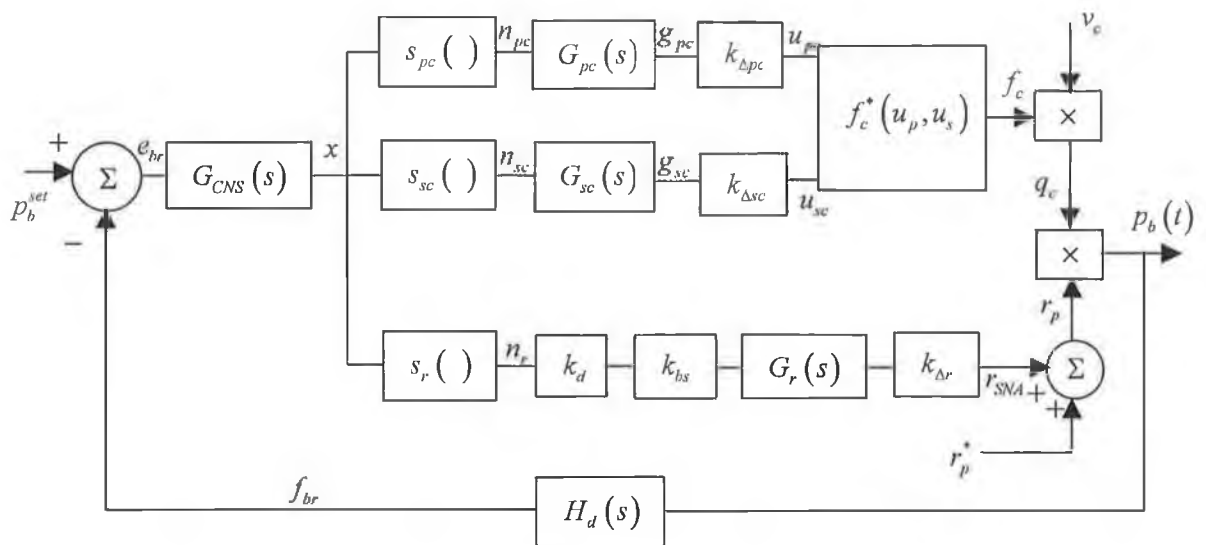


Figure 7.1: The simplified model of the baroreflex including heart and peripheral resistance paths.

Simplifications of the model illustrated in Figure 6.15 to that illustrated in Figure 7.1 are documented in the subsequent section.

### *Reduction in the number of vascular beds*

The simplified model still retains the individuality of cardiac sympathetic, cardiac parasympathetic and peripheral resistance branches, but the multiple sympathetic pathways that control the resistance of the different vascular beds are reduced to one single uniform representation of peripheral resistance control. In this simplified representation, the dynamics of the renal vasculature are chosen as the uniform representation of sympathetic control of the vasculature, since the dynamics of the vasculature are best described for the kidney (see Section 2.2.3.2) and because the kidney also has dominant effects on blood pressure (see Section 2.2.3.3) and receives a large proportion of cardiac output (Dworkin 2000) and is highly innervated (Guild 2002). For these reasons, the kidney may be the key organ of the vasculature involved in the genesis of the slow oscillation (see Section 4.4) (Malpas 2002). Hence,  $G_r(s)$  is as given in Equation (6.7). The cardiac output distribution weights for the individual innervated resistance pathways are averaged to give,  $k_d$ .

Similarly,  $k_{bs}$  is determined as the average of the baroreflex sensitivities for the individual pathways.

*Linearisation of the parasympathetic-sympathetic interaction function*

The nonlinear function of Equation (6.5), which describes the static relationship between parasympathetic ( $u_{pc}$ ) and sympathetic ( $u_{sc}$ ) nerve stimulation frequency and heart rate, is a nonlinear, dual-input, function. A complicated describing function would be required to describe this nonlinearity, and such a describing function may not allow for the level of transparency of the parameters that would enable insightful analysis of baroreflex function. Also, the complicated nonlinear function of Equation (6.5) is not expected to be involved in the genesis of the limit cycle oscillation as it does not contain an inflection, which could give rise to a sustained limit cycle oscillation. When fitted to the data of the rabbit,  $s_{pc} = -8.11$  and  $s_{sc} = 4.87$ . Therefore, Equation (6.5) is linearised to the affine linear function:

$$f_c(t) = s_{pc}u_{pc}(t) + s_{sc}u_{sc}(t) + f_c^0 \quad (7.1)$$

where,

$s_{pc}$  and  $s_{sc}$  are the ‘gains’ related to the parasympathetic and sympathetic nerve activity respectively, and

$f_c^0$  is the autorhythmic heart rate value.

*Describing function approximation of the sigmoid nonlinearities*

The describing function was introduced in Section 4.5.1 and describing function approximations, for the sigmoid nonlinearity, are introduced in Chapter 5. Using the approximation method proposed in Chapter 5, analytical descriptions for the sigmoid nonlinearities of the model are developed.

The sigmoids in the model,  $s_{pc}(\cdot)$ ,  $s_{sc}(\cdot)$  and  $s_r(\cdot)$ , may be described by their describing functions  $N_{pc}^*(M, \omega)$ ,  $N_{sc}(M, \omega)$  and  $N_r(M, \omega)$  respectively. As is the case for the sigmoid in the model illustrated in Figure 4.1, these nonlinearities are all odd and, hence the describing function is real and independent of the input frequency,  $\omega$ . Therefore,  $N_{pc}^*(M, \omega)$ ,  $N_{sc}(M, \omega)$  and  $N_r(M, \omega)$  may be reduced to  $N_{pc}^*(M)$ ,  $N_{sc}(M)$  and  $N_r(M)$  (Slotine 1990).

The describing function analysis method begins with the assumption of a sinusoidal input at  $x$ , in Figure 7.1:

$$x(t) = M \sin(\omega t) \quad (7.2)$$

This assumption is common to describing function analysis of nonlinear systems (Atherton 1982). It is also assumed during the course of this analysis that, during steady-state or limit cycle operation, the harmonics arising in the sigmoidal nonlinearities described by  $s_{pc}(\cdot)$ ,  $s_{sc}(\cdot)$  and  $s_r(\cdot)$  (described by Equations (2.3), and parameterised according to Table 6.2 and 6.3) are of negligible influence due to the low-pass nature of  $G_{pc}$ ,  $G_{sc}$  and  $G_r$  respectively (described by Equations (6.12), (6.13) and (6.14) respectively).

In addition, the multiplier at the output of the nonlinearity introduces double frequency components to the signal. These double frequency components may be ignored as they are also filtered out by  $G_{pc}$ ,  $G_{sc}$  and  $G_r$  when the signal traverses the loop again. These assumptions are supported by examination of the spectrum of  $x(t)$  ( $X(\omega)$ ) attained during simulated limit cycle operation, as shown in Figure 7.2.

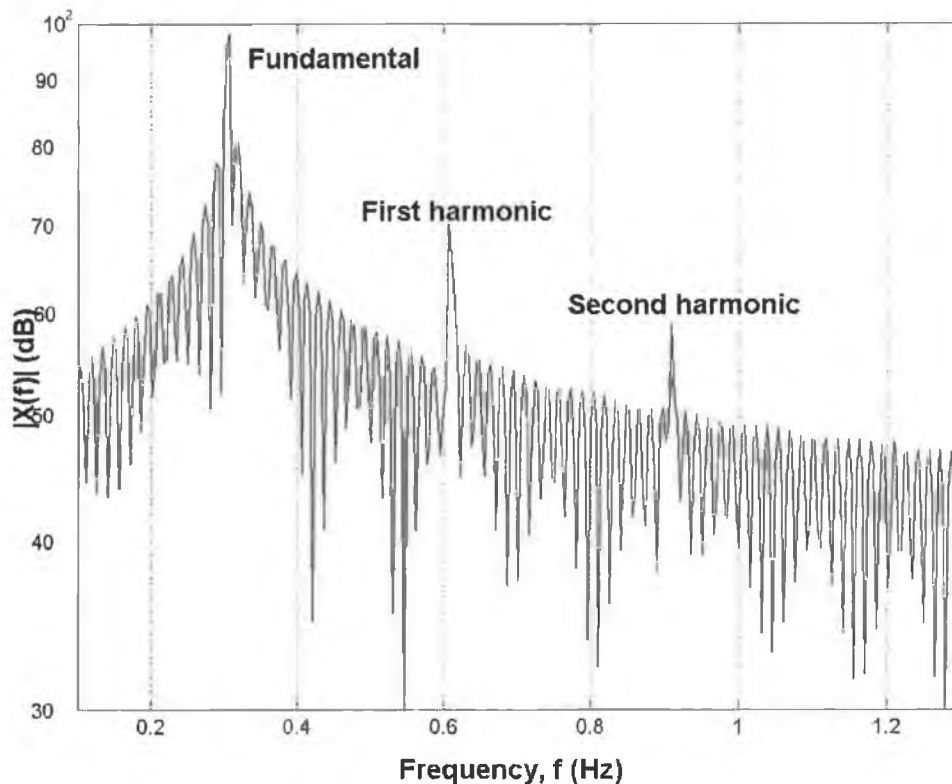


Figure 7.2: Spectrum of  $x(t)$  during limit cycle operation.

### 7.3 Preliminary analytical approaches

A number of different analysis approaches were investigated. The analysis of nonlinear systems based on the use of Poincare maps is a well researched field (Jordan 1987) and may be applicable to the analysis of this model. However, one of the main aims of this study is to investigate which parameters are notably involved in the development of the slow oscillation. Analysis methods such as the Poincare map may not enable this level of insight into system operation. Considering the need for clear insight of baroreflex function and hence, the need for a large level of transparency from response to the model parameters, the describing function technique is proposed as the fundamental basis for the analysis presented in this

chapter. Nonlinear analysis involving describing function techniques allows for the representation of both linear and nonlinear model components by enabling the extension of linear frequency response analysis to the nonlinear case (Lewis 1997). Analytical approximations of the describing functions of the sigmoid nonlinearities have already been introduced (see Chapter 5) and this development enables a purely analytical analysis of models containing the sigmoid (Kinnane 2004).

Three different analysis approaches, all based on the describing function, are introduced in this chapter. These methods are referred to in this text as:

1. Frequency domain analysis, based on the convolution of time domain signals
2. Frequency domain analysis, based on input-output Laplace function
3. Time domain analysis – the development of the conditions for sustained oscillation

A benefit of the frequency domain analysis methods is that graphical representations can be used to facilitate analysis of the system. As an example, the Nyquist diagram may be used in the analysis and determination of a system's stability (see Section 4.5.1 and Figure 4.5). However, emphasis is put on the time domain analysis approach. Although it doesn't enable exploitation of the graphical benefits of the frequency domain analysis methods, it is possible, in theory at least, to develop a set of oscillation conditions which depend directly on the model parameters.

The frequency domain analysis approaches are first introduced (Sections 7.3.1 and 7.3.2), beginning with the frequency domain analysis technique, based on the convolution of the time domain signals at the multiplier at the output of the model. This is followed by the time domain analysis of the model in Section 7.3.3.

### 7.3.1 Frequency domain analysis based on the convolution of the time domain signals

The sine wave of Equation (7.2), is described in the Laplace domain as:

$$X(s) = M \left( \frac{\omega}{s^2 + \omega^2} \right) \quad (7.3)$$

For specific values of amplitude,  $M$ , the describing function gains may be dealt with as amplitude dependent linear gain terms. Given this, the nonlinear model of Figure 7.1 may be represented by the associated linearised model illustrated in Figure 7.3.

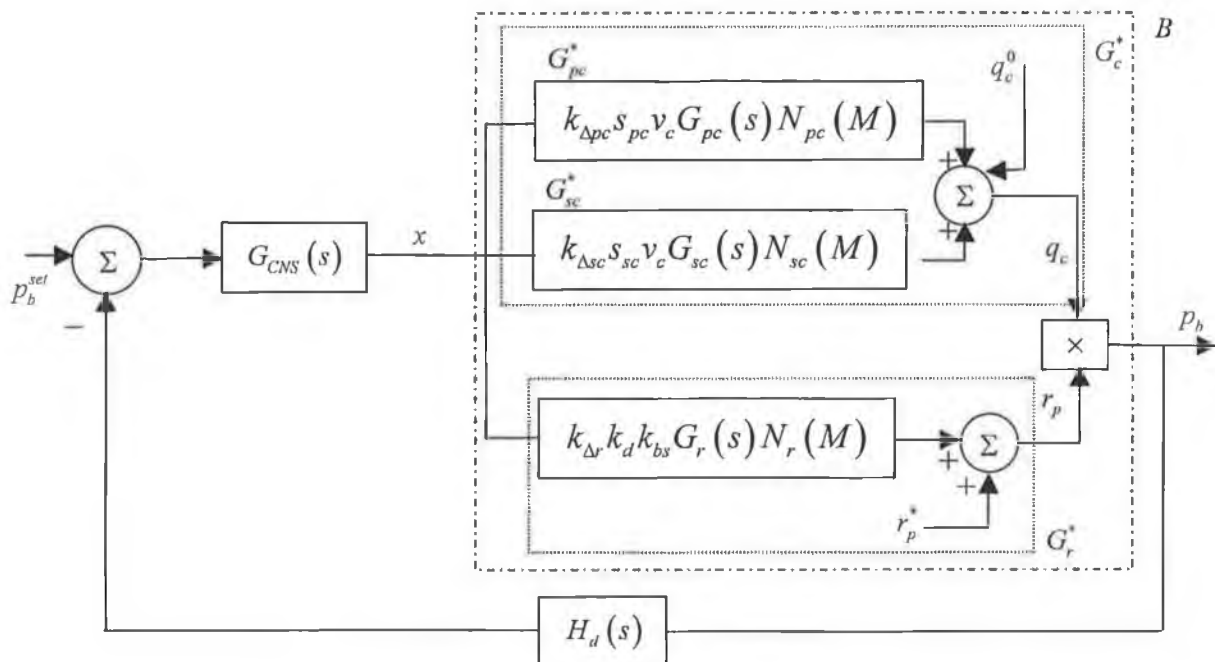


Figure 7.3: The associated linear model structure for frequency domain analysis.

The stroke volume term,  $v_c$ , which multiplies heart rate (Equation 2.2) is incorporated in the associated linear transfer functions of  $G_{pc}^*(s)$  and  $G_{sc}^*(s)$ . Similarly, the gains of the affine linear function described in Equation (7.1),  $s_{pc}$  and  $s_{sc}$ , are incorporated in the associated linear transfer functions. Then the resting cardiac output,  $q_c^0 = f_c^0 v_c$ .

Now, the associated linear transfer functions of the parasympathetic, cardiac sympathetic and vascular sympathetic pathways,  $G_{pc}^*(s)$ ,  $G_{sc}^*(s)$  and  $G_r^*(s)$  are described by:

$$G_{pc}^*(s) = N_{pc}(M)G_{pc}(s)k_{\Delta pc}s_{pc}v_c \quad (7.4)$$

where,

$k_{\Delta pc}$  is the conversion gain in the parasympathetic path (see Section 6.5), and

$G_{pc}(s)$  is as given in Equation (6.4)

also,

$$G_{sc}^*(s) = N_{sc}(M)G_{sc}(s)k_{\Delta sc}s_{sc}v_c \quad (7.5)$$

where,

$k_{\Delta sc}$  is the conversion gain in the sympathetic path (see Section 6.4.1), and

$G_{sc}(s)$  is as given in Equation (6.3)

Finally,

$$G_r^*(s) = N_r(M)k_d k_{bs}G_r(s)k_{\Delta r} + r_p^* \quad (7.6)$$

where,

$k_d$  is the sum of cardiac distribution to the vascular beds (see Section 6.5),

$k_{\Delta r}$  is the conversion gain in the peripheral resistance branch (Section 6.5),

$k_{bs}$  is the sum of baroreflex sensitivities of the different vascular beds, and

$G_r(s)$  is as given in Equation (6.3).

$G_c^*(s)$  is then calculated as:

$$G_c^*(s) = G_{pc}^*(s) + G_{sc}^*(s) + q_c^0 \quad (7.7)$$

The presence of a constant, mean term in Equations (7.6) and (7.7) prevents the development of the transfer functions  $G_r^*(s)$  and  $G_c^*(s)$ . If, conceptually at least, transfer functions can be written, the Laplace representation of the cardiac output signal is then given by:

$$Q_c(s) = G_c^*(s)X(s) \quad (7.8)$$

and the Laplace representation of the total peripheral resistance signal is given by:

$$R_p(s) = G_r^*(s)X(s) \quad (7.9)$$

Equation (2.1) may be represented in the Laplace domain as:

$$P_b(s) = L\{q_c(t)r_p(t)\} \quad (7.10)$$

This may be expanded in the convolution integral (Bronstein 1995) as:

$$P_b(s) = \frac{1}{2\pi i} \int_{x_1-i\infty}^{x_2+i\infty} Q_c(\rho)R_p(s-\rho)d\rho \quad (7.11)$$

where,

$\rho$  is a variable of integration, and

$x_1$  is chosen such that  $\rho$  is in the region of convergence of  $L\{q_c\}$  and such that  $s - \rho$  is in the region of convergence of  $L\{r_p\}$  (Bronstein 1995).

Considering the complexity of the transfer functions,  $G_{pc}(s)$ ,  $G_{sc}(s)$  and  $G_r(s)$ , Equation (7.11) represents a complicated integral but may be calculated, for example, using the residue theorem (Kreyszig 1999). Following calculation of  $P_b(s)$ , an input-output relationship, between  $X(s)$  and  $P_b(s)$  may then be calculated. This is given by:

$$B(s) = \frac{P_b(s)}{X(s)} \quad (7.12)$$

Calculation of the characteristic equation for the system enables the separation of the describing function part ( $N^*(M)$ ) and the linear function ( $B(s)$ ). Hence, when calculated for a range of  $M$  values the locus of  $-1/N^*(M)$  may, in theory, be plotted on the Nyquist plot and the point of intersection of  $-1/N^*(M)$  and the linear dynamical plots may be calculated.

This approach was preliminary investigated for a step input. The complex integral (Equation (7.11)) that results for a sinusoidal input significantly increases the complexity of this analysis approach. This analysis approach was not pursued as it appears that it may not provide as much insight into system operation as other analysis methods and because it also involves lengthy and involved calculations. However, if this analysis approach were to enable analytical calculation of the frequency and amplitude of the limit cycle oscillation, then such an exercise would be worthwhile. This analysis method is left as an area for future research.

### 7.3.2 Frequency domain approach based on the Laplace transform

An alternative analysis approach to the frequency domain approach, based on the convolution of the time domain signals, is the development of an input-output Laplace function between the sinusoidal input and the signal at the output of the model. The signal at the output of the model,  $p_b(t)$ , may be derived using a time domain analysis approach of the model of Figure 7.1. A time domain analysis approach of the model, is documented in Section 7.3.3. Then, it is proposed that  $B(s)$ , in the associated linear model of Figure 7.3, may be calculated as:

$$B(s) = \frac{L\{p_b(t)\}}{X(s)} \quad (7.13)$$

where,  $p_b(t)$  is the blood pressure signal, and

$X(s)$  is as given in Equation (7.3).

This analysis may be developed in the same way as the other frequency domain analysis method, and may allow for the use of Nyquist stability diagrams to analyse the model and solve for the frequency and amplitude of the oscillation. Again, such an approach is left for future research.

An alternative, more tractable and more insightful approach was instead investigated to analyse the complete baroreflex model. This approach is documented in the subsequent section.

### 7.3.3 Development of the conditions for sustained oscillation

This approach is based on the time domain analysis of the traversing signal of the model. Using this approach, conditions for the maintenance of a sustained limit cycle oscillation are developed. It is proposed that these conditions describe the requirements necessary for the slow oscillation in blood pressure to exist. Since these conditions are based on the parameters of the model, they will enable a level of transparency of the parameters of the model. This will allow new insight into aspects of the model involved in the genesis of the slow oscillation.

Referring to the model illustrated in Figure 7.1, the analysis of the model in the time domain is developed as follows. The sine wave signal of Equation (7.2) is input to the nonlinearities described by  $s_{pc}(\cdot)$ ,  $s_{sc}(\cdot)$  and  $s_r(\cdot)$ . The describing functions for these nonlinearities are  $N_{pc}^*(M)$ ,  $N_{sc}(M)$  and  $N_r(M)$  respectively.

As is evident in Figures 6.3, these nonlinearities are not centered at the origin but are offset in the vertical direction (*i.e.* offsets) by  $C_{pc}$ ,  $C_{sc}$  and  $C_r$ .

The output signals of the nonlinearities are periodic functions that may be described using a Fourier series, however, as discussed these harmonics are assumed to disappear. Therefore, the output signals of  $s_{pc}(\cdot)$ ,  $s_{sc}(\cdot)$  and  $s_r(\cdot)$  are:

$$n_{pc}(t) = C_{pc} + N_{pc}^*(M) \sin(\omega t + \phi_{pc}) \quad (7.14)$$

$$n_{sc}(t) = C_{sc} + N_{sc}(M) \sin(\omega t + \phi_{sc}) \quad (7.15)$$

$$n_r(t) = C_r + N_r(M) \sin(\omega t + \phi_r) \quad (7.16)$$

Note that  $\beta_{pc}$  is negative (denoted by  $N_{pc}^*$  in Equation 7.2) so it is convenient to define:

$$n_{pc}(t) = C_{pc} + N_{pc}(M) \sin(\omega t + \phi_{pc} + \pi) \quad (7.17)$$

The nonlinearities of the sympathetic branches to the heart,  $s_{sc}(\ )$ , and the vascular,  $s_r(\ )$ , do not cause a delay to the response of the input. Therefore, they have no influence on the phase of the signal.

Therefore all three signals may be described as:

$$n_{pc}(t) = C_{pc} + N_{pc}(M) \sin(\omega t + \pi) \quad (7.18)$$

$$n_{sc}(t) = C_{sc} + N_{sc}(M) \sin(\omega t) \quad (7.19)$$

$$n_r(t) = C_r + N_r(M) \sin(\omega t) \quad (7.20)$$

This signal is multiplied by the baroreflex sensitivity gain ( $k_{bs}$ ) and by the cardiac output distribution weighting ( $k_d$ ) (see Section 7.2).

The linear dynamical blocks  $G_{pc}(s)$ ,  $G_{sc}(s)$  and  $G_r(s)$  introduce gain ( $|G_{pc}(j\omega)|$ ,  $|G_{sc}(j\omega)|$ ,  $|G_r(j\omega)|$  respectively) and phase ( $\angle G_{pc}(j\omega)$ ,  $\angle G_{sc}(j\omega)$ ,  $\angle G_r(j\omega)$  respectively) to the dynamical signals (Sections 6.4.1, 6.4.2 & 6.5.1). However, these dynamics are of unity d.c. gain (Section 6.4.1, 6.4.2 & 6.5.1) and, hence have no effect on the constant offset values ( $C_{pc}$ ,  $C_{sc}$ , and  $C_r$ ).

The output signals from the dynamical blocks may be described as:

$$g_{pc}(t) = |G_{pc}(j\omega)| N_{pc}(M) \sin(\omega t + \pi + \angle G_{pc}(j\omega)) + C_{pc} \quad (7.21)$$

$$g_{sc}(t) = |G_{sc}(j\omega)| N_{sc}(M) \sin(\omega t + \angle G_{sc}(j\omega)) + C_{sc} \quad (7.22)$$

$$g_r(t) = |G_r(j\omega)| k_d k_{bs} N_r(M) \sin(\omega t + \angle G_r(j\omega)) + k_d k_{bs} C_r \quad (7.23)$$

The signals  $g_{pc}(t)$  and  $g_{sc}(t)$  represent the innervations of the heart by the parasympathetic and cardiac sympathetic nerve pathways. These nerve signals have opposite effects on heart rate and interact in a complex fashion to adjust heart rate (Levy 1984) (Sections 2.2.3.1 and 6.4.3). Levy et al (Levy 1984) developed this relationship by electrically stimulating the nerves for a range of voltages. Hence, as described in Section 6.3.4 and 6.3.5, gain terms are required to transform the range of  $g_{pc}(t)$  and  $g_{sc}(t)$  (which are in terms of heart rate (bpm)) to the range of parasympathetic and cardiac sympathetic nerve stimulation frequencies. These gain values are termed  $k_{\Delta pc}$  and  $k_{\Delta sc}$ .

Therefore, the signals impacting on the nonlinear function describing the parasympathetic- sympathetic interaction are:

$$u_{pc}(t) = k_{\Delta pc} |G_{pc}(j\omega)| N_{pc}(M) \sin(\omega t + \pi + \angle G_{pc}(j\omega)) + k_{\Delta pc} C_{pc} \quad (7.24)$$

$$u_{sc}(t) = k_{\Delta sc} |G_{sc}(j\omega)| N_{sc}(M) \sin(\omega t + \angle G_{sc}(j\omega)) + k_{\Delta sc} C_{sc} \quad (7.25)$$

The dual-input nonlinear function describing the parasympathetic-sympathetic interaction is linearised to the affine function described by Equation (7.1). Using, (7.24) and (7.25) this equation may be expanded to:

$$f_c(t) = s_{pc} k_{\Delta pc} |G_{pc}(j\omega)| N_{pc}(M) \sin(\omega t + \pi + \angle G_{pc}(j\omega)) + s_{sc} k_{\Delta sc} |G_{sc}(j\omega)| N_{sc}(M) \sin(\omega t + \angle G_{sc}(j\omega)) + \bar{f}_c \quad (7.26)$$

where,

$$\bar{f}_c = f_c^0 + s_{pc} k_{\Delta pc} C_{pc} + s_{sc} k_{\Delta sc} C_{sc} \quad (7.27)$$

Then the cardiac output,  $q_c(t)$ , is as given in Equation 2.2:

$$q_c(t) = f_c(t) v_c(t) \quad (7.28)$$

A constant stroke volume,  $v_c$ , is assumed (see Section 6.4.4). Hence,

$$q_c(t) = v_c s_{pc} k_{\Delta pc} |G_{pc}(j\omega)| N_{pc}(M) \sin(\omega t + \pi + \angle G_{pc}(j\omega)) + v_c s_{sc} k_{\Delta sc} |G_{sc}(j\omega)| N_{sc}(M) \sin(\omega t + \angle G_{sc}(j\omega)) + \bar{q}_c \quad (7.29)$$

where,  $\bar{q}_c$ , the mean cardiac output is:

$$\bar{q}_c = v_c \bar{f}_c \quad (7.30)$$

The signal described by Equation (7.30) may be reduced to the form:

$$q_c(t) = K_{sc} \sin(\omega t + \phi_{sc}) + K_{pc} \sin(\omega t + \phi_{pc}) + \bar{q}_c \quad (7.31)$$

where,

$$K_{pc} = v_c s_{pc} k_{\Delta pc} |G_{pc}(j\omega)| N_{pc}(M) \quad (7.32)$$

$$K_{sc} = v_c s_{sc} k_{\Delta sc} |G_{sc}(j\omega)| N_{sc}(M) \quad (7.33)$$

$$\phi_{pc} = \pi + \angle G_{pc}(j\omega) \quad (7.34)$$

$$\phi_{sc} = \angle G_{sc}(j\omega) \quad (7.35)$$

Equation 7.31 may be further reduced to

$$q_c(t) = K_c \sin(\omega t + \phi_c) + q_c^0 \quad (7.36)$$

where,

$$K_c = \sqrt{K_{pc}^2 + K_{sc}^2 - 2K_{pc}K_{sc} \cos(\pi - \phi_{pc} + \phi_{sc})} \quad (7.37)$$

$$\phi_c = \tan^{-1} \left( \frac{K_{pc} \sin(\phi_{pc}) - K_{sc} \sin(\phi_{sc})}{K_{sc} \cos(\phi_{sc}) + K_{pc} \cos(\phi_{pc})} \right) \quad (7.38)$$

Finally, blood pressure  $p_b(t)$  is given as:

$$p_b(t) = q_c(t) r_p(t) \quad (7.39)$$

where,

$$r_p(t) = k_{\Delta r} g_r(t) + r_p^* \quad (7.40)$$

and  $k_{\Delta r}$  is a gain term introduced to scale the range of the output values of the nonlinearity,  $g_r(\cdot)$ , to blood vessel resistance values (see Section 6.5).  $r_p^*$  is the mean peripheral resistance not under neural control (see Section 6.5).

The peripheral resistance signal described by Equation (7.39) may be written as:

$$r_p(t) = K_r \sin(\omega t + \phi_r) + \bar{r} \quad (7.41)$$

where,

$$K_r = k_d |G_r(j\omega)| k_d k_{hs} N_r(M) \quad (7.42)$$

$$\phi_r = \angle G_r(\omega) \quad (7.43)$$

$$\bar{r} = r^* + k_d k_{hs} k_{\Delta r} C_r \quad (7.44)$$

Using 7.36 and 7.41, Equation 7.39 now becomes:

$$p_b(t) = \bar{r}\bar{q}_c + K_r K_c \sin(\omega t + \phi_r) \sin(\omega t + \phi_c) + \bar{r}K_c \sin(\omega t + \phi_r) + \bar{q}_c K_r \sin(\omega t + \phi_c) \quad (7.45)$$

but,

$$K_r K_c \sin(\omega t + \phi_r) \sin(\omega t + \phi_c) = \frac{1}{2}(K_r K_c \cos(2\omega t + \phi_c + \phi_r) + K_r K_c \cos(\phi_c - \phi_r)) \quad (7.46)$$

$$\Rightarrow p_b(t) = \frac{1}{2}(K_r K_c \cos(2\omega t + \phi_c + \phi_r)) + \frac{1}{2}(K_r K_c \cos(\phi_c - \phi_r)) + \bar{r}K_c \sin(\omega t + \phi_r) + \bar{q}_c K_r \sin(\omega t + \phi_c) + \bar{r}\bar{q}_c \quad (7.47)$$

As already discussed at the start of this analysis the double frequency component,  $\frac{1}{2}K_r K_c \cos(2\omega t + \phi_c + \phi_r)$ , will be filtered out by the low-pass dynamics when the signal traverses the loop again, therefore, it may be disregarded at this point as it does not influence the limit cycle oscillation.

Equation (7.36) may be reduced to:

$$p_b(t) = K_{p_b} \sin(\omega t + \phi_{p_b}) + \bar{p}_b \quad (7.48)$$

where,

$$\bar{p}_b = \frac{1}{2}(K_r K_c \cos(\phi_c - \phi_r)) + \bar{r}\bar{q}_c \quad (7.49)$$

$$K_{p_b} = \sqrt{(\bar{r}K_c)^2 + (K_r \bar{p}_b)^2 - 2\bar{p}_b K_r \bar{r}K_c \cos(\pi - \phi_c - \phi_r)} \quad (7.50)$$

$$\phi_{p_b} = \tan^{-1} \left( \frac{\bar{r}K_c \sin(\phi_c) - \bar{p}_b K_r \sin(\phi_r)}{\bar{r}K_c \cos(\phi_c) + \bar{p}_b K_r \cos(\phi_r)} \right) \quad (7.51)$$

Phase  $\zeta_a$  is introduced by the afferent delay in the feedback path. Therefore the feedback signal of the baroreflex model,  $f_{br}(t)$ , is:

$$f_{br}(t) = K_{p_b} \sin(\omega t + \phi_{p_b} + \zeta_a) + \bar{p}_b \quad (7.52)$$

The blood pressure reference signal,  $p_b^{set}(t)$ , is a constant blood pressure reference,  $p_b^{set}$ . Therefore, the signal,  $e_{br}(t)$ , that is input to the high-pass dynamical block,  $G_{CNS}(s)$ , that represent the dynamics of the neural arc (see Equation (6.1)) is:

$$e_{br}(t) = p_b^{set} - f_{br}(t) \quad (7.53)$$

or

$$e_{br}(t) = p_b^{set} - K_{p_b} \sin(\omega t + \phi_{p_b} + \zeta_a) + \bar{p}_b \quad (7.54)$$

The high-pass dynamics of the neural arc introduces gain ( $|G_{CNS}(\omega)|$ ) and phase ( $\angle G_{CNS}(\omega)$ ) to the signal. The processing delay introduces phase  $\zeta_{proc}$ . Hence, after traversing the system, the signal at the input to the nonlinearities is given by:

$$x_{ret}(t) = |G_{CNS}(\omega)| \bar{p}_b - |G_{CNS}(\omega)| K_{p_b} \sin(\omega t + \phi_{p_b} + \angle G_{CNS}(\omega) + \zeta_a + \zeta_{proc}) + |G_{CNS}(\omega)| \bar{p}_b^{set} \quad (7.55)$$

The system will display a sustained oscillation if:

$$x_{ret}(t) = x(t) \quad (7.56)$$

which, from Equations 7.2 and 7.55 gives the three conditions of Equations 7.57, 7.58 and 7.59. The first of these conditions for sustained oscillation is:

$$|G_{CNS}(j\omega)| K_{p_b} = M \quad (7.57)$$

where,  $M$  is the amplitude of the sinusoid of Equation 7.2.

The negative sign in front of the sinusoid is equivalent to a phase shift of  $\pi$  rads. Therefore, the condition for sustained oscillation based on the phase of the system may be written as,

$$-\phi_{p_b} + \angle G_{CNS}(\omega) - \zeta_a - \zeta_{proc} - \pi = 0 \quad (7.58)$$

and in this case where, the blood pressure reference,  $p_b^{set} \neq 0$ . Hence,

$$|G_{CNS}(j\omega)| p_b^{set} - |G_{CNS}(j\omega)| \bar{p}_b = 0 \quad (7.59)$$

Equations 7.57, 7.58 and 7.59 are the conditions for sustained limit cycle oscillation.

### 7.3.4 Numerical example

So as to test the theory developed in the previous section, the conditions necessary for sustained oscillation are tested for a simulated example of the baroreflex model of Figure 6.10. Simulation of the model, for the parameters given in Tables 6.2, 6.3 and 6.5, reveals a 0.34 Hz ( $\sim 2.136$  rads) oscillation in blood pressure with amplitude of 11.66 mmHg, which is typical of experimental measurements (Malpas 2000).

The parameterisation of the model, and justification for the parameters chosen, is documented in Chapter 6. The parameters for the complete baroreflex model presented in Figure 6.7 are documented in Table 6.2, 6.3 and 6.5.

The 'gain' of the nonlinearities, calculable using the describing function, for the parameters listed in Table 6.5 are:

$$N_{pc}(M) = 4.36728 \quad (7.60)$$

$$N_{sc}(M) = N_r(M) = 0.8465 \quad (7.61)$$

The magnitudes of the linear transfer functions  $G_{pc}(s)$ ,  $G_{sc}(s)$ ,  $G_r(s)$  and  $G_{CNS}(s)$  given in Equations (6.3), (6.4), (6.6) and (6.1) are calculated at the frequency of oscillation,  $\omega = 2.135$  rads.

$$G_{pc}(s) = \frac{1}{1+1.22s} \quad (7.62)$$

Then the magnitude factor is given by:

$$|G_{pc}(j\omega)| = \frac{\sqrt{1^2}}{\sqrt{1^2 + 1.22^2 \omega^2}} \quad (7.63)$$

The phase for the dynamical response of the parasympathetic nervous system is calculated as:

$$\angle G_{pc}(j\omega) = \tan^{-1}(0) - \tan^{-1}\left(\frac{1.22\omega}{1}\right) + \tan^{-1}(0.3\omega) = -0.6436 \text{ rads} \quad (7.64)$$

The phase and gains due to the other transfer functions are documented in Table 7.2.

Transfer characteristic	Gain	Phase due to the dynamics	Phase due to the delay
$G_{pc}(s)$	0.3757	-1.2056	-0.6409
$G_{sc}(s)$	0.1088	0.8919	-1.709
$G_k(s)$	0.382	-1.2091	-1.8158
$G_g(s)$	0.382	-1.2091	-1.8158
$G_m(s)$	0.382	-1.2091	-1.8158
$G_s(s)$	0.2422	-1.3255	-1.8158
$H_d(s)$	1	0	-0.4273
$G_{CNS}(s)$	1.27	0.098	-0.8545

Table 7.2: The dynamical gains and phases of the different transfer functions.

The condition equations describing the conditions for limit cycling (Equations (7.57)-(7.59)) are evaluated for the intermediate values listed in Table 7.3.

Parameter	$ G_{CNS}(j\omega) $	$K_{pb}$	$M$	$\phi_{pb}$	$\angle G_{CNS}(j\omega)$	$\zeta_a$	$p_b^{set}$	$\bar{p}_b$	$\zeta_{proc}$
Value	0.0985	9.17	11.65	-1.35	0.098	-0.4273	80	80.2	-0.8545

Table 7.3: The parameters of the condition equations.

The calculation of these equations is documented in Equations (7.66) – (7.68)

$$|G_{CNS}(j\omega)|K_{pb} = 11.64 \approx M \quad (7.65)$$

$$\phi_{pb} + \angle G_{CNS}(\omega) - \zeta_a - \zeta_{proc} - \pi = -5.676 \approx -2\pi \quad (7.66)$$

$$|G_{CNS}(j\omega)|p_b^{set} - |G_{CNS}(j\omega)|\bar{p}_b = -1 \approx 0 \quad (7.67)$$

In Equation (7.68),  $-1 \approx 0$  relative to the values of  $p_b^{set}$  and  $\bar{p}_b$ . The close equality of these equations confirms the validity of the adoption of the reduced model of Figure 7.1.

## 7.4 Discussion

Three different approaches to the analysis of the nonlinear model of the complete baroreflex mechanism were introduced in this Chapter. These methods were based in the time and frequency domain analysis of the model.

The time domain method of analysis was found to be the most tractable of analysis approaches proposed for a system of the complexity of that illustrated in Figure 7.1. This analysis involves the tracking of the traversing signal around the baroreflex feedback loop. The time domain analysis of the model resulted in 3 equations, (Equations (7.57), (7.58) and (7.59)) which describe the conditions for sustained oscillation.

Some comments on the condition equations of Equations (7.57), (7.58) and (7.59) are appropriate:

- Equation (7.59) describes the condition for the mean levels of the model parameters. This condition merely establishes a d.c. equilibrium around the system depicted in Figure 7.1. The condition contains a frequency dependent term,  $\bar{p}_b$ , described in Equation (7.49).
- The gain and phase conditions, given by Equations (7.57) and (7.58), are a pair of nonlinear coupled equations in both frequency,  $\omega$ , and amplitude,  $M$ . Although the gain condition described by Equation (7.57) appears to just contain magnitude terms,  $K_{p_b}$  contains phase terms, as evident in Equation

(7.49). Similarly, the phase condition described by Equation (7.58) is dependent on magnitude terms, via the describing functions gains contained in the description of  $\phi_{p_b}$ .

- The negative feedback pathway introduces a phase of  $\pi$ . The presence of  $\pi$  in Equation (7.58) is interesting because it can be offset by an arbitrary addition or subtraction of  $\pi$  from  $\phi_{p_b}$ .

An aim of this investigation is to attain analytical solutions to  $\omega$  and  $M$ . This would enable determination of the relationships between the different physiological parameters of the system and the presence, absence and change in strength of the slow oscillation. Unfortunately clear analytical solutions to  $\omega$  and  $M$  are difficult, using the time domain analysis, for a number of reasons.

Firstly, due to the fact that the equations are nonlinear, unique solutions may not be attainable. Secondly, the condition equations describe complex, nonlinear relationships between the model parameters and the frequency and amplitude of the slow oscillation. This complexity is introduced at an early stage in the analytical progression through the system. Thirdly, the complexity of the equations is further enhanced by the need for an analytical approximation for the describing function of the sigmoid. Methods of describing function approximation, which enable an analytical description of the describing function of the sigmoid, are described in Chapter 5. Various approximations were developed but these all involve complex, series expansions, which are unwieldy and which add major complexity to the condition equations.

Numerical solutions to the coupled condition equations, which would enable calculation of the frequency ( $\omega$ ) and amplitude ( $M$ ) of the slow oscillation, are possible and will be the target of future research.

However, rather than dwell on calculating analytical solutions for  $\omega$  and  $M$ , the emphasis of this analysis was instead focused on the investigation of the traversing signal, through the baroreflex loop. It is proposed that this analysis approach is sensible as the tracking of the traversing signal, and the effect on the signal of the different components and parameters of the baroreflex as the signal progresses through the system, enables insight into the operation of the short-term blood pressure control mechanisms and the effects of the different sections of the baroreflex responsible for the genesis of the slow oscillation. Advancement of the understanding of the mechanisms involved in the genesis of the slow oscillation is the ultimate goal of this research.

It is clear from the time domain analysis that both the cardiac and the peripheral resistance sides of the baroreflex have important roles to play in mediating the slow oscillation in blood pressure. The derivation of complex and coupled equations which describe the blood pressure signal, alone displays the integrated and sophisticated nature of blood pressure control. The intricate mix of terms involving both cardiac and vascular components displays the collective importance of both sides of the baroreflex in sustaining the slow oscillation. The amplitude and phase of the blood pressure signal are dependent on the phase and amplitude of both the heart rate and total peripheral resistance signals (Equations (7.57) and (7.58)). It is proposed that an intricate balance between the gain, phase and offset parameters of the different pathways of the baroreflex are responsible for the development and maintenance of the slow oscillation. Disturbance of this balance results in the disappearance of the slow oscillation. The slow oscillation is often not observed, particularly in the rabbit, in the control case and it is possible that this is due to variation in the parameters, which result in the conditions of equations (7.57) to (7.59) not being met.

The time domain analysis of the model also clearly shows that the mean levels of neural activity, heart rate and peripheral resistance, play an important role in

maintaining gain and in setting the amplitude of the slow oscillation. This supports the proposed significance of mean SNA, discussed in the previous Chapter.

Analysis of the model via simulation of the parameterised model is also documented in this chapter. This enabled clear identification of the parameters that are significant to the development and maintenance of the slow oscillation. The significant difference in the value of describing function gains along the parasympathetic pathway and the sympathetic pathways is evident from Equations (7.61) and (7.62). The simulation study of the parameterised model confirm that the amplitude of the oscillation in blood pressure is due, to a large extent, to the amplitude of the oscillation via the parasympathetic pathway to the heart (see Equation (7.36) and Equation (7.49)).

Hence, it is proposed that the heart, and in particular the parasympathetic nervous control of the heart, plays a large role in maintaining gain and in mediating the slow oscillation. These conclusions are in contrast to those that have been previously made.

## 7.5 Conclusions

The conclusions of this chapter generally support those of the previous chapter. In the previous chapter conclusions were made following simulation of the complete model of the baroreflex. In this chapter a time domain analysis that analytically describes the working of the model is given. This analysis enables far more insight into the mechanisms of the complete baroreflex than just the simulation of the model would.

Contrary to previous conclusions, this study proposes an important role for the heart in maintaining gain and mediating the slow oscillation in blood pressure. The intricate mix of terms involving both cardiac and peripheral resistance components shows the collective importance of both sides in sustaining oscillations.

In contrast to the generally accepted view that the parasympathetic system is not involved in the genesis of the slow oscillation in blood pressure, a significant role for the parasympathetic pathway in the genesis of the slow oscillation is proposed in this study. Interestingly the gain in the parasympathetic pathway is greater than in the sympathetic pathways to the heart and vasculature. Therefore, it is concluded that the parasympathetic control of the heart plays a significant role in the genesis of the slow oscillation in blood pressure.

Similarly the importance of the mean level of SNA in the genesis of the slow oscillation in blood pressure has at times been down played. This study illustrates that mean SNA is important in maintaining vascular tone, which via the multiplier block plays a significant role in mediating the slow oscillation.

In conclusion, the results of this study might go some way to revising the thinking that the slow oscillation in blood pressure is solely due to the sympathetic control of

the vasculature. This viewpoint is thought to be a shortsighted one considering the similarly describable neural pathways to the heart.

# Chapter 8

## Conclusions

### 8.1 Conclusions

The studies documented in this thesis explore the short-term control mechanisms of blood pressure. The focus of this research is specifically on the nonlinear nature of the blood pressure control mechanisms, and the nonlinear phenomena that they give rise to. Of particular focus is the slow oscillation in blood pressure that exists at 0.1 Hz in the human and at 0.3 Hz in the rabbit, which is proposed to exist as a limit cycle oscillation, developed by nonlinear elements in the baroreflex feedback loop. The means of genesis of this slow oscillation is the major focus of this work and a mathematical modelling approach was undertaken to analyse the nonlinear mechanisms involved.

The results and conclusions of the studies, that form this thesis, are discussed, with respect to the current literature, in the respective chapters of this thesis. In this final chapter, the significance of these research findings is articulated.

It is the opinion of this author, following the comprehensive review of the literature and mechanisms of blood pressure control in Chapter 2 and the detailed analysis which follows of feedback oscillations (particularly in Chapters 4, 6 and 7), that the slow oscillations in blood pressure is primarily the result of a feedback oscillation.

Although, definite conclusions are unfeasible following the analysis of the model of the baroreflex control of peripheral resistance (see Chapter 4), due to the paucity of available relevant information in the literature with which to test the model, changes in the gain characteristics, during different physiological conditions, can be associated with changes in the strength of the slow oscillation.

However, the baroreflex neural feedback paths include both the peripheral resistance and heart sides, as described by the complete baroreflex model in Chapter 6. Results documented in this thesis, highlight the significance of the feedback loops to the heart, which have been previously dismissed by other authors. Hence, though the evidence of feedback oscillation seems very strong (oscillation frequency is within the bound of parameter accuracy, *etc*), it is possibly premature to define the strength of the slow oscillation in blood pressure as an index of purely sympathetic activity to the vasculature, as other neural pathways of the baroreflex have the capability of establishing a slow oscillation, and are, at least, unlikely not to affect the mechanisms of the slow oscillation in blood pressure.

Interestingly, a small body of literature also suggests that the slow oscillation is not completely eliminated following barodenervation. Indeed, such a conflict can have two possible explanations:

- a) There are many conflicting theories in the physiological literature, all of which are supported (to a greater or lesser extent) by a body of experimental evidence. This is indicative of the difficulty of making absolute conclusions with a system as complex as human physiological systems, where it is generally impossible to isolate individual components for analysis and the norm is to provide some evidence of a phenomenon to support a certain theory, though a number of clear counterexamples exist. This allows the science to move forward in an evidential manner, but makes definitive conclusions difficult. It is therefore possible that, at some stage in the future, the presence of slow oscillations in the absence of intact baroreceptor nerves may be explained as a measurement artifact. However, until such conclusive tests are possible, one must go with the overwhelming weight of statistical evidence.

- b) It is also possible that the observed oscillation, in the barodenervated case, is the result of secondary or compensatory effects, which relate indirectly to the neural mechanisms of the baroreflex. For example, it is known that neurally controlled actuators (*e.g.* smooth muscle) are further enhanced and inhibited by hormones and paracrines in the system (*e.g.* angiotensin II and nitric oxide). Therefore there is a possibility that these other, non-neural, feedback mechanisms modulate, or compensate, the actions of the baroreflex.

Finally, one could also surmise that, even if the oscillation in blood pressure does come from a 'central oscillator' in the CNS, local feedback mechanisms within the CNS may be responsible for this. However, the weight of evidence does not support the 'central oscillator' theory (see Section 2.3.3.1). It is somewhat unfortunate that the rabbit, though probably the best documented species in terms of physiological parameters and characteristics, does not appear to exhibit slow oscillations in blood pressure with the same consistency as other species (Chapter 4). There is no doubt that this has, in part at least, contributed to some of the difficulty in making firm conclusions regarding the mechanisms involved in the genesis of the slow oscillation.

This author believes, however, that it is safe to conclude that any feedback oscillations around the slow oscillation frequency are the result of a nonlinear limit cycle, rather than the result of an unlikely set of physiological conditions which would need to be present in order to provide a stable oscillation using linear components. This has important implications for the role of the slow oscillation. The assumption of a nonlinear feedback oscillation, or limit cycle, is supported using a very mild set of assumptions and does not require any belief that the CNS continually adapts in order to maintain the stability of the oscillation. Although the slow oscillation resulted as a consequence of the characteristics of the baroreflex loop, it cannot be categorically asserted that the presence of the slow oscillation is not deliberate, since one might wonder why physiological systems exhibit this phenomenon in the first place. Whatever, the reason (and perhaps the oscillation is only the result of many conflicting design

requirements), the nonlinear avenue is more attractive in not requiring a much bigger issue to be addressed (in the absence of any supporting evidence of a reason for deliberately maintaining the slow oscillation) and is clearly justifiable from a physiological point of view, as soft-limiting characteristics pervade the physiology literature.

A major contribution of this thesis is the insight provided by the comprehensive model of Chapter 6 (and the associated stability analysis in Chapter 7) into the contributions of the various pathways to the slow oscillation. In this author's view, this provides incontrovertible evidence that the heart plays an important role in the genesis of slow oscillations. In the nominal (resting) case, it was seen that oscillations disappear when the cardiac neural pathways are blocked (in the model). This, of course, must be considered within the available accuracy of the physiological parameters, but does indicate a strong role for the cardiac pathways, particularly the parasympathetic pathway. Furthermore, the model of Chapter 6 clearly articulates the important role for mean levels of both cardiac output and peripheral resistance in mediating slow oscillations. In the past, researchers have looked at gain as being the sole issue of importance (De Boer 1987), but due to the explicit relationship between the mean levels and 'gain' in the opposite pathway (obvious from Figure 6.12) it is clear that mean cardiac output and mean peripheral resistance do have indirect 'gain' effects. However, in view of the results of this study, this has been misinterpreted in the past (Liu 2002).

## 8.2 Recommendations for future research

In an area noted for its difficulty in making conclusive experimental measurements and where the body of knowledge advances at an incremental rate, there is much scope for future work related to the research described in this thesis. In particular, the following areas are recommended:

- The model of Chapter 6 was assembled from a range of unconnected physiological experiments, which were, in many cases, undertaken for a

variety of purposes other than those, which are the focus of this thesis. It is therefore likely that there are a number of inter-dependencies, which have not been correctly quantified in the model, due to the (broad) assumption of the theorem of superposition, which clearly does not hold for nonlinear systems. While it is believed that the general structure of the model is correct, there are likely to be some parametric (and possibly some small structural) errors in the model, which can only be eliminated by a concerted experimental validation of the model. This is likely to be an onerous task, given the difficulty of making many physiological measurements (especially neural measurements). However, it is believed that a fully validated model of the full baroreflex system would be of immense value as an ‘experimental’ test-bed for a range of studies.

- The models documented in Chapters 4 and 6 do not include any effectors of blood pressure other than direct neural mechanisms. The importance of other indirect mechanisms, such as hormones and paracrines (e.g. angiotensin II and nitric oxide) has been articulated both in this thesis (though outside the scope of the current work) and elsewhere (Nafz 1997; Barrett 2003). These effects need to be quantified in an extended model, since they affect both the magnitude of the neural effects (through enhancement or opposition) and the timescale on which these effects have influence (since these ‘secondary’ effects normally follow the direct neural response).
- While a set of conditions for oscillation of the combined heart-resistance model of Chapter 6 was developed in Chapter 7, the utility of this result is currently somewhat limited. To increase the usefulness of this result, two extensions of the work are proposed:
  - (a) Since there is currently a very complex relationship between the conditions and the raw physiological parameters, some possible simplifications, which preserve the essence of the result (while improving its transparency) need to be considered. Any simplification would, of course, need to be validated against the original result and it should be

borne in mind that the current set of conditions are already based on a simplified system model (as in Figure 7.1).

- (b) Currently, it is difficult to see how the equations of (7.57) to (7.59) permit an analytical solution for the amplitude and frequency of the slow oscillation. Further to the work recommended in (a), a form of analytical solution may be possible but, in any case, this set of equations will always permit a numerical solution, using one of the many numerical solvers available (e.g. the SOLVE( ) routine in the MATLAB<sup>TM</sup> software suite). There is also a possibility, following numerical solution of the equations for a wide variety of physiological parameters, that relatively simple relationships between the oscillation parameters (amplitude, frequency) and the physiological parameters may be extracted, either through observation or parametric fitting.

# References

- Abarbanel, H. D. I. (1998). "Obtaining order in a world of chaos: Time domain analysis of nonlinear and chaotic signals." *IEEE Signal Processing Magazine* 15: 49-65.
- Abbiw-Jackson, R. M. and W. F. Langford (1998). "Gain-induced oscillations in blood pressure." *Journal of Mathematical Biology* 37: 203-234.
- Akaike, H. (1973). "Maximum likelihood identification of Gaussian autoregressive moving average models." *Biometrika* 60: 255-265.
- Akselrod, S. (1988). "Spectral analysis of fluctuations in cardiovascular parameters: a quantitative tool for the investigation of autonomic control." *Trends in Pharmacological Sciences* 9: 6-9.
- Akselrod, S., D. Gordon, J. B. Madwed, N. C. Snidman, D. C. Shannon and R. J. Cohen (1985). "Hemodynamic regulation: investigation by spectral analysis." *American Journal of Physiology - Heart & Circulatory Physiology* 249: H867-H875.
- Akselrod, S. D., D. Gordon, J. B. Madwed, N. C. Snidman, D. C. Shannon and R. J. Cohen (1981). "Power spectrum analysis of heart rate fluctuations: a quantitative probe of beat-to-beat cardiovascular control." *Science* 213: 220-222.
- Albano, A. M., J. Muench, C. Schwartz, A. I. Mees and P. E. Rapp (1988). "Singular-value decomposition and the Grassberger-Procaccia algorithm." *Physical Review A* 38: 3017-3026.
- Allen, J. and A. Murray (1999). "Modelling the relationship between peripheral blood pressure and blood volume pulses using linear and neural network system identification techniques." *Physiological measurements* 20: 287-301.
- Allison, J. L., K. Sagawa and M. Kumada (1969). "An open-loop analysis of the aortic arch barostatic reflex." *American Journal of Physiology* 217: 1576-1584.
- Altimiras, J. and D. A. Crossley, II (2000). "Control of blood pressure mediated by baroreflex changes of heart rate in the chicken embryo (*Gallus gallus*)." *American Journal of Physiology - Regulatory, Integrative & Comparative Physiology* 278: R980-R986.

- Angell-James, J. E. and M. D. Daly (1970). "Comparison of the reflex vasomotor responses to separate and combined stimulation of the carotid sinus and aortic arch baroreceptors by pulsatile and non-pulsatile pressure in the dog." *Journal of Physiology* 209: 257-293.
- Arai, Y., J. P. Saul, P. Albrecht, L. H. Hartley, L. S. Lilly, R. J. Cohen and W. S. Colucci (1989). "Modulation of cardiac autonomic activity during and immediately after exercise." *American Journal of Physiology - Heart & Circulatory Physiology* 256: H132-H141.
- Atherton, D. P. (1982). Nonlinear control engineering. London, Van Nostrand Reinhold Company Ltd.
- Axler, S. (1997). Linear algebra done right. Berlin, Springer-Verlag.
- Babloyantz, A. a. D., A. (1988). "Is the normal heart a periodic oscillator?" *Biological Cybernetics* 58: 203-211.
- Bai, E.-W. (2002). "A blind approach to the Hammerstein-Wiener model identification." *Automatica* 38: 967-979.
- Barajas, L., L. Liu and K. Powers (1992). "Anatomy of the renal innervation: intrarenal aspects and ganglia of origin." *Canadian Journal of Physiology & Pharmacology* 70: 735-49.
- Barcroft, J. and Y. Nisimaru (1932). "Rhythmical contractions of the spleen." *Journal of Physiology* 74: 294-298.
- Barman, S. M. and G. L. Gebber (1980). "Sympathetic nerve rhythm of brain stem origin." *American Journal of Physiology - Regulatory Integrative & Comparative Physiology* 239: R42-R47.
- Barnett, S. R., R. J. Morin, D. K. Kiely, M. Gagnon, G. Azhar, E. L. Knight, J. C. Nelson and L. A. Lipsitz (1999). "Effects of age and gender on autonomic control of blood pressure dynamics." *Hypertension* 33: 1195-1200.
- Barrett, C., Ramchandra, R, Guild, SJ, Lala, A, Budgett, DM and Malpas, SC. (2003). "What sets the long-term level of renal sympathetic nerve activity, a role for angiotensin II and baroreflexes?" *Circulation Research* 92: 1330-1336.
- Bergen County Technical Schools and Special Services (2004). Distribution of cardiac output. [www.bergen.org/academy/bio/pes/psccardiacoutput.html](http://www.bergen.org/academy/bio/pes/psccardiacoutput.html)
- Berger, R. D., J. P. Saul and R. J. Cohen (1989). "Assessment of autonomic response by broad-band respiration." *IEEE Transactions on Biomedical Engineering* 36: 1061-1065.

- Berger, R. D., J. P. Saul and R. J. Cohen (1989). "Transfer function analysis of autonomic regulation. I. Canine atrial rate response." *American Journal of Physiology - Heart and Circulatory Physiology* 256: H142-H152.
- Bernardi, L., S. Leuzzi, A. Radaelli, C. Passino, J. A. Johnston and P. Sleight (1994). "Low-frequency spontaneous fluctuations of R-R interval and blood pressure in conscious humans: a baroreceptor or central phenomenon?" *Clinical Science* 87: 649-54.
- Berne, R. M. and M. N. Levy (1996). Principles of physiology. St. Louis, Mosby-Year Book Inc.
- Berntson, G. G., J. T. Bigger, D. L. Eckberg, P. Grossman, P. G. Kaufmann, M. Malik, H. N. Nagaraja, S. W. Porges, J. P. Saul, P. H. Stone and M. W. van der Molen (1997). "Heart rate variability: origins, methods, and interpretive caveats." *Psychophysiology* 34: 623-48.
- Bertram, D., C. Barres, Y. Cheng and C. Julien (2000). "Norepinephrine reuptake, baroreflex dynamics, and arterial pressure variability in rats." *American Journal of Physiology - Regulatory Integrative & Comparative Physiology* 279: R1257-R1267.
- Bertram, D., C. Barres, G. Cuisinaud and C. Julien (1998). "The arterial baroreceptor reflex of the rat exhibits positive feedback properties at the frequency of mayer waves." *Journal of Physiology* 513: 251-61.
- Bhargava, V. and D. N. Rao (1970). "Application of describing function technique to memoryless nonlinearities in tandem." *International Journal of Control* 12: 1-8.
- Bigger, J., Jr, J. Fleiss, R. Steinman, L. Rolnitzky, R. Kleiger and J. Rottman (1992). "Frequency domain measures of heart period variability and mortality after myocardial infarction." *Circulation* 85: 164-171.
- Bigger, J. T., J. Fleiss, R. Steinman, L. Rolnitzky, R. Kleiger and J. Rottman (1992). "Correlations among time and frequency domain measures of heart period variability two weeks after acute myocardial infarction." *American Journal of Cardiology* 69: 891-898.
- Borst, C. and J. M. Karemaker (1983). "Time delays in the human baroreceptor reflex." *Journal of the Autonomic Nervous System* 9: 399-409.
- Box, G.E.P., Jenkins G.M. and Reinsel, G.C. (1994). Time series analysis: forecasting and control, Englewood Cliffs, Prentice Hall.

- Brand, P. H., P. J. Metting and S. L. Britton (1988). "Support of arterial blood pressure by major pressor systems in conscious dogs." *American Journal of Physiology - Heart & Circulatory Physiology* 255: H483-H491.
- Brilliant, M. B. (1958). Theory of the analysis of nonlinear systems. Research Laboratory of Electronics. Boston, Massachusetts Institute of Technology.
- Bronk, D. W., L. K. Ferguson, R. Margaria and D. Y. Solant (1936). "The activity of the cardiac sympathetic centers." *American Journal of Physiology* 117: 237-249.
- Bronk, D. W. and G. Stella (1932). "Afferent impulses in the carotid sinus nerve." *Journal of Cell Comparative Physiology* 1: 113-130.
- Bronstein, I. N., K. A. Senendjajew, G. Musiol and H. Muhlig (1995). Taschenbuch der mathematik. Frankfurt am Main, Verlag Harri Deutsch.
- Brooks, V. L. (1995). "Chronic infusion of angiotensin II resets baroreflex control of heart rate by an arterial pressure-independent mechanism." *Hypertension* 26: 420-424.
- Broomhead, D. S. and G. P. King (1986). "Extracting qualitative dynamics from experimental data." *Physica D* 20: 217-236.
- Brown, D. R. (1980). "Receptors under pressure: An update on baroreceptors." *Circulation Research* 46: 1-10.
- Brown, D. R., L. V. Brown, A. Patwardhan and D. C. Randall (1994). "Sympathetic activity and blood pressure are tightly coupled at 0.4 Hz in conscious rats." *American Journal of Physiology - Regulatory, Integrative & Comparative Physiology* 267: R1378-R1384.
- Brown, T. E., L. A. Beightol, J. Koh and D. L. Eckberg (1993). "Important influence of respiration on human RR interval power spectra is largely ignored." *Journal of Applied Physiology* 75: 2310-2317.
- Burgess, D. E., J. C. Hundley, S. G. Li, D. C. Randall and D. R. Brown (1997). "First-order differential-delay equation for the baroreflex predicts the 0.4-hz blood pressure rhythm in rats." *American Journal of Physiology - Regulatory, Integrative & Comparative Physiology* 273: R1878-R1884.
- Burgess, D. E., J. C. Hundley, S.-g. Li, D. C. Randall and D. R. Brown (1997). "Multifiber renal SNA recordings predict mean arterial blood pressure in unanesthetized rat." *American Journal of Physiology - Regulatory Integrative & Comparative Physiology* 273: R851-R857.

- Burke, S. and P. Dorward (1988). "Influence of endogenous opiates and cardiac afferents on renal nerve activity during haemorrhage in conscious rabbits." *Journal of Physiology* 402: 9-27.
- Burrattini, R. and G. Gnudi (1982). "Computer identification of models for the arterial tree impedance: comparison between two simple models and the first experimental results." *Medical and Biological Engineering and Computing* 20: 134-144.
- Buzug, T. and G. Pfister (1992). "Optimal delay time and embedding dimension for delay-time coordinates by analysis of the global static and local dynamical behavior of strange attractors." *Physical Review A* 45: 7073-7084.
- Campbell, K. B., J. A. Ringo, C. Neti and J. E. Alexander (1984). "Informational analysis of left ventricle-systemic arterial interaction." *Annals of Biomedical Engineering* 12: 209-231.
- Cao, L. (1997). "Practical method for determining the minimum embedding dimension of a scalar timeseries." *Physica D* 110: 43-50.
- Casaleggio, A. and S. Braiotta (1997). "Estimation of Lyapunov exponents in ECG time series - the influence of parameters." *Chaos, Solutions and Fractals* 8: 1591-1599.
- Casolo, G. C., P. Stroder, A. Sulla, A. Chelucci, A. Freni and M. Zeraushek (1995). "Heart rate variability and functional severity of congestive heart failure secondary to coronary artery disease." *European Heart Journal* 16: 360-367.
- Cavalcanti, S. (2000). "Arterial baroreflex influence on heart rate variability: a mathematical model-based analysis." *Medical & Biological Engineering & Computing* 38: 189-197.
- Cavalcanti, S. and E. Belardinelli (1996). "Modeling of cardiovascular variability using a differential delay equation." *IEEE Transactions on Biomedical Engineering* 43: 982-989.
- Cawley, R. and G.-H. Hsu (1992). "Local-geometric-projection method for noise reduction in chaotic maps and flows." *Physical Review A* 46: 3057-3082.
- Cerutti, C., C. Barres, M. P. Gustin, C. Julien, M. Lo, C. Paultre, M. Vincent and J. Sassard (1995). "Sympathectomy, sinoaortic denervation and spectral powers of blood pressure and heart rate in lyon rats." *Computer Analysis of Cardiovascular Signals* 13: 243-256.

- Cerutti, C., C. Barres and C. Paultre (1994). "Baroreflex modulation of blood pressure and heart rate variabilities in rats: assessment by spectral analysis." *American Journal of Physiology - Heart & Circulatory Physiology* 266: H1993-H2000.
- Cerutti, C., M. P. Gustin, C. Z. Paultre, M. Lo, C. Julien, M. Vincent and J. Sassard (1991). "Autonomic nervous system and cardiovascular variability in rats: a spectral analysis approach." *American Journal of Physiology - Heart & Circulatory Physiology* 261: H1292-H1299.
- Cevese, A., G. Gulli, E. Polati, L. Gottin and R. Grasso (2001). "Baroreflex and oscillation of heart period at 0.1 Hz studied by alpha-blockade and cross-spectral analysis in healthy humans." *Journal of Physiology - London* 531: 235-244.
- Chalmers, J., S. MacMahon, G. Mancia, J. Whitworth, L. Beilin, L. Hansson, B. Neal, A. Rodgers, C. Ni Mhurchu and T. Clark (1999). "1999 World Health Organization-International Society of Hypertension Guidelines for the management of hypertension. Guidelines sub-committee of the World Health Organization." *Clinical and Experimental Hypertension* 21: 1009-1060.
- Chapuis, B., E. Vidal-Petiot, V. Orea, C. Barres and C. Julien (2004). "Linear modelling analysis of baroreflex control of arterial pressure variability in rats." *Journal of Physiology* 599: 639-649.
- Charlton, J. D. and A. J. Baertschi (1982). "Responses of aortic baroreceptors to changes of aortic blood flow and pressure in rat." *American Journal of Physiology - Heart & Circulatory Physiology* 261: H520-H525.
- Chen, G. and R. J. P. de Figueiredo (1999). "Feedback control of unknown chaotic dynamical systems based on time-series data." *IEEE Transactions on Circuits and Systems* 46: 640-644.
- Chen, P. (1988). "Empirical and theoretical evidence of economic chaos." *Systems Dynamics Review* 4: 81.
- Chon, K. H., R. Mukkamala, K. Toska, T. J. Mullen, A. A. Armoundas and R. J. Cohen (1997). "Linear and nonlinear system identification of autonomic heart-rate modulation." *IEEE Engineering in Medicine and Biology Magazine* 16: 96-115.
- Claesen, S. a. K., R.I. (1994). "Estimation of the largest Lyapunov exponent of an RR interval and its use as an indicator of decreased autonomic heart rate control." *Computers in Cardiology*: 133-136.

- Codd, M. B. (2001). 50 years of heart disease in Ireland: Mortality, morbidity and health services implications. Dublin, Irish Heart Foundation: 1-19.
- Cohen, M. I. and P. M. Gootman (1970). "Periodicities in efferent discharge of splanchnic nerve of the cat." *American Journal of Physiology* 218: 1092-1101.
- Cohen, R. A. (1999). "The potential clinical impact of 20 years of nitric oxide research." *American Journal of Physiology - Heart & Circulatory Physiology* 276: H1404-H1407.
- Cohen, R. A., B. Tesfamariam and R. M. Weisbrod (1990). Endothelium inhibits adrenergic neurotransmission. Endothelium derived vasoactive factors. G. M. Rubanyi and P. M. Vanhoutte. New York, Karger: 206-212.
- Coleridge, H. M., J. C. Coleridge, M. P. Kaufman and A. Dangel (1981). "Operational sensitivity and acute resetting of aortic baroreceptors in dogs." *Circulation Research* 48: 676-84.
- Conlon, K. and C. Kidd (1998). "The role of nitric oxide in the control by the vagal nerves on the heart of the anaesthetised ferret." *Experimental Physiology* 83: 469-480.
- Cooley, R. L., N. Montano, C. Cogliati, P. van de Borne, W. Richenbacher, R. Oren and V. K. Somers (1998). "Evidence for a central origin of the low-frequency oscillation in RR-interval variability." *Circulation* 98: 556-61.
- Coote, J. H. (1988). "The organization of cardiovascular neurons in the spinal cord." *Reviews of Physiology, Biochemistry and Pharmacology* 110: 147-292.
- Coumel, P. (1994). "Paroxysmal atrial fibrillation - a disorder of autonomic tone." *European Heart Journal* 15: 9-16.
- Cowley, A. W., L. F. Liard and A. C. Guyton (1973). "Role of the baroreceptor reflex in daily control of arterial blood pressure and other variables in dogs." *Circulation Research* 32: 564-576.
- Cupples, W. A., P. Novak, V. Novak and F. C. Salevsky (1996). "Spontaneous blood pressure fluctuations and renal blood flow dynamics." *American Journal of Physiology - Renal Physiology* 270: F82-F89.
- Dale, H. H. and W. Feldberg (1934). "The chemical transmission of secretory impulses to the sweat glands of the cat." *The Journal of Physiology* 62: 330-340.
- Damming, M. and F. Mitschke (1993). "Estimation of Lyapunov exponents from time series: the stochastic case." *Physics Letters A* 178: 385-394.

- Davies, T. M. and J. M. M. Nelson (1967). "Sinus arrhythmia in man at rest." *Journal of Applied Physiology* 22: 947-954.
- Davison, E. J. and D. Constantinescu (1971). "A describing function technique for multiple nonlinearities in a single-loop feedback system." *IEEE Transactions on Automatic Control* 16: 56-60.
- De Boer, R., Karemaker, J. and Strackee, J. (1987). "Hemodynamic fluctuations and baroreflex sensitivity in humans: a beat-to-beat model." *American Journal of Physiology - Heart & Circulatory Physiology* 253: H680-H689.
- Dempsey, E. J. a. W., D.T. (2004). "Identification of Hammerstein models with cubic spline nonlinearities." *IEEE Transactions on Biomedical Engineering* 51: 237-245.
- Deutsch, S. and A. Deutsch (1993). *Understanding the Nervous System : An Engineering Perspective*, New York, IEEE Press.
- Di Rienzo, M., G. Parati, P. Castiglioni, S. Omboni, A. U. Ferrari, A. J. Ramirez, A. Pedotti and G. Mancia (1991). "Role of sinoaortic afferents in modulating BP and pulse-interval spectral characteristics in unanesthetized cats." *American Journal of Physiology - Heart & Circulatory Physiology* 261: H1811-H1818.
- Di Virgilio, V., R. Barbieri, L. Mainardi, S. Strano and S. Cerrutti (1997). "A multivariate time-invariant AR method for the analysis of heart rate and arterial blood pressure." *Medical Engineering and Physics* 19: 109-124.
- Diks, C., J. C. van Houwelingen, F. Takens and J. DeGoede (1995). "Reversibility as a criterion for discriminating time series." *Physics Letters A* 201: 221-228.
- Dorward, P. K., W. Riedel, S. L. Burke, J. Gipps and P. I. Korner (1985). "The renal sympathetic baroreflex in the rabbit. Arterial and cardiac baroreceptor influences, resetting, and effect of anesthesia." *Circulation Research* 57: 618-633.
- Dutton, K., S. Thompson and B. Barraclough (1997). *The art of control engineering*. England, Addison Wesley Longman.
- Dworkin, L. D., A. M. Sun and B. M. Brenner (2000). *The renal circulations. The kidney*. B. M. Brenner. Philadelphia, W.B. Saunders Company: 277-318.
- Eckberg, D. L. (1976). "Temporal response patterns of the human sinus node to brief carotid baroreceptor stimuli." *Journal of Physiology - London* 258: 769-782.
- Eckberg, D. L. (1980). "Nonlinearities of the human carotid baroreceptor-cardiac reflex." *Circulation Research* 47: 208-16.

- Eckberg, D. L. (1983). "Human sinus arrhythmia: noninvasive measure of parasympathetic cardiac control." *Journal of Applied Physiology* 54: 962-966.
- Eckberg, D. L. (1997). "Sympathovagal Balance : A Critical Appraisal." *Circulation* 96: 3224-3232.
- Eckberg, D. L. and P. Sleight (1992). *Human Baroreflexes in Health and Disease*. Oxford, Clarendon.
- Eckmann, J.-P. and D. Ruelle (1985). "Ergodic Theory of chaos and strange attractors." *Reviews of Modern Physics* 57: 617-656.
- Eisenhofer, G., P. Friberg, B. Rundqvist, A. A. Quyyumi, G. Lambert, D. M. Kaye, I. J. Kopin, D. S. Goldstein and M. D. Esler (1996). "Cardiac Sympathetic Nerve Function in Congestive Heart Failure." *Circulation* 93: 1667-1676.
- Electrophysiology, T. F. o. t. E. S. o. C. t. N. A. S. o. P. (1996). "Heart Rate Variability : Standards of Measurement, Physiological Interpretation, and Clinical Use." *Circulation* 93: 1043-1065.
- Esler, M., D. Kaye, G. Lambert, D. Esler and G. Jennings (1997). "Adrenergic nervous system in heart failure." *American Journal of Cardiology* 80: 7L-14L.
- Eyal, S. and S. Akselrod (2000). "Bifurcations in a simple model of the cardiovascular system." *Methods of Information in Medicine* 39: 118-121.
- Fagius, J. and B. G. Wallin (1980). "Sympathetic reflex latencies and conduction velocities in normal man." *Journal of Physiology - London* 47: 429-443.
- Farmer, J. D. and J. J. Sidorowich (1987). "Predicting chaotic time series." *Physical Review Letters* 59: 845-848.
- Faustmann, P. M. and R. E. Ganz (1994). "Central cardio autonomic disorganization in interictal states of epilepsy detected by phase space analysis." *International Journal of Neuroscience* 78: 43-47.
- Feldberg, W. and J. H. Gaddum (1934). "The chemical transmitter at synapses in a sympathetic ganglion." *The Journal of Physiology* 81: 305-319.
- Flepp, L., R. Holzner, E. Brun, M. Finardi and R. Badii (1991). "Model identification by periodic-orbit analysis for NMR-laser chaos." *Physical Review Letters* 67: 2244-2247.
- Fouad, F. M., R. C. Tarazi, C. M. Ferrario, S. Figaly and C. Alicandri (1984). "Assessment of parasympathetic control of heart rate by a non-invasive method." *American Journal of Physiology - Heart & Circulatory Physiology* 246: H838-H842.

- Fox, S. I. (1996). Human physiology. Dubuque, Wm. C. Brown Publishers.
- Franz, G. N., A. M. Scher and C. Ito (1971). "Small signal characteristics of carotid sinus baroreceptors of rabbits." *Journal of Applied Physiology* 30: 527-535.
- Fraser, A. M. and Swinney (1986). "Independent coordinates for strange attractors from mutual information." *Physical Review A* 33: 1134-1140.
- Fuji, K., D. D. Heistad and F. M. Faraci (1990). "Vasomotion of basilar arteries in vivo." *American Journal of Physiology - Heart & Circulatory Physiology* 258: H1829-H1834.
- Furchgott, R. F. and J. V. Zawadzi (1980). "The obligatory role of the endothelial cells in the relaxation of arterial smooth muscle by acetylcholine." *Nature* 288: 373-376.
- Ganz, R. E. and P. M. Faustmann (1994). "A chaos theory approach to autonomic dysfunction in multiple sclerosis." *Journal of Neurology* 241: 348-349.
- Ganz, R. E., G. Wiebels, K. H. Skacker, P. M. Faustmann and C. W. Zimmermann (1993). "The Lyapunov exponents of heart rate dynamics as a sensitive marker of central autonomic organization: An exemplary study of early multiple sclerosis." *International Journal of Neuroscience* 71: 29-36.
- Gebber, G. L. and S. M. Barman (1980). "Basis for 2-6 cycle/s rhythm in sympathetic nerve discharge." *American Journal of Physiology - Regulatory Integrative & Comparative Physiology* 239: R48-R56.
- Glick, G. and E. Braunwald (1964). "Relative roles of the sympathetic and parasympathetic nervous systems in the reflex control of heart rate." *Circulation Research* 16: 363-375.
- Goldberger, A. L. (1996). "Non-linear dynamics for clinicians: chaos theory, fractals, and complexity at the bedside." *Lancet* 347: 1312-4.
- Goldstein, D. S. (1981). "Plasma norepinephrine during stress in essential hypertension." *Hypertension* 3: 551-6.
- Grady, H. C. and E. M. A. Bullivant (1992). "Renal blood flow varies during normal activity in conscious unrestrained rats." *American Journal of Physiology - Regulatory Integrative & Comparative Physiology* 262: R926-R932.
- Gran, R. and M. Rimer (1965). "Stability analysis of systems with multiple nonlinearities." *IEEE Transactions on Automatic Control* 10: 94-97.
- Grassberger, P. and I. Procaccia (1983). "Characterization of strange attractors." *Physical Review Letters* 50: 346-349.

- Grassberger, P. and I. Procaccia (1983). "Estimation of the Kolmogorov entropy from a chaotic signal." *Physical Review A* 28: 2591-2593.
- Grassberger, P. and I. Procaccia (1983). "Measuring the strangeness of a strange attractor." *Physica D* 9: 189-203.
- Grassberger, P., T. Schreiber and C. Schaffrath (1991). "Non-linear time sequence analysis." *International Journal of Bifurcation and Chaos* 1: 521.
- Grassi, G. (1998). "Role of the sympathetic nervous system in human hypertension." *Journal of Hypertension* 16: 1979-87.
- Grassi, G., B. M. Cattaneo, G. Seravalle, A. Lanfranchi and G. Mancia (1998). "Baroreflex control of sympathetic nerve activity in essential and secondary hypertension." *Hypertension* 31: 68-72.
- Grasso, R., G. Rizzi, F. Schena and A. Cevese (1995). "Arterial baroreceptors are not essential for low frequency oscillation of arterial pressure." *Journal of Autonomic Nervous System* 50: 323-331.
- Green, J. H. and P. F. Heffron (1968). "Studies upon the relationship between baroreceptor and sympathetic activity." *Quarterly Journal of Experimental Physiology* 53: 23-32.
- Grisk, O. and H. M. Stauss (2002). "Frequency response modulation of mesenteric and renal vascular resistance." *American Journal of Physiology - Regulatory Integrative & Comparative Physiology* 282: R1468-R1476.
- Grodins, F. S. (1963). *Control Theory and Biological Systems*. New York, Columbia University Press.
- Gu, C. X., P. F. Juranka and C. E. Morris (2001). "Stretch-Activation and Stretch-Inactivation of Shaker-IR, a Voltage-Gated K<sup>+</sup> Channel." *Biophysical Journal* 80: 2678-2693.
- Guild, S. J. (2002). *Understanding variations in renal blood flow in mammals*. Auckland, University of Auckland.
- Guild, S.-J., P. C. Austin, M. Navakatikyan, J. V. Ringwood and S. C. Malpas (2001). "Dynamic relationship between sympathetic nerve activity and renal blood flow: a frequency domain approach." *American Journal of Physiology - Regulatory Integrative & Comparative Physiology* 281: R206-610.
- Guyton, A. C. (1987). *Human physiology and mechanisms of disease*. Philadelphia, W.B. Saunders Company.
- Guyton, A. C. (1991). *Textbook of medical physiology*. Philadelphia, W.B. Saunders.

- Guyton, A. C., H. M. Batson, C. M. Smith and G. G. Armstrong (1951). "Method for studying competence of the body's blood pressure regulatory mechanisms and effect of pressoreceptor denervation." *American Journal of Physiology* 164: 360-368.
- Guyton, A. C., T. G. Coleman and H. J. Granger (1972). "Circulation: overall regulation." *Annual Reviews Physiology* 34: 13-46.
- Guyton, A. C. and J. E. Hall (1996). Textbook of medical physiology. Philadelphia, W.B. Saunders.
- Guzzetti, S., M. G. Signorini, C. Cogliati, S. Mezzetti, A. Porta, S. Cerutti and A. Malliani (1996). "Non-linear dynamics and chaotic indices in heart rate variability of normal subjects and heart-transplanted patients." *Cardiovascular Research* 31: 441-446.
- Hagerman, I., Berglund, M., Lorin, M., Nowak, J. and Sylven, C. (1996). "Chaos-related deterministic regulation of heart rate variability in time and frequency domains: effects of autonomic blockade and exercise." *Cardiovascular Research* 31: 410-418.
- Hales, S. (1733). Statistical essays: containing haemastatics. London, Innys, Manby and Woodward.
- Hamner, J. W., R. J. Morin, J. L. Rudolph and J. A. Taylor (2001). "Inconsistent link between low-frequency oscillations: R-R interval responses to augmented Mayer waves." *Journal of Applied Physiology* 90: 1559-1564.
- Hayano, J., F. Yasuma, A. Okada, S. Mukai and T. Fujinami (1996). "Respiratory sinus arrhythmia. A phenomenon improving pulmonary gas exchange and circulatory efficiency." *Circulation* 94: 842-7.
- Head, G. and R. McCarty (1987). "Vagal and sympathetic components of the heart rate range and gain of the baroreceptor-heart rate reflex in conscious rats." *Journal of the Autonomic Nervous System* 21: 203-213.
- Head, G. A. and S. L. Burke (2001). "Renal And Cardiac Sympathetic Baroreflexes In Hypertensive Rabbits." *Clinical and Experimental Pharmacology and Physiology* 28: 972-975.
- Hilborn, R. C. (2001). Chaos and nonlinear dynamics: An introduction for scientists and engineers. New York, Oxford University Press.
- Holohan, A. (2000). On calculating the describing function. Irish Signals and Systems Conference, Dublin.

- Holstein Rathlou, N. H., J. He, A. J. Wagner and D. J. Marsh (1995). "Patterns of blood pressure variability in normotensive and hypertensive rats." *American Journal of Physiology - Regulatory Integrative & Comparative Physiology* 269: R1230-R1239.
- Holstein Rathlou, N. H. and D. J. Marsh (1994). "A dynamic model of renal blood flow autoregulation." *Bulletin of Mathematical Biology* 56: 411-29.
- Holstein Rathlou, N. H. and D. J. Marsh (1994). "A dynamic model of renal blood flow autoregulation." *Bulletin of Mathematical Biology* 56: 411-429.
- Holstein-Rathlou, N.-H. (1993). "Oscillations and chaos in renal blood flow control." *Journal of the American Society of Nephrology* 4: 1275-1287.
- Holstein-Rathlou, N. H., F. M. Karlsen and P. P. Leyssac (1998). "Blood pressure variability and kidney function." *Fundamental & Clinical Pharmacology* 12: 29s-34s.
- Holstein-Rathlou, N.-H. and D. J. Marsh (1994). "Renal blood flow regulation and arterial pressure fluctuations: A case study in nonlinear dynamics." *Physiological Reviews* 74: 637-681.
- Houle, M. S. and G. E. Billman (1999). "Low-frequency component of the heart rate variability spectrum: a poor marker of sympathetic activity." *American Journal of Physiology - Heart & Circulatory Physiology* 45: H215-H223.
- Hyndman, B. W. (1974). "The role of rhythms in homeostasis." *Kybernetik* 15: 227-236.
- Hyndman, B. W., R. I. Kitney and B. M. Sayers (1971). "Spontaneous rhythms in physiological control systems." *Nature* 233: 339-41.
- Igler, F. O., J. H. Donegan, K. C. Hoo, M. E. Korn and J. M. Kampine (1981). "Chronic localized hypotension and resetting of carotid sinus baroreceptors." *Circulation Research* 49: 649-654.
- Iida, N. (1999). "Nitric oxide mediates sympathetic vasoconstriction at supraspinal, spinal, and synaptic levels." *American Journal of Physiology - Heart & Circulatory Physiology* 276: H918-H925.
- Ikeda, Y., T. Kawada, M. Sugimachi, O. Kawaguchi, T. Shishido, T. Sato, H. Miyano, W. Matsuura, J. Alexander and K. Sunagawa (1996). "Neural arc of baroreflex optimizes dynamic pressure regulation in achieving both stability and quickness." *American Journal of Physiology - Heart & Circulatory Physiology* 40: H882-H890.

- Imaizumi, T., Y. Harasawa, S. Ando, M. Sugimachi and A. Takeshita (1994). "Transfer function analysis from arterial baroreceptor afferent activity to renal nerve activity in rabbits." *American Journal of Physiology - Heart & Circulatory Physiology* 266: H36-H42.
- Inoue, K., S. Miyake, M. Kumashiro, H. Ogata, T. Ueta and T. Akatsu (1991). "Power spectral analysis of blood pressure variability in traumatic quadriplegic humans." *American Journal of Physiology - Heart & Circulatory Physiology* 260: H842-H847.
- Iriki, M., P. Dorward and P. Korner (1977). "Baroreflex "resetting" by arterial hypoxia in the renal and cardiac sympathetic nerves of the rabbit." *Pflugers Archiv* 370: 1-7.
- Iriki, M., E. Kozawa, P. Korner and P. Dorward (1979). "Arterial and cardiopulmonary baroreceptor and chemoreceptor influences and interaction on ear sympathetic nerve discharge in the rabbit." *Japanese Journal of Physiology* 29: 551-558.
- Iriki, M., W. Riedel and E. Simon (1972). "Patterns of differentiation in various sympathetic efferents induced by changes of blood gas composition and by central thermal stimulation in anaesthetised rabbits." *Japanese Journal of Physiology* 22: 585-602.
- Jacob, H. J., A. Ramanathan, S. G. Pan, M. J. Brody and G. A. Myers (1995). "Spectral analysis of arterial pressure lability in rats with sinoaortic deafferentation." *American Journal of Physiology - Regulatory Integrative & Comparative Physiology* 38: R1481-R1488.
- James, T. N. (1966). "Cholinergic mechanisms in the sinus node." *Circulation Research* 14: 347-357.
- Janig, W. (1985). "Organisation of the lumbar sympathetic outflow to skeletal muscle and skin of the cat hindlimb and tail." *Reviews of Physiology, Biochemistry and Pharmacology* 102: 119-213.
- Janssen, B. J. A., P. J. A. Leenders and J. F. M. Smits (2000). "Short-term and long-term blood pressure and heart rate variability in the mouse." *American Journal of Physiology - Regulatory Integrative & Comparative Physiology* 278: R215-R225.
- Janssen, B. J. A., S. C. Malpas, S. L. Burke and G. A. Head (1997). "Frequency-dependent modulation of renal blood flow by renal nerve activity in conscious

- rabbits." *American Journal of Physiology - Regulatory, Integrative & Comparative Physiology* 273: R597-R608.
- Janssen, B. J. A., J. Oosting, D. W. Slaaf, P. B. Persson and H. A. J. Struijkerboudier (1995). "Hemodynamic basis of oscillations in systemic arterial pressure in conscious rats." *American Journal of Physiology - Heart & Circulatory Physiology* 269: H62-H71.
- Johnson, C. D. and M. P. Gilbey (1998). "Effects of aortic nerve stimulation on discharges of sympathetic neurons innervating rat tail artery and vein." *American Journal of Physiology - Regulatory, Integrative & Comparative Physiology* 275: R942-R949.
- Jordan, D. W. a. S., P. (1987). *Nonlinear ordinary differential equations*. Oxford, Clarendon press.
- Jud, H. G. (1964). "Limit cycle determination for parallel linear and nonlinear elements." *IEEE Transactions on Automatic Control* 9: 183-184.
- Julius, S. (1996). "The evidence for a pathophysiologic significance of the sympathetic overactivity in hypertension." *Clinical & Experimental Hypertension* 18: 305-21.
- Julius, S. and S. Nesbitt (1996). "Sympathetic overactivity in hypertension. A moving target." *American Journal of Hypertension* 9: 113S-120S.
- Just, A., U. Wittmann, H. Ehmke and H. R. Kirchheim (1998). "Autoregulation of renal blood flow in the conscious dog and the contribution of the tubuloglomerular feedback." *Journal of Physiology* 506: 275-90.
- Just, A., U. Wittmann, B. Nafz, C. D. Wagner, H. Ehmke, H. R. Kirchheim and P. B. Persson (1994). "The blood pressure buffering capacity of nitric oxide by comparison to the baroreceptor reflex." *American Journal of Physiology - Heart & Circulatory Physiology* 267: H521-H527.
- Kaneko, K. and I. Tsuda (1996). *Complex systems: chaos and beyond. A conservative approach with applications in life sciences*. Berlin, Springer-Verlag.
- Kanoh, H. (1984). *Analysis of a mathematical model. Mechanisms of blood pressure waves*. K. Mayakawa, H. P. Koepchen and C. Polosa. Berlin, Springer and Verlag: 241-254.
- Kantz, H. and T. Schreiber (1997). *Nonlinear time series analysis. Nonlinear time series analysis*. Cambridge, Cambridge University Press.

- Karemaker, J. M. (1999). "Autonomic integration: the physiological basis of cardiovascular variability." *Journal of Physiology - London* 517: 316.
- Kashihara, K., T. Kawada, Y. Yanagiya, K. Uemura, M. Inagaki, H. Takaki, M. Sugimachi and K. Sunagawa (2003). "Bezold-Jarisch reflex attenuates dynamic gain of baroreflex neural arc." *American Journal of Physiology - Heart & Circulatory Physiology* 285: H833-H840.
- Katona, P. G. and F. Jih (1975). "Respiratory sinus arrhythmia: noninvasive measure of parasympathetic cardiac control." *Journal of Applied Physiology* 39: 801-805.
- Katz, A. M. (1992). *Physiology of the heart*, Lippincott Williams & Wilkins.
- Kawada, T., Y. Ikeda, M. Sugimachi, T. Shishido, O. Kawaguchi, T. Yamazaki, J. Alexander and K. Sunagawa (1996). "Bidirectional augmentation of heart rate regulation by autonomic nervous system in rabbits." *American Journal of Physiology - Heart & Circulatory Physiology* 40: H288-H295.
- Kawada, T., T. Sato, M. Inagaki, T. Shishido, T. Tatewaki, Y. Yanagiya, C. Zheng, M. Sugimachi and K. Sunagawa (2000). "Closed-loop identification of carotid sinus baroreflex transfer characteristics using electrical stimulation." *Japanese Journal of Physiology* 50: 371-380.
- Kawada, T., T. Shishido, M. Inagaki, T. Tatewaki, C. Zheng, Y. Yanagiya, M. Sugimachi and K. Sunagawa (2001). "Differential dynamic baroreflex regulation of cardiac and renal sympathetic nerve activities." *American Journal of Physiology - Heart & Circulatory Physiology* 280: H1581-H1607.
- Kawada, T., M. Sugimachi, T. Sato, H. Miyano, T. Shishido, H. Miyashita, R. Yoshimura, H. Takaki, J. Alexander and K. Sunagawa (1997). "Closed-loop identification of carotid sinus baroreflex open-loop transfer characteristics in rabbits." *American Journal of Physiology - Heart & Circulatory Physiology* 273: H1024-H1031.
- Kawada, T., M. Sugimachi, T. Shishido, H. Miyano, Y. Ikeda, R. Yoshimura, T. Sato, H. Takaki, J. Alexander and K. Sunagawa (1997). "Dynamic vagosympathetic interaction augments heart rate response irrespective of stimulation patterns." *American Journal of Physiology - Heart & Circulatory Physiology* 272: H2180-H2187.
- Kawada, T., M. Sugimachi, T. Shishido, H. Miyano, T. Sato, R. Yoshimura, H. Miyashita, T. Nakahara, J. Alexander, Jr. and K. Sunagawa (1999).

- "Simultaneous identification of static and dynamic vagosympathetic interactions in regulating heart rate." *American Journal of Physiology - Regulatory Integrative & Comparative Physiology* 276: R782-R789.
- Kawada, T., K. Uemura, K. Kashihara, A. Kamiya, M. Sugimachi and K. Sunagawa (2004). "A derivative-sigmoidal model reproduces operating point-dependent baroreflex neural arc transfer characteristics." *American Journal of Physiology - Heart & Circulatory Physiology* 286: H2272-H2279.
- Kawada, T., Y. Yanagiya, K. Uemura, T. Miyamoto, C. Zheng, M. Li, M. Sugimachi and K. Sunagawa (2003). "Input-size dependence of the baroreflex neural arc transfer characteristics." *American Journal of Physiology - Regulatory Integrative & Comparative Physiology* 284: H404-H415.
- Kawada, T., C. Zheng, Y. Yanagiya, K. Uemura, T. Miyamoto, M. Inagaki, T. Shishido, M. Sugimachi and K. Sunagawa (2002). "High-cut characteristics of the baroreflex neural arc preserve baroreflex gain against pulsatile pressure." *American Journal of Physiology - Heart & Circulatory Physiology* 282: H1149-H1156.
- Kennel, M. B., R. Brown and H. D. I. Abarbanel (1992). "Determining minimum embedding dimension using a geometrical construction." *Physical Review A* 45: 3403-3411.
- Kent, B. B., J. W. Drane, B. Blumenstein and J. W. Manning (1972). "A mathematical model to assess changes in the baroreceptor reflex." *Cardiology* 57: 295-310.
- Kezdi, P. and E. Geller (1968). "Baroreceptor control of postganglionic sympathetic nerve discharge." *American Journal of Physiology* 214: 427-435.
- King, G. P., R. Jones and D. S. Broomhead (1987). "Phase portraits from a time series: a singular system approach." *Nuclear Physics B*. 2: 379.
- Kingwell, B. A., G. A. McPherson and P. I. Korner (1991). "Assessment of gain of tachycardia and bradycardia responses of cardiac baroreflex." *American Journal of Physiology - Heart & Circulatory Physiology* 260: H1254-H1263.
- Kinnane, O. P., J. V. Ringwood, D. P. Kelly and S. C. Malpas (2004). Describing function approximations for biomedical applications. Proceedings of the Irish Signals and Systems Conference, Belfast.
- Kinnane, O. P., J. V. Ringwood, R. Ramchandra, C. J. Barrett, B. L. Leonard and S. C. Malpas (2003). Deterministic chaos in blood pressure signals during

- different physiological conditions. Proceedings of the IFAC Symposium on Modelling and Control in Biomedical Systems, Melbourne.
- Kinnane, O. P., Ringwood, J.V. and Malpas, S.C. (2004). "Predicting the slow oscillation in blood pressure using nonlinear analysis." *Under review, awaiting resubmission.*
- Kitney, R. I. (1979). "A nonlinear model for studying oscillations in the blood pressure control system." *Journal of Biomedical Engineering* 1: 89-99.
- Koch, E. (1931). Die reflektorische selbststeuerung des kreislaufes. Ergebnisse der kreislaufforschung. B. Kisch. Dresden, Steinkopff.
- Koh, J., T. Brown, L. Beightol, C. Ha and D. Eckberg (1994). "Human autonomic rhythms: vagal cardiac mechanisms in tetraplegic subjects." *Journal of Physiology - London* 474: 483-495.
- Koizumi, k., H. Seller, A. Kaufman and C. M. Brooks (1971). "Pattern of sympathetic discharges and their relation to baroreceptor and respiratory activities." *Brain Research* 27: 281-294.
- Korner, P. (1972). "The central nervous system and physiological mechanisms of optimal cardiovascular control." *Austalian Journal of Experimental Biology and Medical Science* 49: 319-343
- Korner, P., J. Shaw, M. West and J. Oliver (1972). "Central nervous system control of baroreceptor reflexes in the rabbit." *Circulation Research* 31: 637-652.
- Korner, P., J. Shaw, M. West and J. Oliver (1972). "Central nervous system control of baroreceptor reflexes in the rabbit." *Circulation Research XXXI*: 637-652.
- Korner, P. I. (1975). "Central and peripheral 'resetting' of the baroreceptor system." *Clin Exp Pharmacol Physiol Suppl.* 2: 171-178.
- Korner, P. I. (1995). "Cardiac baroreflex in hypertension: role of the heart and angiotensin II." *Clinical and Experimental Hypertension* 17: 425-439.
- Korner, P. I. (1995). "Cardiac baroreflex in hypertension: role of the heart and angiotensin II." *Clin Exp Hypertension* 17: 425-439.
- Korner, P. I. and G. A. Head (1994). Baroreflexes in hypertension. Central neural Mechanisms in cardiovascular regulation. G. Kunos and J. Ciriello. Boston,Basel,Berlin,, Birkhauser. 2: 356-374.
- Korner, P. I., J. R. Oliver, P. Sleight, J. P. Chalmers and J. S. Robinson (1974). "Effects of clonidine on the baroreceptor-heart rate reflex and on single aortic

- baroreceptor fibre discharge." *European Journal of Pharmacology* 28: 189-198.
- Korner, P. I., J. Shaw, J. W. Malcom, J. R. Oliver and R. G. Hilder (1973). "Integrative reflex control of heart rate in the rabbit during hypoxia and hyperventilation." *Circulation Research* 33: 63-73.
- Korner, P. I., M. J. West, J. Shaw and J. B. Uther (1974). "'Steady-state' properties of the baroreceptor-heart rate reflex in essential hypertension in man." *Clinical and Experimental Pharmacology and Physiology* 1: 65-76.
- Kostelich, E. J. and T. Schreiber (1993). "Noise reduction in chaotic time-series data: a survey of common methods." *Phys. Rev. E* 48: 1752.
- Kostelich, E. J. and J. A. Yorke (1988). "Noise Reduction in dynamical systems." *Physical Review A* 38: 1649-1652.
- Kostelich, E. J. and J. A. Yorke (1990). "Noise reduction: Finding the simplest dynamical system consistent with the data." *Physica D* 41: 183-196.
- Kreyszig, E. (1999). *Advanced Engineering Mathematics*. Singapore, Peter Janzow.
- Krieger, E. M. (1970). "Time course of baroreceptor resetting in acute hypertension." *American Journal of Physiology* 218: 486-490.
- Kubo, T., T. Imaizumi, Y. Harasawa, S. I. Ando, T. Tagawa, T. Endo, M. Shiramoto and A. Takeshita (1996). "Transfer function analysis of central arc of aortic baroreceptor reflex in rabbits." *American Journal of Physiology - Heart & Circulatory Physiology* 39: H1054-H1062.
- Landgren, S. (1952). "The baroreceptor activity in the carotid sinus nerve and the distensibility of the sinus wall." *Acta Physiol Scand* 26: 35-56.
- Landgren, S. (1952). "On the excitation mechanism of the carotid baroreceptors." *Acta Physiol Scand* 26: 1-34.
- Lanfranchi, P. A. and V. K. Somers (2002). "Arterial baroreflex function and cardiovascular variability: interactions and implications." *American Journal of Physiology - Regulatory Integrative & Comparative Physiology* 283: R815-R826.
- Larovere, M. T., J. T. Bigger, F. I. Marcus, A. Mortara and P. J. Schwartz (1998). "Baroreflex sensitivity and heart-rate variability in prediction of total cardiac mortality after myocardial infarction." *Lancet* 351: 478-484.

- Larovere, M. T. and P. J. Schwartz (1997). "Baroreflex sensitivity as a cardiac and arrhythmia mortality risk stratifier." *Pace-Pacing & Clinical Electrophysiology* 20: 2602-2613.
- Le Fevre, M. E., S.-J. Guild, R. Ramchandra, C. J. Barrett and S. C. Malpas (2003). "Role of angiotensin II in the neural control of renal function." *Hypertension* 41: 583-591.
- Leonard, B. L., M. A. Navakatikyan and S. C. Malpas (2000). "Differential regulation of the oscillations in sympathetic nerve activity and renal blood flow following volume expansion." *Autonomic Neuroscience* 83: 19-28.
- Levy, M. N. (1971). "Sympathetic-parasympathetic interactions in the heart." *Circulation Research* 29: 437-445.
- Levy, M. N. (1984). Cardiac sympathetic-parasympathetic interactions. Federation Proceedings.
- Levy, M. N., P. J. Martin, T. Iano and H. Zieske (1969). "Paradoxical effects of vagus nerve stimulation on heart rate in dogs." 303-314.
- Levy, M. N. and H. Zieske (1969). "Comparison of cardiac effects of vagus nerve stimulation and of acetylcholine infusions." *American Journal of Physiology* 216: 890-897.
- Lewis, P. H. and C. Yang (1997). Basic Control Systems Engineering, Prentice-Hall Inc.
- Leyssac, P. P. and L. Baumbach (1983). "An oscillating intratubular pressure response to alterations in the loop of Henle flow in the rat kidney." *Acta. Physiol. Scand.* 117: 415-419.
- Liebert, W., K. Pawelzik and H. G. Schuster (1991). "Optimal embedding of chaotic attractors from topological considerations." *Europhysics Letters* 14: 521.
- Little, J. N. and L. Shure (1992). Signal processing toolbox for use with MATLAB: user's guide. Massachusetts, Mathworks Inc.
- Littler, W. A., M. J. West, A. J. Honour and P. Sleight (1978). "The variability of arterial pressure." *American Heart Journal* 95: 180-186.
- Liu, H.-K., S.-J. Guild, J. V. Ringwood, C. J. Barrett, B. L. Leonard, S.-K. Nguang, M. A. Navakatikyan and S. C. Malpas (2002). "Dynamic baroreflex control of blood pressure: influence of the heart vs. peripheral resistance." *American Journal of Physiology - Regulatory Integrative & Comparative Physiology* 283: R533-R542.

- Ljung, L. (1999). *System identification: Theory for the user* (2nd ed.). Englewood Cliffs, NJ., Prentice-Hall.
- Lohmeier, T. E. (2001). "The sympathetic nervous system and long-term blood pressure regulation." *American Journal of Hypertension* 14: 147S-154S.
- Lohmeier, T. E. (2003). "Interactions Between Angiotensin II and Baroreflexes in Long-Term Regulation of Renal Sympathetic Nerve Activity." *Circulation Research* 92: 1282-1284.
- Lombardi, F. (2000). "Chaos Theory, Heart Rate Variability, and Arrhythmic Mortality." *Circulation* 101: 8-10.
- Lovell, N., B. Henry, A. Avolio, B. Cellar, D. Carlson and M. Brunner (1997). Nonlinear chaotic dynamics of mean arterial pressure after carotid baroreceptor isolation. 19th International Conference - IEEE/EMBS, Chicago, IEEE.
- Ludwig, C. (1847). "Beitrage zur kenntnis des einflusses der respirationsbewegungen auf den blutumlauf im aortensystem." *Arch. Anat. Physiol.*: 242-302.
- Luff, S. E., S. G. Hengstberger, E. M. McLachlan and W. P. Anderson (1992). "Distribution of sympathetic neuroeffector junctions in the juxtaglomerular region of the rabbit kidney." *Journal of the Autonomic Nervous System* 40: 239-53.
- Madwed, J. B., P. Albrecht, R. G. Mark and R. J. Cohen (1989). "Low - frequency oscillations in arterial pressure and heart rate: a simple computer model." *American Journal of Physiology - Heart & Circulatory Physiology* 256: H1573-H1579.
- Malik, M. and A. J. Camm (1990). "Heart rate variability." *Clinical Cardiology* 13: 570-576.
- Malliani, A. (1999). "The pattern of sympathovagal balance explored in the frequency domain." *News in Physiological Sciences* 14: 111-117.
- Malliani, A., F. Lombardi, M. Pagani and M. S. Cerutti (1994). "Power spectral analysis of cardiovascular variability in patients at risk for sudden cardiac death." *Journal of Cardiovascular Electrophysiology* 5: 274-286.
- Malliani, A., M. Pagani, F. Lombardi and S. Cerutti (1991). "Cardiovascular neural regulation explored in the frequency domain." *Circulation* 84: 482-92.

- Malpas, S. (2002). "Neural influences on cardiovascular variability: possibilities and pitfalls." *American Journal of Physiology - Heart & Circulatory Physiology* 282: H6-H20.
- Malpas, S., S.-J. Guild, R. Evans and G. F. DiBona (2003). "Responsiveness of the Renal Vasculature: Relating Electrical Stimulation to Endogenous Nerve Activity Is Problematic." *American Journal of Physiology - Renal Physiology* 284: F594-F596.
- Malpas, S. C. (1995). "A new model for the generation of sympathetic nerve activity." *Clinical & Experimental Pharmacology & Physiology* 22: 11-15.
- Malpas, S. C. (1998). "The rhythmicity of sympathetic nerve activity." *Progress in Neurobiology* 56: 65-96.
- Malpas, S. C. (2004). "What sets the long-term level of sympathetic nerve activity: is there a role for arterial baroreceptors?" *American Journal of Physiology - Regulatory Integrative & Comparative Physiology* 286: R1-R12.
- Malpas, S. C., R. D. Bendle, G. A. Head and J. H. Ricketts (1996). "Frequency and amplitude of sympathetic discharges by baroreflexes during hypoxia in conscious rabbits." *American Journal of Physiology - Heart & Circulatory Physiology* 271: H2563-H2574.
- Malpas, S. C. and D. E. Burgess (2000). "Renal SNA as the primary mediator of slow oscillations in blood pressure during hemorrhage." *American Journal of Physiology - Regulatory Integrative & Comparative Physiology* 279: R1299-R1306.
- Malpas, S. C. and R. G. Evans (1998). "Do different levels and patterns of sympathetic activation all provoke renal vasoconstriction?" *Journal of the Autonomic Nervous System* 69: 72-82.
- Malpas, S. C., R. G. Evans, G. A. Head and E. V. Lukoshkova (1998). "Contribution of renal nerves to renal blood flow variability during hemorrhage." *American Journal of Physiology - Regulatory Integrative & Comparative Physiology* 274: R1283-R1294.
- Malpas, S. C., A. S. Groom and G. A. Head (1997). "Baroreflex control of heart rate and cardiac hypertrophy in angiotensin ii-induced hypertension in rabbits." *Hypertension* 29: 1284-1290.
- Malpas, S. C., T. A. Hore, M. Navakatykyan, E. V. Lukoshkova, S. K. Nguang and P. C. Austin (1999). "Resonance in the renal vasculature evoked by activation of

- the sympathetic nerves." *American Journal of Physiology - Regulatory Integrative & Comparative Physiology* 276: R1311-R1319.
- Malpas, S. C. and B. L. Leonard (2000). "Neural regulation of renal blood flow: A re-examination." *Clinical & Experimental Pharmacology & Physiology* 27: 956-964.
- Malpas, S. C., B. L. Leonard, S.-J. Guild, J. V. Ringwood, M. Navakatikyan, P. C. Austin, G. A. Head and D. E. Burgess (2001). "The sympathetic nervous system's role in regulating blood pressure variability." *IEEE: Engineering in Medicine and Biology Magazine*.
- Malpas, S. C. and I. Ninomiya (1992). "A new approach to analysis of synchronized sympathetic nerve activity." *American Journal of Physiology - Heart & Circulatory Physiology* 263: H1311-H1317.
- Malpas, S. C., A. Shweta, W. P. Anderson and G. A. Head (1996). "Functional response to graded increases in renal nerve activity during hypoxia in conscious rabbits." *American Journal of Physiology - Regulatory Integrative & Comparative Physiology* 271: R1489-R1499.
- Mancia, G., A. U. Ferrari, L. Gregorini, G. Parati, G. Pomidossi, G. Bertinieri, G. Grassi, M. Di Rienzo, A. Pedotti and A. Zanchetti (1983). "Blood pressure and heart rate variabilities in normotensive and hypertensive human beings." *Circulation Research* 53: 96-104.
- Mancia, G., G. Parati, M. Di Rienzo and A. Zanchetti (1997). Blood pressure variability. Handbook of hypertension, Pathophysiology of hypertension. A. Zanchetti and G. Mancia. 17: 116-169.
- Mancia, G. and A. Zanchetti (1986). Blood pressure variability. Handbook of hypertension. A. Zanchetti and R. Tarazi. Amsterdam, Elsevier Science Publishing Co. Inc. 7: 125-152.
- Marieb, E. N. (2003). Essentials of human anatomy & physiology. San Francisco, Pearson Education Inc.
- Marquardt, D. W. (1963). "An algorithm for least-squares estimates of nonlinear parameters." *Journal of the Society of Industrial and Applied Mathematics* 11: 431-441.
- Marshall, J. M. (1981). "Interactions between the response to stimulation of peripheral chemoreceptors and baroreceptors: the importance of

- chemoreceptor activation of the defence areas." *Journal of Autonomic Nervous System* 3: 389-400.
- Marshall, J. M. (1994). "Peripheral chemoreceptors and cardiovascular regulation." *Physiological Reviews* 74: 544-584.
- Mayer, S. (1876). "Uber spontane blutdruckschwankungen." *Sitzungsberichte Kaiserlich Akad Wissenschaft Mathemat-Naturwissenschaft Classe* 74: 281-307.
- McAllen, R. M. and C. N. May (1990). "The conduction velocity of the descending spinal pathway to the renal sympathetic nerve in the cat." *Journal of Autonomic Nervous System* 30: 139-142.
- McAreevey, D., J. M. Neilson, D. J. Ewing and D. C. Russell (1989). "Cardiac parasympathetic activity during the early hours of acute myocardial infarction." *British Heart Journal* 62: 165-170.
- McCance, A. J., P. A. Thompson and J. C. Forfar (1993). "Increased cardiac sympathetic nervous activity in patients with unstable coronary heart disease." *European Heart Journal* 14: 751-757.
- Mees, A. I. and A. R. Bergen (1975). "Describing function revisited." *IEEE Transactions on Automatic Control* 20: 473-478.
- Mees, A. I., P. E. Rapp and L. S. Jennings (1987). "Singular value decomposition and embedding dimension." *Physical Review A* 37: 340-346.
- Mende, W., H. Herzel and K. Wermke (1990). "Bifurcations and chaos in newborn infant cries." *Physics Letters A* 145: 418-424.
- Michaels, D. C., E. P. Matyas and J. Jalife (1987). "Mechanisms of sinoatrial pacemaker synchronization: a new hypothesis." *Circulation Research* 61: 704-714.
- Millar, C. M. W., C. N. Bishop and E. B. Raftery (1978). "Circadian variation of blood pressure." *Lancet* 1: 789-795.
- Miyawaki, T., P. Pilowsky, Q. J. Sun, J. Minson, S. Suzuki, L. Arnold, I. Llewellynsmith and J. Chalmers (1995). "Central inspiration increases barosensitivity of neurons in rat rostral ventrolateral medulla." *American Journal of Physiology - Regulatory Integrative & Comparative Physiology* 268: R909-R918.

- Mokrane, A., A. R. LeBlanc and R. Nadeau (1995). "Transfer function analysis of vagal control of heart rate during synchronized vagal stimulation." *American Journal of Physiology - Heart & Circulatory Physiology* 269: H1931-H1940.
- Mokrane, A. and R. Nadeau (1998). "Dynamics of heart rate response to sympathetic nerve stimulation." *American Journal of Physiology - Heart & Circulatory Physiology* 275: H995-H1001.
- Montano, N., C. Cogliati, A. Porta, M. Pagani, A. Malliani, K. Narkiewicz, F. M. Abboud, C. Birkett and V. K. Somers (1998). "Central vagotonic effects of atropine modulate spectral oscillations of sympathetic nerve activity." *Circulation* 98: 1394-9.
- Montano, N., T. G. Ruscone, A. Porta, F. Lombardi, M. Pagani and A. Malliani (1994). "Power spectrum analysis of heart rate variability to assess the changes in sympathovagal balance during graded orthostatic tilt." *Circulation* 90: 1826-1831.
- Mrowka, R., A. Patzak, E. Schubert and P. B. Persson (1996). "Linear and non-linear properties of heart rate in postnatal maturation." *Cardiovascular Research* 31: 447-454.
- Mrowka, R., H. M. Strauss, C. D. Wagner, B. Nafz, A. Patzak and P. B. Persson (1995). "Non-linear analysis of the cardiovascular control system in rat strains with differing hemodynamic characteristics." *Computers in Cardiology*: 313-315.
- Mullen, T. J., M. L. Appel, R. Mukkamala, J. M. Mathias and R. J. Cohen (1997). "System identification of closed-loop cardiovascular control: Effects of posture and autonomic blockade." *American Journal of Physiology - Heart & Circulatory Physiology* 272: H448-H461.
- Munakata, M., A. Aihara, Y. Imai, T. Noshiro, S. Ito and K. Yoshinaga (1999). "Altered sympathetic and vagal modulations of the cardiovascular system in patients with pheochromocytoma: Their relations to orthostatic hypotension." *American Journal of Hypertension* 12: 572-580.
- Murata, K., P. J. Landrigan and S. Araki (1992). "Effects of age, heart rate, gender, tobacco and alcohol ingestion on R-R interval variability in human ECG." *Journal of the Autonomic Nervous System* 37: 199-206.

- Nafz, B., A. Just, H. M. Stauss, C. D. Wagner, H. Ehmke, H. R. Kirchheim and P. Persson (1986). "Blood pressure variability is buffered by nitric oxide." *Journal of the Autonomic Nervous System* 57: 181-183.
- Nafz, B., C. Wagner and P. Persson (1997). "Endogenous nitric oxide buffers blood pressure variability between 0.2 and 0.6 Hz in the conscious rat." *American Journal of Physiology - Heart & Circulatory Physiology* 272: H632-H637.
- Nakahara, T., T. Kawada, M. Sugimachi, H. Miyano, T. Sato, T. Shishido, R. Yoshimura, H. Miyashita, M. Inagaki, J. Alexander and K. Sunagawa (1999). "Neuronal uptake affects dynamic characteristics of heart rate response to sympathetic stimulation." *American Journal of Physiology - Regulatory Integrative & Comparative Physiology*. 46: R140-R146.
- Nakata, A., S. Takata, T. Yuasa, A. Shimakura, M. Maruyama, H. Nagai, S. Sakagami and K.-I. Kobayashi (1998). "Spectral analysis of heart rate, arterial pressure, and muscle sympathetic nerve activity in normal humans." *American Journal of Physiology - Heart & Circulatory Physiology* 274: H1211-H1217.
- Navakatikyan, M. A., B. L. Leonard, R. G. Evans and S. C. Malpas (2000). "Modelling the neural control of intrarenal blood flow." *Clinical and Experimental Pharmacology Physiology* 27: 650-652.
- Ninomiya, I., T. Akiyama and N. Nishiura (1990). "Mechanism of cardiac-related synchronized cardiac sympathetic nerve activity in awake cats." *American Journal of Physiology - Regulatory Integrative & Comparative Physiology* 259: R499-R506.
- Ninomiya, I. and S. Fujita (1976). "Reflex effects of thermal stimulation on sympathetic nerve activity to skin and kidney." *American Journal of Physiology* 230: 271-278.
- Ninomiya, I., N. Nisimaru and H. Irisawa (1971). "Sympathetic nerve activity to the spleen, kidney, and heart in response to baroreceptor input." *American Journal of Physiology* 221: 1346-1351.
- Nishimaru, N. (1971). "Comparison of gastric and renal nerve activity." *American Journal of Physiology* 220: 1303-1308.
- Nisimaru, Y. (1984). A story of the spleen, the fourth grade blood pressure change. Mechanisms of blood pressure waves. K. Miyakawa, H. P. Koepchen and C. Polosa. New York, Springer-Verlag: 341-346.

- Nolan, J., A. D. Flapan, S. Capewell, T. M. MacDonald, J. M. Neilson and D. J. Ewing (1992). "Decreased cardiac parasympathetic activity in chronic heart failure and its relation to left ventricular function." *British Heart Journal* 67: 482-485.
- O'Leary, D. S. and D. J. Woodbury (1996). "Role of cardiac output in mediating arterial blood pressure oscillations." *American Journal of Physiology - Regulatory Integrative & Comparative Physiology* 271: R641-R646.
- Olufsen, M. S. (1999). "Structured tree outflow condition for blood flow in larger systemic arteries." *American Journal of Physiology - Heart & Circulatory Physiology* 276: H257-H268.
- Olufsen, M. S., C. S. Peskin, W. Y. Kim, E. M. Pedersen, A. Nadim and J. Larsen (2000). "Numerical simulation and experimental validation of blood flow in arteries with structured-tree outflow conditions." *Annals of Biomedical Engineering* 28: 1281-1299.
- Ottesen, J. T. (1997). "Modelling of the baroreflex-feedback mechanism with time-delay." *Journal of Mathematical Biology* 36: 41-63.
- Ottesen, J. T. (1997). "Nonlinearity of baroreceptor nerves." *Surveys of Mathematics for Industry* 7: 187-201.
- Ottesen, J. T. (2000). "Modelling the dynamical baroreflex-feedback control." *Mathematical and Computer Modelling* 31: 167-173.
- Packard, N. H., J. P. Crutchfield, J. D. Farmer and R. S. Shaw (1980). "Geometry from a time series." *Physical Review Letters* 45: 712-716.
- Pagani, M., F. Lombardi, S. Guzzetti, O. Rimoldi, R. Furlan, P. Pizzinelli, G. Sandrone, G. Malfatto, S. Dell'Orto and E. Piccaluga (1986). "Power spectral analysis of heart rate and arterial pressure variabilities as a marker of sympatho-vagal interaction in man and conscious dog." *Circulation Research* 59: 178-93.
- Panas, E. a. N., V. (2000). "Are oil markets chaotic? A nonlinear dynamic analysis." *Energy Economics* 22: 549-568.
- Parati, G., M. Di Rienzo, L. Ulian, C. Santucci, A. Girard, J. L. Elghozi and G. Mancia (1998). "Clinical relevance blood pressure variability." *Journal of Hypertension - Supplement* 16: S25-S33.
- Parati, G. and G. Mancia (2001). "Blood pressure variability as a risk factor." *Blood Pressure Monitoring* 6: 341-347.

- Parati, G., A. Ravogli, A. Frattola, A. Groppelli, L. Ulian, C. Santucci and G. Mancia (1994). "Blood pressure variability: clinical implications and effects of antihypertensive treatment." *Journal of Hypertension - Supplement* 12: S35-S40.
- Parati, G., J. P. Saul, M. Di Rienzo and G. Mancia (1995). "Spectral Analysis of Blood Pressure and Heart Rate Variability in Evaluating Cardiovascular Regulation : A Critical Appraisal." *Hypertension* 25: 1276-1286.
- Parati, G., L. Ulian, C. Santucci, S. Omboni and G. Mancia (1995). "Blood pressure variability, cardiovascular risk and antihypertensive treatment." *Journal of Hypertension* 13: 27-34.
- Parlitz, U. (1992). "Identification of true and spurious Lyapunov exponents from time series." *International Journal of Bifurcation and Chaos* 2: 155-165.
- Patzak, A., K. Lipke, W. Orlow, R. Mrowka, H. M. Stauss, E. Windt, P. B. Persson and E. Schubert (1996). "Development of the heart rate power spectra reveals neonatal peculiarities of cardio-respiratory control." *American Journal of Physiology - Regulatory Integrative & Comparative Physiology* 271: R1025-R1032.
- Pavlov, A. N., Janson, N.B., Anishchenko, V.S., Gridnev, V.I. and Dovgalevsky, P.Y. (2000). "Diagnostic of cardio-vascular disease with help of largest Lyapunov exponent of RR-sequences." *Chaos, Solutions and Fractals* 11: 807-814.
- Penaz, J. (1978). "Mayer waves: history and methodology." *Automedica* 2: 135-141.
- Persson, P. B. (1997). "Spectrum analysis of cardiovascular time series." *American Journal of Physiology - Regulatory Integrative & Comparative Physiology* 273: R1201-R1210.
- Persson, P. B., J. E. Baumann, H. Ehmke, B. Nafz, U. Wittmann and H. R. Kirchheim (1992). "Phasic and 24-hr blood pressure control by endothelium-derived relaing factor in conscious dogs." *American Journal of Physiology - Heart & Circulatory Physiology* 262: H1395-H1400.
- Persson, P. B., H. Ehmke and H. R. Kirchheim (1989). "Cardiopulmonary-arterial baroreceptor interaction in the control of blood pressure." *News in Physiological Sciences* 4: 56-59.
- Petiot, E., C. Barres, B. Chapuis and C. Julien (2001). "Frequency response of renal sympathetic nervous activity to aortic depressor nerve stimulation in the anaesthetized rat." *Journal of Physiology - London* 537: 949-959.

- Pickering, T. G., B. Gribbin and P. Sleight (1972). "Comparison of the reflex heart rate response to rising and falling arterial pressure in man." *Cardiovascular Research* 6: 277-283.
- Pilowsky, P. (1995). "Good vibrations? respiratory rhythms in the central control of blood pressure." *Clinical and Experimental Pharmacology and Physiology* 22: 594-604.
- Polosa, C. (1967). "The silent period of sympathetic preganglionic neurons." *Canadian Journal of Physiology and Pharmacology* 45: 1033-1045.
- Poon, C.-S. and M. Barahona (2001). Titration of chaos with added noise. Proceedings of the National Academy of Science, USA.
- Preiss, G. and C. Polosa (1974). "Patterns of sympathetic neuron activity associated with Mayer waves." *American Journal of Physiology* 226: 724-30.
- Radhakrishna, R. K. A., D. N. Dutt and V. K. Yeragani (2000). "Nonlinear measures of heart rate time series: influence of posture and controlled breathing." *Autonomic Neuroscience: Basic and Clinical* 83: 148-158.
- Radojicic, I., D. Mandic and D. Vulic (2001). "On the presence of deterministic chaos in heart rate variability signals." *Computers in Cardiology* 28: 465-468.
- Ramchandra, R. (2003). Unpublished results.
- Ramchandra, R., C. J. Barrett and S. C. Malpas (2003). "Chronic blockade of nitric oxide does not produce hypertension in baroreceptor denervated rabbits." *Hypertension* 42: 974-977.
- Rao, R. K. A., Dutt, D.N. and Yeragani, V.K. (2000). "Nonlinear measures of heart rate time series: influence of posture and controlled breathing." *Autonomic Neuroscience: Basic and Clinical* 83: 148-158.
- Rao, R. K. A. and V. K. Yeragani (2001). "Decreased chaos and increased nonlinearity of heart rate time series in patients with panic disorder." *Autonomic Neuroscience: Basic and Clinical* 88: 99-108.
- Rees, D. D., R. M. Palmer and S. Moncada (1989). Role of endothelium-derived nitric oxide in the regulation of blood pressure. Proceedings of the National Academy of Science, USA.
- Richardson, D. R., D. C. Randall and D. F. Speck (1998). Cardiopulmonary system. Madison, Connecticut, Fence Creek Publishing.
- Ricketts, J. H. and G. A. Head (1999). "A five-parameter logistic equation for investigating asymmetry of curvature in baroreflex studies." *American Journal*

- of Physiology - Regulatory Integrative & Comparative Physiology* 46: R441-R454.
- Rideout, V. (1991). *Mathematical and computer modelling of Physiological Systems*, Medical Physics Publishing.
- Ringwood, J., O. Kinnane and S. Malpas (2005). Prediction of low frequency blood pressure oscillations via a combined heart/resistance model. *Proceedings of the IFAC World Congress, Prague*.
- Ringwood, J. V. and S. C. Malpas (2001). "Slow oscillations in blood pressure via a nonlinear feedback model." *American Journal of Physiology - Regulatory Integrative & Comparative Physiology* 280: R1105-R1115.
- Rissanen, J. (1978). "Modelling by shortest data description." *Automatica* 14: 465-471.
- Rosenbaum, M. and D. Race (1968). "Frequency response characteristics of vascular resistance vessels." *American Journal of Physiology* 125(6): 1397-1402.
- Rosenstein, M., J. J. Collins and C. J. De Luca (1993). "A practical method for calculating largest Lyapunov exponents from small data sets." *Physica D* 65: 117-134.
- Rosenstein, M., J. J. Collins and C. J. De Luca (1994). "Reconstruction expansion as a geometry based framework for choosing proper delay times." *Physica D* 73: 189-208.
- Rubanyi, M. G., A. D. Freay, K. Kauser, A. Johns and D. R. Harder (1990). "Mechanoreception by the endothelium: Mediators and mechanisms of pressure- and flow- induced vascular responses." *Blood Vessels* 27: 246-257.
- Rudas, L., A. A. Crossman, C. A. Morillo, J. R. Halliwill, K. U. O. Tahvanainen, T. A. Kuusela and D. L. Eckberg (1999). "Human sympathetic and vagal baroreflex responses to sequential nitroprusside and phenylephrine." *American Journal of Physiology - Heart & Circulatory Physiology* 45: H1691-H1698.
- Ryan, S. M., A. L. Goldberger, S. M. Pincus, J. Mietus and L. A. Lipsitz (1994). "Gender- and age- related differences in heart rate dynamics: Are women more complex than men?" *Journal of the American College of Cardiology* 24: 1700-1707.
- Sagawa, K. and K. Watanabe (1965). "Summation of bilateral carotid sinus signals in the barostatic reflex." *American Journal of Physiology*: 1278-1286.

- Sano, M. and Y. Sawada (1985). "Measurement of the Lyapunov spectrum from a chaotic time series." *Physical Review Letters* 55: 1082-1085.
- Sato, T., T. Kawada, M. Inagaki, T. Shishido, M. Sugimachi and K. Sunagawa (2003). "Dynamics of sympathetic baroreflex control of arterial pressure in rats." *American Journal of Physiology - Regulatory, Integrative & Comparative Physiology* 285: R262-R270.
- Sato, T., T. Kawada, M. Inagaki, T. Shishido, H. Takaki, M. Sugimachi and K. Sunagawa (1999). "New analytic framework for understanding sympathetic baroreflex control of arterial pressure." *American Journal of Physiology - Heart & Circulatory Physiology* 276: H2251-H2261.
- Sato, T., T. Kawada, T. Shishido, H. Miyano, M. Inagaki, H. Miyashita, M. Sugimachi, M. M. Knuepfer and K. Sunagawa (1998). "Dynamic transduction properties of in situ baroreceptors of rabbit aortic depressor nerve." *American Journal of Physiology - Heart & Circulatory Physiology* 274: H358-H365.
- Sauer, T. (1992). "A noise reduction method for signals from nonlinear systems." *Physica D* 58: 193-201.
- Saul, J. P., R. D. Berger, P. Albrecht, S. P. Stein, M. H. Chen and R. J. Cohen (1991). "Transfer function analysis of the circulation: unique insights into cardiovascular regulation." *American Journal of Physiology - Heart & Circulatory Physiology* 261: H1231-H1245.
- Saul, J. P., R. F. Rea, D. L. Eckberg, R. D. Berger and R. J. Cohen (1990). "Heart rate and muscle sympathetic nerve variability during reflex changes of autonomic activity." *American Journal of Physiology - Heart & Circulatory Physiology* 258: H713-H721.
- Scarpa, A. (1974). *Tabulae neurologicae ad illustrandam historiam anatomicam cardiacorum nervorum, noni nervorum cerebri, glossopharyngaei et pharyngaei ex octavo cerebri*. Ticini, Balthassarem Comini.
- Scher, A. M. and A. C. Young (1963). "Servoanalysis of carotid sinus reflex effects on peripheral resistance." *Circulation Research* 12: 152-162.
- Schreiber, T. (1993). "Extremely simple nonlinear noise reduction method." *Physical Review E* 47: 2401-2404.
- Schreiber, T. and P. Grassberger (1991). "A simple noise-reduction method for real data." *Physics Letters A* 160: 411.

- Seals, D. R., N. O. Suwarno, M. J. Joyner, C. Iber, J. G. Copeland and J. A. Dempsey (1993). "Respiratory modulation of muscle sympathetic nerve activity in intact and lung denervated humans." *Circulation Research* 72: 440-454.
- Seidel, H. (1997). Nonlinear dynamics of physiological rhythms. Berlin, Technischen Universitat Berlin.
- Seidel, H. and H. Herzel (1995). Modelling heart rate variability due to respiration and baroreflex. Modelling the dynamics of biological systems. E. Mosekilde and O. G. Mouritsen. Berlin, Springer-Verlag.
- Seidel, H. and H. Herzel (1998). "Bifurcations in a nonlinear model of the baroreceptor-cardiac reflex." *Physica D* 115: 145-160.
- Seidel, H., H. Herzel and D. L. Eckberg (1997). "Phase dependencies of the human baroreceptor reflex." *American Journal of Physiology* 272: H2040-53.
- Seller, H. (1991). Central baroreceptor reflex pathways. Baroreceptor reflexes: integrative functions and clinical aspects. P. B. Persson and H. R. Kirchheim. Heidelberg, Germany, Springer-Verlag.
- Seydnejad, S. R. and R. I. Kitney (2001). "Modeling of Mayer waves generation mechanisms." *IEEE Engineering in Medicine and Biology Magazine* 20: 92-100.
- Sherwood, L. (1997). Human physiology: from cells to systems, USA, Wadsworth Publishing Company.
- Shirai, M., K. Matsukawa, N. Nishiura and I. Ninomiya (1995). "Effects of baroreceptor reflex on efferent pulmonary sympathetic nerve activity in anesthetized cat." *American Journal of Physiology - Regulatory Integrative & Comparative Physiology* 37: R1078-R1083.
- Signorini, M. G. and S. Cerrutti (1994). Lyapunov exponents calculated from heart rate variability time series. International conference of the IEEE EMBC Society, Baltimore.
- Signorini, M. G., F. Marchetti and S. Cerutti (2001). "Applying nonlinear noise reduction in the analysis of heart rate variability." *IEEE: Engineering in Medicine and Biology Magazine* 20: 59-68.
- Sleight, P. (2004). "Arterial baroreflexes can determine long-term blood pressure: Baroreceptors and hypertension: time for are-think?" *Experimental Physiology* 89: 337-341.

- Sleight, P., M. T. Larovere, A. Mortara, G. Pinna, R. Maestri, S. Leuzzi, B. Bianchini, L. Tavazzi and L. Bernardi (1995). "Physiology and pathophysiology of heart rate and blood pressure variability in humans: is power spectral analysis largely an index of baroreflex gain?" *Clinical Science* 88: 103-109.
- Slotine, J.-J. and W. Li (1990). *Applied nonlinear control*, Englewood Cliffs, New Jersey, Wiley.
- Stauss, H. M. (2002). "Baroreceptor reflex function." *American Journal of Physiology - Regulatory Integrative & Comparative Physiology* 283: R284-R286.
- Stauss, H. M. (2003). "Heart rate variability." *American Journal of Physiology - Regulatory Integrative & Comparative Physiology* 285: R927-R931.
- Stauss, H. M., E. A. Anderson, W. G. Haynes and K. C. Kregel (1998). "Frequency response characteristics of sympathetically mediated vasomotor waves in humans." *American Journal of Physiology - Heart & Circulatory Physiology* 43: H1277-H1283.
- Stauss, H. M., A. Godecke, R. Mrowka, J. Schrader and P. B. Persson (1999). "Enhanced blood pressure variability in eNOS knockout mice." *Hypertension* 33: 1359-1363.
- Stauss, H. M. and K. C. Kregel (1996). "Frequency response characteristic of sympathetic-mediated vasomotor waves in conscious rats." *American Journal of Physiology - Heart & Circulatory Physiology* 271: H1416-H1422.
- Stauss, H. M., R. Mrowka, B. Nafz, A. Patzak, T. Unger and P. B. Persson (1995). "Does low frequency power of arterial blood pressure reflect sympathetic tone?" *Journal of Autonomic Nervous System* 54: 145-154.
- Stauss, H. M. and P. B. Persson (2000). "Role of nitric oxide in buffering short-term blood pressure fluctuations." *News in Physiological Sciences* 15: 229-233.
- Stauss, H. M., P. B. Persson, A. K. Johnson and K. C. Kregel (1997). "Frequency-response characteristics of autonomic nervous system function in conscious rats." *American Journal of Physiology - Heart & Circulatory Physiology* 273: H786-H795.
- Stauss, H. M., J. U. Stegmann, P. B. Persson and H. J. Habler (1999). "Frequency response characteristics of sympathetic transmission to skin vascular smooth muscles in rats." *American Journal of Physiology - Regulatory Integrative & Comparative Physiology* 46: R591-R600.

- Suga, H., H. Sagawa and D. P. Kostiuk (1976). "Controls of the ventricular contractility assessed by pressure-volume ratio,  $E_{\max}$ ." *Cardiovascular Research* 10: 582-592.
- Suga, H., H. Sagawa and A. Shoukas (1974). "Carotid sinus baroreflex effects on instantaneous pressure-volume ration of the canine left ventricle." *Journal of Physiology Society Japan* 36: 106-107.
- Sugihara, G., W. Allan, D. Sobel and K. D. Allan (1996). Nonlinear control of heart rate variability in human infants. Proceedings of the National Academy of Sciences, USA.
- Sugihara, G. and R. M. May (1990). "Nonlinear forecasting as a way of distinguishing chaos from measurement error in time series." *Nature* 344: 734-741.
- Sugimachi, M., T. Imaizumi, K. Sunagawa, Y. Hirooka, K. Todaka, A. Takeshita and M. Nakamura (1990). "A new method to identify dynamic transduction properties of aortic baroreceptors." *American Journal of Physiology - Heart & Circulatory Physiology* 258: H887-H895.
- Sun, H., R. Gaspo, N. Leblanc and S. Nattel (1998). "Cellular Mechanisms of Atrial Contractile Dysfunction Caused by Sustained Atrial Tachycardia." *Circulation* 98: 719-727.
- Szego, G. (1975). Orthogonal polynomials. New York, American Mathematical Society.
- Taher, M. F., A. B. P. Cecchini, M. A. Allen, S. R. Gobran, R. C. Gorman, B. L. Guthrie, K. A. Lingenfelter, S. Y. Rabbany, P. M. Rolchigo, J. Melbin and A. Noordergraaf (1988). "Baroreceptor responses derived from a fundamental concept." *Annals of Biomedical Engineering* 16: 429-443.
- Takens, F. (1981). Determining strange attractors in turbulence. Lecture Notes in Mathematics. D. A. Rand and L. S. Young. Berlin, Springer-Verlag. 898: 366-381.
- Taylor, J. A., D. L. Carr, C. W. Myers and D. L. Eckberg (1998). "Mechanisms underlying very-low-frequency RR-interval oscillations in humans." *Circulation* 98: 547-555.
- Taylor, J. A. and D. L. Eckberg (1996). "Fundamental relations between short-term RR interval and arterial pressure oscillations in humans." *Circulation* 93: 1527-1532.

- Taylor, J. A., T. D. Williams, D. R. Seals and K. P. Davy (1998). "Low-frequency arterial pressure fluctuations do not reflect sympathetic outflow - gender and age differences." *American Journal of Physiology - Heart & Circulatory Physiology* 43: H1194-H1201.
- Teich, M. C., S. B. Lowen, B. M. Jost, K. Vibe-Rheymer and C. Heneghan (2000). Heart rate variability: measures and models. Nonlinear biomedical signal processing. M. Akay. New York, IEEE Press: 159-213.
- Terui, N., Y. Saeki and M. Kumada (1987). "Confluence of barosensory and nonbarosensory inputs at neurons in the ventrolateral medulla in rabbits." *Canadian Journal of Physiology and Pharmacology* 65: 1584-1590.
- Theiler, J. (1987). "Efficient algorithm for estimating the correlation dimension from a set of discrete points." *Physical Review E* 36: 4456-4462.
- Theiler, J. and D. Prichard (1996). "Constrained-realization Monte-Carlo method for hypothesis testing." *Physica D* 94: 221-235.
- Theiler, J. S., A. Eubank, B. Longtin, B. Galdrikian and J. Doyne Farmer (1992). "Testing for nonlinearity in time series: the method of surrogate data." *Physica D* 58: 77-94.
- Thoren, P. and J. V. Jones (1977). "Characteristics of aortic baroreceptor C-fibres in the rabbit." *Acta Physiologica Scandinavica* 99: 448-56.
- Thrasher, T. N. (2002). "Unloading arterial baroreceptors causes neurogenic hypertension." *American Journal of Physiology - Regulatory, Integrative & Comparative Physiology* 282: R1044-R1053.
- Thrasher, T. N. (2004). "Baroreceptors and the long-term control of blood pressure." *Experimental Physiology* 89: 331-335.
- Tortora, G. J. and S. R. Grabowski (2003). Principles of anatomy and physiology. New York, John Wiley & Sons, Inc.
- Triedman, J. K., M. H. Perrott, R. J. Cohen and J. P. Saul (1995). "Respiratory sinus arrhythmia: time domain characterization using autoregressive moving average analysis." *American Journal of Physiology - Heart & Circulatory Physiology* 268: H2232-H2238.
- Ursino, M., G. Fabbri and E. Belardinelli (1992). "A mathematical analysis of vasomotion in the peripheral vascular bed." *Cardioscience* 3: 13-25.

- Ursino, M. and C. A. Lodi (1998). "Interaction among autoregulation, CO<sub>2</sub> reactivity, and intracranial pressure: a mathematical model." *American Journal of Physiology - Heart & Circulatory Physiology* 274: H1715-H1728.
- Ursino, M. and E. Magosso (2003). "Role of short-term cardiovascular regulation in heart period variability: a modelling study." *American Journal of Physiology - Heart & Circulatory Physiology* 284: H1479-H1493.
- Valentinuzzi, M. E. and L. A. Geddes (1974). "The central component of the respiratory heart rate response." *Cardiovascular Research* 12: 87-103.
- Vandeborne, P., N. Montano, B. Zimmerman, M. Pagani and V. K. Somers (1997). "Relationship between repeated measures of hemodynamics, muscle sympathetic nerve activity, and their spectral oscillations." *Circulation* 96: 4326-4332.
- Wagner, C. D., Mrowka, R., Nafz, B. and Persson, P.B. (1995). "Complexity and "chaos" in blood pressure after baroreceptor denervation of conscious dogs." *American Journal of Physiology - Heart & Circulatory Physiology* 269: H1760-H1766.
- Wagner, C. D., B. Nafz and P. B. Persson (1996). "Chaos in blood pressure." *Cardiovascular Research* 31: 380-387.
- Wallin, B. G. and R. Rea (1988). "Spinal sympathetic conduction velocity in humans." *Journal of the Autonomic Nervous System* 24: 221-225.
- Warner, H. R. (1958). "The frequency-dependent nature of blood pressure regulation by the carotid sinus studied with an electric analog." *Circulation Research* 6: 35-40.
- Warner, H. R. and A. Cox (1962). "A mathematical model of heart rate control by sympathetic and vagus efferent information." *Journal of Applied Physiology* 17: 349-355.
- Warner, M. R. and R. O. Russell (1969). "Effect of combined sympathetic and vagal stimulation on heart rate in the dog." *Circulation Research* 24: 567-573.
- Weinstock, M., P. I. Korner, G. A. Head and P. K. Dorward (1988). "Differentiation of cardiac baroreflex properties by cuff and drug methods in two rabbit strains." *American Journal of Physiology - Regulatory Integrative & Comparative Physiology* 255: R654-R664.
- Wesseling, K. H., J. J. Settels, G. Walstra, H. J. Van Esch and J. H. Donders (1982). Baromodulation as the cause of short term blood pressure variability?

- International Conference on Applications of Physics to Medicine and Biology, Trieste, World Scientific.
- Westerhof, N., G. Elizinga and P. Sipkema (1971). "An artificial arterial system for pumping hearts." *Journal of Applied Physiology* 31: 776-781.
- Whittam, A. M., Clayton, R.H., Lord, S.W., McComb, J.M and Murray, A. (2000). "Heart rate and blood pressure variability in normal subjects compared with data from beat-to-beat models developed from de Boer's model of the cardiovascular system." *Physiological Measurements* 21: 305-318.
- Williams, G. P. (1997). *Chaos theory tamed*. London, Taylor & Francis Limited.
- Wolf, A., J. B. Swift, H. L. Swinney and J. A. Vastano (1985). "Determining Lyapunov exponents from a time series." *Physica D* 16: 285-317.
- Woon, S. K. and H. Nicholson (1977). "Describing functions, limit cycles and reduced models in nonlinear systems." *Electronics Letters* 13: 185-187.
- Yamazaki, T. and K. Sagawa (1989). "Summation of sinoartical baroreflexes depends on size of input signals." *American Journal of Physiology - Heart & Circulatory Physiology* 257: H465-H472.
- Yamazaki, Y., T. Karakida and S. Homma (1990). "Conduction velocity of motor nerve and cervical sympathetic and vagus nerve in streptozotocin diabetic rats." *Neuroscience Letters* 113: 29-33.
- Yang, T., M. D. Jacobstein and M. N. Levy (1984). "Synchronisation of automatic cells in S-A node during vagal stimulation in dogs." *American Journal of Physiology - Heart & Circulatory Physiology* 246: H585-H591.
- Yeragani, V. K. (1995). "Heart rate and blood pressure variability: implications for psychiatric research." *Neuropsychobiology* 32: 182-191.
- Yeragani, V. K., R. K. A. Rao, M. R. Smitha, R. B. Pohl, R. Balon and K. Srinivasan (2002). "Diminished chaos in heart rate time series in patients with major depression." *Biological Psychiatry* 51: 733-744.
- Yeragani, V. K., Rao, R., Jayaraman, A., Pohl, R., Balon, R. and Glitz, D. (2002). "Heart rate time series: decreased chaos after intravenous lactate and increased non-linearity after isoproterenol in normal subjects." *Psychiatry Research* 109: 81-92.
- Yeragani, V. k., K. Srinivasan, S. Vempati, R. Pohl and R. Balon (1993). "Fractal dimension of heart rate time series: an effective measure of autonomic function." *Journal of Applied Physiology* 75: 2429-2438.

- Yip, K.-P., N. H. Holstein Rathlou and D. J. Marsh (1991). "Chaos in blood flow control in genetic and renovascular hypertensive rats." *American Journal of Physiology - Renal Fluid Electrolyte Physiology* 261: F400-F408.
- Yip, K.-P., D. J. Marsh and N.-H. Holstein-Rathlou (1995). "Evidence of low dimensional chaos in renal blood flow control in genetic and experimental hypertension." *Physica D* 80: 95-104.
- Yip, K.-P., D. J. Marsh and N.-H. Holstein-Rathlou (1995). "Evidence of low dimensional chaos in renal blood flow control in genetic and experimental hypertension." *Physica D*. 80: 95-104.
- Yuasa, S., X. Li, H. Hitomi, M. Hashimoto, H. Fujioka, H. Kiyomoto, K. Uchida, T. Shoji, N. Takahashi, S. Miki, A. Miyatake, K. Mizushige and H. Matsuo (2000). "Sodium sensitivity and sympathetic nervous system in hypertension induced by long-term nitric oxide blockade in rats." *Clinical Experimental Pharmacological Physiology* 27: 18-24.
- Zak, S. H. (2001). *Systems and control*. New York, Oxford University Press.
- Zaza, A. and F. Lombardi (2001). "Autonomic indexes based on the analysis of heart rate variability: a view from the sinus node." *Cardiovascular Research* 50: 434-442.
- Zhang, T. and E. J. Johns (1994). "Analysis of renal sympathetic nerve activity using chaotic theory and power spectral analysis in Wistar and SPSHR." *Journal of Physiology* 20: 481.
- Zhang, T. a. J., E.J. (1998). "Chaotic characteristics of renal nerve peak interval sequence in normotensive and hypertensive rats." *Clinical and Experimental Pharmacology and Physiology* 25: 896-903.
- Zhong, S., S. M. Barman and G. L. Gebber (1992). "Effect of brain stem lesions on 10-Hz and 2- to 6Hz rhythms in sympathetic discharge." *American Journal of Physiology - Regulatory Integrative & Comparative Physiology* 262: R1015-R1024.
- Zhu, Y. (1999). Parametric Wiener model identification for control. Proceedings of the IFAC World Congress, Beijing 37-42.
- Zweiner, U., D. Hoyer, R. Bauer, B. Luthke, B. Walter, K. Schmidt, S. Hallmeyer, B. Kratzsch and M. Eiselt (1996). "Deterministic-chaotic and periodic properties of heart rate and arterial pressure fluctuations and their mediation in piglets." *Cardiovascular Research* 31.